

## **ABSTRACT**

BREEN, MIYUKI. Predicting the Biochemical Response of Vertebrate Endocrine Systems to Endocrine Active Chemicals. (Under the direction of Rory Conolly and Alun Lloyd).

There is international concern regarding effects of endocrine-active environmental contaminants and commercial products on the health of humans and wildlife. A large number of environmental contaminants may disrupt the endocrine system during critical stages of development, which can result in adverse outcomes in humans and wildlife. Endocrine active chemicals (EACs) are exogenous chemicals that can cause adverse health effects in intact organisms, affecting reproduction and development in both humans and wildlife by inducing adverse hormonal changes in the tightly regulated endocrine pathways. The main focus of research on EACs has been on vertebrate species, driven by the need for human and ecological risk assessments and drug development. To enhance the interpretation and quantitative application of measurement data in risk assessments and drug development, this dissertation describes mathematical computational models of vertebrate endocrine systems.

The first project was to develop a mechanistic computational model of steroidogenesis in human H295R cells. We previously developed a computational model that describes the biosynthetic pathways for the conversion of cholesterol (CHOL) to steroids, and the kinetics for enzyme inhibition by the EAC, metyrapone (MET). In this work, we extended our dynamic model by including a cell proliferation model supported by additional experiments, and by adding a pathway for the biosynthesis of oxysterols (OXY). The extended steroidogenesis model predictions closely correspond to the measured time-course concentrations of CHOL and 14 steroids both in the cells and in the medium, and the calculated time-course concentrations of OXY from control and MET-exposed cells.

The second project was to develop a mechanistic computational model of the Hypothalamic-Pituitary-Gonadal (HPG) axis for a model vertebrate, the fathead minnow (*Pimephales promelas*). A series of time-course fadrozole (FAD) exposure experiments were performed: the data indicate adaptive changes (i.e., compensation) in plasma 17 $\beta$ -estradiol (E2) levels occurring during exposure and “overshoot” occurring post-exposure. In the first part of this research, we developed a dynamic model that includes a regulatory feedback loop within the HPG axis that can mediate adaptive responses to FAD. The HPG axis model predictions closely correspond to the time-course measurements of plasma E2 for lower FAD test concentrations, and the model accurately predicted cytochrome P450 (CYP) 19A mRNA fold changes and plasma E2 dose-response from the 4-day study. The main limitation of the model was the large overestimation of a plasma E2 concentration for higher FAD test concentrations. In the second part of this research, we addressed this limitation by extending the model to include a pathway for protein synthesis of *cyp19a*. As a result, the extended model significantly improved the model fit for the dynamic E2 concentrations at high dose.

These mechanistic modeling capabilities could help define mechanisms of action for poorly characterized chemicals and mixtures for predictive risk assessments, and to screen drug candidates in the early phase of drug development. These studies demonstrate the value of mechanistic computational modeling to examine and predict the possible dynamic behaviors and to formulate and test hypotheses to increase understanding of the biochemical responses of vertebrate endocrine systems to EACs.

© Copyright 2014 by Miyuki Breen

All Rights Reserved

Predicting the Biochemical Response of Vertebrate Endocrine Systems to  
Endocrine Active Chemicals

by  
Miyuki Breen

A dissertation submitted to the Graduate Faculty of  
North Carolina State University  
in partial fulfillment of the  
requirements for the degree of  
Doctor of Philosophy

Biomathematics

Raleigh, North Carolina

2014

APPROVED BY:

---

Alun L. Lloyd  
Committee Co-Chair

---

Sharon R. Lubkin

---

Rory B. Conolly  
Committee Co-Chair

---

R. Woodrow Setzer

---

Karen H. Watanabe

## DEDICATION

To Hannah Mai Breen, my beautiful daughter, who was brought to me by God's grace. *You* stepped into *my life* and brought me true happiness. *You* have blessed *my life* with your sincere love and your precious adorable smiles. I dedicate my dissertation work to *you*.

“Keep your dreams alive. Understand to achieve anything requires faith and belief in yourself, vision, hard work, determination, and dedication. Remember all things are possible for those who believe.”

- Gail Devers

## **BIOGRAPHY**

Miyuki Breen was born and raised on a farm in a small town in Japan. When she was ten years old, her father and grandfather were hospitalized at the same time; her father being disabled in an accident and her grandfather having developed Alzheimer's disease, which forced her mother to quit her job to take care of them. To help support her family, Miyuki worked as a newspaper deliverer, waitress, and cashier, and she finished high school by receiving the Japanese National Achievement Scholarship. In spite of hardship, she was successful academically and always sought to attend college - despite everybody's opposition, even from teachers. After high school, she left the countryside and moved to Tokyo, where she worked as a technician for a defense industry company during the day to accumulate financial resources and attend a junior college at night to reinforce her academic foundation. Tokyo is also where she met her future American husband. In 1994, she immigrated to the United States to tie the knot with Michael Scott Breen. Miyuki and Michael were blessed to have their beautiful daughter, Hannah Mai Breen, in 2007.

Miyuki Breen's strong desire for learning has helped her to excel in many academic settings. She received numerous awards, scholarships, and fellowships, and gained the opportunities to attend numerous research programs and scientific meetings throughout her undergraduate and graduate studies. Related to her doctoral research on endocrine disrupting chemicals (EDCs), she authored six refereed publications and 25 peer-reviewed abstracts, including four award winning scientific posters from graduate student/postdoctoral paper competitions (North Carolina Society of Toxicology Spring Meeting 2008, 2009, 2010; Gordon Research Conference: Environmental Endocrine Disruptors 2008). In addition, she

was selected as one of six student participants to attend the 2009 SETAC Workshop: A Vision and Strategy for Ecotoxicology in the 21st Century - Defining Adverse Outcome Pathways Associated with Ecological Risk. Moreover, she has been an active member of professional societies. During her doctoral program, she has served as the student representative of the Society of Toxicology Biological Modeling Specialty Section, a member of the Society of Toxicology Graduate Student Leadership Committee Professional Development Subcommittee, and a peer-reviewer for the International Journal of Toxicology.

Miyuki Breen received a bachelor's degree (double major in applied mathematics and statistics, minor in computer sciences) with Summa Cum Laude honors from the University of Akron, OH in 2002, and a master's degree in biomathematics from North Carolina State University, Raleigh, NC in 2007. In 2008, she started her Doctor of Philosophy in the Biomathematics Program at North Carolina State University under the direction of Dr. Rory B. Conolly from the United States Environmental Protection Agency (U.S. EPA) and Dr. Alun L. Lloyd from North Carolina State University (NCSU).

## ACKNOWLEDGMENTS

I would like to express my deepest gratitude and appreciations to my dear husband, Michael Breen, for his continuous support as a collaborator giving me helpful suggestions to my research and editing my papers, and as a marriage partner helping me to take care of our daughter during long hours of writing, model development, and model analysis.

I would like to thank my U.S. EPA advisor, Dr. Rory B. Conolly, and my NCSU advisor, Dr. Alun L. Lloyd for their guidance and mentorship. Their knowledge and guidance facilitated success of publishing research papers in well-respected journals and presenting research at numerous scientific meetings. I would like to thank my committee members, Drs. Sharon R. Lubkin, Karen H. Watanabe, and R. Woodrow Setzer for their guidance and helpful suggestions. I greatly appreciate the support and expertise provided by my collaborators, Drs. Daniel L. Villeneuve, Gerald T. Ankley, and Natsuko Terasaki. Without their experimental expertise and measurement data, we could not have successfully developed mechanistic mathematical models for our research. I also greatly appreciate the guidance and support giving by fellow Society of Toxicology Biological Modeling Specialty Section officers and U.S. EPA researchers, Drs. Hisham A. El-Masri and Cecilia Tan. I gained valuable experience as an active member of professional societies and working with them. I would like to acknowledge the North Carolina State University/Environmental Protection Agency Cooperative Training Program in Environmental Science Research with North Carolina State University, and Oak Ridge Institute for Science and Education Research Participation at Environmental Protection Agency for providing me with financial support.

I would like to express my sincere gratitude and appreciation to my undergraduate advisor, Dr. Judith A. Palagallo from the University of Akron. She was the first mentor and dear friend who introduced me to the wonderful world of mathematical research with continuous guidance, support, and encouragement. Without her guidance, I would not have gained so many valuable research opportunities and experiences in my earlier years to inspire me to continue onto graduate programs. I am also grateful to a fellow science graduate student/mom/mathematics science teacher, Angela Costello, and a fellow microbiology professor/mom, Alice Lee, for sharing a passion for mathematics and science, and an art of balancing graduate school and parenthood. Their story inspired and encouraged me to continue on my graduate studies in mathematical science, and guided me in realizing that I am not alone in this journey of graduate school/parenthood. Last, but not least, I would like to extend special thanks to my extraordinary family and friends, Joseph Breen, Machio & Kinuko Kanno, Sheila & Carey Demers, Patrick & Cyndi Breen, Mary & James Puracchio, Rachel Vilandre, Diane Hom, Christopher Larson, Donna & James Millet, Donna Howard, Christine Sandez, James Huggard, Suli & Jon Meulenberg, Manjri Lall, Jennifer Peterson, Nadeesha & Anthony Andrady, Levon & Mary Martin, and May Shih for providing me encouragements and helping me to maintain my sanity during difficult times. You have been my best cheerleaders.

## TABLE OF CONTENTS

<b>LIST OF TABLES .....</b>	<b>ix</b>
<b>LIST OF FIGURES .....</b>	<b>x</b>
<b>1. INTRODUCTION AND BACKGROUND .....</b>	<b>1</b>
Introduction .....	1
Vertebrate Endocrine System.....	1
Endocrine Active Chemicals .....	3
Adrenal Steroidogenesis in H295R Cells.....	4
Mechanistic Computational Model of Steroidogenesis in H295R Cells.....	5
Computational Model of Fathead Minnow Hypothalamic-Pituitary-Gonadal Axis .....	8
References .....	11
<b>2. MECHANISTIC COMPUTATIONAL MODEL OF STEROIDOGENESIS IN H295R CELLS: ROLE OF OXYSTEROLS AND CELL PROLIFERATION TO IMPROVE PREDICTABILITY OF BIOCHEMICAL RESPONSE TO ENDOCRINE ACTIVE CHEMICAL – METYRAPONE .....</b>	<b>15</b>
Abstract .....	16
Introduction .....	16
Materials and Methods .....	17
Results .....	20
Discussion .....	23
Acknowledgments .....	28
References .....	28
Supplementary Data .....	30
<b>3. DEVELOPING PREDICTIVE APPROACHES TO CHARACTERIZE ADAPTIVE RESPONSES OF THE REPRODUCTIVE ENDOCRINE AXIS TO AROMATASE INHIBITION: II. COMPUTATIONAL MODELING .....</b>	<b>45</b>
Abstract .....	46
Introduction .....	46
Materials and Methods .....	47
Results .....	51
Discussion .....	56
Acknowledgments .....	58
References .....	58
Supplementary Data .....	60

<b>4. COMPUTATIONAL MODEL OF THE FATHEAD MINNOW HYPOTHALAMIC-PITUITARY-GONADAL AXIS: INCORPORATING PROTEIN SYNTHESIS TO IMPROVE PREDICTABILITY OF BIOCHEMICAL RESPONSE TO ENDOCRINE ACTIVE CHEMICALS .....</b>	<b>75</b>
Abstract .....	77
Introduction .....	78
Materials and Methods .....	80
Results .....	87
Discussion .....	89
Acknowledgments .....	92
References .....	100
Supplementary Data .....	102
<b>5. COMMENTARY ON THE PARAMETER IDENTIFICATION ISSUE .....</b>	<b>108</b>
Standard Error and Correlation Coefficient Calculation .....	111
Identifiability Analysis .....	116
References .....	120
<b>6. CONCLUSIONS .....</b>	<b>123</b>
<b>7. APPENDICES .....</b>	<b>127</b>
Appendix A. Computational Model of Steroidogenesis in Human H295R Cells to Predict Biochemical Response to Endocrine-Active Chemicals: Model Development for Metyrapone .....	128
Appendix B. Developing Predictive Approaches to Characterize Adaptive Responses of the Reproductive Endocrine Axis to Aromatase Inhibition: I. Data Generation in a Small Fish Model .....	153

## LIST OF TABLES

Table 2.1	Estimated Transport Equilibrium Parameters (dimensionless) from Model Fit of Steroids Corresponding to Given $q$ Parameter.....	22
Table 2.2	Estimated Parameters of Metabolic Pathway.....	22
Table 2.S1	Quantitative Ranges for Cholesterol and Steroids.....	39
Table 3.1	Physiological Constant for Weights, Volumes, Blood Flows, and Partition Coefficients (PC).....	50
Table 3.2	Fixed Biochemical Parameters.....	51
Table 3.3	Estimated Biochemical Parameters.....	51
Table 4.1	Estimated Biochemical Parameters.....	94
Table 5.1	Standard Errors for Estimated Transport Equilibrium Parameters.....	114
Table 5.2	Standard Errors for Estimated Parameters of Metabolic Pathway.....	115

## LIST OF FIGURES

Figure 2.1	Graphical Representation of the Two Compartment Model and Model Parameters with Equilibrium Constants.....	19
Figure 2.2	Time-Course of Measured and Model-Predicted Number of Viable Cells.....	20
Figure 2.3	Time-Course of Total Number of Measured CHOL and Steroid Molecules, and Calculated OXY Molecules.....	21
Figure 2.4	Model Evaluation of CHOL and OXY. ....	22
Figure 2.5	Model Evaluation of Steroids for Control Cells. ....	24
Figure 2.6	Model Evaluation of Steroids for MET-Exposed Cells.....	25
Figure 2.7	Relative Sensitivities for Model-Predicted ALDO and CORT.....	26
Figure 2.8	Relative Sensitivities for Model-Predicted T and E2.....	27
Figure 2.S1	Graphical Representation of Model Parameters with Reversible Transport Processes. ....	40
Figure 2.S2	Measured Number and Percentage of Viable H295R Cells. ....	41
Figure 2.S3	Time-Course of Number of Calculated OXY Molecules. ....	42
Figure 2.S4	Model Evaluation of Intracellular Steroids for Control Cells. ....	43
Figure 2.S5	Model Evaluation of Intracellular Steroids in MET-Exposed Cells.....	44
Figure 3.1	Overview of Experimental Design. ....	47
Figure 3.2	Graphical Representation of Physiological Model of HPG Axis. ....	48

Figure 3.3	Graphical Representation of Biochemical Processes within the Six Compartments of the Model. ....	49
Figure 3.4	Measurements of Plasma E2 and Ovary CYP19A mRNA.....	52
Figure 3.5	Model Evaluation of Venous E2 and Ovary CYP19A mRNA.....	53
Figure 3.6	Modeled Dose Response During FAD Exposure. ....	54
Figure 3.7	Relative Sensitivities for Model-Predicted E2 Plotted for Biochemical Model Parameters. ....	55
Figure 3.8	Relative Sensitivities for Model-Predicted CYP19A mRNA Plotted for Biochemical Model Parameters. ....	56
Figure 3.S1	Model Predictions Plotted as a Function of FAD Concentration and Time.....	72
Figure 3.S2	Relative Sensitivities for Model-Predicted E2 Plotted for Cardiovascular Parameters.....	73
Figure 3.S3	Relative Sensitivities for Model-Predicted CYP19A mRNA E2 Plotted for Cardiovascular Parameters.. ....	74
Figure 4.1	Graphical Representation of Biochemical Processes within the Six Compartments of the Model. ....	93
Figure 4.2	Model Evaluation of Venous E2 and Ovary CYP19A mRNA.....	95
Figure 4.3	Modeled Dose Response During FAD Exposure. ....	96
Figure 4.4	Model Predictions Plotted as a Function of FAD Concentration and Time.....	97
Figure 4.5	Relative Sensitivities for Model-Predicted E2 Plotted for Biochemical Model Parameters. ....	98

Figure 4.6	Relative Sensitivities for Model-Predicted CYP19A mRNA Plotted for Biochemical Model Parameters. ....	99
Figure 5.1	Heat Map of Correlation Coefficients for Metabolic Pathway parameters of the H295R Model. ....	116

## **1. INTRODUCTION AND BACKGROUND**

### **Introduction**

The endocrine system consists of a series of glands that signal each other by secreting chemicals called hormones into the blood. These hormones travel to target tissues to regulate various critical functions, which include metabolism, reproduction, growth and development. Exposure to endocrine active chemicals (EACs) can affect reproduction and development in both humans and wildlife by inducing adverse hormonal changes in the tightly regulated endocrine pathways. Chemicals capable of acting as EACs are ubiquitous with environmental sources that include household detergents, pesticides, plastics, pharmaceutical estrogens, industrial chemicals, and byproducts of incineration and fuel combustion. Colborn *et al.* (1993) reported that a large number of environmental contaminants may disrupt the endocrine system during critical stages of development, which can result in adverse outcomes in humans and wildlife. To identify and regulate chemicals that have the potential to impact the endocrine system, government programs have been established both in North America and Europe (Nichols *et al.*, 2011). The main focus of research on EACs has been on vertebrate species, driven by the need for human and ecological risk assessments and drug development.

### **Vertebrate Endocrine System**

The endocrine system regulates various processes vital for life. It is a dynamic control system of the body which coordinates responses of a target tissue to internal and external signals. The primary function of the endocrine system is to maintain a balanced physiological

system that can sustain a dynamic equilibrium by avoiding large fluctuations in hormone levels and their responses. By integrating specialized responses of individual organs, the endocrine system allows the desired cellular environment to be maintained. The physiological processes regulated by the endocrine system include short- and long-term metabolism, reproduction, growth, functions of the gut, kidneys, and cardiovascular system, and stress responses.

The endocrine system is organized to stabilize the cellular environment by a seesaw-type mechanism. The seesaw-type mechanism operates by feedback signals between the target cells and the regulating cells, with the result that secretion of a target cell-stimulating hormone is altered by the products of the target cells. The balance of the two sides of the seesaw is determined by a programmed set point, which determines the level at which each side of the seesaw will respond to signals from the other side. The preprogrammed set point represents the optimal physiological condition. The endocrine system is organs and tissues integrate their information using crosstalk, where signaling from hormones are shared between different biological pathways, and responses to hormones can activate multiple responses in the organism.

The endocrine system, which originated during the early evolution of fish, is highly conserved across vertebrate species. Hence, the components of the endocrine system are fundamentally the same for all vertebrates. Specialized endocrine glands of the brain-pituitary system in vertebrates include the hypothalamus, pituitary, thyroid, adrenal, gonads (testes or ovaries), pancreas, and parathyroid.

Glands of the endocrine system signal each other by secreting hormones into the blood, which travel to target tissues to regulate critical functions. The brain initiates the process by sending neural signals. The hypothalamus responds to these neural signals and secretes hormones into the blood and transported to the pituitary. In response, the pituitary secretes different hormones that travel to specific downstream endocrine glands, such as the thyroid, adrenal gland, and gonads. In response, these glands release hormones that travel to target tissues to regulate specific physiological processes. Hormones produced by the thyroid regulate general metabolic rate, growth and possibly embryonic development. Hormones secreted by the adrenal gland are involved in stress responses, osmoregulation and carbohydrate metabolism. The hormones released by the gonads control reproduction. To maintain control of these physiological processes, some hormones secreted by the downstream glands travel back to the hypothalamus and pituitary to form a closed-loop negative feedback control system.

### **Endocrine Active Chemicals**

EACs are exogenous chemicals that cause effects by either receptor- or nonreceptor-mediated mechanisms. Receptor-mediated EACs mimic or block endogenous hormone activity by acting as receptor agonists or antagonists. Agonists bind to hormone receptors and promote hormone activity, whereas the antagonists bind to hormone receptors and block hormone activity. Nonreceptor-mediated EACs inhibit the activity of enzymatic reactions for various biological pathways, such as steroid biosynthesis.

There is international concern regarding the effects of various environmental contaminants and commercial products on the health of humans and wildlife (Cooper and Kavlock 1997; Daston *et al.*, 2003; Hutchinson *et al.*, 2006; Zacharewski 1998). The feminization of male smallmouth bass in the Potomac River due to exposure to water pollutants is a well known example of the potential effects of EACs (Buzdar *et al.*, 2007). The U.S. Environmental Protection Agency developed and implemented an endocrine disruptor screening program (EDSP) to screen for endocrine disrupting properties of chemicals in drinking water and pesticides used in food production, which is required by the Safe Drinking Water Act Amendments (1996) and the Food Quality Protection Act (1996). The EDSP is designed as a two-tiered screening and testing process to identify chemicals that can interact with the endocrine system (Tier 1), and to characterize their dose-response (Tier 2). In particular, the EDSP examines the effect of chemicals that act as agonists or antagonists of estrogen and androgen receptors (Chu *et al.*, 2009; Henley and Korach 2006), and other EACs that can cause effects by nonreceptor-mediated mechanisms (Harvey and Everett 2003; Ulleras *et al.*, 2008; Villeneuve *et al.*, 2007).

### **Adrenal Steroidogenesis in H295R Cells**

Steroids are a class of hormones synthesized in the gonads and adrenal glands, which have an important role in a wide range of physiological and pathological processes, such as stress response, development, growth, reproduction, metabolism, aging, and hormone-sensitive cancers (Portier 2002; Ulleras *et al.*, 2008). Steroids are derived from cholesterol through a series of biochemical reactions mediated by multiple cytochrome P450 (CYP)

enzymes and hydroxysteroid dehydrogenases (HSD), primarily synthesized in the ovaries, testes, and adrenal tissue (Miller *et al.*, 1988; Payne *et al.*, 2004). The activity of these steroidogenic enzymes and the subsequent production rate of steroids can be altered by various environmental and pharmacologic EACs (Sanderson *et al.*, 2002; Walsh *et al.*, 2000).

The human adrenocortical carcinoma cell line H295R is the only *in vitro* assay that can be used to evaluate EAC effects across the entire steroidogenesis pathway since H295R cells express all the key enzymes involved in steroidogenesis and they have the ability to produce all the adrenocortical steroids (Gazdar *et al.*, 1990; Rainey *et al.*, 1994; Staels *et al.*, 1993). The H295R cell line was selected as an *in vitro* steroidogenesis assay to detect chemicals that affect steroid biosynthesis in the EDSP Tier 1 battery of screening assays (2009). Moreover, this assay coupled with a mechanistic computational model supports the recommendations of the National Research Council's report *Toxicology Testing in the 21<sup>st</sup> Century* (National Research Council, 2007). The report advises the use of *in vitro* systems to evaluate a broad range of chemicals and outcomes at a reduced cost, with fewer animals, and develop a sound scientific basis to assess effects from environmental agents.

### **Mechanistic Computational Model of Steroidogenesis in H295R Cells**

To increase the understanding and quantitative use of data from the *in vitro* steroidogenesis assay for human and ecological risk assessments, we developed a mechanistic computational model of steroidogenesis in H295R cells. Our research goal is to better understand the dose-response behaviors of EACs. Each of these EACs can inhibit different steroidogenic enzymes, which alter the production rate of steroids. Laboratory

experiments can measure the level of steroids after chemical exposures, but measurements of the metabolic reaction rates for each enzyme are not feasible. However, knowledge of the metabolic reaction rates and steroid transport rates is essential to fully understand the dynamic dose-response behavior of EACs. Development of a mechanistic computational model of steroidogenesis, and estimation of the metabolic reaction rates and steroid transport rates helps us gain this essential knowledge.

Other models of steroid synthesis have been previously reported in the literature. Murphy *et al.* (2005) developed a model for vitellogenesis, a steroid-controlled process, in female fish. To model steroidogenesis in ovaries, they combined all reactions occurring between the release of gonadotropin and the production of testosterone (T) into one Hill equation. Selgrade and Schlosser (1999) developed a mathematical model to predict plasma levels of 17 $\beta$ -estradiol (E2) during different stages of the menstrual cycle in women from luteinizing hormone (LH) and follicle-stimulating hormone (FSH) concentrations. E2 concentrations were modeled as a weighted sum of LH concentration, growth follicle stage, and preovulatory stage. These models lack the ability to predict responses to EACs that inhibit specific steroidogenic enzymes, since they do not include any reactions in the metabolic pathway for steroid synthesis. Breen *et al.* (2007) developed a mechanistic model of the metabolic pathway for ovarian steroidogenesis in female fish. Metabolic reaction and transport rates were estimated under the assumption that the steroidogenic pathway is operating at steady-state. Becker *et al.* (1980) developed a probabilistic model of the metabolic pathway for testicular steroidogenesis. They estimated transition probabilities for the reactions in the pathway from *ex vivo* preparations of rat and rabbit testes. Since ovarian

and testicular steroidogenesis do not express all the key enzymes for steroidogenesis and lack the ability to produce all the adrenocortical steroids, these computational models do not include the metabolic pathways for the major adrenal steroids, such as aldosterone and cortisol.

In this work, we developed a mechanistic model for the synthesis and transport of adrenocortical steroids, and their biochemical response to the competitive steroidogenic enzyme inhibitor metyrapone (MET), a model EAC. Since the structure of the metabolic reaction pathway for steroid synthesis is well established, a mechanistic model was chosen to better understand the biological mechanism for the response to chemical exposures. The model was based on an *in vitro* steroidogenesis experimental design with two compartments: culture medium and human adrenal cells. The model describes cholesterol transport from the medium into the cells, conversion of cholesterol into steroids in the cells, transport of the steroids and EAC between the cells and medium, and inhibition of specific steroidogenic enzymes by the EAC. The computational model was developed and evaluated for an EAC using dose-response experimental data, which includes measured concentrations of cholesterol, 14 steroids [pregnenolone (PREG), 17 $\alpha$ -hydroxy-pregnenolone (HPREG), dehydroepiandrosterone (DHEA), progesterone (PROG), 17 $\alpha$ -hydroxy-progesterone (HPROG), androstenedione (DIONE), testosterone (T), deoxycorticosterone (DCORTICO), corticosterone (CORTICO), aldosterone (ALDO), 11-deoxycortisol (DCORT) cortisol (CORT), estrone (E1), and 17-beta-estradiol (E2)] in H295R cells and medium, and the EAC, metyrapone (MET). The data were obtained from an *in vitro* steroidogenesis assay using the

human H295R adrenocarcinoma cell line. An iterative optimization algorithm was used to estimate the metabolic reaction rate constants and steroid transport rate constants.

We previously developed a mechanistic computational model that describes the biosynthetic pathways for conversion of cholesterol to adrenocortical steroids, and the kinetics for enzyme inhibition by the MET. The primary focus was on steroid synthesis (Breen *et al.*, 2010). The key limitations of the previous steroidogenesis model were the large underestimation and overestimation of CHOL concentrations in cells and medium, respectively, and the potential confounding effects of cell proliferation and viability on the time-course concentrations of the steroids. In Chapter 2, we describe the extended model and additional critical experiments performed to address key limitations of the previously developed model. In addition, the details of the previous steroidogenesis model are provided in Appendix A.

### **Computational Model of Fathead Minnow Hypothalamic-Pituitary-Gonadal Axis**

Dose-response and time-course behaviors of endocrine effects in organisms exposed to environmental chemicals are major determinants of health risk. The NRC report *Toxicology Testing in the 21<sup>st</sup> Century* emphasizes that adaptive changes within organisms exposed to environmental stress can alter dose-response behaviors to minimize the effects of the stressors (National Research Council, 2007). As the field of toxicology evolved, characterization of adaptation to modern toxicology stressors became critical (National Research Council, 2007). Better understanding of the adaptive mechanisms is needed to refine descriptions of dose-response behavior for risk assessments. To increase the

understanding and characterization of the adaptive responses to toxicant stress, we developed a mechanistic computational model of the Hypothalamic-Pituitary-Gonadal (HPG) axis for a model vertebrate, the fathead minnow (*Pimephales promelas*). Our research goal is to better understand the dose-response behaviors and how the feedback regulatory loops in the HPG axis generate adaptive responses to toxicant stress.

Other models of the HPG axis have been previously reported in the literature. Watanabe *et al.* (2009) developed a model for male fathead minnows exposed to  $17\alpha$ -ethinylestradiol or  $17\beta$ -estradiol (E2) to predict plasma sex-steroid hormones and vitellogenin (Vtg) concentrations, and Li *et al.* (2011) extended the model for female fathead minnows exposed to  $17\alpha$ -ethinylestradiol or  $17\beta$ -trenbolone. Murphy *et al.* (2005) developed a model for female sciaenid fish exposed to PCBs and cadmium to predict Vtg concentrations, and Kim *et al.* (2006) developed a model for salmonids to describe normal functioning. Barton and Andersen (1998) developed a model for rats to simulate hormone levels in testes and blood. Pechstein *et al.* (2000) and Tornøe *et al.* (2007) developed a model for humans to describe changes in luteinizing hormone (LH) and testosterone (T) concentrations following treatment with the LH-releasing hormone antagonist, cetrorelix, and the gonadotropin-releasing hormone (GnRH) agonist, triptorelin, as well as the GnRH receptor blocker, degarelix, respectively.

In this work, we developed a mechanistic mathematical model of the HPG axis in female fathead minnows to predict the dose-response and time-course behaviors for endocrine effects of the aromatase inhibitor, fadrozole (FAD). Fadrozole is a model EAC that competitively inhibits the steroidogenic enzyme, aromatase cytochrome P450 (CYP) 19A. To

support development of a computational dynamic model of the HPG axis to predict complex dose-response time-course behaviors that may occur *in vivo*, a series of time-course FAD exposure experiments were performed (Villeneuve *et al.*, 2009, 2013). One of the experiments, Villeneuve *et al.* (2013), is described in Appendix B. Data from three separate experiments to characterize the response of female fathead minnows to FAD exposure were utilized for model development. We observed adaptive changes (compensation) in plasma E2 levels during exposure, which resulted in a period of increased E2 production/concentrations, relative to controls, immediately following removal of the inhibitor (an overshoot), particularly at lower FAD test concentrations (Villeneuve *et al.*, 2009). In Chapter 3, we describe the computational model of the HPG axis, which characterizes the adaptive responses to aromatase inhibition (Breen *et al.*, 2013). In this study, we developed an HPG axis model that includes a regulatory feedback loop within the HPG axis that can mediate adaptive responses to EAC. The computational model of the HPG axis was developed based on knowledge of biological mechanisms, and the model consists of six tissue compartments: gill, brain (as an organ including hypothalamic-pituitary complex), ovary, liver, venous blood, and rest of body. These six compartments, which are involved in the HPG axis signaling and feedback control, are configured to be consistent with the cardiovascular system of the exposed fish. Model parameters were estimated using E2 concentrations for three lower FAD test concentrations by an iterative optimization algorithm.

The focus of Breen *et al.* (2013) was to capture compensation and overshoot of plasma E2 concentration for lower FAD concentrations. The main limitation of Breen *et al.* (2013) was the large overestimation of a plasma E2 concentration for higher FAD test

concentrations. To address this limitation, we extended the model by Breen *et al.* (2013). In Chapter 4, we describe the extended model of the HPG axis, which includes the pathway for protein synthesis of *cyp19a* (aromatase). Model parameters were estimated using E2 concentrations for all four FAD test concentrations and an iterative optimization algorithm. The extended model improved the predictability of the biochemical response to EACs.

In our study, mathematical models were developed based on knowledge of biological mechanisms, and model parameters were estimated using biological data generated from experiments. Since many of the model parameters are not directly measurable, the estimation of unknown model parameters and identifiability play a central role in model development. In Chapter 5, we address parameter identification issues associated with the HPG axis model of fathead minnows.

## REFERENCES

- Barton HA, Andersen ME. (1998). A model for pharmacokinetics and physiological feedback among hormones of the testicular-pituitary axis in adult male rats: A framework for evaluating effects of endocrine active compounds. *Toxicol. Sci.* **45**, 174-187.
- Becker S, Chubb C, Ewing L. (1980). Mathematical model of steroidogenesis in rat and rabbit testes. *Am. J. Physiol.* **239**, 184-195.
- Blazer, V, Iwanowicz, L and Iwanowicz, D. (2007). Intersex (testicular oocytes) in smallmouth bass from the Potomac River and selected nearby drainages. *J. Aquat. Anim. Health.* **19**, 242-253.
- Breen MS, Breen M, Terasaki N, Yamazaki M, Conolly RB. (2010). Computational model of steroidogenesis in human H295R cells to predict biochemical response to endocrine-active chemicals: model development for metyrapone. *Environ. Health Perspect.* **118**, 265-72.

Breen MS, Villeneuve DL, Breen M, Ankley GT, Conolly RB. (2007). Mechanistic computational model of ovarian steroidogenesis to predict biochemical responses to endocrine active compounds. *Ann. Biomed. Eng.* **35**, 970-981.

Chu WL, Shiizaki K, Kawanishi M, Kondo M, Yagi T. (2009). Validation of a new yeast-based reporter assay consisting of human estrogen receptors alpha/beta and coactivator SRC-1: Application for detection of estrogenic activity in environmental samples. *Environ. Toxicol.* **24**, 413-521.

Colborn T, vom Saal FS, Soto AM. (1993). Developmental effects of endocrine-disrupting chemicals in wildlife and humans. *Environ. Health Perspect.* **101**, 378-384.

Cooper RL, Kavlock RJ. (1997). Endocrine disruptors and reproductive development: a weight-of-evidence overview. *J. Endocrinol.* **152**, 159-166.

Daston GP, Cook JC, Kavlock RJ. (2003). Uncertainties for endocrine disrupters: our view on progress. *Toxicol. Sci.* **74**, 245-252.

Food Quality Protection Act of 1996. (1996). Public Law 104 -107.

Gazdar AF, Oie HK, Shackleton CH, Chen TR, Triche TJ, Myers CE. (1990). Establishment and characterization of a human adrenocortical carcinoma cell line that expresses multiple pathways of steroid biosynthesis. *Cancer Res.* **50**, 5488-5496.

Harvey PW, Everett DJ. (2003). The adrenal cortex and steroidogenesis as cellular and molecular targets for toxicity: critical omissions from regulatory endocrine disrupter screening strategies for human health? *J. Appl. Toxicol.* **23**, 81-87.

Henley DV, Korach KS. (2006). Endocrine-disrupting chemicals use distinct mechanisms of action to modulate endocrine system function. *Endocrinology* **147** Suppl, S25-32.

Hutchinson TH, Ankley GT, Segner H, Tyler CR. (2006). Screening and testing for endocrine disruption in fish-biomarkers as "signposts," not "traffic lights," in risk assessment. *Environ. Health Perspect.* **114**, 106-114.

Kim J, Hayton WL, Schultz IR. (2006). Modeling the brain-pituitary-gonad axis in salmon. *Mar. Environ. Res.* **62** Suppl, S426-432.

- Li, Z, Kroll, KJ, Jensen, KM, Villeneuve, DL, Ankley, GT, Brian, JV, Sepúlveda, MS, Orlando, EF, Lazorchak, JM, Kostich, M, Armstrong, B, Denslow, ND, and Watanabe, KH (2011). A computational model of the hypothalamic - pituitary - gonadal axis in female fathead minnows (*Pimephales promelas*) exposed to 17 $\alpha$ -ethynylestradiol and 17 $\beta$ -trenbolone. *BMC Syst Biol.* **5**, 63.
- Miller WL. (1988). Molecular biology of steroid hormone synthesis. *Endocr. Rev.* **9**, 295-318.
- Murphy CA, Rose KA, Thomas P. (2005). Modeling vitellogenesis in female fish exposed to environmental stressors: predicting the effects of endocrine disturbance due to exposure to a PCB mixture and cadmium. *Reprod. Toxicol.* **19**, 395-409.
- National Research Council. (2007). Toxicity Testing in the 21st Century: A Vision and a strategy. National Academy Press, Washington, DC
- Nichols JW, Breen M, Denver RJ, Distefano JJ 3rd, Edwards JS, Hoke RA, Volz DC, Zhang X. (2011). Predicting chemical impacts on vertebrate endocrine systems. *Environ. Toxicol. Chem.* **30**, 39-51.
- Payne AH, Hales DB. 2004. Overview of steroidogenic enzymes in the pathway from cholesterol to active steroid hormones. *Endocr Rev* 25(6): 947-970.
- Pechstein B, Nagaraja NV, Hermann R, Romeis P, Locher M, Derendorf H. (2000). Pharmacokinetic-pharmacodynamic modeling of testosterone and luteinizing hormone suppression by cetrorelix in healthy volunteers. *J. Clin. Pharmacol.* **40**, 266-274.
- Portier CJ. (2002). Endocrine dismodulation and cancer. *Neuro. Endocrinol. Lett.* **23** Suppl, 43-47.
- Rainey WE, Bird IM, Mason JJ. (1994). The NCI-H295 cell line: a pluripotent model for human adrenocortical studies. *Mol. Cell Endocrinol.* **100**, 45-50.
- Safe Drinking Water Act Amendments of 1996. (1996). Public Law 104-182.
- Sanderson JT, Boerma J, Lansbergen GW, van den Berg M. (2002). Induction and inhibition of aromatase (CYP19) activity by various classes of pesticides in H295R human adrenocortical carcinoma cells. *Toxicol. Appl. Pharmacol.* **182**, 44-54.
- Selgrade JF, Schlosser PM. (1999). A model for the production of ovarian hormones during the menstrual cycle. *Fields Institute Communications* **21**, 429-446.
- Staels B, Hum DW, Miller WL. (1993). Regulation of steroidogenesis in NCI-H295 cells: a cellular model of the human fetal adrenal. *Mol. Endocrinol.* **7**, 423-433.

Tornøe CW, Agerso H, Senderovitz T, Nielsen HA, Madsen H, Karlsson MO, Jonsson EN. (2007). Population pharmacokinetic/pharmacodynamic (PK/PD) modelling of the hypothalamic-pituitary-gonadal axis following treatment with GnRH analogues. *Br. J. Clin. Pharmacol.* **63**, 648-664.

Ulleras E, Ohlsson A, Oskarsson A. (2008). Secretion of cortisol and aldosterone as a vulnerable target for adrenal endocrine disruption - screening of 30 selected chemicals in the human H295R cell model. *J. Appl. Toxicol.* **28**, 1045-1053.

U.S. Environmental Protection Agency (2009). Endocrine Disruptor Screening Program (EDSP): announcing the availability of the Tier 1 screening battery and related test guidelines. Federal Register. Vol. 74, No. 202, October 21, 2009, Page 54415-54422.

Villeneuve DL, Ankley GT, Makynen EA, Blake LS, Greene KJ, Higley EB, Newsted JL, Giesy JP, Hecker M. (2007). Comparison of fathead minnow ovary explant and H295R cell-based steroidogenesis assays for identifying endocrine-active chemicals. *Ecotoxicol. Environ. Saf.* **68**, 20-32.

Villeneuve, DL, Breen, M, Bencic, DC, Cavallin, JE, Jensen, KM, Makynen, EA, Thomas, LM, Wehmas, LC, Conoll, RB, Ankley, GT. (2013). Developing Predictive approaches to characterize adaptive responses of the reproductive endocrine axis to aromatase inhibition: I. Data Generation in a Small Fish Model. *Toxicol. Sci.* **133**, 225-233.

Villeneuve, DL, Mueller, ND, Martinovic, D, Makynen, EA, Kahl, MD, Jensen, KM, Durhan, EJ, Cavallin, JE, Bencic, D, Ankley, GT. (2009). Direct effects, compensation, and recovery in female fathead minnows exposed to a model aromatase inhibitor. *Environ Health Perspect.* 117, 624-631.

Walsh LP, Kuratko CN, Stocco DM. (2000). Econazole and miconazole inhibit steroidogenesis and disrupt steroidogenic acute regulatory (StAR) protein expression post-transcriptionally. *J. Steroid. Biochem. Mol. Biol.* **75**, 229-236.

Watanabe KH, Li Z, Kroll KJ, Villeneuve DL, Garcia-Reyero N, Orlando EF, Sepúlveda MS, Collette TW, Ekman DR, Ankley GT, Denslow ND. (2009). A computational model of the hypothalamic-pituitary-gonadal axis in male fathead minnows exposed to 17alpha-ethinylestradiol and 17beta-estradiol. *Toxicol. Sci.* **109**, 180-92.

Zacharewski T. (1998). Identification and assessment of endocrine disruptors: limitations of in vivo and in vitro assays. *Environ. Health Perspect.* **106**, 577-582.

**2. MECHANISTIC COMPUTATIONAL MODEL OF STEROIDOGENESIS IN H295R CELLS: ROLE OF OXYSTEROLS AND CELL PROLIFERATION TO IMPROVE PREDICTABILITY OF BIOCHEMICAL RESPONSE TO ENDOCRINE ACTIVE CHEMICAL – METYRAPONE**

Miyuki Breen, Michael S. Breen, Natsuko Terasaki, Makoto Yamazaki, Alun L. Lloyd, Rory B. Conolly

Published in Toxicological Sciences: 2011; 123: 80-93

Reprinted with permission from Oxford University Press

Miyuki Breen was primarily responsible for model development, simulation, analysis of results, and manuscript writing.

# Mechanistic Computational Model of Steroidogenesis in H295R Cells: Role of Oxysterols and Cell Proliferation to Improve Predictability of Biochemical Response to Endocrine Active Chemical—Metyrapone

Miyuki Breen,\*† Michael S. Breen,‡ Natsuko Terasaki,§ Makoto Yamazaki,§ Alun L. Lloyd,† and Rory B. Conolly\*,<sup>1</sup>

\*Integrated Systems Toxicology Division, National Health and Environmental Effects Research Laboratory, U.S. Environmental Protection Agency, Research Triangle Park, North Carolina 27711; †Biomathematics Graduate Program, Department of Mathematics, North Carolina State University, Raleigh, North Carolina 27695; ‡Human Exposure and Atmospheric Sciences Division, National Exposure Research Laboratory, U.S. Environmental Protection Agency, Research Triangle Park, North Carolina 27711; and §Safety Research Laboratory, Mitsubishi Tanabe Pharma Corporation, Kisarazu, Chiba 292-0818, Japan

<sup>1</sup>To whom correspondence should be addressed at Office of Research and Development, National Health and Environmental Effects Research Laboratory, U.S. Environmental Protection Agency, 109 T. W. Alexander Drive, Mail B105-03, Research Triangle Park, NC 27711. Fax: (919) 541-0694.  
E-mail: conolly.rory@epa.gov

Received December 28, 2010; accepted June 14, 2011

The human adrenocortical carcinoma cell line H295R is being used as an *in vitro* steroidogenesis screening assay to assess the impact of endocrine active chemicals (EACs) capable of altering steroid biosynthesis. To enhance the interpretation and quantitative application of measurement data in risk assessments, we are developing a mechanistic computational model of adrenal steroidogenesis in H295R cells to predict the synthesis of steroids from cholesterol (CHOL) and their biochemical response to EACs. We previously developed a deterministic model that describes the biosynthetic pathways for the conversion of CHOL to steroids and the kinetics for enzyme inhibition by the EAC, metyrapone (MET). In this study, we extended our dynamic model by (1) including a cell proliferation model supported by additional experiments and (2) adding a pathway for the biosynthesis of oxysterols (OXY), which are endogenous products of CHOL not linked to steroidogenesis. The cell proliferation model predictions closely matched the time-course measurements of the number of viable H295R cells. The extended steroidogenesis model estimates closely correspond to the measured time-course concentrations of CHOL and 14 adrenal steroids both in the cells and in the medium and the calculated time-course concentrations of OXY from control and MET-exposed cells. Our study demonstrates the improvement of the extended, more biologically realistic model to predict CHOL and steroid concentrations in H295R cells and medium and their dynamic biochemical response to the EAC, MET. This mechanistic modeling capability could help define mechanisms of action for poorly characterized chemicals for predictive risk assessments.

**Key Words:** endocrine disrupting chemicals; mechanistic computational model; *in vitro* toxicology; metyrapone; H295R cells; steroid biosynthesis.

endocrine disrupting properties of chemicals in drinking water and pesticides. This legislation addresses the concern that various environmental chemical contaminants may alter the endocrine system of humans and wildlife with subsequent adverse outcomes and disease. Based on this legislation, an endocrine disruptor screening program (EDSP) was developed by the U.S. Environmental Protection Agency (U.S. EPA, 1998). The EDSP is designed as a two-tiered screening and testing process to identify chemicals that can interact with the endocrine system (Tier 1) and to characterize their dose-response (Tier 2). In the EDSP Tier 1 battery of screening assays (U.S. EPA, 2009), the human adrenocortical carcinoma cell line H295R was selected as an *in vitro* steroidogenesis assay to detect chemicals that affect steroid biosynthesis.

As a screening tool, the *in vitro* H295R steroidogenesis assay has several strengths. This assay can be used to evaluate the effects across the entire steroidogenesis pathway because H295R cells express all the key enzymes for steroidogenesis and have the ability to produce all the adrenocortical steroids as well as sex steroids (Gazdar *et al.*, 1990; Rainey *et al.*, 1994; Staels *et al.*, 1993). The screen is rapid and inexpensive and can detect chemicals that either inhibit or induce steroidogenesis (U.S. EPA, 2009). Furthermore, this assay coupled with a mechanistic computational model supports the recommendations by the National Research Council (NRC) report regarding a vision and strategy for toxicology testing in the 21st century (NRC, 2007). The NRC report recommends the use of *in vitro* systems to assess mechanisms of action for a large number of chemicals while reducing the number of animals and testing cost for *in vivo* assays (Andersen and Krewski, 2010).

To increase the understanding and quantitative use of data from the *in vitro* H295R steroidogenesis assay for human

The Safe Drinking Water Act Amendments (1996) and the Food Quality Protection Act (1996) require screening for

and ecological risk assessments, we are developing a mechanistic computational model of steroidogenesis in H295R cells. We previously developed a deterministic model that describes the biosynthetic pathways for conversion of cholesterol (CHOL) to adrenocortical steroids and the kinetics for enzyme inhibition by the competitive steroidogenic enzyme inhibitor, metyrapone (MET), a model endocrine active chemical (EAC) with a well-characterized mechanism of action (Breen *et al.*, 2010). Metyrapone is used as a clinical diagnostic test for pituitary adrenocorticotrophic dysfunction. In the present paper, we extended the model and performed additional critical experiments to address key limitations of the previously described model.

The primary focus of the previous work was on steroid synthesis (Breen *et al.*, 2010). The main limitation of the previous steroidogenesis model was the large underestimation and overestimation of CHOL concentrations in cells and medium, respectively. In the present paper, we addressed this limitation by investigating CHOL utilization. Because CHOL metabolism is responsible for the biosynthesis of steroids and oxysterols (OXY) (Bjorkhem, 2002; Javitt, 2008; Nishimura *et al.*, 2005; Schroeffer, 2000), we extended the previous model by adding the pathway for OXY biosynthesis. We examined the hypothesis that metabolism of CHOL into OXY may reduce the large discrepancy between measured and model-predicted concentrations of CHOL in cells and medium.

The OXY, similar to steroid hormones, are endogenous products of CHOL. The OXY are formed in many tissues, including adrenal tissue, through CHOL oxygenation reactions mediated by different cytochrome P450 enzymes or reactive oxygen species (Adams *et al.*, 2004; Bjorkhem, 2002; Schroeffer, 2000). The OXY possess potent regulatory functions in a broad range of biological mechanisms, including CHOL homeostasis, apoptosis, calcium uptake, and cell differentiation (Bjorkhem, 2002; Javitt, 2008; Nishimura *et al.*, 2005; Schroeffer, 2000).

Another key limitation of the previous steroidogenesis model is the potential confounding effects of cell proliferation and viability on the time-course concentrations of the steroids. Because the proliferation of H295R cells can be substantial (Logie *et al.*, 1999), we addressed this limitation by performing additional experiments and developing a cell proliferation model. Cell proliferation and viability experiments for control and EAC-exposed H295R cells were performed, and the data were used for parameter estimation and model evaluation. The cell proliferation model was then linked with the steroidogenesis model to control for this confounding.

The contribution of this study is the extension of a previously developed steroidogenesis model (Breen *et al.*, 2010) by including (1) a pathway for OXY biosynthesis and (2) cell proliferation model. The extended model was evaluated with measurements of CHOL and 14 steroids in H295R cells and medium, measurements from an H295R cell proliferation and

viability assay, and OXY concentrations determined from a molecular balance formulation.

## MATERIALS AND METHODS

We first describe the H295R cell proliferation and steroidogenesis experiments and the calculation of OXY concentrations. Then, we present the mathematical models for cell proliferation, pathways for OXY and steroid biosynthesis, and procedures for parameter estimation and sensitivity analysis.

**H295R cell proliferation assay.** We performed a cell proliferation study following the experimental method as the previously described H295R steroidogenesis assay for control and two concentrations of MET (1 and 10  $\mu$ M) (Breen *et al.*, 2010). The MET concentrations were selected based on cytotoxicity and clinical data. Using a cell viability assay, no significant cytotoxicity was observed at these two concentrations after treatment for 3 days. Clinical observations show mean plasma peak concentrations of 2.2 and 16.3  $\mu$ M at 4 and 1 h following administration of 750 mg MET, respectively (www.pharma.us.novartis.com).

For the cell proliferation assay,  $6 \times 10^5$  cells were initially incubated for 72 h (prestimuli incubation period). At poststimuli incubation periods of 0, 24, 48, and 72 h, all cells were separated and removed from six replicate wells. The number and percentage of viable cells in each well were then determined using a cell analyzer (Vi-CELL XR; Beckman Coulter, Fullerton, CA).

For statistical analysis of the cell viability data, two-way ANOVA test was used to determine differences between the mean numbers of viable cells across treatments (MET doses), using sampling times as a blocking factor to control variability due to differences across sampling time. Differences were considered significant at  $p \leq 0.05$ .

**Steroidogenesis assay with H295R cells.** We performed *in vitro* experimental studies with H295R cells: a control study with samples collected at five time points (0, 8, 24, 48, and 72 h) and a MET study with two MET concentrations (1 and 10  $\mu$ M) with samples analyzed at four time points (8, 24, 48, and 72 h). The start time of the experiments was after changing the medium, adding stimuli for activation of steroidogenesis, and including the concentrations of MET. The details were previously described (Breen *et al.*, 2010). Briefly, the medium and cells were separately removed from four replicate wells at each time point. The cells were sonicated in 100  $\mu$ l of distilled water to produce a cell lysate, which included all the cellular membranes. The CHOL concentrations in the medium and cell lysate were measured using a commercial kit (Wako Pure Chemical Industries, Ltd, Osaka, Japan) based on a CHOL oxidase method. Steroid concentrations in the medium and cell lysate were measured using liquid chromatography/mass spectrometry for 12 steroids (pregnenolone [PREG], 17 $\alpha$ -hydroxy-pregnenolone [HPREG], dehydroepiandrosterone [DHEA], progesterone [PROG], 17 $\alpha$ -hydroxy-progesterone [HPROG], androstenedione [DIONE], testosterone [T], deoxycorticosterone [DCORTICO], corticosterone [CORTICO], aldosterone [ALDO], 11-deoxycortisol [DCORT], and cortisol [CORT]) and ELISA for two additional steroids (estrone [E1] and 17 $\beta$ -estradiol [E2]). The steroid concentrations were adjusted for the recovery of each steroid, with a recovery range between 81.7 and 94.1%. The quantitative ranges for CHOL and each steroid in cells and medium are provided in Supplementary Table S1.

**Oxysterols calculated from measurements of cholesterol and steroids.** Because no OXY measurements are available, all OXY molecules were lumped together, and the OXY concentrations were calculated based on a molecular balance formulation. To determine OXY concentrations, we made four assumptions. First, we assumed no degradation of CHOL, OXY, and steroids. This assumption is supported by other studies reporting little or no degradation of various steroids across 72 h, our experimental duration (Evans *et al.*, 2001; Garde and Hansen, 2005; Wickings and Nieschlag, 1976). Second, we assumed no *de novo* synthesis of CHOL because CHOL is abundant in our experiments and is unlikely to be synthesized. Third, because OXY data are unavailable, we

assumed no OXY transport between cells and medium. Fourth, we assumed that the sum of number of CHOL, OXY, and steroid molecules is conserved across time. We determined OXY concentrations from the molecular balance equation, which equates the quantity of molecules (i.e., CHOL, OXY, and steroids) at the initial time to those at later times, as described by

$$\begin{aligned} V_{\text{cell}}^i \left( C_{\text{CHOL,cell}}^{d,i} + C_{\text{OXY,cell}}^{d,i} + \sum_{x=1}^{14} C_{x,\text{cell}}^{d,i} \right) + V_{\text{med}} \left( C_{\text{CHOL,med}}^{d,i} + \sum_{x=1}^{14} C_{x,\text{med}}^{d,i} \right) \\ = V_{\text{cell}}^{i-1} \left( C_{\text{CHOL,cell}}^{d,i-1} + C_{\text{OXY,cell}}^{d,i-1} + \sum_{x=1}^{14} C_{x,\text{cell}}^{d,i-1} \right) \\ + V_{\text{med}} \left( C_{\text{CHOL,med}}^{d,i-1} + \sum_{x=1}^{14} C_{x,\text{med}}^{d,i-1} \right), \end{aligned} \quad (1)$$

where  $C_{\text{CHOL,cell}}^{d,i}$  and  $C_{\text{CHOL,med}}^{d,i}$  are the measured concentrations of CHOL in cells and medium at the  $i$ th time and  $d$ th MET dose (including control) for  $d = 1, 2, 3$  (0, 1, 10  $\mu\text{M}$ ) and  $i = 1, \dots, 5$  (0, 8, 24, 48, 72 h), respectively;  $C_{x,\text{cell}}^{d,i}$  and  $C_{x,\text{med}}^{d,i}$  are the measured concentrations of steroid  $x$  in cells and medium at the  $i$ th time and  $d$ th MET dose, respectively;  $C_{\text{OXY,cell}}^{d,i}$  are the calculated concentrations of OXY in cells at the  $i$ th time and  $d$ th MET dose;  $V_{\text{cell}}^i$  is the volume of cells at the  $i$ th time, as predicted by the cell proliferation model described below; and  $V_{\text{med}}$  is the volume of medium. To solve Equation (1) for  $C_{\text{OXY,cell}}^{d,i}$ , the initial OXY concentrations in cells are assumed to be zero:  $C_{\text{OXY,cell}}^{d,i=1} = 0$ . We calculated OXY for one experiment because medium concentrations of E1 and E2 at time equals zero were below blank sample concentrations in replicate experiments. We obtained the equation for  $C_{\text{OXY,cell}}^{d,i}$  as

$$\begin{aligned} C_{\text{OXY,cell}}^{d,i} = \left( C_{\text{CHOL,cell}}^{d,i-1} - C_{\text{CHOL,cell}}^{d,i} + \sum_{x=1}^{14} C_{x,\text{cell}}^{d,i-1} - \sum_{x=1}^{14} C_{x,\text{cell}}^{d,i} \right) \\ + \frac{V_{\text{med}}}{V_{\text{cell}}^i} \left( C_{\text{CHOL,med}}^{d,i-1} - C_{\text{CHOL,med}}^{d,i} + \sum_{x=1}^{14} C_{x,\text{med}}^{d,i-1} - \sum_{x=1}^{14} C_{x,\text{med}}^{d,i} \right). \end{aligned} \quad (2)$$

**Mathematical model of cell proliferation.** To predict the number of viable H295R cells per well across time,  $N_{\text{cell}}(t)$ , we developed a cell proliferation model. We assumed an exponential cell population growth as described by

$$N_{\text{cell}}(t) = N_{\text{cell}}(-72) e^{k_p(t+72)}, \quad (3)$$

where  $N_{\text{cell}}(-72)$  is the initial number of viable cells and  $k_p$  is the proliferation rate. The least squares method was used to estimate  $k_p$  with time-course data from the control experiments. By taking logs of Equation (3), we obtained a least squares estimate for  $k_p$  as

$$k_p^* = [\mathbf{T}' \mathbf{T}]^{-1} \mathbf{T}' \mathbf{X}, \quad (4)$$

where  $k_p^*$  is the least squares estimate of  $k_p$ ,  $\mathbf{X}$  is a 25-element vector, and  $\mathbf{T}' = [0 \ 72 \ 96 \ 120 \ 144 \ \dots \ 72 \ 96 \ 120 \ 144]$ . The vector  $\mathbf{X}$  is defined as

$$\begin{aligned} \mathbf{X} = \left[ 0 \ \ln \left( \frac{N_{\text{cell}}(t=0, r=1)}{N_{\text{cell}}(-72)} \right) \ \ln \left( \frac{N_{\text{cell}}(t=24, r=1)}{N_{\text{cell}}(-72)} \right) \right. \\ \left. \ln \left( \frac{N_{\text{cell}}(t=48, r=1)}{N_{\text{cell}}(-72)} \right) \ \ln \left( \frac{N_{\text{cell}}(t=72, r=1)}{N_{\text{cell}}(-72)} \right) \ \dots \right. \\ \left. \ln \left( \frac{N_{\text{cell}}(t=72, r=6)}{N_{\text{cell}}(-72)} \right) \right], \end{aligned} \quad (5)$$

for  $t = 0, 24, 48, 72$ , and  $r = 1, 2, \dots, 6$ , where  $N_{\text{cell}}(t, r)$  is the measured number of viable cells at time  $t$  and replicate  $r$ . Negative time denotes time before stimuli added to initiate steroid biosynthesis (prestimuli). Positive time denotes incubation time with stimuli (poststimuli).

The cell proliferation model was used to estimate the volume of viable cells. From Equation (3), we determined the volume of viable cells per well across time,  $V_{\text{cell}}(t)$ , as

$$V_{\text{cell}}(t) = V_{\text{cell}}(-72) e^{k_p(t+72)}, \quad (6)$$

where  $V_{\text{cell}}(-72)$  is the initial volume of viable cells per well. The  $V_{\text{cell}}(-72)$  is obtained by multiplying  $N_{\text{cell}}(-72)$  by the overall mean volume of an individual H295R cell from control and the two MET concentrations (1 and 10  $\mu\text{M}$ ), which was previously determined to be 1499  $\mu\text{m}^3$  (Breen *et al.*, 2010). The overall mean volume was used since the mean volumes changed only slightly between controls and the two MET concentrations.

The  $V_{\text{cell}}(t)$  was used to compensate for steroid dilution in the cell lysate. We determined the concentration of steroid  $x$  in cells,  $C_{\text{cell},x}(t)$ , by

$$C_{\text{cell},x}(t) = C_{\text{lysate},x}(t) \left( \frac{V_{\text{lysate}}(t)}{V_{\text{cell}}(t)} \right), \quad (7)$$

where  $C_{\text{lysate},x}(t)$  is the measured concentration of steroid  $x$  in the cell lysate at time  $t$  and is the volume of cell lysate at time  $t$ . The  $V_{\text{lysate}}(t)$  is the sum of  $V_{\text{cell}}(t)$  and the volume of distilled water. This  $V_{\text{cell}}(t)$  was also used in the dynamic molecular balance equations to determine the time-course concentrations of CHOL, OXY, and the 14 steroids.

**Overview of mathematical model for metabolic and transport pathways.** The computational model is based on the experimental design with two compartments: culture medium and H295R cells (Fig. 1). The model includes two distinct metabolic pathways originating from CHOL: OXY biosynthesis and steroid biosynthesis. The OXY biosynthesis pathway includes conversion of CHOL into OXY. The steroid biosynthesis pathway includes the conversion of CHOL into 14 steroids (PREG, HPREG, DHEA, PROG, HPROG, DIONE, T, DCORTICO, CORTICO, ALDO, DCORT, CORT, E1, and E2) and the inhibition of the steroidogenic enzymes by MET.

The transport pathways for the model include cellular uptake of CHOL and MET and import and secretion of the steroids. The transport of OXY between the cells and medium is not included in the model because no data are available. The details and supporting literature data for the biological pathways of steroid biosynthesis and transport were previously described (Breen *et al.*, 2010). Below, we first describe the details of the metabolic and transport pathways. Then, the dynamic molecular balance equations, which couple the metabolic and transport pathways, are described. The complete set of equations is provided in the Supplementary data.

**Metabolic pathways.** In the extended model, the conversion of CHOL into OXY is described by a first-order rate equation (Fig. 1B). The metabolic pathway that converts CHOL into the 14 steroids consists of 17 enzymatic reactions catalyzed by nine different proteins (Fig. 1A) (Payne and Hales, 2004). As described in the previous model (Breen *et al.*, 2010), we assumed that the substrate concentration is much less than the Michaelis constant (substrate concentration that yields a half-maximal reaction rate). Thus, the rate of product formation increases linearly with substrate concentration as described by a first-order rate equation (Fig. 1B).

Various EACs can inhibit the enzymes in the steroidogenesis metabolic pathway. In this study, we examined the response of H295R cells exposed to the EAC, MET, which is a competitive inhibitor of cytochrome P450 11 $\beta$ -hydroxylase (CYP11B1) (Harvey and Everett, 2003; Harvey *et al.*, 2007). For the two CYP11B1 enzymatic reactions competitively inhibited by MET: conversion of DCORTICO to CORTICO and conversion of DCORT to CORT (Fig. 1A), the kinetic parameters  $k_{16}$  and  $k_{17}$  are divided by  $\alpha_{\text{CORTICO}}(t) = 1 + (C_{\text{MET,cell}}(t)/k_{41})$  and  $\alpha_{\text{CORT}}(t) = 1 + (C_{\text{MET,cell}}(t)/k_{42})$ , respectively, where  $k_{41}$  and  $k_{42}$  are MET inhibition constants (Fig. 1B).

**Transport pathways.** The model used for the transport of CHOL and the steroids between cells and medium was previously described (Breen *et al.*, 2010). Briefly, we model the transport rate of CHOL from the medium as a first-order process (Fig. 1B). We model the secretion and uptake rates for each steroid as reversible first-order processes ( $k_{+x}$  and  $k_{-x}$  for secretion and uptake of steroid  $x$ , respectively) (Supplementary Fig. S1).

**FIG. 1.** (A) Graphical representation of the two compartment model (culture medium and cells) for biosynthesis of OXY and steroids in H295R cells, and enzyme inhibition by MET. Cell uptake of CHOL from medium is depicted by the broad gray arrow labeled with the steroidogenic acute regulatory protein (StAR). Irreversible metabolic reaction for biosynthesis of OXY from CHOL is depicted by white arrow labeled with OXY enzymes (OE). Irreversible metabolic reactions for biosynthesis of 14 steroids (PREG, HPREG, DHEA, PROG, HPROG, DIONE, T, E1, E2, DCORTICO, CORTICO, ALDO, DCORT, and CORT) from CHOL are depicted by arrows, with each pattern representing a unique enzyme. Enzymes labeled next to metabolic reactions they catalyze are: CYP450 side-chain-cleavage (CYP11A), CYP450c17 $\alpha$ -hydroxylase (CYP17H), CYP450c17,20-lyase (CYP17L), 3 $\beta$ -hydroxydehydrogenase type 2 (3 $\beta$ HSD2), 17 $\beta$ -hydroxydehydrogenase type 1 (17 $\beta$ HSD1), CYP450 aromatase (CYP19), CYP450 21 $\alpha$ -hydroxylase (CYP21A), CYP450 11 $\beta$ -hydroxylase type 1 (CYP11B1), and aldosterone synthase (CYP11B2). Bidirectional thin gray arrows depict reversible steroid transport between medium and cells. The EAC, MET, is shown as enzyme inhibitor of CYP11B1. (B) Graphical representation of model parameters, which consists of first-order rate constants for CHOL uptake into cells,  $k_1$ , and for each metabolic process,  $k_0$ ,  $k_2$ – $k_{18}$ . For quasi-equilibrium analysis, equilibrium constants are  $q_{19}$ – $q_{32}$ . Partition coefficient for MET is  $q_{40}$ . Enzyme inhibition constants for MET are  $k_{41}$  and  $k_{42}$  for CORTICO and CORT pathways, respectively.

As described in the previous model (Breen *et al.*, 2010), we assume no degradation of MET, and MET diffuses into the cells and reaches equilibrium with the MET concentration in the medium

$$C_{\text{MET,cell}}(t) = q_{40} C_{\text{MET,med}}(t), \quad (8)$$

where  $q_{40}$  is the equilibrium coefficient, and  $C_{\text{MET,cell}}(t)$  and  $C_{\text{MET,med}}(t)$  are the

cell and medium MET concentrations at time  $t$ , respectively (Fig. 1B). To calculate  $C_{\text{MET,cell}}(t)$ , we need to account for the  $V_{\text{cell}}(t)$  and  $V_{\text{med}}$ . We obtained the equation for  $C_{\text{MET,cell}}(t)$  by solving the molecular balance equation

$$V_{\text{cell}}(t)C_{\text{MET,cell}}(t) + V_{\text{med}}C_{\text{MET,med}}(t) = V_{\text{cell}}(t)C_{\text{MET,cell}}(0) + V_{\text{med}}C_{\text{MET,med}}(0), \quad (9)$$

for  $C_{\text{MET,med}}(t)$  and substituted into Equation (8) with  $C_{\text{MET,cell}}(0) = 0$  to yield

$$C_{\text{MET,cell}}(t) = \left( \frac{q_{40}}{1 + q_{40} V_{\text{cell}}(t)/V_{\text{med}}} \right) C_{\text{MET,med}}(0). \quad (10)$$

**Dynamic molecular balances.** The time-course of the steroids, CHOL, and OXY are described by dynamic molecular balance equations (Supplementary data). The general dynamic molecular balance equations for the steroids in cells and medium are

$$\frac{d(V_{\text{cell}}(t)C_{x,\text{cell}}(t))}{dt} = P_{x,\text{cell}}(t) - U_{x,\text{cell}}(t) + I_{x,\text{cell}}(t) - S_{x,\text{cell}}(t), \quad (11)$$

and

$$V_{\text{med}} \frac{dC_{x,\text{med}}(t)}{dt} = S_{x,\text{cell}}(t) - I_{x,\text{cell}}(t), \quad (12)$$

where  $C_{x,med}(t)$  is the concentration of steroid  $x$  in medium at time  $t$ ;  $P_{x,cell}(t)$  and  $U_{x,cell}(t)$  are the production and utilization rates of steroid  $x$  in cells at time  $t$ , respectively;  $I_{x,cell}(t)$  and  $S_{x,cell}(t)$  are the cell import and secretion rates of steroid  $x$  at time  $t$ , respectively. The first two terms on the right side of Equation (11) represent the net metabolic reaction rate of steroid  $x$  and the last two terms represent the net cellular uptake or release rate of steroid  $x$ . The time-courses of CHOL and OXY are calculated in the same manner as the time-courses of the steroids.

**Quasi-equilibrium analysis.** Based on the evidence that steroid transport between the cells and medium is rapid and reversible, as described in the previous model (Breen *et al.*, 2010), we assume the steroid concentrations in the cells and medium are operating near equilibrium. Because the steroids are involved in the larger network consisting of the metabolic pathway of steroidogenesis, this is considered as quasi-equilibrium.

For quasi-equilibrium, the reversible transport rates ( $k_{+x}$  and  $k_{-x}$  for secretion and import of steroid  $x$ , respectively) are assumed to be much greater than the metabolic reaction rates. The concentration of steroid  $x$  in the cells and medium rapidly reaches equilibrium to yield

$$\frac{C_{x,\text{med}}(t)}{C_{x,\text{cell}}(t)} = \frac{k_{+x}}{k_{-x}} = q_x, \quad (13)$$

where  $q_x$  is the equilibrium constant of steroid  $x$  transport. By solving Equation (13) for  $C_{x,\text{med}}(t)$ , we obtain an algebraic equation for each steroid in the medium as

$$C_{x,\text{med}}(t) = q_x C_{x,\text{cell}}(t). \quad (14)$$

To determine the dynamic molecular balance equations for the steroids in cells for quasi-equilibrium, we sum the molecules of steroid  $x$  in the cells and medium based on Equations (11 and 12) and substitute Equation (14) for  $C_{x,med}(t)$  to yield

$$\begin{aligned} \frac{d(V_{\text{cell}}(t)C_{x,\text{cell}}(t) + V_{\text{med}}C_{x,\text{med}}(t))}{dt} &= \frac{d[(V_{\text{cell}}(t) + V_{\text{med}}q_x)C_{x,\text{cell}}(t)]}{dt} \\ &= P_{x,\text{cell}}(t) - U_{x,\text{cell}}(t). \end{aligned} \quad (15)$$

We obtain a system of equations consisting of a differential equation for each steroid in the cells from Equation (15) as

$$\frac{dC_{x,\text{cell}}(t)}{dt} = \frac{1}{V_{\text{cell}}(t) + V_{\text{med}}q_x} \left( P_{x,\text{cell}}(t) - U_{x,\text{cell}}(t) - C_{x,\text{cell}}(t) \frac{dV_{\text{cell}}(t)}{dt} \right), \quad (16)$$

where

$$\frac{dV_{\text{cell}}(t)}{dt} = k_p V_{\text{cell}}(-72) e^{k_p(t+72)} = k_p V_{\text{cell}}(t). \quad (17)$$

Equation (17) was obtained by differentiating Equation (6) with respect to time. The quasi-equilibrium assumption reduces the number of the model parameters to 36 parameters: 14 transport equilibrium constants ( $q_{19}, q_{20}, \dots, q_{32}$ ), 18 metabolic rate constants ( $k_0, k_2, k_3, \dots, k_{18}$ ), CHOL import rate ( $k_1$ ), 2 enzyme inhibition constants for MET ( $k_{41}$  and  $k_{42}$ ), and the partition coefficient for MET ( $q_{40}$ ). These dynamic molecular balance equations for quasi-equilibrium and the 36 parameters are used in all subsequent analysis (Supplementary data).

**Parameter estimation.** The parameters for the transport and metabolic pathways were independently estimated using the mean concentrations from replicate experiments. For the transport pathway, the equilibrium constants ( $q_{19}, q_{20}, \dots, q_{32}$ ) were estimated with the time-course data from the control and MET studies using the least squares method. From Equation (14), we obtained a least squares estimate for  $q_x$  as

$$q_x^* = [\underline{C}_{x,\text{cell}}' \quad \underline{C}_{x,\text{cell}}']^{-1} \underline{C}_{x,\text{cell}}' \underline{C}_{x,\text{med}}, \quad (18)$$

where  $q_x^*$  is the least squares estimate of the equilibrium constant for steroid  $x$  transport, and  $\underline{C}_{x,\text{cell}}' = [C_{x,\text{cell}}^{d=1,i=1} \quad C_{x,\text{cell}}^{d=1,i=2} \quad \dots \quad C_{x,\text{cell}}^{d=3,i=5}]$  and  $\underline{C}_{x,\text{med}}' = [C_{x,\text{med}}^{d=1,i=1} \quad C_{x,\text{med}}^{d=1,i=2} \quad \dots \quad C_{x,\text{med}}^{d=3,i=5}]$  are the measured concentrations in the cells and medium at the  $i$ th time and  $d$ th MET dose (including control), respectively.

For the metabolic pathway, the parameters ( $k_0, k_1, k_2, \dots, k_{18}, k_{41}, k_{42}$ ) were estimated with the time-course data from the control and MET studies. The weighted least squares method was used to estimate these parameters instead of the least squares method to account for CHOL and all the steroids concentrations that vary by several orders of magnitude. Let  $C_{\text{CHOL},\text{cell}}^d(t_i; \underline{k})$  and  $C_{\text{OXY},\text{cell}}^d(t_i; \underline{k})$  be the model-predicted concentrations of CHOL and OXY in the cells at the  $i$ th time,  $t_i$ , for the  $d$ th MET dose (including control),  $\underline{k}$  with parameter set  $\underline{k} = (k_0, k_1, k_2, \dots, k_{18}, k_{41}, k_{42})$  for  $d = 1, \dots, 3$ , and  $i = 1, \dots, 5$ , respectively;  $C_{x,\text{cell}}^d(t_i; \underline{k})$  be the model-predicted concentrations of steroid  $x$  in the cells at time  $t_i$  for the MET dose,  $\underline{k}$  with parameter set  $\underline{k}$ ;  $\bar{C}_{\text{CHOL},\text{cell}}^d$  and  $\bar{C}_{\text{OXY},\text{cell}}^d$  be the mean measured concentration of CHOL and calculated concentration of OXY in the cells across time, respectively;  $\bar{C}_{x,\text{cell}}^d$  be the mean measured concentration of steroid  $x$  in the cells across time. Then, the weighted least squares estimate,  $\underline{k}^* = (k_0^*, k_1^*, k_2^*, \dots, k_{18}^*, k_{41}^*, k_{42}^*)$ , is the parameter values  $\underline{k}$ , which minimizes the cost function

$$J(\underline{k}) = \sum_{d=1}^3 \frac{1}{\bar{C}_{\text{CHOL},\text{cell}}^d} \sum_{i=1}^5 \left( C_{\text{CHOL},\text{cell}}^d(t_i; \underline{k}) - C_{\text{CHOL},\text{cell}}^d(t_i; \bar{C}_{\text{CHOL},\text{cell}}^d) \right)^2 + \sum_{d=1}^3 \frac{1}{\bar{C}_{\text{OXY},\text{cell}}^d} \sum_{i=1}^5 \left( C_{\text{OXY},\text{cell}}^d(t_i; \underline{k}) - C_{\text{OXY},\text{cell}}^d(t_i; \bar{C}_{\text{OXY},\text{cell}}^d) \right)^2 + \sum_{x=1}^{14} \sum_{d=1}^3 \frac{1}{\bar{C}_{x,\text{cell}}^d} \sum_{i=1}^5 \left( C_{x,\text{cell}}^d(t_i; \underline{k}) - C_{x,\text{cell}}^d(t_i; \bar{C}_{x,\text{cell}}^d) \right)^2. \quad (19)$$

Parameters for the metabolic pathway were estimated with a nonlinear optimization algorithm using MATLAB R2010a (Mathworks, Natick, MA) software. The Nelder-Mead simplex method was used due to its relative insensitivity to the initial parameter values as compared with other common methods, such as Newton's method and its robustness to discontinuities (Nelder and Mead, 1965).

**Sensitivity analysis.** We performed a sensitivity analysis to examine parameter uncertainty using the method previously described (Breen *et al.*,

2010). Briefly, the sensitivity function relates changes of the model output to changes in the model parameters. We calculated relative sensitivity functions  $R_{x,\text{med},k_i}(t)$  and  $R_{x,\text{med},q_i}(t)$  with respect to parameters  $k_i$  and  $q_i$ , respectively, for each of the model-predicted concentrations in the medium,  $C_{x,\text{med}}$ , and each MET dose (including control). MATLAB was used to numerically solve the partial derivatives in  $R_{x,\text{med},k_i}(t)$  and  $R_{x,\text{med},q_i}(t)$ . To rank the relative sensitivities, we calculated the L2 norm across time for each relative sensitivity function as described by

$$\text{L2 norm}(R_{x,\text{med},k_i}) = \sqrt{\int |R_{x,\text{med},k_i}(t)|^2 dt} \quad (20)$$

and

$$\text{L2 norm}(R_{x,\text{med},q_i}) = \sqrt{\int |R_{x,\text{med},q_i}(t)|^2 dt}. \quad (21)$$

## RESULTS

### Cell Proliferation—Estimated Parameter and Model Evaluation

The time-course measurements for the number of viable cells per well (Supplementary Fig. S2A) and percentage of viable cells per well (Supplementary Fig. S2B) are shown for each MET dose. The percentage of viable cells per well across all measurements was  $91.8 \pm 2.3\%$  (mean  $\pm$  SD). The mean number of viable cells measured across MET doses (control, 1, and 10  $\mu\text{M}$ ) was not statistically different ( $p = 0.41$ ). Therefore, control data were used to estimate the value of  $k_p$ , which was determined to be 0.00878/h. The model-predicted number of viable cells was compared with time-course measurements from the control experiments (Fig. 2). The model predictions closely correspond to the mean time-course data.

### Calculated Oxysterols

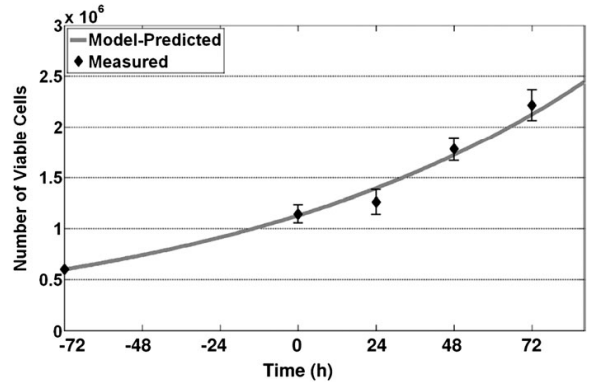


**FIG. 2.** Time-course of measured and model-predicted number of viable cells. Measurements were plotted at 72 h prestimuli and four poststimuli incubation periods of 0, 24, 48, and 72 h (mean  $\pm$  SD) for control experiments. Negative time denotes time before stimuli added to initiate steroid biosynthesis (prestimuli). Positive time denotes incubation time with stimuli (poststimuli).

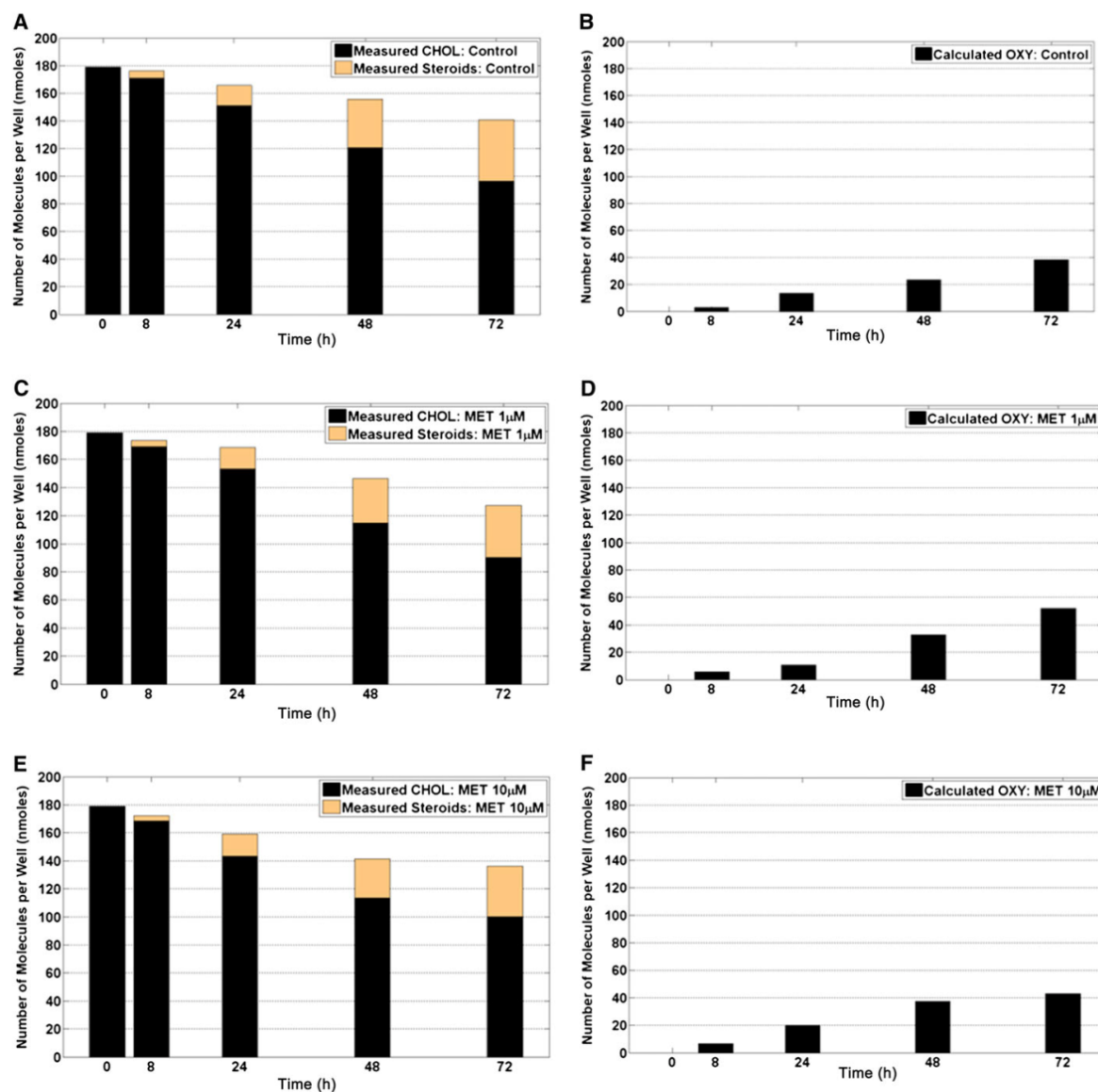


**FIG. 3.** Left column shows time-course of total (sum in cells and medium) number of measured CHOL and steroid molecules in control (A), 1 μM (C), and 10 μM (E) MET-exposed cells. Right column shows time-course for number of calculated OXY molecules for control (B), 1 μM (D), and 10 μM (F) MET-exposed cells. To calculate OXY concentrations, measured concentrations of CHOL and each steroid are needed. Because medium concentrations of two steroids (E1 and E2) at time  $t = 0$  were considered valid (i.e., above blank sample concentrations) only in one experiment, the single experiment was used to calculate OXY concentrations.

Figure 3 shows the time-course for the sum of measured number of CHOL and steroid molecules and the calculated number of OXY molecules at each MET dose (control, 1, and 10 μM). For each MET dose, the calculated number of OXY molecules monotonically increased across time. The number of OXY molecules showed no apparent pattern with increasing MET dose (Supplementary Fig. S3).

#### Transport Pathways for Steroids

Table 1 shows the estimated transport equilibrium parameters. As described in the previous model (Breen *et al.*, 2010), the MET transport equilibrium,  $q_{40}$ , could not be determined from the data because MET was not measured in the cells. Therefore,  $q_{40}$  was set equal to  $q_{22}$ , the CORTICO transport equilibrium, because the partition coefficients for MET

TABLE 1  
Estimated Transport Equilibrium Parameters (dimensionless)  
from Model Fit of Steroids Corresponding to Given  $q$  Parameter

Parameter	Value
$q_{19}$	0.013
$q_{20}$	0.005
$q_{21}$	0.041
$q_{22}$	0.056
$q_{23}$	0.091
$q_{24}$	0.061
$q_{25}$	0.021
$q_{26}$	0.042
$q_{27}$	0.068
$q_{28}$	0.038
$q_{29}$	0.040
$q_{30}$	0.027
$q_{31}$	0.044
$q_{32}$	0.035
$q_{40}$	0.056 <sup>a</sup>

<sup>a</sup>Metyrapone transport equilibrium ( $q_{40}$ ) set to CORTICO transport equilibrium ( $q_{22}$ ); see text for details.

(XLogP = 2.0) and CORTICO (XLogP = 1.9) are similar (PubChem database).

#### Metabolic Pathways for OXY and Steroid Biosynthesis

Table 2 shows the estimated parameters for the metabolic pathways. The convergence time for the nonlinear parameter estimation was typically around 10 min on an Intel Core 2 Duo processor using MATLAB.

TABLE 2  
Estimated Parameters of Metabolic Pathway

Parameters	Value	Units
$k_0$	0.014	Per h
$k_1$	0.016	Per h
$k_2$	0.011	Per h
$k_3$	0.757	Per h
$k_4$	1.268	Per h
$k_5$	0.814	Per h
$k_6$	11.153	Per h
$k_7$	7.217	Per h
$k_8$	0.177	Per h
$k_9$	1.754	Per h
$k_{10}$	0.048	Per h
$k_{11}$	6.479	Per h
$k_{12}$	12.188	Per h
$k_{13}$	0.595	Per h
$k_{14}$	0.001	Per h
$k_{15}$	0.091	Per h
$k_{16}$	0.637	Per h
$k_{17}$	0.247	Per h
$k_{18}$	0.122	Per h
$k_{41}$	63.566	nM
$k_{42}$	25.208	nM

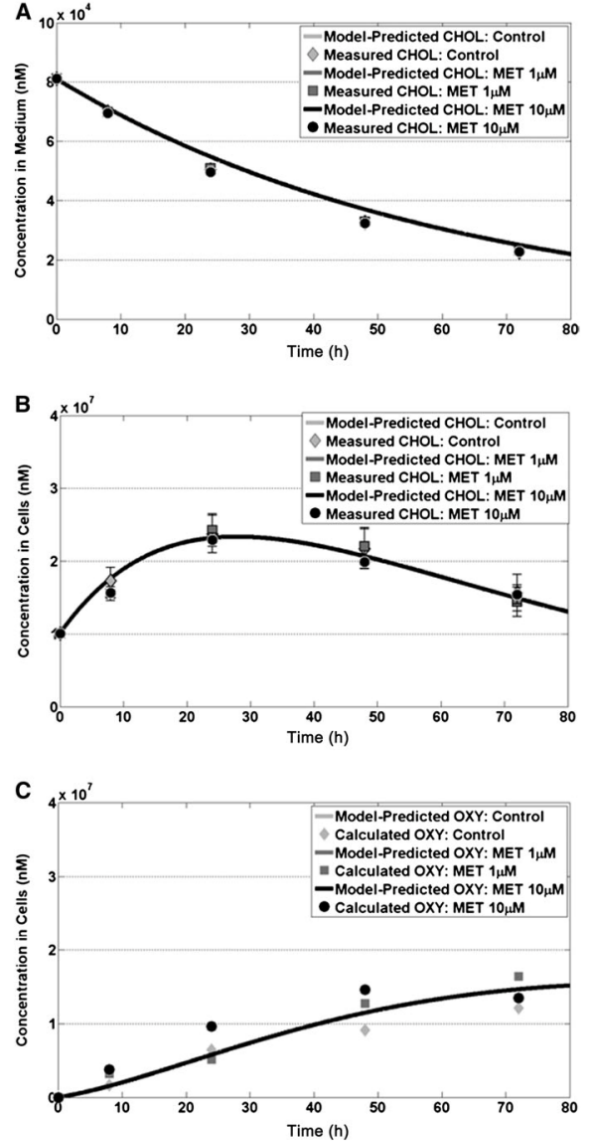


FIG. 4. Model evaluation of CHOL and OXY for control and MET-exposed cells. Time-course of model-predicted concentrations were plotted and compared with concentrations (mean  $\pm$  SD) measured at five sampling times for CHOL in medium (A), CHOL in cells (B), and calculated for OXY in cells (C). To calculate OXY concentrations, measured concentrations of CHOL and each steroid are needed. Because medium concentrations of two steroids (E1 and E2) at time  $t = 0$  were considered valid (i.e., above blank sample concentrations) only in one experiment, the single experiment was used to calculate OXY concentrations.

For CHOL and OXY, we compared model-predicted concentrations with time-course data from control and MET-exposed cells (Fig. 4). Model-predicted concentrations correspond well to the mean time-course data for CHOL both in the

cells and in the medium and OXY in cells. For MET-exposed cells, model-predicted and measured concentrations of CHOL and calculated concentrations of OXY remained approximately unchanged from controls as MET increased.

For CHOL in medium and cells, the extended model performed remarkably better than the previous model (Breen *et al.*, 2010). For CHOL in medium, the extended model overestimated the mean measurements by 9, 13, and 11% at 24, 48, and 72 h, respectively, whereas the previous model overestimated the mean measurements by 43, 96, and 153% at 24, 48, and 72 h, respectively. For CHOL in cells, the extended model overestimated the mean measurements by 2, 4, and 5% at 24, 48, and 72 h, respectively, whereas the previous model underestimated the mean measurements by 52, 53, and 47% at 24, 48, and 72 h, respectively.

For the 14 steroids, we compared model-predicted concentrations with time-course measurements from control and MET-exposed cells. Overall, model-predicted concentrations correspond closely to the mean time-course measurements in cells (Supplementary Fig. S4) and medium (Fig. 5) for control cells. As compared with the previous model (Breen *et al.*, 2010), the extended model better captured the mean time-course behavior for the five steroids (PROG, HPROG, DHEA, HPREG, and PREG), which increased until 48 h and then sharply decreased at 72 h (Figs. 5B, 5C, and 5E). For these five steroids, the extended model predictions increased until 40–50 h and then decreased (Figs. 5B, 5C, and 5E), whereas the previous model predictions monotonically increased across time (Breen *et al.*, 2010). For the other steroids in control cells, the extended model performed similar to the previous model. A detailed evaluation was reported previously (Breen *et al.*, 2010).

For MET-exposed cells, we compared model-predicted steroid concentrations with time-course measurements. For three steroids (ALDO, CORTICO, and CORT) downstream from the enzyme inhibited by MET (CYP11B1), the model-predicted concentrations correspond well to the mean time-course measurements both in the cells (Supplementary Fig. S5) and in the medium (Figs. 6A–C). For two steroids (DCORTICO and DCORT) immediately upstream from CYP11B1, the model-predicted concentrations correspond closely to the mean time-course data both in the cells (Supplementary Fig. S5) and in the medium (Figs. 6D and 6E), which remained approximately unchanged at 8, 24, and 48 h as MET increased and slightly increased at 72 h as MET increased. For the other nine steroids further upstream from CYP11B1, model-predicted and measured concentrations remained approximately unchanged from controls as MET increased (data not shown). For five steroids (ALDO, CORTICO, CORT, DCORTICO, and DCORT), the extended and previous models showed similar results for MET-exposed cells.

#### Sensitivity Analysis

Figures 7 and 8 show the relative sensitivities for the four primary steroids: ALDO, CORT, T, and E2. For ALDO,  $k_{18}$  was highly sensitive at each MET dose, and eight parameters were

moderately sensitive: parameters associated with transport pathways ( $k_1$ ,  $q_{21}$ , and  $q_{22}$ ), metabolic pathways ( $k_2$ ,  $k_5$ , and  $k_{16}$ ), and MET-mediated enzyme inhibition ( $q_{40}$  and  $k_{41}$ ). For CORT,  $q_{27}$  and  $k_{17}$  were highly sensitive, and two parameters associated with MET-mediated enzyme inhibition ( $q_{40}$  and  $k_{42}$ ) were moderately sensitive. For steroids T and E2, the parameters associated with MET ( $q_{40}$ ,  $k_{41}$ , and  $k_{42}$ ) were not sensitive, and the sensitivity of all parameters was unchanged with increasing MET dose. For T,  $k_{10}$  was highly sensitive, and six parameters were moderately sensitive: parameters associated with transport pathways ( $k_1$  and  $q_{29}$ ) and metabolic pathways ( $k_2$ ,  $k_3$ ,  $k_9$ , and  $k_{12}$ ). For E2, six parameters were moderately sensitive: parameters associated with transport pathways ( $q_{29}$ ,  $q_{30}$ , and  $q_{32}$ ) and metabolic pathways ( $k_2$ ,  $k_{13}$ , and  $k_{15}$ ). The E1 pathway appears to be the preferred pathway for E2 synthesis because E2 was sensitive to the E1 pathway ( $k_{13}$  and  $k_{15}$ ) and not sensitive to the T pathway ( $k_{10}$  and  $k_{14}$ ). This preferred pathway result is consistent with our previous study of ovarian steroidogenesis (Breen *et al.*, 2007). The sensitivity analysis orders the inputs by importance, identifying main contributors to the variation in the outcome of a model. Parameters with high sensitivity are more important and significant for the model output than parameters with low sensitivity.

## DISCUSSION

We extended a computational model of adrenal steroidogenesis to include (1) a cell proliferation model to account for time-varying number of viable cells and (2) a metabolic pathway for biosynthesis of OXY to examine the hypothesis that metabolism of CHOL into OXY improves the model fit for CHOL. Experiments were designed and performed to evaluate the cell proliferation model. The extended model and cell proliferation experiments addressed key limitations of the previous model (Breen *et al.*, 2010) by (1) removing the confounding effects of cell proliferation from the steroidogenesis model, (2) reducing the large discrepancy between the measured and model-predicted concentrations of CHOL both in the medium and in the cells, and (3) allowing the steroidogenesis model to more accurately capture the observed dynamic behavior. Furthermore, the model's predictive ability improved considerably with only a slight increase in the model complexity by adding one parameter for cell proliferation and one parameter for OXY biosynthesis.

#### Metabolic Pathway for Oxysterols

In the previous steroidogenesis model, we developed a steroidogenesis model and evaluated its ability to predict only the steroid concentrations for MET-exposed H295R cells (Breen *et al.*, 2010). The present study was initiated after we discovered that (1) the differences between the model-predicted and measured CHOL concentrations both in the medium and in the cells were large and (2) the sum of the number of measured CHOL and steroids molecules was not conserved across time.

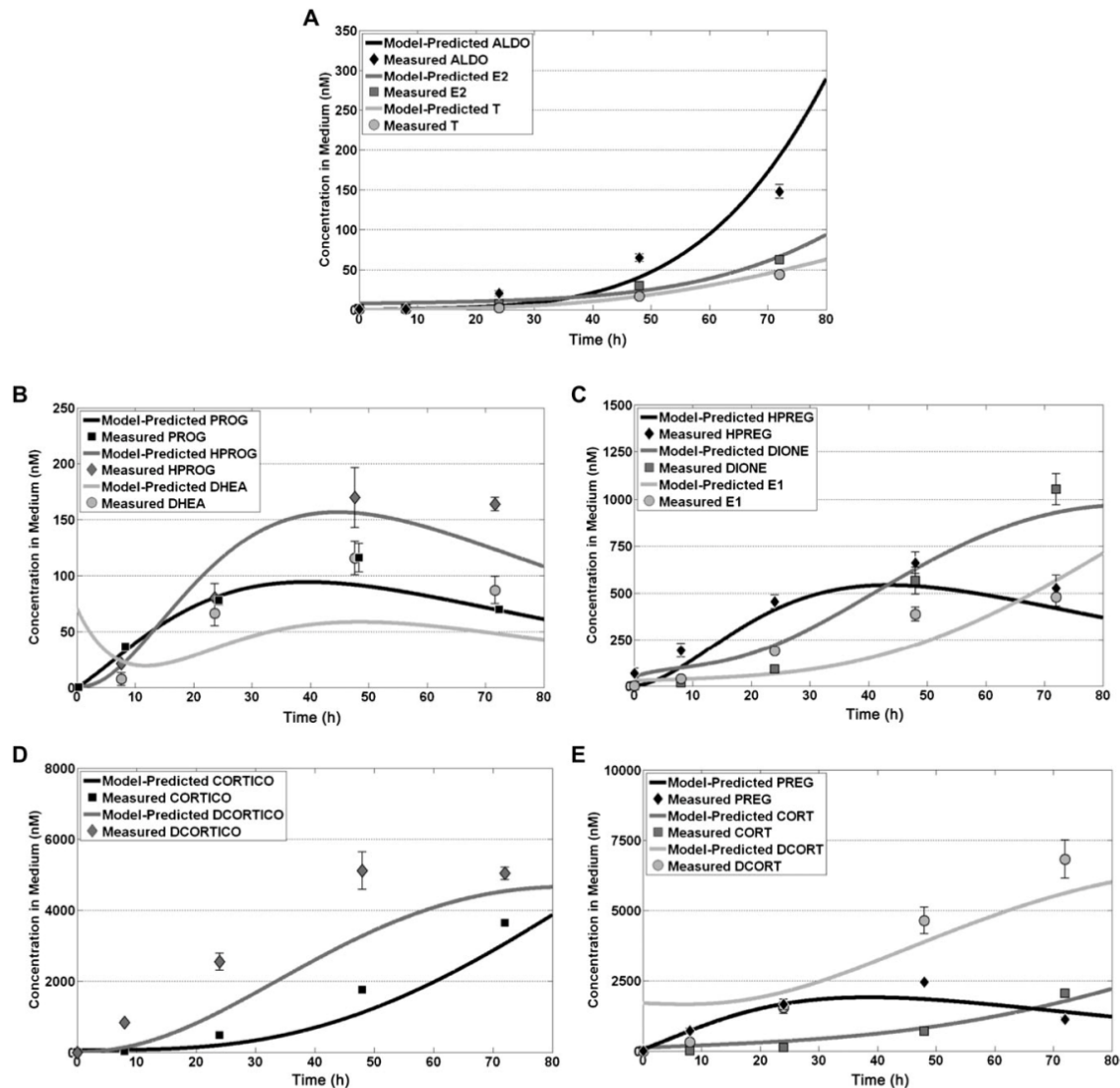


**FIG. 5.** Model evaluation of steroids for control cells. Time-course of model-predicted concentrations in medium were plotted and compared with concentrations (mean  $\pm$  SD) measured at five sampling times for ALDO, E2, and T (A); PROG, HPROG, and DHEA (B); HPREG, DIONE, and E1 (C); CORTICO and DCORTICO (D); and PREG, CORT, and DCORT (E).

To explain the lack of a molecular balance in the data, we examined the hypothesis that other metabolic pathways were needed in the model. The literature shows that OXY biosynthesis is a primary pathway for CHOL metabolism, and the pathway is present in adrenal tissue. To test this hypothesis, we (1) included the OXY metabolic pathway in the extended model, (2) calculated OXY concentrations, (3) estimated model parameters, and (4) evaluated the model-predicted concentrations of CHOL, OXY, and all 14 steroids both in the cells and in the medium.

The results support our hypothesis. By including the OXY metabolic pathway, the extended model significantly improved the model fit for CHOL both in the medium and in the cells as compared with the previous model. Moreover, the model-predicted and calculated OXY concentrations closely correspond. Close correspondence of model-predicted and measured CHOL and 14 steroids supports our model assumption of no degradation of CHOL, OXY, and steroids.

Besides the pathway for conversion of CHOL to OXY, we examined alternative biologically realistic hypotheses to allow for

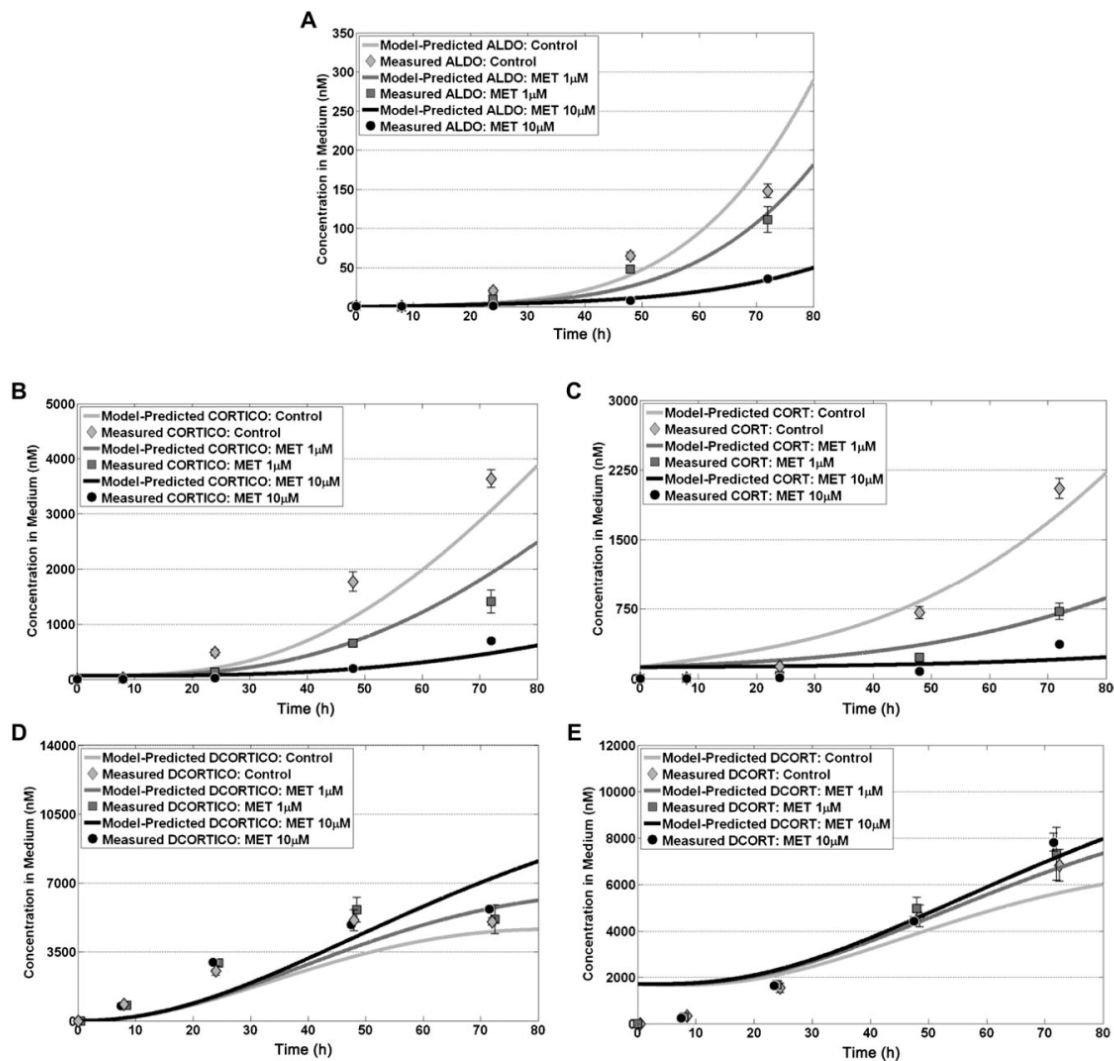


**FIG. 6.** Model evaluation of steroids for MET-exposed cells. Time-course of model-predicted concentrations in medium were plotted and compared with concentrations (mean  $\pm$  SD) measured at five sampling times for ALDO (A); CORTICO (B); CORT (C); DCORTICO (D); and DCORT (E). For controls, model-predicted and measured concentrations are same as shown in Figure 5.

a molecular balance. One alternative hypothesis is an unaccounted form of CHOL because CHOL is distributed in various cell membranes and compartments with a high abundance in the plasma membrane, endocytic recycling compartment, and Golgi complex (Ikonen, 2008). Another alternative hypothesis is a pathway for conversion of CHOL to CHOL esters because CHOL is a biosynthetic precursor of steroid hormones, OXY, and CHOL esters in all cells (Ikonen, 2008). However, in this study, the assay used to measure CHOL concentrations in cells includes CHOL esters and all the cellular membranes and compartments that can contain CHOL and CHOL esters. Because this CHOL

measurement accounts for free, membrane-bound, and esterified CHOL, these alternative hypotheses are not supported.

#### Dynamic Steroid Behavior

For the previous model, the dynamic steroid predictions for all 14 steroids had the same qualitative behavior, increasing monotonically across time (0–80 h). Although the mean measured concentrations for nine steroids increased monotonically, the mean measurements for five steroids (PROG, HPROG, DHEA, HPREG, and PREG) increased until 48 h and then decreased at 72 h. This was a key limitation of the

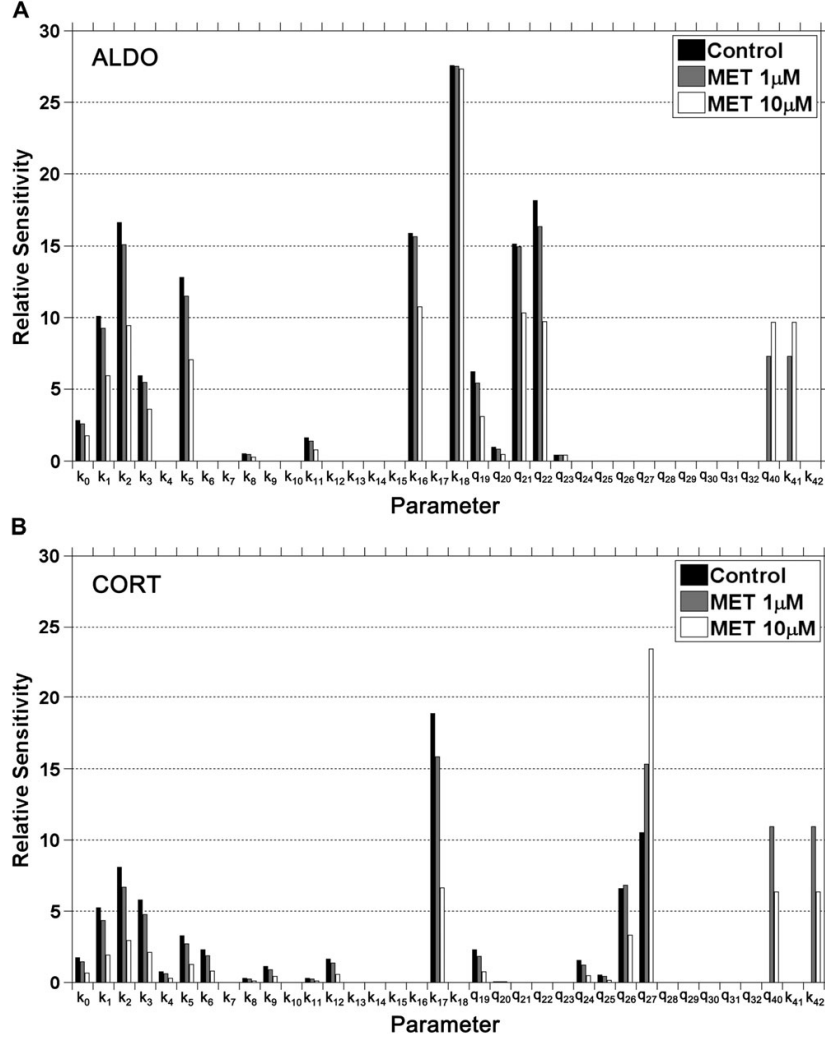


**FIG. 7.** Relative sensitivities for model-predicted ALDO (A) and CORT (B) plotted for 36 model parameters ( $k_0$ – $k_{18}$ ,  $q_{19}$ – $q_{32}$ ,  $q_{40}$ ,  $k_{41}$ – $k_{42}$ ) for control and MET-exposed cells. Each bar represents L2 norm of relative sensitivities across time (0–80h) and indicates the degree to which changes in parameter values lead to changes in model outputs.

previous model. By including cell proliferation, the extended model captures this observed time-course behavior for each steroid. One possible factor responsible for this behavior is the increasing number of enzymes due to cell proliferation. This is further evidence that the more biologically realistic features of the extended model allow for a better representation of the observed time-course behavior of steroidogenesis.

#### *Future Applications of Extended Model*

There are several potential applications for the extended model. First, the model's better ability to predict the time-course

of CHOL concentrations both in the medium and in the cells will be critical for EAC that affect upstream metabolic (e.g., inhibition of steroidogenic enzyme CYP11A) or signaling processes, which may affect CHOL levels. Second, the more biologically realistic model may improve the accuracy for low concentration extrapolations of concentration-response curves for other EACs with environmental concentrations below experimental levels. Environmental concentrations of MET are unknown. Third, the model can be simply modified with EAC-specific enzyme inhibition constants to predict the biochemical response for other EACs that competitively inhibit steroidogenic

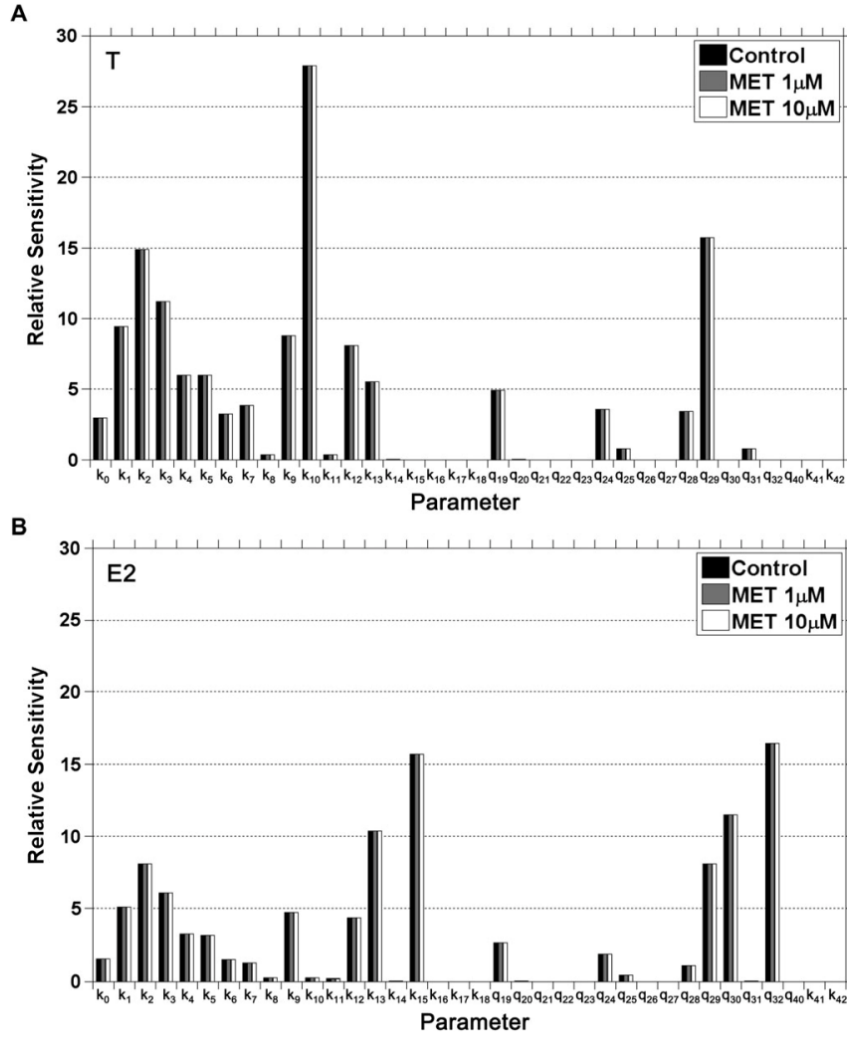


**FIG. 8.** Relative sensitivities for model-predicted T (A) and E2 (B) plotted for 36 model parameters ( $k_0$ – $k_{18}$ ,  $q_{19}$ – $q_{32}$ ,  $q_{40}$ ,  $k_{41}$ – $k_{42}$ ) for control and MET-exposed cells. Each bar represents L2 norm of relative sensitivities across time (0–80 h) and indicates the degree to which changes in parameter values lead to changes in model outputs.

enzymes. Fourth, our *in vitro* model could be extended to predict the *in vivo* response. The steroidogenesis model would need to be linked to a multiorgan systems model, which includes the regulatory feedback of the hypothalamus-pituitary-adrenal axis, and refined based on additional experiments. This extension of the current model would require a significant research effort. Finally, with further model refinement and evaluation, the model can be used to help identify mechanisms of action for EACs by predicting the enzyme inhibition constants for poorly characterized EACs and for screening assays that typically measure only a few steroids in the medium.

#### Limitations

There are some limitations to our extended model based on the model structure and assumptions and data available for model evaluation. First, the extended model structure and parameter values are based on MET concentrations at or below 10 $\mu$ M. At higher MET concentrations, the proliferation rate and viability of the cells can be altered and inhibition of additional steroidogenic enzymes can occur. Therefore, the extended model may not accurately extrapolate at higher MET concentrations without including a cell proliferation model and enzyme inhibition constants that are dose dependent. Second, our model

assumption of first-order enzyme kinetics, which reduced the model complexity while maintaining the model's predictive ability, is only applicable for nonsaturable enzyme kinetics. For highly concentrated or potent EACs, first-order enzyme kinetics may need to be replaced by saturable enzyme kinetics (e.g., Michaelis-Menten). Third, transport of OXY between the cells and medium is not included in the model because the OXY data are unavailable. This may result in the overestimation of OXY in the cells. Experiments that measure the time-course of OXY are needed to further evaluate the OXY metabolic and transport pathways. Finally, the extended model structure is based on EACs that are competitive enzyme inhibitors. For EACs with different mechanisms of action (e.g., activating or antagonizing steroid hormone receptors and inducing steroidogenic enzymes), model refinements will be needed (Sanderson, 2006). These refinements may require additional model-guided experiments for other pathways, such as gene regulation and upstream signaling pathways.

### Conclusions

We extended a previous steroidogenesis model by including a cell proliferation model and a pathway for OXY biosynthesis. The cell proliferation model, which was independently evaluated with experimental data, removed the confounding of cell proliferation from the steroid biosynthesis and its biochemical response to EAC. The inclusion of the metabolic pathway for OXY biosynthesis significantly improved the model fit for CHOL and allowed the model to capture the dynamic behavior of steroids both in the medium and in the cells. Our study demonstrates the significant improvement of the extended, more biologically realistic model to estimate CHOL and adrenal steroid concentrations both in H295R cells and in medium and their dynamic biochemical response to the EAC, MET. This mechanistic modeling capability could help define mechanisms of action for poorly characterized chemicals and mixtures for predictive risk assessments and to screen drug candidates based on steroidogenic effects in the early phase of drug development.

### SUPPLEMENTARY DATA

Supplementary data are available online at <http://toxsci.oxfordjournals.org/>.

### FUNDING

North Carolina State University/Environmental Protection Agency Cooperative Training Program in Environmental Sciences Research (Training Agreement CT833235-01-0 to M.B.) with North Carolina State University.

### ACKNOWLEDGMENTS

We thank Hisham El-Masri and Daniel Villeneuve for their review comments and helpful suggestions. Although this

manuscript was reviewed by the U.S. EPA and approved for publication, it may not reflect official Agency policy. Mention of trade names or commercial products does not constitute endorsement or recommendation for use.

### REFERENCES

- Adams, C. M., Reitz, J., De Brabander, J. K., Feramisco, J. D., Li, L., Brown, M. S., and Goldstein, J. L. (2004). Cholesterol and 25-hydroxycholesterol inhibit activation of SREBPs by different mechanisms, both involving SCAP and Insigs. *J. Biol. Chem.* **279**, 52772–52780.
- Andersen, M. E., and Krewski, D. (2010). The vision of toxicity testing in the 21st century: moving from discussion to action. *Toxicol. Sci.* **117**, 17–24.
- Bjorkhem, I. (2002). Do oxysterols control cholesterol homeostasis? *J. Clin. Invest.* **110**, 725–730.
- Breen, M. S., Breen, M., Terasaki, N., Yamazaki, M., and Conolly, R. B. (2010). Computational model of steroidogenesis in human H295R cells to predict biochemical response to endocrine-active chemicals: model development for metyrapone. *Environ. Health Perspect.* **118**, 265–272.
- Breen, M. S., Villeneuve, D. L., Breen, M., Ankly, G. T., and Conolly, R. B. (2007). Mechanistic computational model of ovarian steroidogenesis to predict biochemical responses to endocrine active compounds. *Ann. Biomed. Eng.* **35**, 970–981.
- Evans, M. J., Livesey, J. H., Ellis, M. J., and Yandle, T. G. (2001). Effect of anticoagulants and storage temperatures on stability of plasma and serum hormones. *Clin. Biochem.* **34**, 107–112.
- Food Quality Protection Act. (1996). *Public Law 104–170*. U.S. Senate and House of Representatives, Washington, DC.
- Garde, A. H., and Hansen, A. M. (2005). Long-term stability of salivary cortisol. *Scand. J. Clin. Lab. Investig.* **65**, 433–436.
- Gazdar, A. F., Oie, H. K., Shackleton, C. H., Chen, T. R., Triche, T. J., Myers, C. E., Chrousos, G. P., Brennan, M. F., Stein, C. A., and La Rocca, R. V. (1990). Establishment and characterization of a human adrenocortical carcinoma cell line that expresses multiple pathways of steroid biosynthesis. *Cancer Res.* **50**, 5488–5496.
- Harvey, P. W., and Everett, D. J. (2003). The adrenal cortex and steroidogenesis as cellular and molecular targets for toxicity: critical omissions from regulatory endocrine disrupter screening strategies for human health? *J. Appl. Toxicol.* **23**, 81–87.
- Harvey, P. W., Everett, D. J., and Springall, C. J. (2007). Adrenal toxicology: a strategy for assessment of functional toxicity to the adrenal cortex and steroidogenesis. *J. Appl. Toxicol.* **27**, 103–115.
- Ikonen, E. (2008). Cellular cholesterol trafficking and compartmentalization. *Mol. Cell Biol.* **9**, 125–138.
- Javitt, N. B. (2008). Oxysterols: novel biologic roles for the 21st century. *Steroids* **73**, 149–157.
- Logie, A., Boulle, N., Gaston, V., Perin, L., Boudou, P., Le Bouc, Y., and Gicquel, C. (1999). Autocrine role of IGF-II in proliferation of human adrenocortical carcinoma NCI H295R cell line. *J. Mol. Endocrinol.* **23**, 23–32.
- National Research Council. (2007). *Toxicity Testing in the 21st Century: A Vision and a Strategy*. National Academy Press, Washington, DC.
- Nelder, J. A., and Mead, R. (1965). A simplex method for function minimization. *Comput. J.* **7**, 308–313.
- Nishimura, T., Inoue, T., Shibata, N., Sekine, A., Takabe, W., Noguchi, N., and Arai, H. (2005). Inhibition of cholesterol biosynthesis by 25-hydroxycholesterol is independent of OSBP. *Genes Cells* **10**, 793–801.

- Payne, A. H., and Hales, D. B. (2004). Overview of steroidogenic enzymes in the pathway from cholesterol to active steroid hormones. *Endocr. Rev.* **25**, 947–970.
- Rainey, W. E., Bird, I. M., and Mason, J. I. (1994). The NCI-H295R cell line: a pluripotent model for human adrenocortical studies. *Mol. Cell. Endocrinol.* **100**, 45–50.
- Safe Drinking Water Act Amendments. (1996). *Public Law 104–182*. U.S. Senate and House of Representatives, Washington, DC.
- Sanderson, J. T. (2006). The steroid hormone biosynthesis pathway as a target for endocrine-disrupting chemicals. *Toxicol. Sci.* **94**, 3–21.
- Schroepfer, G. (2000). Oxysterols: modulators of cholesterol metabolism and other processes. *Physiol. Rev.* **80**, 361–554.
- Staels, B., Hum, D. W., and Miller, W. L. (1993). Regulation of steroidogenesis in NCI-H295R cells: a cellular model of the human fetal adrenal. *Mol. Endocrinol.* **7**, 423–433.
- U.S. Environmental Protection Agency (U.S. EPA). (1998). *Endocrine Disruptor Screening Program*. Vol. 63 No. 154, pp, 42852– 42855. Federal Register, Washington, DC.
- U.S. Environmental Protection Agency (U.S. EPA). (2009). *Endocrine Disruptor Screening Program (EDSP): Announcing the Availability of the Tier 1 Screening Battery and Related Test Guidelines*. Vol. 74, No. 202, pp. 54415–54422; Federal Register, Washington, DC.
- Wickings, E. J., and Nieschlag, E. (1976). Stability of testosterone and androstenedione in blood and plasma samples. *Clin. Chim. Acta* **71**, 439–443.

## Supplementary Data to:

### **Mechanistic Computational Model of Steroidogenesis in H295R Cells: Role of Oxysterols and Cell Proliferation to Improve Predictability of Biochemical Response to Endocrine Active Chemical - Metirapone**

Miyuki Breen,<sup>\*,†</sup> Michael S. Breen,<sup>‡</sup> Natsuko Terasaki,<sup>§</sup> Makoto Yamazaki,<sup>§</sup> Alun L. Lloyd,<sup>†</sup>  
Rory B. Conolly<sup>\*</sup>

<sup>\*</sup> National Health and Environmental Effects Research Laboratory, U.S. Environmental Protection Agency, Research Triangle Park, NC 27711, USA

<sup>†</sup> Biomathematics Program, Department of Mathematics, North Carolina State University, Raleigh, NC 27695, USA

<sup>‡</sup> National Exposure Research Laboratory, U.S. Environmental Protection Agency, 109 T.W. Alexander Drive, Mail E205-02, Research Triangle Park, NC 27711, USA

<sup>§</sup> Safety Research Laboratory, Mitsubishi Tanabe Pharma Corporation, Kisarazu, Chiba 292-0818, Japan

## 1. Dynamic molecular balance equations in cells and medium

CHOL in cells:

$$\frac{dV_{\text{cell}}(t)C_{\text{CHOL,cell}}(t)}{dt} = k_1V_{\text{med}}C_{\text{CHOL,med}}(t) - (k_0 + k_2)V_{\text{cell}}(t)C_{\text{CHOL,cell}}(t);$$

$$C_{\text{CHOL,cell}}(0) = 1.01 \times 10^7 \text{ nM}$$

OXY in cells:

$$\frac{dV_{\text{cell}}(t)C_{\text{OXY,cell}}(t)}{dt} = k_0V_{\text{cell}}(t)C_{\text{CHOL,cell}}(t);$$

$$C_{\text{OXY,cell}}(0) = 0$$

PREG in cells:

$$\frac{dV_{\text{cell}}(t)C_{\text{PREG,cell}}(t)}{dt} = k_2V_{\text{cell}}(t)C_{\text{CHOL,cell}}(t) - (k_3 + k_5 + k_{+19})V_{\text{cell}}(t)C_{\text{PREG,cell}}(t) + k_{-19}V_{\text{med}}C_{\text{PREG,med}}(t);$$

$$C_{\text{PREG,cell}}(0) = 5.07 \times 10^3 \text{ nM}$$

HPREG in cells:

$$\frac{dV_{\text{cell}}(t)C_{\text{HPREG,cell}}(t)}{dt} = k_3V_{\text{cell}}(t)C_{\text{PREG,cell}}(t) - (k_4 + k_6 + k_{+24})V_{\text{cell}}(t)C_{\text{HPREG,cell}}(t) + k_{-24}V_{\text{med}}C_{\text{HPREG,med}}(t);$$

$$C_{\text{HPREG,cell}}(0) = 0$$

DHEA in cells:

$$\frac{dV_{\text{cell}}(t)C_{\text{DHEA,cell}}(t)}{dt} = k_4V_{\text{cell}}(t)C_{\text{HPREG,cell}}(t) - (k_7 + k_{+28})V_{\text{cell}}(t)C_{\text{DHEA,cell}}(t) + k_{-28}V_{\text{med}}C_{\text{DHEA,med}}(t);$$

$$C_{\text{DHEA,cell}}(0) = 1.87 \times 10^3 \text{ nM}$$

PROG in cells:

$$\frac{dV_{\text{cell}}(t)C_{\text{PROG,cell}}(t)}{dt} = k_5V_{\text{cell}}(t)C_{\text{PREG,cell}}(t) - (k_8 + k_{11} + k_{+20})V_{\text{cell}}(t)C_{\text{PROG,cell}}(t) + k_{20}V_{\text{med}}C_{\text{PROG,med}}(t);$$

$$C_{\text{PROG,cell}}(0) = 17.09 \text{ nM}$$

HPROG in cells:

$$\frac{dV_{\text{cell}}(t)C_{\text{HPROG,cell}}(t)}{dt} = k_6 V_{\text{cell}}(t)C_{\text{HPREG,cell}}(t) + k_8 V_{\text{cell}}(t)C_{\text{PROG,cell}}(t) - (k_9 + k_{12} + k_{+25})V_{\text{cell}}(t)C_{\text{HPROG,cell}}(t) + k_{-25}V_{\text{med}}C_{\text{HPROG,med}}(t);$$

$$C_{\text{HPROG,cell}}(0) = 55.31 \text{ nM}$$

DIONE in cells:

$$\frac{dV_{\text{cell}}(t)C_{\text{DIONE,cell}}(t)}{dt} = k_7 V_{\text{cell}}(t)C_{\text{DHEA,cell}}(t) + k_9 V_{\text{cell}}(t)C_{\text{HPROG,cell}}(t) - (k_{10} + k_{13} + k_{+29})V_{\text{cell}}(t)C_{\text{DIONE,cell}}(t) + k_{-29}V_{\text{med}}C_{\text{DIONE,med}}(t);$$

$$C_{\text{DIONE,cell}}(0) = 1.25 \times 10^3 \text{ nM}$$

T in cells:

$$\frac{dV_{\text{cell}}(t)C_{\text{T,cell}}(t)}{dt} = k_{10} V_{\text{cell}}(t)C_{\text{DIONE,cell}}(t) - (k_{14} + k_{+31})V_{\text{cell}}(t)C_{\text{T,cell}}(t) + k_{-31}V_{\text{med}}C_{\text{T,med}}(t);$$

$$C_{\text{T,cell}}(0) = 0$$

E1 in cells:

$$\frac{dV_{\text{cell}}(t)C_{\text{E1,cell}}(t)}{dt} = k_{13} V_{\text{cell}}(t)C_{\text{DIONE,cell}}(t) - (k_{15} + k_{+30})V_{\text{cell}}(t)C_{\text{E1,cell}}(t) + k_{-30}V_{\text{med}}C_{\text{E1,med}}(t);$$

$$C_{\text{E1,cell}}(0) = 1.12 \times 10^3 \text{ nM}$$

E2 in cells:

$$\frac{dV_{\text{cell}}(t)C_{\text{E2,ovv}}(t)}{dt} = k_{14} V_{\text{cell}}(t)C_{\text{T,cell}}(t) + k_{15} V_{\text{cell}}(t)C_{\text{E1,cell}}(t) - k_{+32}V_{\text{cell}}(t)C_{\text{E2,cell}}(t) + k_{-32}V_{\text{med}}C_{\text{E2,med}}(t);$$

$$C_{\text{E2,cell}}(0) = 228.70 \text{ nM}$$

DCORTICO in cells:

$$\frac{dV_{\text{cell}}(t)C_{\text{DCORTICO,cell}}(t)}{dt} = k_{11} V_{\text{cell}}(t)C_{\text{PROG,cell}}(t) - \left( \frac{k_{16}}{\alpha_{\text{CORTICO}}} + k_{+21} \right) V_{\text{cell}}(t)C_{\text{DCORTICO,cell}}(t) + k_{-21}V_{\text{med}}C_{\text{DCORTICO,med}}(t);$$

$$C_{\text{DCORTICO,cell}}(0) = 448.95 \text{ nM}$$

CORTICO in cells:

$$\frac{dV_{\text{cell}}(t)C_{\text{CORTICO,cell}}(t)}{dt} = \frac{k_{16}}{\alpha_{\text{CORTICO}}}V_{\text{cell}}(t)C_{\text{DCORTICO,cell}}(t) - (k_{18} + k_{+22})V_{\text{cell}}(t)C_{\text{CORTICO,cell}}(t) + k_{-22}V_{\text{med}}C_{\text{CORTICO,med}}(t);$$

$$C_{\text{CORTICO,cell}}(0) = 1.22 \times 10^3 \text{ nM}$$

ALDO in cells:

$$\frac{dV_{\text{cell}}(t)C_{\text{ALDO,cell}}(t)}{dt} = k_{18}V_{\text{cell}}(t)C_{\text{CORTICO,cell}}(t) - k_{+23}V_{\text{cell}}(t)C_{\text{ALDO,cell}}(t) + k_{-23}V_{\text{med}}C_{\text{ALDO,med}}(t);$$

$$C_{\text{ALDO,cell}}(0) = 0$$

DCORT in cells:

$$\frac{dV_{\text{cell}}(t)C_{\text{DCORT,cell}}(t)}{dt} = k_{12}V_{\text{cell}}(t)C_{\text{HPROG,cell}}(t) - \left( \frac{k_{17}}{\alpha_{\text{CORT}}} + k_{+26} \right) V_{\text{cell}}(t)C_{\text{DCORT,cell}}(t) + k_{-26}V_{\text{med}}C_{\text{DCORT,med}}(t);$$

$$C_{\text{DCORT,cell}}(0) = 4.06 \times 10^4 \text{ nM}$$

CORT in cells:

$$\frac{dV_{\text{cell}}(t)C_{\text{CORT,cell}}(t)}{dt} = \frac{k_{17}}{\alpha_{\text{CORT}}}V_{\text{cell}}(t)C_{\text{DCORT,cell}}(t) - k_{+27}V_{\text{cell}}(t)C_{\text{CORT,cell}}(t) + k_{-27}V_{\text{med}}C_{\text{CORT,med}}(t);$$

$$C_{\text{CORT,cell}}(0) = 1.84 \times 10^3 \text{ nM}$$

CHOL in medium:

$$\frac{dC_{\text{CHOL,med}}(t)}{dt} = -k_1C_{\text{CHOL,med}}(t); \quad C_{\text{CHOL,med}}(0) = 8.11 \times 10^4 \text{ nM}$$

PREG in medium:

$$V_{\text{med}} \frac{dC_{\text{PREG,med}}(t)}{dt} = k_{+19}V_{\text{cell}}(t)C_{\text{PREG,cell}}(t) - k_{-19}V_{\text{med}}C_{\text{PREG,med}}(t); \quad C_{\text{PREG,med}}(0) = 0.85 \text{ nM}$$

HPREG in medium:

$$V_{\text{med}} \frac{dC_{\text{HPREG,med}}(t)}{dt} = k_{+24}V_{\text{cell}}(t)C_{\text{HPREG,cell}}(t) - k_{-24}V_{\text{med}}C_{\text{HPREG,med}}(t); \quad C_{\text{HPREG,med}}(0) = 69.45 \text{ nM}$$

DHEA in medium:

$$V_{\text{med}} \frac{dC_{\text{DHEA,med}}(t)}{dt} = k_{+28} V_{\text{cell}}(t) C_{\text{DHEA,cell}}(t) - k_{-28} V_{\text{med}} C_{\text{DHEA,med}}(t); \quad C_{\text{DHEA,med}}(0) = 0$$

PROG in medium:

$$V_{\text{med}} \frac{dC_{\text{PROG,med}}(t)}{dt} = k_{+20} V_{\text{cell}}(t) C_{\text{PROG,cell}}(t) - k_{-20} V_{\text{med}} C_{\text{PROG,med}}(t); \quad C_{\text{PROG,med}}(0) = 0.03 \text{ nM}$$

HPROG in medium:

$$V_{\text{med}} \frac{dC_{\text{HPROG,med}}(t)}{dt} = k_{+25} V_{\text{cell}}(t) C_{\text{HPROG,cell}}(t) - k_{-25} V_{\text{med}} C_{\text{HPROG,med}}(t); \quad C_{\text{HPROG,med}}(0) = 0$$

DIONE in medium:

$$V_{\text{med}} \frac{dC_{\text{DIONE,med}}(t)}{dt} = k_{+29} V_{\text{cell}}(t) C_{\text{DIONE,cell}}(t) - k_{-29} V_{\text{med}} C_{\text{DIONE,med}}(t); \quad C_{\text{DIONE,med}}(0) = 0.80 \text{ nM}$$

T in medium:

$$V_{\text{med}} \frac{dC_{\text{T,med}}(t)}{dt} = k_{+31} V_{\text{cell}}(t) C_{\text{T,cell}}(t) - k_{-31} V_{\text{med}} C_{\text{T,med}}(t); \quad C_{\text{T,med}}(0) = 0.80 \text{ nM}$$

E1 in medium:

$$V_{\text{med}} \frac{dC_{\text{E1,med}}(t)}{dt} = k_{+30} V_{\text{cell}}(t) C_{\text{E1,cell}}(t) - k_{-30} V_{\text{med}} C_{\text{E1,med}}(t); \quad C_{\text{E1,med}}(0) = 0.11 \text{ nM}$$

E2 in medium:

$$V_{\text{med}} \frac{dC_{\text{E2,med}}(t)}{dt} = k_{+32} V_{\text{cell}}(t) C_{\text{E2,cell}}(t) - k_{-32} V_{\text{med}} C_{\text{E2,med}}(t); \quad C_{\text{E2,med}}(0) = 1.21 \text{ nM}$$

DCORTICO in medium:

$$V_{\text{med}} \frac{dC_{\text{DCORTICO,med}}(t)}{dt} = k_{+21} V_{\text{cell}}(t) C_{\text{DCORTICO,cell}}(t) - k_{-21} V_{\text{med}} C_{\text{DCORTICO,med}}(t); \quad C_{\text{DCORTICO,med}}(0) = 0 \text{ nM}$$

CORTICO in medium:

$$V_{\text{med}} \frac{dC_{\text{CORTICO,med}}(t)}{dt} = k_{+22} V_{\text{cell}}(t) C_{\text{CORTICO,cell}}(t) - k_{-22} V_{\text{med}} C_{\text{CORTICO,med}}(t); \quad C_{\text{CORTICO,med}}(0) = 0.11 \text{ nM}$$

ALDO in medium:

$$V_{\text{med}} \frac{dC_{\text{ALDO,med}}(t)}{dt} = k_{+23} V_{\text{cell}}(t) C_{\text{ALDO,cell}}(t) - k_{-23} V_{\text{med}} C_{\text{ALDO,med}}(t); \quad C_{\text{ALDO,med}}(0) = 0.91 \text{ nM}$$

DCORT in medium:

$$V_{\text{med}} \frac{dC_{\text{DCORT,med}}(t)}{dt} = k_{+26} V_{\text{cell}}(t) C_{\text{DCORT,cell}}(t) - k_{-26} V_{\text{med}} C_{\text{DCORT,med}}(t); \quad C_{\text{DCORT,med}}(0) = 0 \text{ nM}$$

CORT in medium:

$$V_{\text{med}} \frac{dC_{\text{CORT,med}}(t)}{dt} = k_{+27} V_{\text{cell}}(t) C_{\text{CORT,cell}}(t) - k_{-27} V_{\text{med}} C_{\text{CORT,med}}(t); \quad C_{\text{CORT,med}}(0) = 0.03 \text{ nM}$$

## 2. Molecular balance equations for quasi-equilibrium

CHOL in cells:

$$\frac{dC_{\text{CHOL,cell}}(t)}{dt} = \left( \frac{1}{V_{\text{cell}}(t)} \right) \left[ k_1 V_{\text{med}} C_{\text{CHOL,med}}(t) - (k_0 + k_2 + k_p) V_{\text{cell}}(t) C_{\text{CHOL,cell}}(t) \right];$$

$$C_{\text{CHOL,cell}}(0) = 1.01 \times 10^7 \text{ nM}$$

OXY in cells:

$$\frac{dC_{\text{OXY,cell}}(t)}{dt} = k_0 C_{\text{CHOL,cell}}(t) - k_p C_{\text{OXY,cell}}(t);$$

$$C_{\text{OXY,cell}}(0) = 0$$

PREG in cells:

$$\frac{dC_{\text{PREG,cell}}(t)}{dt} = \left( \frac{1}{V_{\text{cell}}(t) + V_{\text{med}}q_{19}} \right) \left[ k_2 V_{\text{cell}}(t) C_{\text{CHOL,cell}}(t) - (k_3 + k_5 + k_p) V_{\text{cell}}(t) C_{\text{PREG,cell}}(t) \right];$$

$$C_{\text{PREG,cell}}(0) = 5.07 \times 10^3 \text{ nM}$$

HPREG in cells:

$$\frac{dC_{\text{HPREG,cell}}(t)}{dt} = \left( \frac{1}{V_{\text{cell}}(t) + V_{\text{med}}q_{24}} \right) \left[ k_3 V_{\text{cell}}(t) C_{\text{PREG,cell}}(t) - (k_4 + k_6 + k_p) V_{\text{cell}}(t) C_{\text{HPREG,cell}}(t) \right];$$

$$C_{\text{HPREG,cell}}(0) = 0$$

DHEA in cells:

$$\frac{dC_{\text{DHEA,cell}}(t)}{dt} = \left( \frac{1}{V_{\text{cell}}(t) + V_{\text{med}}q_{28}} \right) \left[ k_4 V_{\text{cell}}(t) C_{\text{HPREG,cell}}(t) - (k_7 + k_p) V_{\text{cell}}(t) C_{\text{DHEA,cell}}(t) \right];$$

$$C_{\text{DHEA,cell}}(0) = 1.87 \times 10^3 \text{ nM}$$

PROG in cells:

$$\frac{dC_{\text{PROG,cell}}(t)}{dt} = \left( \frac{1}{V_{\text{cell}}(t) + V_{\text{med}}q_{20}} \right) \left[ k_5 V_{\text{cell}}(t) C_{\text{PREG,cell}}(t) - (k_8 + k_{11} + k_p) V_{\text{cell}}(t) C_{\text{PROG,cell}}(t) \right];$$

$$C_{\text{PROG,cell}}(0) = 17.09 \text{ nM}$$

HPROG in cells:

$$\frac{dC_{\text{HPROG,cell}}(t)}{dt} = \left( \frac{1}{V_{\text{cell}}(t) + V_{\text{med}}q_{25}} \right) \left[ k_6 V_{\text{cell}}(t) C_{\text{HPREG,cell}}(t) + k_8 V_{\text{cell}}(t) C_{\text{PROG,cell}}(t) - (k_9 + k_{12} + k_p) V_{\text{cell}}(t) C_{\text{HPROG,cell}}(t) \right];$$

$$C_{\text{HPROG,cell}}(0) = 55.31 \text{ nM}$$

DIONE in cells:

$$\frac{dC_{\text{DIONE,cell}}(t)}{dt} = \left( \frac{1}{V_{\text{cell}}(t) + V_{\text{med}}q_{29}} \right) \left[ k_7 V_{\text{cell}}(t) C_{\text{DHEA,cell}}(t) + k_9 V_{\text{cell}}(t) C_{\text{HPROG,cell}}(t) - (k_{10} + k_{13} + k_p) V_{\text{cell}}(t) C_{\text{DIONE,cell}}(t) \right];$$

$$C_{\text{DIONE,cell}}(0) = 1.25 \times 10^3 \text{ nM}$$

T in cells:

$$\frac{dC_{T,cell}(t)}{dt} = \left( \frac{1}{V_{cell}(t) + V_{med}q_{31}} \right) \left[ k_{10}V_{cell}(t)C_{DIONE,cell}(t) - (k_{14} + k_p)V_{cell}(t)C_{T,cell}(t) \right];$$

$$C_{T,cell}(0) = 0$$

E1 in cells:

$$\frac{dC_{E1,cell}(t)}{dt} = \left( \frac{1}{V_{cell}(t) + V_{med}q_{30}} \right) \left[ k_{13}V_{cell}(t)C_{DIONE,cell}(t) - (k_{15} + k_p)V_{cell}(t)C_{E1,cell}(t) \right];$$

$$C_{E1,cell}(0) = 1.12 \times 10^3 \text{ nM}$$

E2 in cells:

$$\frac{dC_{E2,cell}(t)}{dt} = \left( \frac{1}{V_{cell}(t) + V_{med}q_{32}} \right) \left[ k_{14}V_{cell}(t)C_{T,cell}(t) + k_{15}V_{cell}(t)C_{E1,cell}(t) - k_pV_{cell}(t)C_{E2,cell}(t) \right];$$

$$C_{E2,cell}(0) = 228.70 \text{ nM}$$

DCORTICO in cells:

$$\frac{dC_{DCORTICO,cell}(t)}{dt} = \left( \frac{1}{V_{cell}(t) + V_{med}q_{21}} \right) \left[ k_{11}V_{cell}(t)C_{PROG,cell}(t) - \left( \frac{k_{16}}{\alpha_{CORTICO}} + k_p \right) V_{cell}(t)C_{DCORTICO,cell}(t) \right];$$

$$C_{DCORTICO,cell}(0) = 448.95 \text{ nM}$$

CORTICO in cells:

$$\frac{dC_{CORTICO,cell}(t)}{dt} = \left( \frac{1}{V_{cell}(t) + V_{med}q_{22}} \right) \left[ \frac{k_{16}}{\alpha_{CORTICO}} V_{cell}(t)C_{DCORTICO,cell}(t) - (k_{18} + k_p)V_{cell}(t)C_{CORTICO,cell}(t) \right];$$

$$C_{CORTICO,cell}(0) = 1.22 \times 10^3 \text{ nM}$$

ALDO in cells:

$$\frac{dC_{ALDO,cell}(t)}{dt} = \left( \frac{1}{V_{cell}(t) + V_{med}q_{23}} \right) \left[ k_{18}V_{cell}(t)C_{CORTICO,cell}(t) - k_pV_{cell}(t)C_{ALDO,cell}(t) \right];$$

$$C_{ALDO,cell}(0) = 0$$

DCORT in cells:

$$\frac{dC_{\text{DCORT,cell}}(t)}{dt} = \left( \frac{1}{V_{\text{cell}}(t) + V_{\text{med}}q_{26}} \right) \left[ k_{12}V_{\text{cell}}(t)C_{\text{HPROG,cell}}(t) - \left( \frac{k_{17}}{\alpha_{\text{CORT}}} + k_p \right) V_{\text{cell}}(t)C_{\text{DCORT,cell}}(t) \right];$$

$$C_{\text{DCORT,cell}}(0) = 4.06 \times 10^4 \text{ nM}$$

CORT in cells:

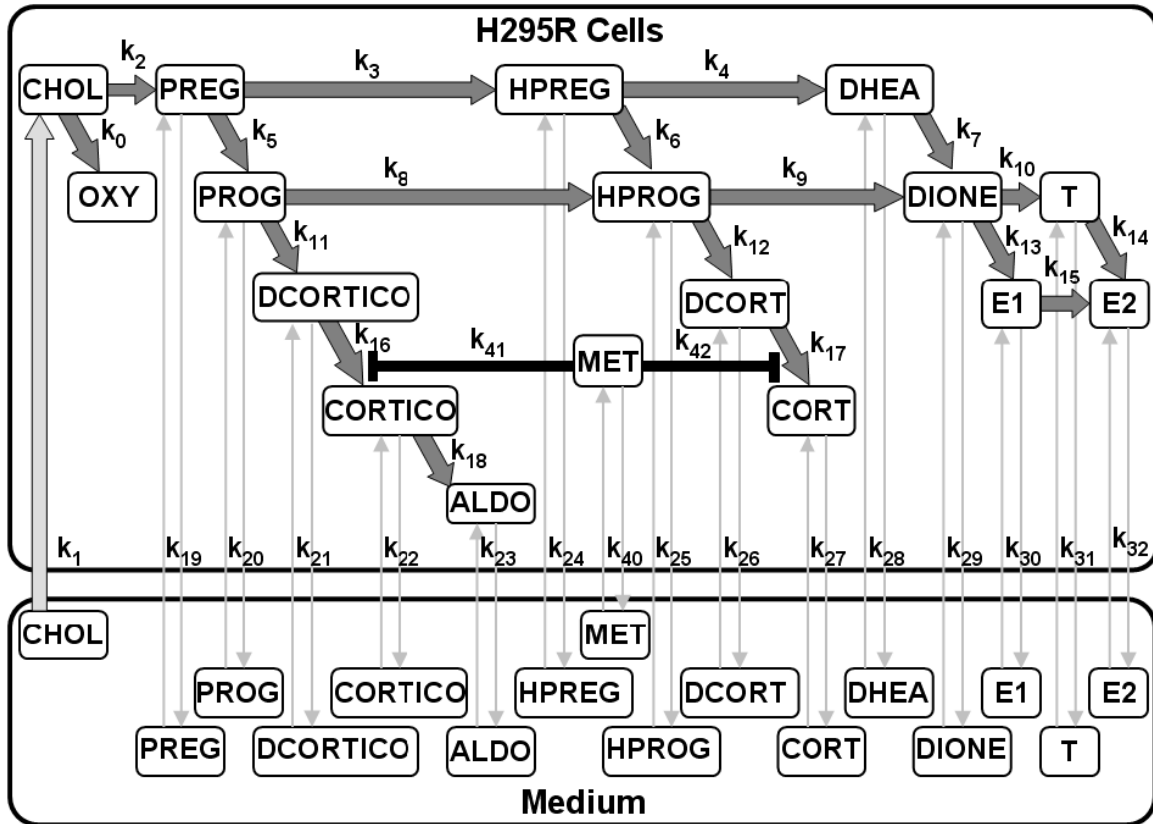
$$\frac{dC_{\text{CORT,cell}}(t)}{dt} = \left( \frac{1}{V_{\text{cell}}(t) + V_{\text{med}}q_{27}} \right) \left[ \frac{k_{17}}{\alpha_{\text{CORT}}} V_{\text{cell}}(t)C_{\text{DCORT,cell}}(t) - k_p V_{\text{cell}}(t)C_{\text{CORT,cell}}(t) \right];$$

$$C_{\text{CORT,cell}}(0) = 1.84 \times 10^3 \text{ nM}$$

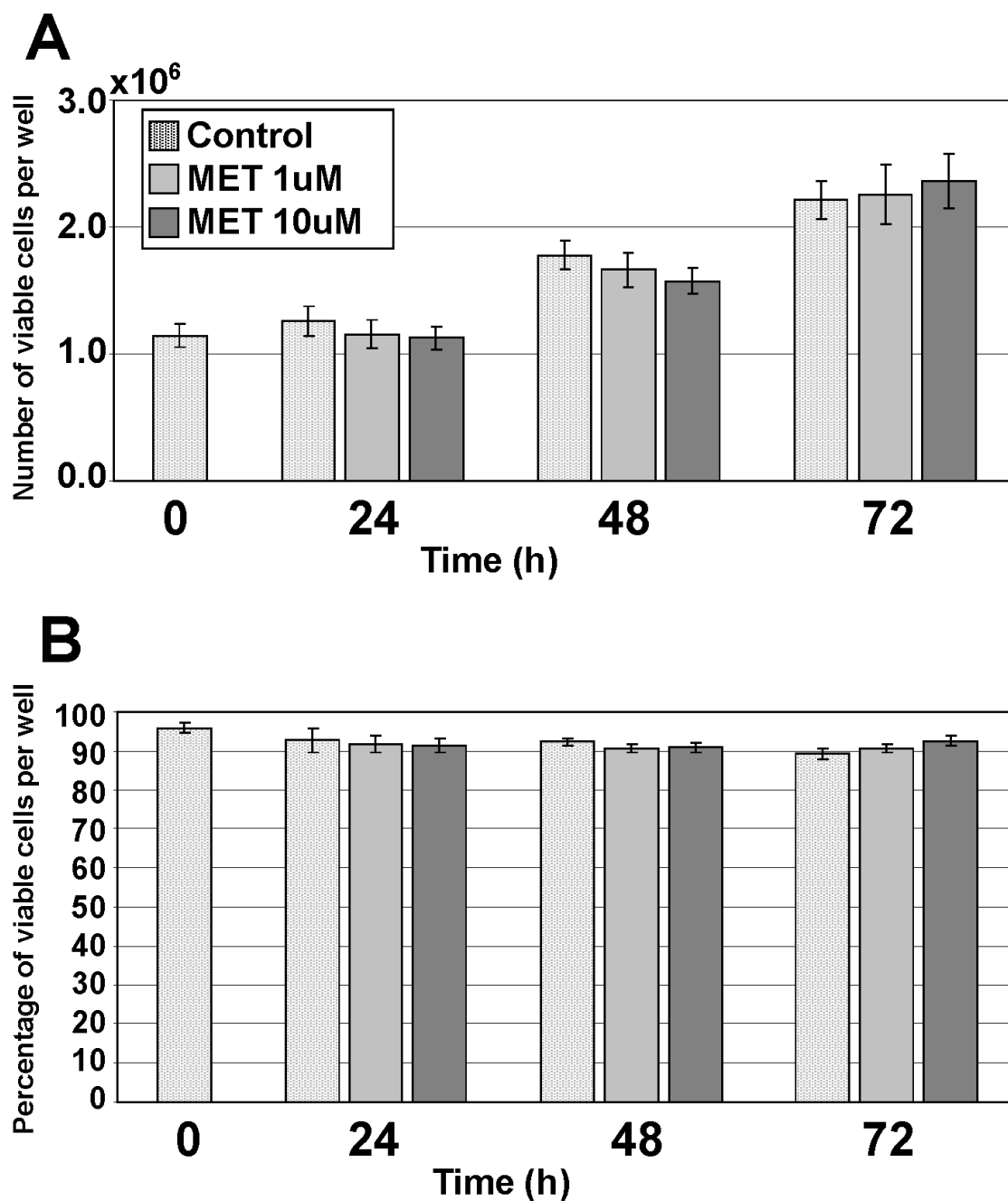
**Supplemental Material, Table 1. Quantitative ranges for cholesterol and steroids in cells and medium**

Steroid	Quantitative range (nM)	
	Cells <sup>1</sup>	Medium
CHOL	$2.4 \times 10^6 - 3.9 \times 10^7$	$4.0 \times 10^4 - 6.5 \times 10^5$
PREG	$6.8 \times 10^3 - 6.8 \times 10^5$	$15.8 - 1.6 \times 10^3$
HPREG	$6.4 \times 10^3 - 6.4 \times 10^5$	$15.0 - 1.5 \times 10^3$
DHEA	$7.4 \times 10^3 - 7.4 \times 10^5$	$17.3 - 1.7 \times 10^3$
PROG	$1.4 \times 10^3 - 6.8 \times 10^5$	$3.2 - 1.6 \times 10^3$
HPROG	$1.3 \times 10^3 - 6.4 \times 10^5$	$3.0 - 1.5 \times 10^3$
DIONE	$1.5 \times 10^3 - 7.5 \times 10^5$	$3.5 - 1.7 \times 10^3$
T	$1.5 \times 10^3 - 7.5 \times 10^5$	$3.5 - 1.7 \times 10^3$
E1	$8.2 \times 10^2 - 8.1 \times 10^4$	$5.5 - 5.5 \times 10^2$
E2	$2.6 \times 10^2 - 5.4 \times 10^3$	$5.5 - 1.1 \times 10^2$
DCORTICO	$6.5 \times 10^3 - 3.2 \times 10^6$	$15.1 - 7.6 \times 10^3$
CORTICO	$6.2 \times 10^3 - 3.1 \times 10^6$	$14.4 - 7.2 \times 10^3$
ALDO	$1.1 \times 10^3 - 6.0 \times 10^5$	$2.8 - 1.4 \times 10^3$
DCORT	$6.2 \times 10^3 - 3.1 \times 10^6$	$14.4 - 7.2 \times 10^3$
CORT	$5.9 \times 10^3 - 3.0 \times 10^6$	$13.8 - 6.9 \times 10^3$

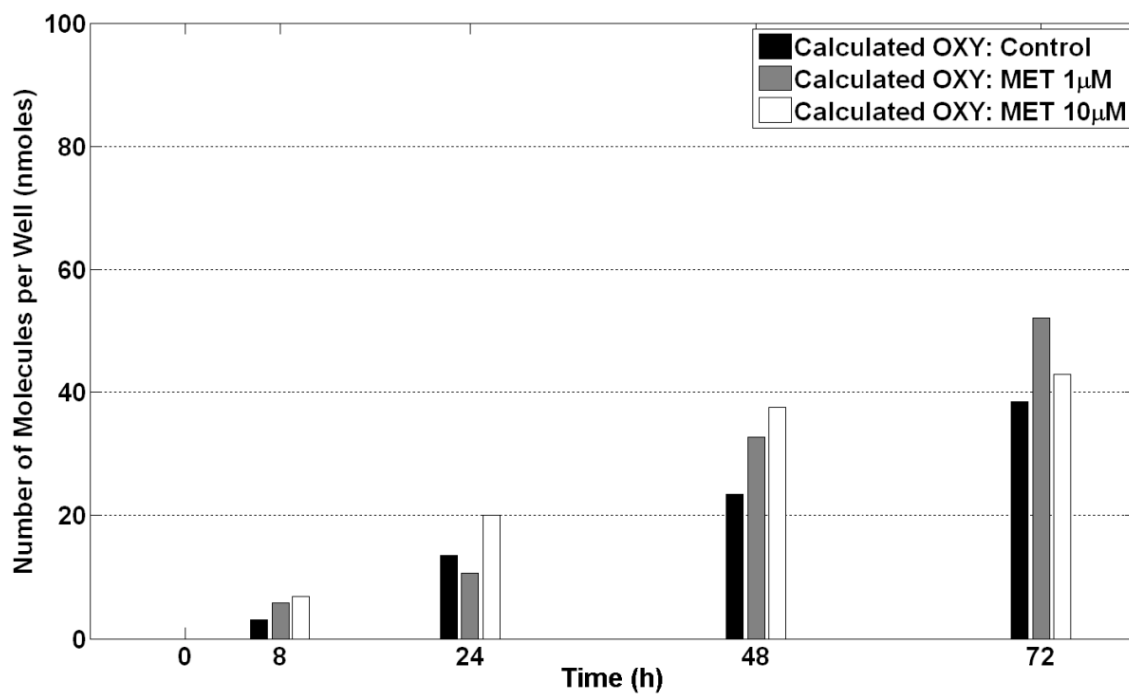
<sup>1</sup> Based on estimated volume of viable cells per well at time = 0 h



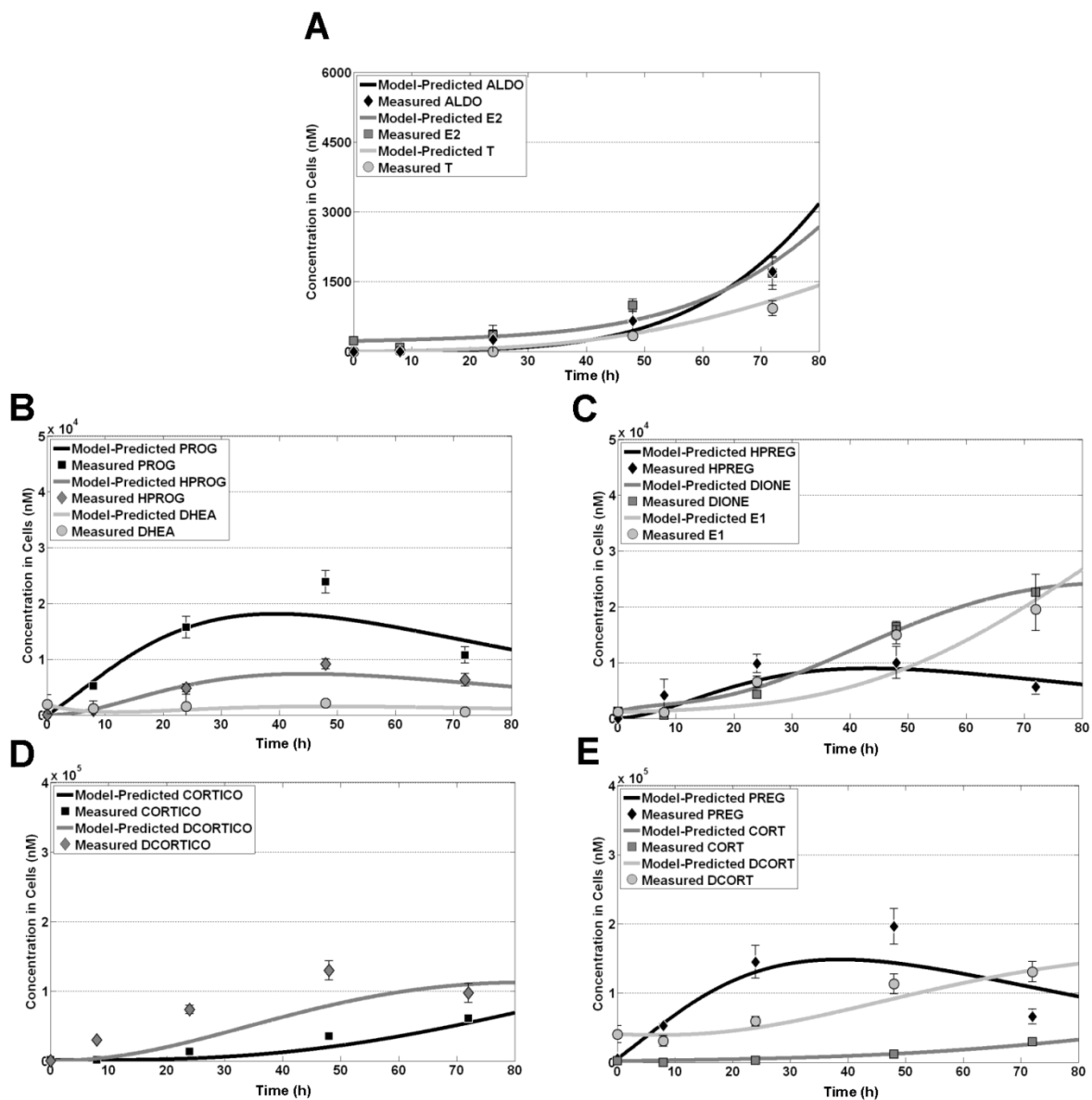
**Supplementary Figure S1.** Graphical representation of the parameters for the mathematical H295R steroidogenesis model. First-order rate constant for cholesterol uptake into the cells is  $k_1$ . First-order rate constants for metabolic processes are:  $k_0, k_2$ -  $k_{18}$ . Reversible first-order rate constants for transport processes ( $k_{+x}$  and  $k_{-x}$  for secretion and import of steroid  $x$ ; respectively) are  $k_{19}$ -  $k_{32}$ . Enzyme inhibition constants for MET are  $k_{41}$  and  $k_{42}$  for CORTICO and CORT pathways, respectively.



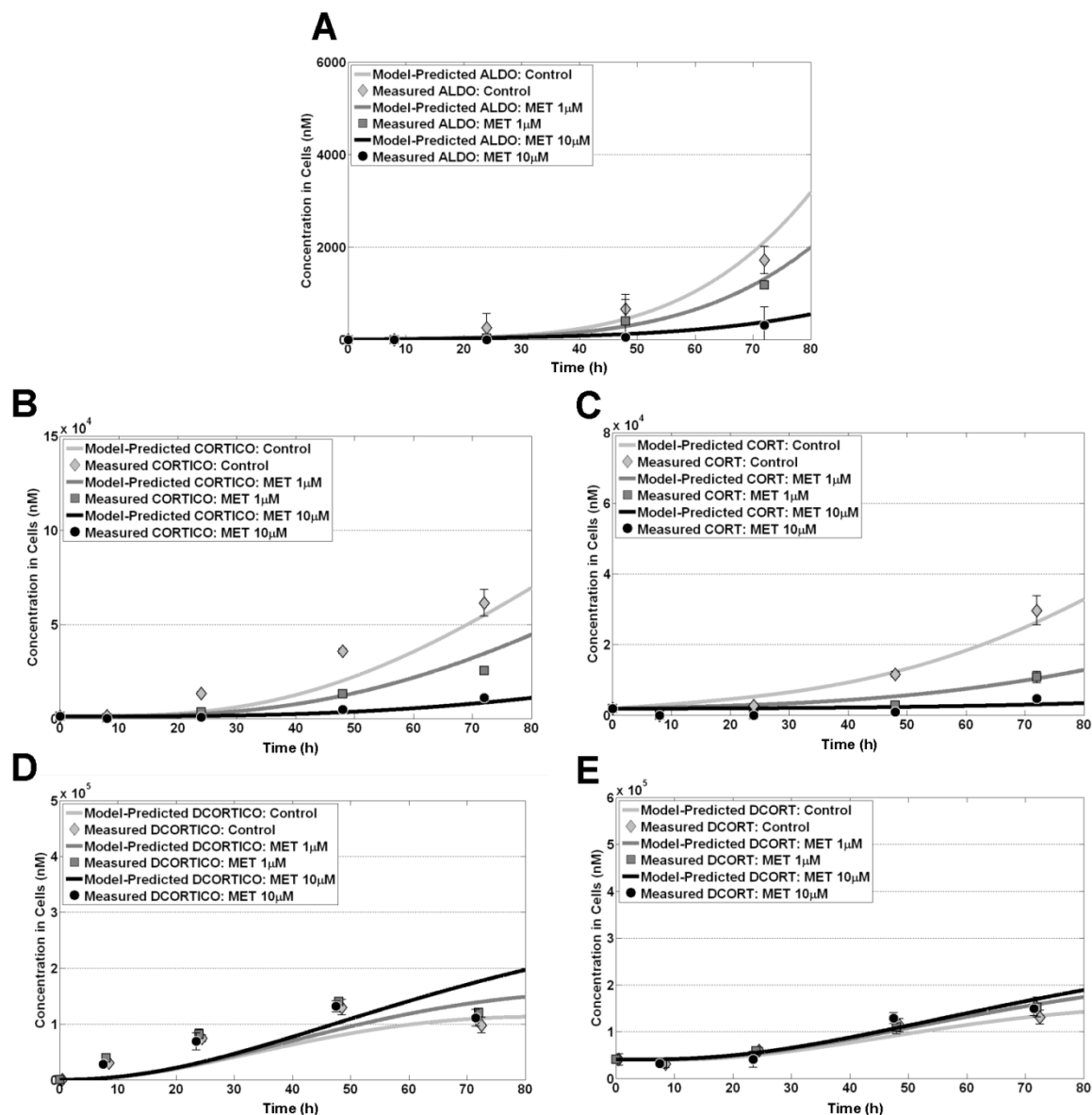
**Supplementary Figure S2.** From cell viability experiments, measured number (A) and percentage (B) of viable H295R cells (mean  $\pm$  SD) were plotted at four post-stimuli incubation periods of 0, 24, 48, 72 h for control and two MET concentrations.



**Supplementary Figure S3.** Time-course of number of calculated OXY molecules for control, 1 μM, and 10 μM MET-exposed cells. Results shown for one experiment since medium concentrations of E1 and E2 at time  $t = 0$  were below sample concentrations in replicate experiments.



**Supplementary Figure S4.** Model evaluation of intracellular steroids for control cells. Time-course of model-predicted concentrations in cells were plotted, and compared to concentrations (mean  $\pm$  SD) measured at five sampling times for ALDO, E2, T (A); PROG, HPROG, DHEA (B); HPREG, DIONE, E1 (C); CORTICO, DCORTICO (D); PREG, CORT, DCORT (E).



**Supplementary Figure S5.** Model evaluation of intracellular steroids in MET-exposed cells. Time-course of model-predicted concentrations in cells were plotted, and compared to concentrations (mean  $\pm$  SD) measured at five sampling times for ALDO (A); CORTICO (B); CORT (C); DCORTICO (D); DCORT (E). For controls, model-predicted and measured concentrations are same as shown in Supplementary Figure S4.

**3. DEVELOPING PREDICTIVE APPROACHES TO CHARACTERIZE ADAPTIVE RESPONSES OF THE REPRODUCTIVE ENDOCRINE AXIS TO AROMATASE INHIBITION: II. COMPUTATIONAL MODELING**

Miyuki Breen, Daniel L. Villeneuve, Gerald T. Ankley, David C. Bencic, Michael S. Breen, Karen H. Watanabe, Alun L. Lloyd, Rory B. Conolly

Published in Toxicological Sciences: 2013; 133: 234-247

Reprinted with permission from Oxford University Press

Miyuki Breen was primarily responsible for model development, simulation, analysis of results, and manuscript writing.

# Developing Predictive Approaches to Characterize Adaptive Responses of the Reproductive Endocrine Axis to Aromatase Inhibition:

## II. Computational Modeling

Miyuki Breen,<sup>\*,†</sup> Daniel L. Villeneuve,<sup>‡</sup> Gerald T. Ankley,<sup>‡</sup> David C. Bencic,<sup>§</sup> Michael S. Breen,<sup>¶</sup> Karen H. Watanabe,<sup>||</sup> Alun L. Lloyd,<sup>†</sup> and Rory B. Conolly<sup>\*,1</sup>

<sup>\*</sup>Integrated Systems Toxicology Division, National Health and Environmental Effects Research Laboratory, U.S. Environmental Protection Agency, Research Triangle Park, North Carolina 27711; <sup>†</sup>Biomathematics Graduate Program, Department of Mathematics, North Carolina State University, Raleigh, North Carolina 27695; <sup>‡</sup>Mid-Continent Ecology Division, National Health and Environmental Effects Research Laboratory, U.S. Environmental Protection Agency, Duluth, Minnesota 55804; <sup>§</sup>Ecological Exposure Research Division, National Exposure Research Laboratory, U.S. Environmental Protection Agency, Cincinnati, Ohio; <sup>¶</sup>National Exposure Research Laboratory, U.S. Environmental Protection Agency, Research Triangle Park, North Carolina 27711; and <sup>||</sup>Department of Environmental and Biomolecular Systems, Oregon Health & Science University, Beaverton, Oregon 97006

<sup>1</sup>To whom correspondence should be addressed at U.S. Environmental Protection Agency, Office of Research and Development, National Health and Environmental Effects Research Laboratory, 109 TW Alexander Dr, Mail B105-03, Research Triangle Park, NC 27711. Fax: 919-541-4284. E-mail: [conolly.rory@epa.gov](mailto:conolly.rory@epa.gov).

Received December 4, 2012; accepted February 27, 2013

Endocrine-disrupting chemicals can affect reproduction and development in humans and wildlife. We developed a computational model of the hypothalamic-pituitary-gonadal (HPG) axis in female fathead minnows to predict dose-response and time-course (DRTC) behaviors for endocrine effects of the aromatase inhibitor, fadrozole (FAD). The model describes adaptive responses to endocrine stress involving regulated secretion of a generic gonadotropin (LH/FSH) from the hypothalamic-pituitary complex. For model development, we used plasma 17 $\beta$ -estradiol (E2) concentrations and ovarian cytochrome P450 (CYP) 19A aromatase mRNA data from two time-course experiments, each of which included both an exposure and a depuration phase, and plasma E2 data from a third 4-day study. Model parameters were estimated using E2 concentrations for 0, 0.5, and 3  $\mu$ g/l FAD exposure concentrations, and good fits to these data were obtained. The model accurately predicted CYP19A mRNA fold changes for controls and three FAD doses (0, 0.5, and 3  $\mu$ g/l) and plasma E2 dose response from the 4-day study. Comparing the model-predicted DRTC with experimental data provided insight into how the feedback control mechanisms in the HPG axis mediate these changes: specifically, adaptive changes in plasma E2 levels occurring during exposure and “overshoot” occurring postexposure. This study demonstrates the value of mechanistic modeling to examine and predict dynamic behaviors in perturbed systems. As this work progresses, we will obtain a refined understanding of how adaptive responses within the vertebrate HPG axis affect DRTC behaviors for aromatase inhibitors and other types of endocrine-active chemicals and apply that knowledge in support of risk assessments.

**Key Words:** endocrine disruptors; biological modeling; non-mammalian species; dose response; biomarkers.

There is international concern regarding effects of endocrine-active environmental contaminants and commercial products on the health of humans and wildlife (Cooper and Kavlock, 1997; Daston *et al.*, 2003; Hutchinson *et al.*, 2006; Zacharewski, 1998). The dose-response and time-course (DRTC) behaviors of those chemicals are major determinants of health risk. In addition to adsorption, distribution, metabolism, and elimination, physiological adaptation (compensation) can affect DRTC behaviors. Characterization of adaptation is critical to modern toxicology as the field evolves from reliance on whole animal testing with apical endpoints toward predictive approaches anchored in understanding modes of action (National Research Council, 2007). The main goal of our current research was to develop a computational model of adaptive mechanisms in the hypothalamic-pituitary-gonadal (HPG) axis for a model vertebrate, the fathead minnow (*Pimephales promelas*).

Several computational models of the HPG axis have been described. For example, models have been developed to predict plasma sex-steroid concentrations and/or vitellogenin (egg yolk protein) concentrations in male fathead minnows exposed to estrogenic chemicals like 17 $\alpha$ -ethinylestradiol or 17 $\beta$ -estradiol (E2) (Watanabe *et al.*, 2009), in female fathead minnows exposed to 17 $\alpha$ -ethinylestradiol or 17 $\beta$ -trenbolone (Li *et al.*, 2011), and in female sciaenid fish exposed to PCBs and cadmium (Murphy *et al.*, 2005). Kim *et al.* (2006) developed a computational model to describe normal functioning of the HPG axis in salmonids. Barton and Andersen (1998) developed a model of the HPG axis in rats to simulate hormone levels in testes and blood. HPG axis models for humans have been

developed to describe changes in luteinizing hormone (LH) and testosterone (T) concentrations following treatment with the gonadotropin-releasing hormone (GnRH) agonist, triptorelin, and the GnRH receptor blocker, degarelix, (Tornøe *et al.*, 2007), as well as the LH-releasing hormone antagonist, cetrorelix (Pechstein *et al.*, 2000).

To increase our understanding of mechanisms of compensation and recovery, we developed a computational model of the HPG axis in female fathead minnows to predict DRTC behaviors for effects of the aromatase inhibitor, fadrozole (FAD). FAD is a model endocrine-active chemical that competitively inhibits the steroidogenic enzyme, aromatase cytochrome P450 (CYP) 19A. Although FAD is not ecologically relevant, there are a variety of environmental contaminants that can inhibit aromatase activity and elicit similar effects (Petkov *et al.*, 2009; Vinggaard *et al.*, 2000). Our model includes a feedback regulatory loop within the HPG axis that mediates adaptive responses to endocrine-active chemical stressors by controlling the secretion of LH and follicle-stimulating hormone (FSH) from a generalized hypothalamic-pituitary complex.

In developing our model, we drew upon data from three separate experiments in which responses of female fathead minnows to FAD exposure were characterized. In the first study (experiment 1), fathead minnows were exposed to FAD via water at 0, 3, or 30  $\mu\text{g/l}$  for 8 days followed by an 8-day recovery phase, with samples collected for various endpoints, including plasma E2 and ovarian CYP19A mRNA (Villeneuve *et al.*, 2009). To increase our understanding of adaptive responses, an additional follow-up experiment was conducted (experiment 2, companion study). Fathead minnows were exposed to 0, 0.5, or 30  $\mu\text{g}$  FAD/l for 8 days followed by 4, 8, 12, 16, or 20 days of recovery in control water, and various endpoints, including plasma E2 and ovarian CYP19A mRNA, were analyzed (Villeneuve *et al.*, 2013—companion paper). Plasma E2 and ovarian CYP19A mRNA data from these two experiments, including recovery, were used for parameter estimation and model evaluation. Experimental design for experiments 1 and 2 are shown in Figure 1. To further evaluate our model, model predictions were tested against plasma E2 data from a third experiment (experiment 3) in which fathead minnows were exposed to 0, 0.04, 0.2, 1, or 5  $\mu\text{g}$  FAD/l for 4 days (Ralston-Hooper *et al.*, 2013).

The measurements from experiments 1 and 2 indicated adaptive changes (compensation) in plasma E2 levels during exposure, which resulted in a period of increased E2 production/concentrations, relative to controls, immediately following removal of the inhibitor (an overshoot), particularly at lower FAD test concentrations (Villeneuve *et al.*, 2009). This type of behavior is not limited to FAD, but it is commonly observed with other endocrine-active chemicals that impact a variety of other pathways: inhibition of CYP11A, CYP17, 3 $\beta$ -hydroxysteroid dehydrogenase, and, even, agonism of the androgen receptor (Ankley *et al.*, 2009, 2011, 2012; Ekman *et al.*, 2011). Moreover,

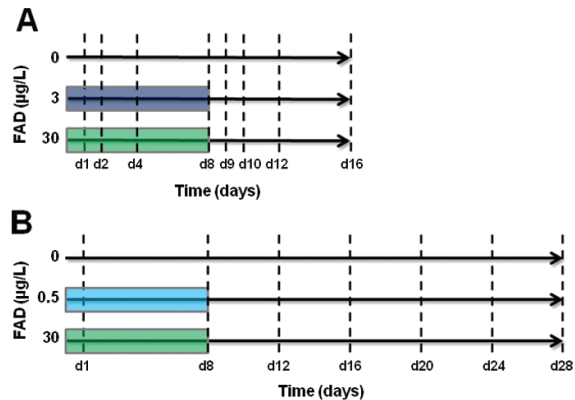


FIG. 1. Overview of design for (A) experiment 1 (Villeneuve *et al.*, 2009) and (B) the portion of experiment 2 (Villeneuve *et al.*, 2013—companion paper). Boxes indicate periods of exposure to FAD. Periods with no box indicates exposure to control water. Vertical dashed lines represents sampling times (days). This figure can be viewed in color online.

although our experimental model was a fish species, due to the significant conservation of the HPG axis structure and function, our model should be broadly extrapolatable to any vertebrate species. The model is intended to aid characterizing how regulatory feedback loops within the vertebrate endocrine axis mediate adaptive responses to endocrine-disrupting chemicals.

## MATERIALS AND METHODS

**Mathematical model of HPG axis.** The computational model of the HPG axis for FAD-exposed female fathead minnows was developed based on knowledge of biological mechanisms. The model consists of six tissue compartments: gill, brain (as a tissue including hypothalamic-pituitary complex), ovary, liver, venous blood, and rest of body (Figs. 2 and 3). The configuration of the compartments involved in HPG axis signaling and feedback control is consistent with the cardiovascular system of the exposed fish. However, because an arterial blood compartment is not essential for this model, it was not included. The model includes a generalized regulatory feedback loop that mediates adaptive responses to endocrine stress within the HPG axis. This negative regulatory loop controls the secretion of gonadotropins (LH and FSH). The time-varying concentrations of substrates are described by dynamic mass balances. We express the dynamic mass balance for the substrates in compartment  $y$  with volume  $V_y$  as

$$V_y \frac{dC_{xy}}{dt} = P_{xy} - U_{xy} - D_{xy} + I_{xy} - S_{xy}, \quad (1)$$

where  $C_{xy}$  is the concentration of substrate  $x$  in compartment  $y$ ,  $P_{xy}$  is the production rate of substrate  $x$  in compartment  $y$ ,  $U_{xy}$  is the utilization rate of substrate  $x$  in compartment  $y$ ,  $D_{xy}$  is the degradation rate of substrate  $x$  in compartment  $y$ ,  $I_{xy}$  is the import rate of substrate  $x$  into compartment  $y$ , and  $S_{xy}$  is the secretion rate of substrate  $x$  from compartment  $y$ . The first two terms on the right side of Equation 1 represent the net metabolic reaction rate of substrate  $x$ . The last two terms represent the net uptake or release rate of substrate  $x$  in compartment  $y$ . The complete set of equations is provided in the Supplementary data. The model code can be obtained from RC at

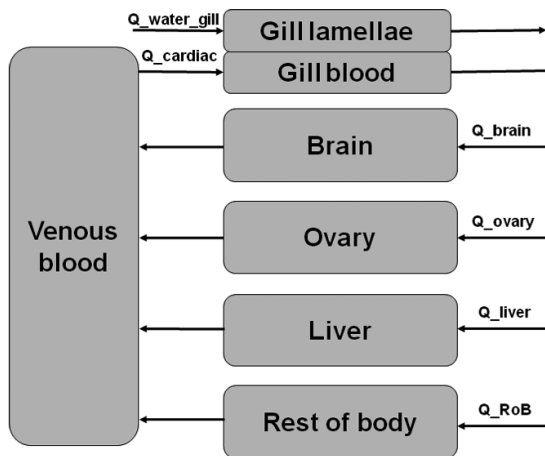


**FIG. 2.** Graphical representation of physiological model of HPG axis for FAD-exposed female fathead minnows. The physiological model consists of water flow through gill lamellae and blood flows between six compartments: gill blood, brain, ovary, liver, rest of body, and venous blood. The parameter values for water and blood flows are shown in Table 1.

conolly.roy@epa.gov. The model for each tissue compartment is described in detail below.

**Gill compartment.** The gill serves as the major route for uptake of FAD from water by fish. There are no data on FAD uptake into skin. However, the rate of uptake into skin and from skin into the systemic circulation is likely to be much slower than via the gills because the gills provide a well-perfused, intimate interface between tank water and fish blood. The computational model thus reflects this assumption that uptake via the gills is the main route of FAD entry into the fish, with skin being at most a minor route that is not quantitatively important. The gill compartment is broken into two subcompartments: gill lamellae and gill blood. The gill lamellae are gas-exchange units with thin-walled, sac-like structures. FAD enters the gills via inspired water with uptake into the venous blood compartment, and FAD is removed from the gills via expired water with release from arterial blood. To determine the FAD concentration in the gill blood, we assume a rapid equilibrium for FAD between water in the gill lamellae and gill blood. No metabolism of substrates is included in the gill compartment. The gills' uptake and elimination of FAD are described by an algebraic expression for the mass balance of FAD entering and leaving the gills based on the method by Ramsey and Andersen (1984).

**Brain compartment.** We represent the brain-pituitary system as a generalized brain compartment. The brain-pituitary system communicates with hormone messengers, and endocrine glands produce and secrete the hormones to subsequent target tissues and glands. The brain initiates the process by sending neural signals. The hypothalamus responds to these neural signals by releasing GnRH, which is transported to the pituitary (Levavi-Sivan *et al.*, 2010). In response to GnRH, the pituitary secretes LH and FSH into the blood that travel to the ovaries and initiates synthesis and secretion of hormones such as T and E2 via G protein-coupled receptor (GPCR) signaling. As part of a closed-loop negative feedback control system, specific hormones secreted by the ovaries (e.g., E2) are transported in the blood to the hypothalamus and pituitary to inhibit secretion of the initial hormone messengers (GnRH, LH, and FSH) (Chang *et al.*, 2009; Levavi-Sivan *et al.*, 2010; Trudeau, 1997).

Because empirical data for the peptide hormone messengers are unavailable, GnRH is not included in our model, and LH and FSH are represented as a generalized gonadotropin (LH/FSH) in our model. The model has zero-order synthesis, first-order release, and first-order degradation of LH/FSH in the brain

compartment. The release of LH/FSH from the brain can be inhibited by E2 secreted from ovary (Chang *et al.*, 2009; Levavi-Sivan *et al.*, 2010; Trudeau, 1997). We model this negative feedback system, which controls the secretion of LH/FSH, by using the Hill function for a repressor with the Hill coefficient set to one. The E2 and FAD are imported into the brain compartment and secreted into the venous blood compartment by blood flow-limited kinetics.

**Ovary compartment.** The pituitary secretes LH and FSH into the blood that travels to the target ovary tissue, where LH and FSH bind to LH and FSH receptors to regulate steroidogenesis in the ovary. In our simplified model, LH/FSH in the venous blood compartment reversibly binds to LH/FSH receptors at the ovarian cell surface to control the synthesis of CYP19A mRNA, which in turn regulates E2 production in the ovary compartment. The model has zero-order synthesis of CYP19A mRNA (basal rate), and CYP19A mRNA synthesis is stimulated by LH/FSH-receptor complex. Synthesized CYP19A mRNA is translated to *cyp19a* (aromatase) by Michaelis-Menten kinetics. Both CYP19A mRNA and *cyp19a* are degraded in the ovary by first-order clearance.

Estradiol and FAD are absorbed into the ovary compartment and secreted into the venous blood compartment by blood flow-limited kinetics. Because intermediate steroid hormone concentrations are unavailable, we did not include a detailed metabolic pathway for steroidogenesis in the present model. Instead, the model includes the conversion of T into E2 by *cyp19a* and competitive inhibition of *cyp19a* by FAD. The concentration of T was set to a literature-reported constant value (Watanabe *et al.*, 2007). The metabolism of T to E2 and the FAD inhibition of *cyp19a* are described by Michaelis-Menten kinetics for competitive inhibition.

**Liver compartment.** Estradiol and FAD are absorbed into the liver compartment and secreted into the venous blood compartment by blood flow-limited kinetics. The model has first-order degradation of E2 and FAD in the liver compartment.

**Venous blood compartment.** E2 and FAD from all the tissue compartments enter the venous blood compartment, as described by blood flow-limited kinetics, and are transported into the gill blood compartment. The LH/FSH are transported into the venous blood compartment and degraded by first-order kinetics. Because LH/FSH are proteins, they do not enter any tissues; however, they will bind to the LH/FSH receptors at the ovarian cell surface to stimulate the synthesis of CYP19A mRNA in the ovary compartment. Free LH/FSH, free LH/FSH receptors at the ovarian cell surface, and LH/FSH-receptor complex dynamics are described in the model.

**Rest of body compartment.** The rest of body compartment includes all tissues except gill, brain, ovary, and liver. E2 and FAD are absorbed into this compartment and secreted into the venous blood compartment by blood flow-limited kinetics.

**Parameter estimation.** The model utilizes physiological and biochemical parameters including tissue compartment volumes, blood flow rates, equilibrium partition coefficients, and biochemical reaction rates (i.e., transcription, translation, metabolism, transport, and degradation). Volumes of the major tissue compartments (ovary, liver, brain) and the whole body were measured in this study. The other physiological parameter values were calculated based on the literature (Table 1). Cardiac output and blood flows were based on measurements from rainbow trout (Nichols *et al.*, 1990, 2004) and were allometrically scaled as described elsewhere (Li *et al.*, 2011; Watanabe *et al.*, 2009). However, cardiac output and blood flows were not scaled for differences in temperature (i.e., 12°C typical for rainbow trout vs. 25°C for fathead minnow). The equilibrium tissue:blood partition coefficients for E2 and blood:water and tissue:blood partition coefficients for FAD were assumed to be one based on our experimental results, which validated our model assumption that plasma concentrations of FAD were likely similar to water concentration. There were 21 biochemical parameters affecting the DRTC behaviors of CYP19A mRNA and E2 for the endocrine effects of FAD: five parameters were obtained from the literature, and 16 parameters were estimated using the mean E2 concentrations from fathead minnow studies. To capture adaptive changes in plasma E2 levels occurring during exposure and a subsequent "overshoot" behavior

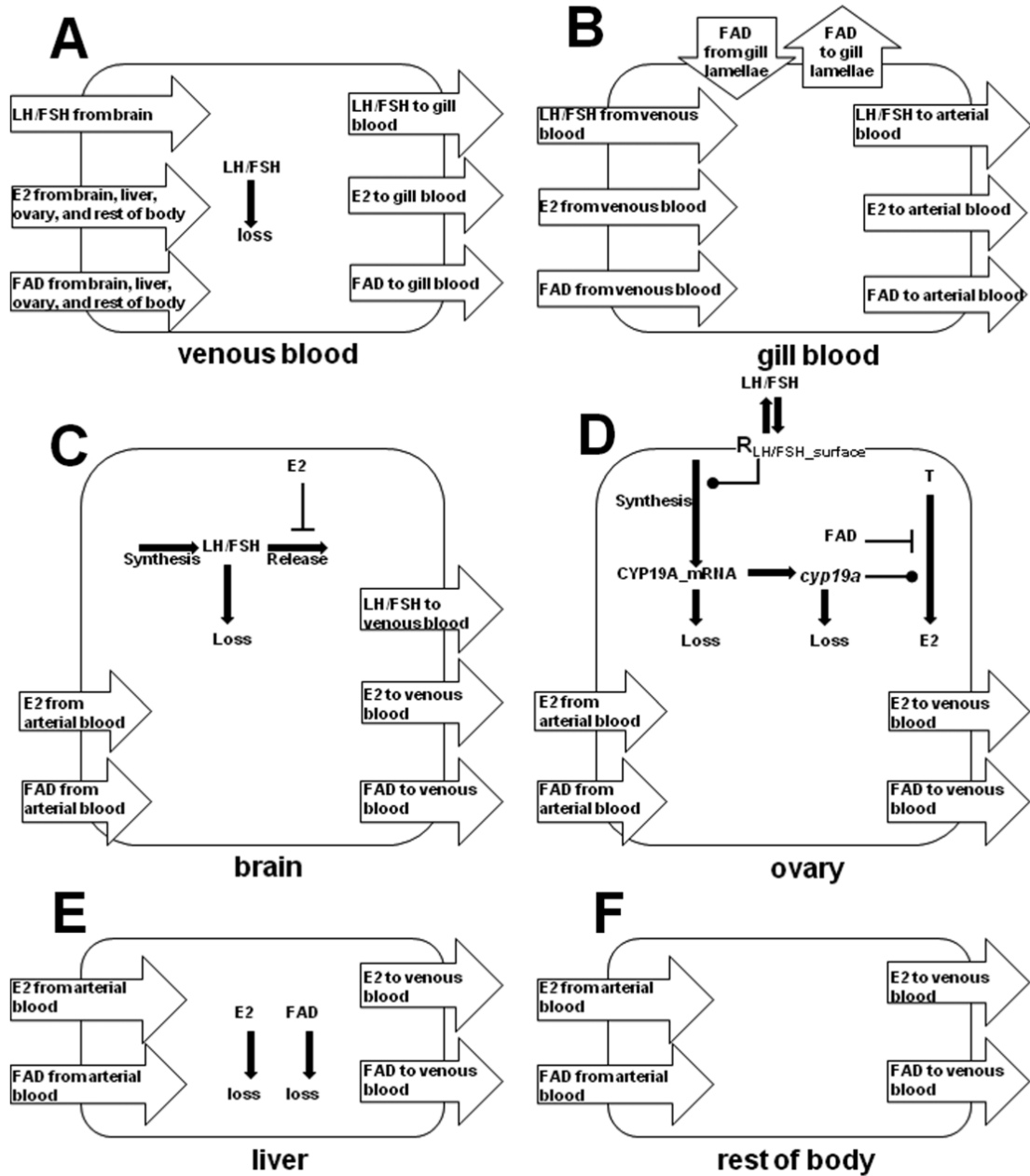


**FIG. 3.** Graphical representation of biochemical processes within the six compartments of the model: venous blood (A), gill blood (B), brain (C), ovary (D), liver (E), and rest of body (F). In the venous blood (A), processes include uptake and release of LH/FSH, E2, and FAD; degradation of LH/FSH. In the gill (B), processes include uptake and release of LH/FSH, E2, and FAD; FAD transport from gill lamellae to gill blood. In the brain (C), processes include uptake and release of FAD and E2; LH/FSH synthesis, release, and degradation; E2-mediated inhibition of LH/FSH release into venous blood. In the ovary (D), processes include uptake and release of FAD and E2; reversible binding of LH/FSH in blood to LH/FSH receptors on cell membrane (surface); LH/FSH receptor-mediated activation of CYP19A\_mRNA synthesis; translation of CYP19A\_mRNA into *cyp19a*; degradation of CYP19A\_mRNA and *cyp19a*; conversion of T into E2 catalyzed by *cyp19a*; enzyme inhibition of *cyp19a* by FAD. In the liver (E), processes include uptake and release of E2 and FAD; degradation of E2 and FAD. In the rest of body (F), processes include uptake and release of FAD and E2.

TABLE 1  
Physiological Constant for Weights, Volumes, Blood Flows, and Partition Coefficients (PC)

Parameter description	Symbol	Compartment	Value	Reference
Weight of whole body	Wt_body	Whole body	$9.451 \times 10^{-4}$ kg	Measured
Volume of whole body	V_body	Whole body	$9.470 \times 10^{-4}$ l	Measured
Cardiac output	Q_cardiac	Whole body	$1.110 \times 10^{-2}$ l/h	$2.06 \text{ Wt\_body}^{0.75}$ based on Nichols <i>et al.</i> (2004), Watanabe <i>et al.</i> (2009), Li <i>et al.</i> (2011)
Weight of gills	Wt_gill	Gill	$1.578 \times 10^{-5}$ kg	Nichols <i>et al.</i> (1996)
Volume of gills	V_gill	Gill	$1.578 \times 10^{-5}$ l	Assumed gill density is 1 kg/l (water density)
Water flow through gills	Q_water_gill	Gill	$5.714 \times 10^{-2}$ l/h	$10.6 \text{ Wt\_body}^{0.75}$ based on Nichols <i>et al.</i> (2004), Watanabe <i>et al.</i> (2009), Li <i>et al.</i> (2011)
Weight of ovary	Wt_ovary	Ovary	$1.488 \times 10^{-4}$ kg	Measured
Volume of ovary	V_ovary	Ovary	$1.440 \times 10^{-4}$ l	Weight/density (1.02 kg/l) from Breen <i>et al.</i> (2007)
Blood flow to ovary	Q_ovary	Ovary	$6.292 \times 10^{-3}$ l/h	$3.6 \text{ Q\_cardiac}(\text{Wt\_ovary}/\text{Wt\_body})$ based on Nichols <i>et al.</i> (1990), Watanabe <i>et al.</i> (2009), Li <i>et al.</i> (2011)
Weight of liver	Wt_liver	Liver	$2.305 \times 10^{-5}$ kg	Measured
Volume of liver	V_liver	Liver	$2.400 \times 10^{-5}$ l	Measured
Blood flow to liver	Q_liver	Liver	$6.500 \times 10^{-4}$ l/h	$2.4 \text{ Q\_cardiac}(\text{Wt\_liver}/\text{Wt\_body})$ based on Nichols <i>et al.</i> (1990), Watanabe <i>et al.</i> (2009), Li <i>et al.</i> (2011)
Weight of brain	Wt_brain	Brain	$1.004 \times 10^{-5}$ kg	Measured
Volume of brain	V_brain	Brain	$1.200 \times 10^{-5}$ l	Measured
Blood flow to brain	Q_brain	Brain	$4.247 \times 10^{-4}$ l/h	$3.6 \text{ Q\_cardiac}(\text{Wt\_brain}/\text{Wt\_body})$ based on Nichols <i>et al.</i> (1990), Watanabe <i>et al.</i> (2009), Li <i>et al.</i> (2011)
Weight of venous	Wt_venous	Venous blood	$2.448 \times 10^{-5}$ kg	Nichols <i>et al.</i> (1996), Robinson <i>et al.</i> (1992)
Volume of venous	V_venous	Venous blood	$2.448 \times 10^{-5}$ l	Weight/density of water (1 kg/l)
Volume of rest of body	V_RoB	Rest of body	$7.267 \times 10^{-4}$ l	$\text{V\_body} - \text{Volume of other organs}$
Blood flow to rest of body	Q_RoB	Rest of body	$3.738 \times 10^{-3}$ l/h	$\text{Q\_cardiac} - \text{Blood flow to other organs}$
Water:blood PC for FAD	P_FAD_water:blood	Gill	1	Assumed
Ovary:blood PC for FAD	P_FAD_ovary:blood	Ovary	1	Assumed
Ovary:blood PC for E2	P_E2_ovary:blood	Ovary	1	Assumed
Liver:blood PC for FAD	P_FAD_liver:blood	Liver	1	Assumed
Liver:blood PC for E2	P_E2_liver:blood	Liver	1	Assumed
Brain:blood PC for FAD	P_FAD_brain:blood	Brain	1	Assumed
Brain:blood PC for E2	P_E2_brain:blood	Brain	1	Assumed
Rest of body:blood PC for FAD	P_FAD_RoB:blood	Rest of body	1	Assumed
Rest of body:blood PC for E2	P_E2_RoB:blood	Rest of body	1	Assumed

occurring postexposure for 3  $\mu\text{g/l}$  FAD dose, model parameters were estimated using E2 concentrations for 0, 0.5, and 3  $\mu\text{g/l}$  FAD doses. The CYP19A mRNA data were not used to estimate model parameters because we validated our model predictions using this dataset. We incorporated measured data from both experiments described above in both parameter estimation and model evaluation.

Using the least squares method, eight parameters in the ovary compartment ( $k_{\text{syn\_mRNA\_basal}}$ ,  $k_{\text{syn\_mRNA\_max}}$ ,  $k_{\text{loss\_mRNA}}$ ,  $V_{\text{max\_syn\_CYP19A}}$ ,  $K_{\text{m\_syn\_CYP19A}}$ ,  $k_{\text{loss\_CYP19A}}$ ,  $K_{\text{FAD}}$ ,  $K_{\text{E2}}$ ), two parameters in the liver compartment ( $k_{\text{loss\_FAD}}$ ,  $k_{\text{loss\_E2}}$ ), four parameters in the brain compartment ( $k_{\text{loss\_LHFSH}}$ ,  $k_{\text{loss\_LHFSH}}$ ,  $k_{\text{loss\_LHFSH}}$ ,  $k_{\text{loss\_LHFSH}}$ ), and two parameters in the venous blood compartment ( $k_{\text{loss\_LHFSH}}$ ,  $k_{\text{loss\_LHFSH}}$ ) were estimated with the time-course data of E2 from the fathead minnow studies. We let  $n_d$  be the number of time points in the time-course data of E2 for the  $d$ th FAD dose (including control);  $C_{\text{E2,blood}}^{d,i}$  be the measured E2 plasma concentrations for the  $d$ th FAD dose at the  $i$ th time;  $C_{\text{E2,blood}}^d(t; \bar{k})$  be the model-predicted concentrations of E2 in the venous blood compartment at the  $i$ th time,  $t_p$ , for the  $d$ th FAD dose (including control),  $C_{\text{FAD}}^d$ , with parameter set

$$\bar{k} = (k_{\text{syn\_mRNA\_basal}}, k_{\text{syn\_mRNA\_max}}, k_{\text{loss\_mRNA}}, V_{\text{max\_syn\_CYP19A}}, K_{\text{m\_syn\_CYP19A}}, k_{\text{loss\_CYP19A}}, K_{\text{FAD}}, K_{\text{E2}}, k_{\text{loss\_FAD}}, k_{\text{loss\_E2}}, k_{\text{loss\_LHFSH}}, k_{\text{loss\_LHFSH}}, k_{\text{loss\_LHFSH}}, k_{\text{loss\_LHFSH}}, k_{\text{loss\_LHFSH}}, k_{\text{loss\_LHFSH}})$$

for  $d = 1, 2, 3$ , and  $i = 1, \dots, n_d$ . Then, the least squares estimate,

$$\bar{k}^* = (k_{\text{syn\_mRNA\_basal}}^*, k_{\text{syn\_mRNA\_max}}^*, k_{\text{loss\_mRNA}}^*, V_{\text{max\_syn\_CYP19A}}^*, K_{\text{m\_syn\_CYP19A}}^*, k_{\text{loss\_CYP19A}}^*, K_{\text{FAD}}^*, K_{\text{E2}}^*, k_{\text{loss\_FAD}}^*, k_{\text{loss\_E2}}^*, k_{\text{loss\_LHFSH}}^*, k_{\text{loss\_LHFSH}}^*, k_{\text{loss\_LHFSH}}^*, k_{\text{loss\_LHFSH}}^*, k_{\text{loss\_LHFSH}}^*, k_{\text{loss\_LHFSH}}^*)$$

is the parameter values  $\bar{k}^*$ , which minimizes the cost function

$$J(\bar{k}) = \sum_{d=1}^3 \sum_{i=1}^{n_d} [C_{\text{E2,blood}}^{d,i} - C_{\text{E2,blood}}^d(t_i; C_{\text{FAD}}^d, \bar{k})]^2. \quad (2)$$

Parameters were estimated with a nonlinear optimization algorithm using MATLAB R2010a (Mathworks, Natick, MA) software. The Nelder-Mead simplex method was used due to its relative insensitivity to the initial parameter values compared with other common methods, such as Newton's method, and its robustness to discontinuities (Nelder and Mead, 1965).

**Sensitivity analysis.** To examine model parameter uncertainty, we performed a sensitivity analysis on 25 parameters: 6 cardiovascular parameters in Table 1 and 19 biochemical parameters in Tables 2 and 3. The sensitivity function relates changes of the model output (plasma E2 concentrations and

TABLE 2  
Fixed Biochemical Parameters

Parameter description	Symbol	Compartment	Value	Reference
Catalysis rate for CYP19A	$k_{cat\_CYP19A}$	Ovary	$6.0093 \times 10^{-4}/h$	Zhao <i>et al.</i> (2001)
Michaelis constant for T	$K_{m\_T}$	Ovary	$0.0096 \mu\text{mol/l}$	Zhao <i>et al.</i> (2001)
Concentration of T	$C_T$	Ovary	$1.4146 \times 10^{-2} \mu\text{mol/l}$	Watanabe <i>et al.</i> (2007)
Total amount of LH/FSH receptor	$A_{R\_LHFSH\_total}$	Ovary	$2.88 \times 10^{-7} \mu\text{mol}$	Miwa <i>et al.</i> (1994)
Binding rate of LH/FSH (blood) to LH/FSH receptor (ovary)	$k_{LHFSH\_on}$	Venous blood	$0.2 \times 10^{-3}/(\mu\text{mol/h})$	Watanabe <i>et al.</i> (2009)

TABLE 3  
Estimated Parameters

Parameter description	Symbol	Compartment	Value
Basal synthesis rate of CYP19A mRNA	$k_{syn\_mRNA\_basal}$	Ovary	$1.474 \times 10^{-5} \mu\text{mol/h}$
Maximum synthesis rate of CYP19A mRNA	$k_{syn\_mRNA\_max}$	Ovary	$9.250 \times 10^{-1} \mu\text{mol/h}$
Degradation rate of CYP19A mRNA	$k_{loss\_mRNA}$	Ovary	$1.494 \times 10^{-2}/h$
Maximum synthesis rate of CYP19A	$V_{max\_syn\_CYP19A}$	Ovary	$3.149 \times 10^{-3} \mu\text{mol/h}$
Michaelis constant for synthesis of CYP19A	$K_{m\_syn\_CYP19A}$	Ovary	$6.537 \times 10^3 \mu\text{mol/l}$
Degradation rate of CYP19A	$k_{loss\_CYP19A}$	Ovary	$1.374 \times 10^{-2}/h$
Inhibition constant of FAD	$K_{i\_FAD}$	Ovary	$1.981 \times 10^{-3} \mu\text{mol/l}$
Activation constant for synthesis of CYP19A mRNA	$K_{a\_syn\_mRNA}$	Ovary	$2.278 \times 10^{-20} \mu\text{mol/l}$
Degradation rate of FAD	$k_{loss\_FAD}$	Liver	$4.698 \times 10^1/h$
Degradation rate of E2	$k_{loss\_E2}$	Liver	$1.167 \times 10^1/h$
Zero-order synthesis rate of LH/FSH	$k_{0\_syn\_LHFSH}$	Brain	$1.726 \times 10^{-9} \mu\text{mol/h}$
Degradation rate of LH/FSH	$k_{loss\_LHFSH}$	Brain	$3.407 \times 10^1/h$
Releasing rate of LH/FSH	$k_{LHFSH}$	Brain	$1.534 \times 10^{-2}/h$
Inhibition constant of E2	$K_{i\_E2}$	Brain	$5.311 \times 10^{-5} \mu\text{mol/l}$
Releasing rate of LH/FSH (blood) from LH/FSH receptor (ovary)	$k_{LHFSH\_off}$	Venous blood	$8.004 \times 10^{-1}/h$
Degradation rate of LH/FSH	$k_{loss\_LHFSH}$	Venous blood	$1.831 \times 10^1/h$

ovarian expression of CYP19A mRNA) to changes in the model parameters. We calculated relative sensitivity functions  $R_{E2,blood,k_i}(t)$  and  $R_{mRNA,ovary,k_i}(t)$  with respect to parameter  $k_i$  for each of the model-predicted concentrations  $C_{E2,blood}$  and fold changes of CYP19AmRNA in the ovary compartment  $F_{mRNA,ovary}$ , respectively, as described by

$$R_{E2,blood,k_i}(t) = \left( \frac{k_i}{C_{E2,blood}(t)} \right) \frac{\partial C_{E2,blood}(t)}{\partial k_i} \quad (3)$$

and

$$R_{mRNA,ovary,k_i}(t) = \left( \frac{k_i}{F_{mRNA,ovary}(t)} \right) \frac{\partial F_{mRNA,ovary}(t)}{\partial k_i}. \quad (4)$$

MATLAB was used to numerically calculate the partial derivatives in  $R_{E2,blood,k_i}(t)$  and  $R_{mRNA,ovary,k_i}(t)$  (Equations 3 and 4) for control and each FAD dose. To rank the relative sensitivities, we calculated the  $L^2$  norm across time for each relative sensitivity function as described by

$$L^2 \text{ norm}(R_{E2,blood,k_i}) = \sqrt{\int |R_{E2,blood,k_i}(t)|^2 dt} \quad (5)$$

and

$$L^2 \text{ norm}(R_{mRNA,ovary,k_i}) = \sqrt{\int |R_{mRNA,ovary,k_i}(t)|^2 dt}. \quad (6)$$

Magnitudes of the relative sensitivities relate the degree to which changes in parameter values lead to changes in model outputs. The sensitivity analysis orders the inputs by importance, identifying the main contributors to the variation in the model outcome. Parameters with high sensitivity are more important for the model output than parameters with low sensitivity.

## RESULTS

### FAD Exposure Data

Exposure to 0.5  $\mu\text{g}$  FAD/l had no considerable effect on either E2 concentrations or CYP19A mRNA expression (Fig. 4). For the 3  $\mu\text{g/l}$  FAD group, E2 concentrations were greatly reduced after 2 days of exposure but recovered to the control level between 2 and 8 days of exposure, exceeded those of controls at 1 day postexposure, and returned to control levels after 2 days postexposure (Fig. 4A). Expression of CYP19A mRNA was greatly elevated after 4 or 8 days of exposure and returned to control levels postexposure period (Fig. 4B). As one would predict, exposure to 30  $\mu\text{g}$  FAD/l had the most considerable effect on E2 concentrations and CYP19A mRNA abundance. The E2 concentrations were greatly reduced within 1 day of exposure to FAD, remained greatly reduced throughout the exposure period, and then rebounded back to the control level during recovery (Fig. 4A). Expression of CYP19A mRNA was greatly elevated at 2 days of exposure and thereafter, but returned to control levels during depuration (Fig. 4B).

### Mathematical Model of HPG Axis

The physiological constants for tissue weights, tissue volumes, blood flows, and partition coefficients are shown in

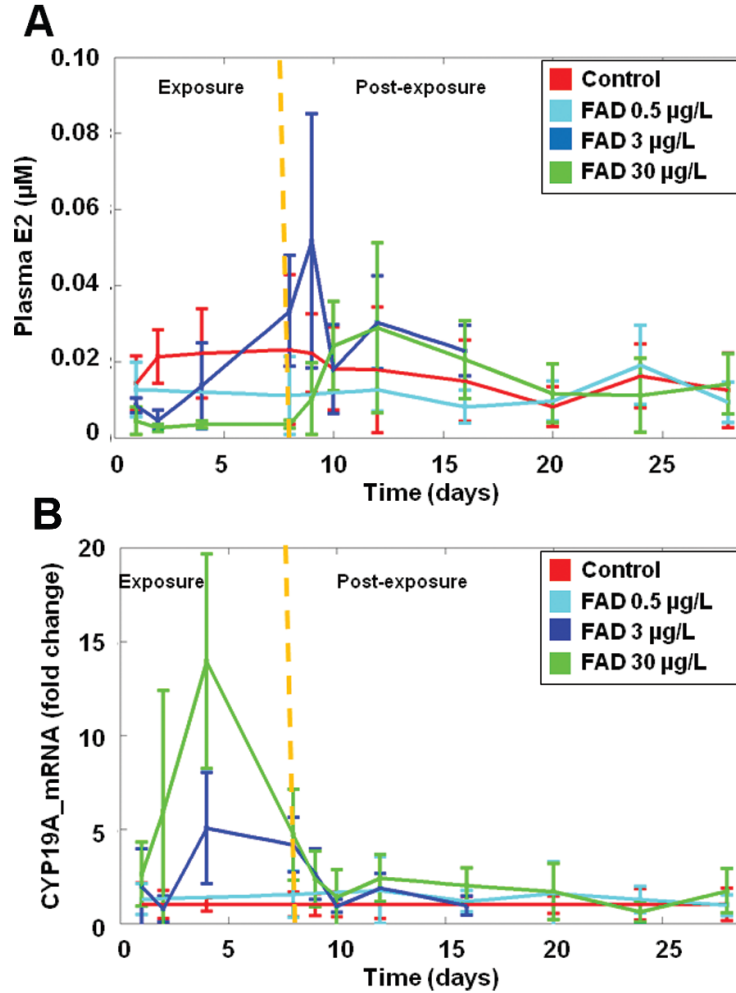


**FIG. 4.** Measurements of plasma E2 (A) and ovary CYP19A\_mRNA (B) for control and three FAD concentrations (0.5, 3, and 30 µg/L). Measurements (mean  $\pm$  SD) of E2 concentrations and CYP19A\_mRNA fold changes relative to controls were plotted from two experiments: control data includes four sampling times during exposure and seven sampling times postexposure; 0.5 µg/L—two sampling times during exposure and five sampling times postexposure; 3 µg/L—four sampling times during exposure and four sampling times postexposure; 30 µg/L—four sampling times during exposure and seven sampling times postexposure.  $n = 16$  for most conditions (combination of treatment and time point) with two experiments (control and FAD concentration of 30 µg/L at d1, d8, d12, and d16) and  $n = 8$  for most conditions with one experiment. Vertical dashed line indicates period of FAD exposure. This figure can be viewed in color online.

**Table 1.** The five literature-derived biochemical parameters and the biochemical parameters estimated by fitting the model predictions to the measured mean plasma E2 concentrations for 0, 0.5, and 3 µg/L FAD doses are shown in **Tables 2 and 3**, respectively. The time for convergence to the solution for the nonlinear parameter estimation was typically around 3 h on an Intel Core 2 Duo processor using MATLAB.

We compared the model-predicted concentrations of venous E2 with time-course measurements of plasma E2. For the FAD doses used for parameter estimation (0, 0.5, and 3 µg/L), the model-predicted E2 concentrations correspond closely to the

mean time-course measurements (**Figs. 5A–C**). For the 3 µg FAD/l treatment, the model captured the plasma E2 compensation during exposure and the overshoot and return to control level postexposure (**Fig. 5C**). For the high FAD dose (30 µg/L), which was not included for parameter estimation, the model-predicted E2 concentrations during exposure also correspond closely to the mean time-course measurements (**Fig. 5D**). However, the model overpredicted E2 concentrations postexposure (**Fig. 5D**). **Figure 6A** shows the modeled venous E2 dose response during FAD exposure on days 1, 4, and 8. The model predictions monotonically decreased across dose, with FAD exposure on day 1

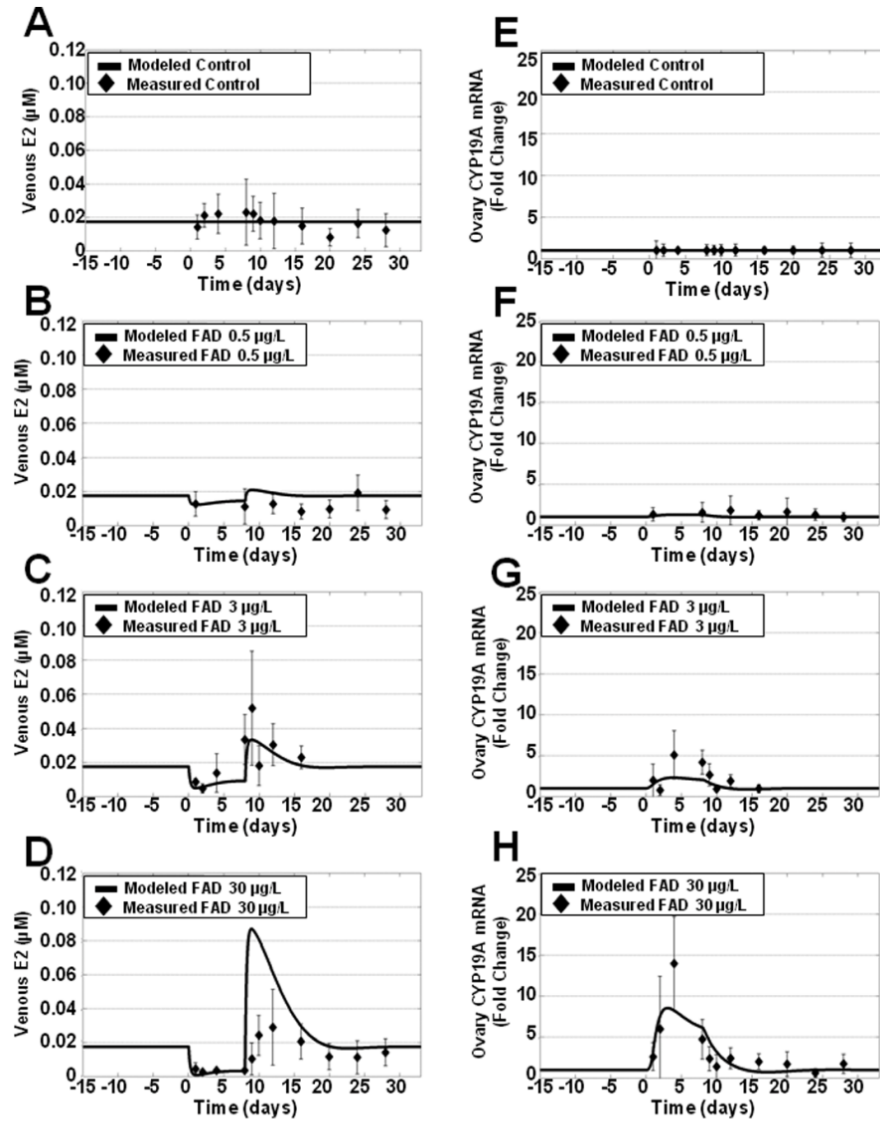
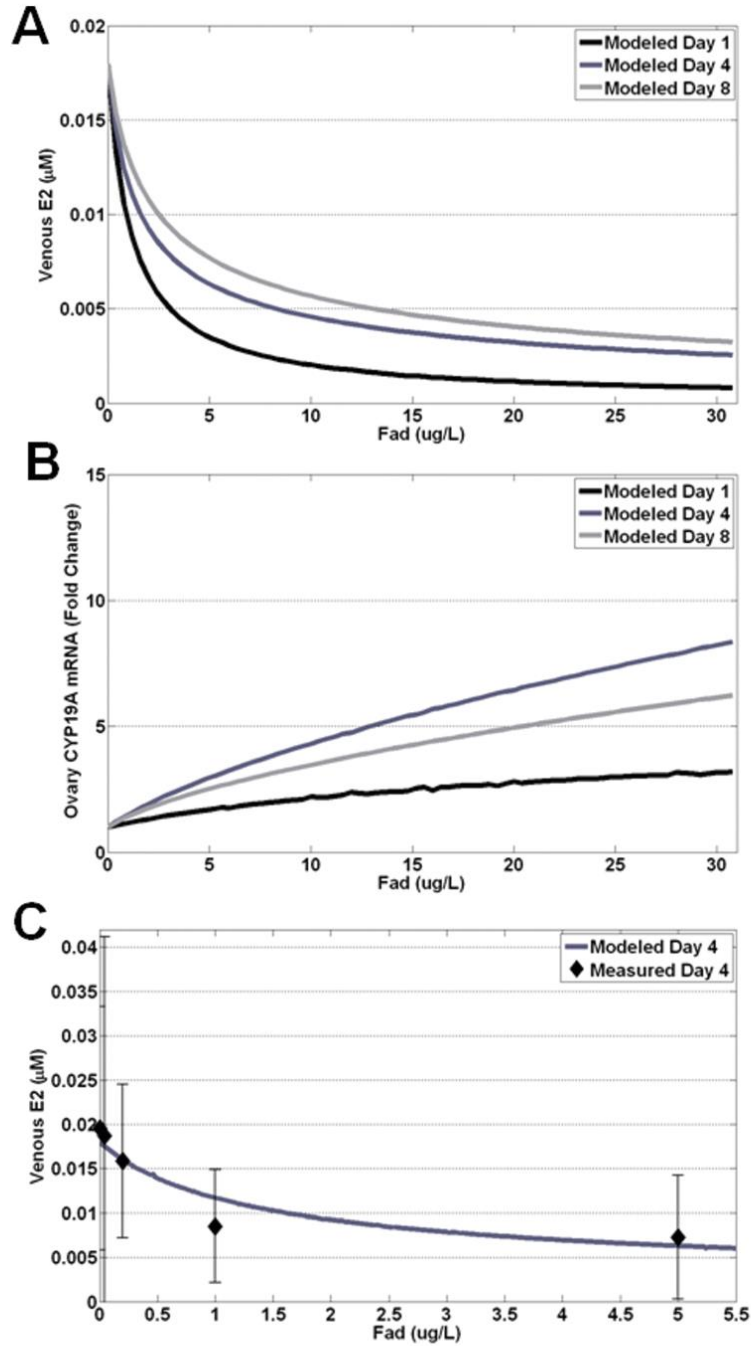


FIG. 5. Model evaluation for control and three FAD concentrations (0.5, 3, and 30  $\mu\text{g/L}$ ). Model predictions were plotted as a function of days during pre-exposure (–15 to 0 days), exposure to FAD (0–8 days), and postexposure (8–33 days) and compared with measurements (mean  $\pm$  SD) for plasma E2 concentrations (A–D) and ovary CYP19A\_mRNA fold changes relative to controls (E–H). Model predictions were compared with measurement data from two experiments: control data include four sampling times during exposure and seven sampling times postexposure; 0.5  $\mu\text{g/L}$ —two sampling times during exposure and five sampling times postexposure; 3  $\mu\text{g/L}$ —four sampling times during exposure and four sampling times postexposure; 30  $\mu\text{g/L}$ —four sampling times during exposure and seven sampling times postexposure. Vertical dashed lines indicate period of FAD exposure.

having the lowest venous E2 concentration and day 8 having the highest venous E2 concentration. Additionally, the model predictions are plotted as a function of FAD concentration and time for venous E2 concentrations (Supplementary fig. S1A).

For model validation, we compared the model-predicted and measured ovary CYP19A mRNA changes. Although

the measurements were not used for parameter optimization, measured ovary CYP19A mRNA fold changes correspond well to the time-course data for control and the three FAD doses (Figs. 5E–H). Figure 6B shows the modeled ovary *cyp19a* dose response during FAD exposure on days 1, 4, and 8. The model predictions monotonically increased across dose, with



**FIG. 6.** Modeled dose response during FAD exposure. Model predictions were plotted as a function of FAD concentrations for venous E2 concentrations (A,C) and ovary CYP19A\_mRNA fold changes relative to controls (B) during exposure to FAD on days 1, 4, and 8. For day 4 (C), measured venous E2 concentrations for five FAD concentrations (0, 0.04, 0.2, 1, and 5  $\mu\text{g/l}$ ) with  $n = 11$  or 12 were plotted with model predictions. Same model predictions are shown in (A) and (C) for FAD concentrations between 0 and 5.5  $\mu\text{g/l}$ .

FAD exposure on day 4 having the highest ovary CYP19A mRNA and day 1 having the lowest ovary CYP19A mRNA. Additionally, the model predictions are plotted as a function of FAD concentration and time for ovary CYP19A mRNA fold changes (Supplementary fig. S1B).

To further validate our model, we tested model predictions against plasma E2 data from the 4 days exposure study that was not included in our model development. The model-predicted dose-response curve for venous E2 corresponds well to plasma E2 measurements, even with all five FAD doses (0, 0.04, 0.2, 1,

and 5  $\mu\text{g FAD/l}$ ) different from the FAD doses used for model calibration (Fig. 6C).

### Sensitivity Analysis

Figs. 7A, B and 8A, B show the relative sensitivities for modeled E2 and CYP19A mRNA, respectively, plotted as a function of the 19 biochemical model parameters for control and three FAD test concentrations (0.5, 3, and 30  $\mu\text{g/l}$ ) during exposure and postexposure, respectively. Overall, E2 (Figs. 7A and B) and CYP19A mRNA (Figs. 8A and B) were highly to

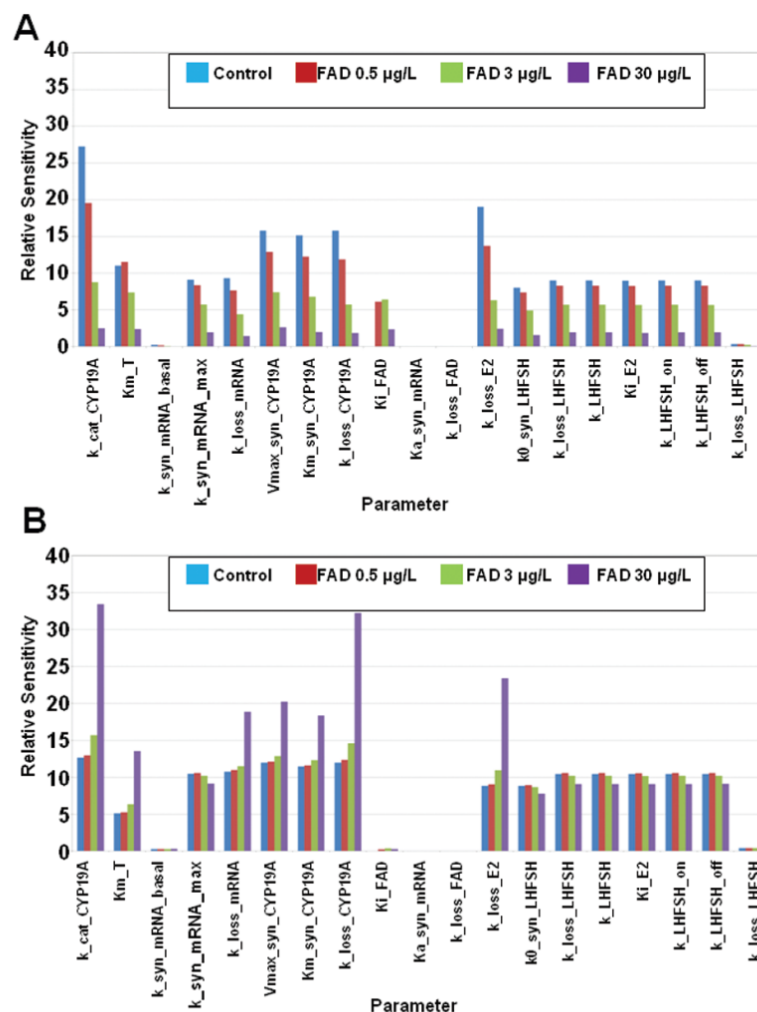
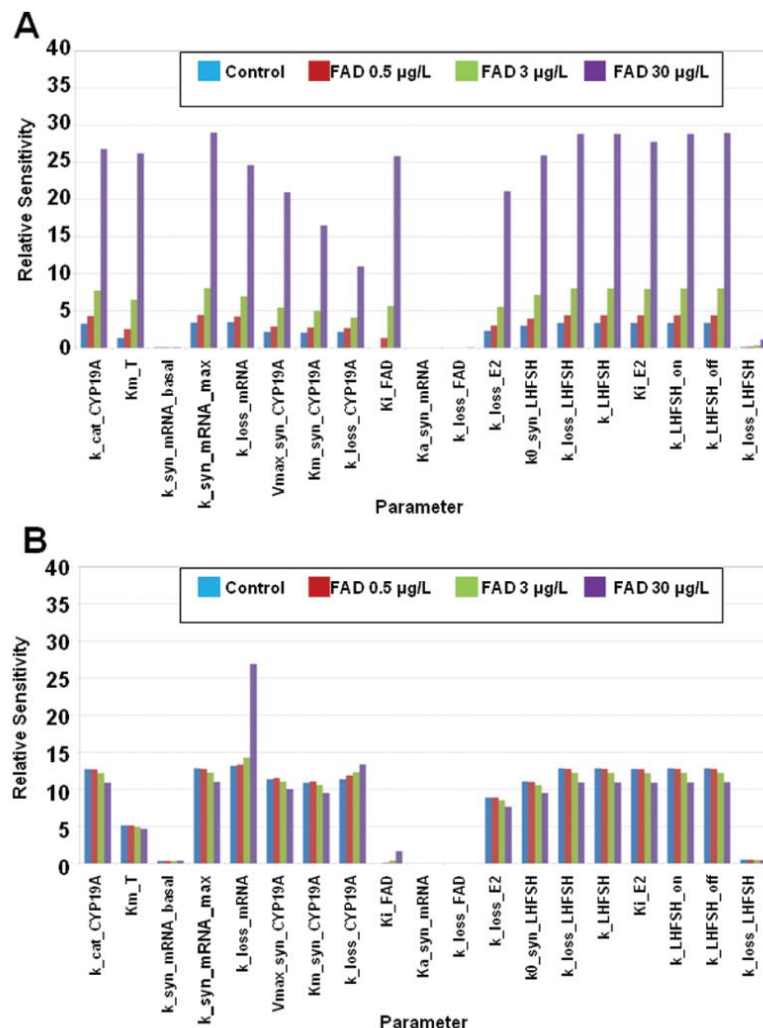


FIG. 7. Relative sensitivities for modeled E2 plotted as a function of the 19 biochemical model parameters for control and three FAD concentrations (0.5, 3, and 30  $\mu\text{g/l}$ ). Each bar represents the  $L^2$  norm of the relative sensitivities across time during exposure (0–8 days; A) and postexposure (8–33 days; B). The values indicate the degree to which changes in parameter values lead to changes in model outputs. This figure can be viewed in color online.



**FIG. 8.** Relative sensitivities for modeled CYP19A\_mRNA plotted as a function of the 19 biochemical model parameters for control and three FAD concentrations (0.5, 3, and 30 µg/l). Each bar represents the  $L^2$  norm of the relative sensitivities across time during exposure (0–8 days; A) and postexposure (8–33 days; B). The values indicate the degree to which changes in parameter values lead to changes in model outputs. This figure can be viewed in color online.

moderately sensitive to the model parameters during exposure and postexposure, except for a few parameters ( $k_{syn\_mRNA\_basal}$ ,  $K_{a\_syn\_mRNA}$ ,  $k_{loss\_FAD}$ ,  $k_{loss\_LHFSH}$ ).

Supplementary figures 2SA,B and 3SA,B show the relative sensitivities for modeled E2 and CYP19A mRNA, respectively, plotted as a function of the six cardiovascular model parameters for control and three FAD test concentrations (0.5, 3, and 30 µg/l) during exposure and postexposure, respectively. Both E2 (Supplementary figs. 2SA and B) and CYP19A mRNA (Supplementary figs. 3SA and B) were most sensitive to

cardiac output ( $Q_{cardiac}$ ) and highly sensitive to blood flow to ovary ( $Q_{ovary}$ ) and rest of body ( $Q_{RoB}$ ) during exposure and postexposure.

## DISCUSSION

To predict the DRTC behaviors for endocrine effects of the aromatase inhibitor, FAD, we developed a mechanistic mathematical model and estimated biochemical parameters for the HPG

axis in female fathead minnows. Experimental gene expression and steroid data were used to develop the computational model. To examine the adaptive responses to FAD, a regulatory feedback loop within the HPG axis that can mediate adaptive responses to endocrine-active chemicals was included in the model. Sensitivity analysis indicates that the regulatory feedback loop plays an important role in our model because E2 and CYP19A mRNA were highly to moderately sensitive to the parameters ( $k_{\text{LHFSH}}$ ,  $K_{\text{E2}}$ ) associated with the feedback control loop. The model closely fits the dynamic E2 concentrations for baseline, 0.5, and 3  $\mu\text{g/l}$  FAD test groups. The model also predicts dynamic CYP19A mRNA fold changes for baseline and three (0.5, 3, and 30  $\mu\text{g/l}$ ) FAD concentrations and venous E2 dose response during FAD exposure (0, 0.04, 0.2, 1, and 5  $\mu\text{g FAD/l}$ ) on day 4.

Our HPG axis model with one negative feedback loop was capable of simulating several important DRTC phenomenon observed empirically. The model predicts declining estradiol concentrations following initial exposure to FAD. Through the feedback loop incorporated into the model, declining E2 concentrations stimulate increased release of a generalized gonadotropin (LH/FSH), leading to increased transcription of CYP19A mRNA and an assumed parallel increase in aromatase activity. The increased aromatase transcription and activity confronted with a constant level of inhibition lead to a modest increase in the predicted venous E2 concentrations over an 8-day period of exposure, which is particularly evident at the 3  $\mu\text{g/l}$  FAD dose. Although the model slightly underpredicts the magnitude of increased E2 production over the course of the exposure period, the general behavior of the model prediction was consistent with that observed empirically. Immediately after chemical removal, the model successfully predicts a brief period over which circulating E2 concentrations in the FAD-treated fish exceed those of controls before gradually returning to normal levels, as CYP19A mRNA transcription and assumed activity decline back to baseline levels. Although ovarian CYP19A mRNA data and plasma E2 data from the 4-day exposure study were not included in model development, the model also captures dynamic CYP19A mRNA fold changes and venous E2 dose response during FAD exposure on day 4. Therefore, our mechanistic model provides a reasonable simulation of critical DRTC behaviors observed *in vivo*.

There are some limitations to our model based on the model structure and assumptions and data available for model evaluation. First, although our feedback mechanism results in a gradual increase in venous E2 concentrations over the course of exposure at the 3  $\mu\text{g/l}$  FAD dose, the model underpredicts the magnitude of compensation observed *in vivo*. This could suggest, for instance, that the current model underestimates the degree of increase in aromatase activity that is currently predicted from a specific fold-change increase in CYP19A mRNA transcription. This is a relationship that could be investigated via additional time-course experiments, as methods to measure both aromatase activity and CYP19A mRNA transcripts are well developed (Villeneuve *et al.*, 2006). Other parameters such as the rate and magnitude of feedback response per unit change in circulating E2 may also play a

role, but the precise mechanisms of the feedback response are not well understood nor can specific measurements of gonadotropin peptide concentrations be made readily for cyprinid fish species like the fathead minnow. Similarly, it is recognized that the ovary of an asynchronous spawning fish species, like fathead minnow, contains a heterogeneous collection of oocytes and ovarian follicles at multiple different stages of development. It is expected that these subpopulations of ovarian cells likely have differential sensitivity or capacity to respond to endocrine feedback (e.g., mediated by FSH/LH); thus, changes in the overall distribution of these different populations in the ovary could also influence the relative magnitudes of response. However, most experiments to date have focused data collection on the tissue level of resolution. Data collected at the level of specific subpopulations of oocytes and ovarian follicles within the ovary are lacking. Second, although our feedback mechanism results in postexposure “overshoot” in venous E2 concentrations at the 30  $\mu\text{g/l}$  FAD dose, the model overpredicts the magnitude of postexposure “overshoot” that was observed *in vivo*. It is likely that there are additional biological phenomena operating *in vivo* that impose limits on the overall magnitude/strength of the compensatory response and the corresponding “overshoot” that occurs when the inhibitor is abruptly removed from the system. Thus, we explored whether the compensatory response may be limited by electron transfer because aromatase and other microsomal type II cytochrome P450 enzymes depend on electron transfer from P450 oxidoreductase for their function (Miller, 2005). We hypothesized that unless the redox partners for aromatase were also induced as part of a compensatory response, electron transfer efficiency could become the limiting rate of estradiol synthesis, even if aromatase transcription and presumably translation continued to increase. We extended our model to evaluate whether such a mechanism could improve the ability of the model to fit the empirical data; however, that was not the case. (Dynamic molecular balance equations for the extended model are provided in the [Supplementary data](#).) Another possible explanation is that E2 production becomes substrate limited. Specifically, T is the C19 steroid precursor that undergoes aromatization to form E2. Within the ovary, T production is localized within the theca cells, whereas aromatization to E2 takes place in the granulosa cells (Yaron, 1995). Some of the key proteins that are rate limiting for T production include StAR and CYP11A (Miller, 1988; Stocco, 2001). It is notable that whereas targets thought to be directly involved in stimulating E2 production by granulosa cells (*cyp19a* and FSHR) were robustly induced in both experiments (Villeneuve *et al.*, 2009, 2013—companion paper), CYP11A and StAR expression was either transiently induced (Villeneuve *et al.*, 2009) or not at all (Villeneuve *et al.* 2013—companion paper). This suggests the possibility that the availability of T could impose limits on the degree of compensatory E2 production that could be achieved by increasing *cyp19a* transcription and translation. In the present experiments, plasma volumes were insufficient to allow for quantification of both E2 and T.

To better understand adaptive responses to endocrine stress, we further investigated another potential feedback regulatory loop within the HPG axis. Based on the observation of an apparent tight, parallel coupling between plasma E2 concentrations and CYP19A mRNA expression in fish exposed to 30 µg FAD/l, we hypothesized an autocrine feedback whereby the internalization of LH/FSH receptors could be stimulated by E2 in ovary to provide a more rapid feedback response to alterations in E2 synthesis rates. This hypothesis was based on the knowledge that many GPCRs go through cycling to and from the cell membrane (McArdle *et al.* 2002). There is sufficient characterization to support the idea that LHR and FSHR undergo this type of cycling (Krishnamurthy *et al.*, 2003). Therefore, we extended our model to include such an additional autocrine feedback loop, which regulates LH and FSH receptor recycling in the ovary. (Dynamic molecular balance equations for the extended model are provided in the [Supplementary data](#).) We hypothesized that the LH/FSH receptors cycle between the ovarian cell surface and cytosol, and the receptors must be at the cell surface to be activated by reversible binding of LH/FSH. However, the extended model with an additional feedback regulatory loop did not improve the model fit for plasma E2 or ovary CYP19A mRNA considerably. This is another example of how the model can be used as a preliminary hypothesis testing tool before proceeding with more expensive and time-consuming experimentation.

There are several potential extensions and applications for our model. First, investigations of other regulatory mechanisms for different test concentrations/doses could be guided by this work. For example, in future studies, we plan to investigate other possible regulatory mechanisms for higher treatment groups using genomic (e.g., microarray) technologies in combination with targeted experiments to quantitatively define the relationships among key events. Second, the model can be extended to endocrine-active chemicals that impact other pathways, including endocrine-active chemicals with multiple modes of action. For instance, in future studies, we plan to extend our model to other aromatase inhibitors with multiple modes of action, such as Prochloraz, an antifungal pesticide with relevance for human risk assessments. Thus, our approach can be expanded to other chemicals that interact with the HPG axis to ultimately provide a generic capability for generating useful predictions of DRTC for disruptions of the HPG axis in fish. Third, our fish model could be modified for other vertebrate species including humans. The endocrine system, which originated during the early evolution of fish, is highly conserved across vertebrate species. Hence, the components of the endocrine system are fundamentally the same for all vertebrates. With the appropriate *in vivo* aromatase inhibition data from other vertebrate species, our model could be modified and reparameterized. Because the modeling approach taken is extendable to other chemicals that interact with the HPG axis and other vertebrate species, it could, with substantial further development, provide a generic capability for generating useful predictions of DRTC for disruptions of the HPG axis for both human and ecological risk assessments.

Comparing model-predicted DRTC with experimental data provided insight into how the feedback control mechanisms embedded in the HPG axis mediate the dynamic dose-response changes. This study demonstrates the value of mechanistic computational modeling to examine and predict the possible dynamic behaviors and to formulate and test hypotheses. As this work progresses, we will obtain a refined understanding of how adaptive responses within the vertebrate HPG axis can affect DRTC behaviors for aromatase inhibitor and other types of endocrine-active chemicals and apply that knowledge in support of risk assessments.

## SUPPLEMENTARY DATA

Supplementary data are available online at <http://toxsci.oxfordjournals.org/>.

## FUNDING

North Carolina State University/Environmental Protection Agency Cooperative Training Program in Environmental Sciences Research (Training Agreement CT833235-01-0 to M.B.).

## ACKNOWLEDGMENTS

We thank Hisham El-Masri and Richard Judson for their review comments and helpful suggestions. Although this manuscript was reviewed by the U.S. Environmental Protection Agency and approved for publication, it may not reflect official Agency policy. Mention of trade names or commercial products does not constitute endorsement or recommendation for use.

## REFERENCES

- Ankley, G. T., Bencic, D. C., Cavallin, J. E., Jensen, K. M., Kahl, M. D., Makynen, E. A., Martinovic, D., Mueller, N. D., Wehmas, L. C., and Villeneuve, D. L. (2009). Dynamic nature of alterations in the endocrine system of fathead minnows exposed to the fungicide prochloraz. *Toxicol. Sci.* **112**, 344–353.
- Ankley, G. T., Cavallin, J. E., Durhan, E. J., Jensen, K. M., Kahl, M. D., Makynen, E. A., Martinovic-Weigelt, D., Wehmas, L. C., and Villeneuve, D. L. (2011). Temporal evaluation of effects of a model 3 $\beta$ -hydroxysteroid dehydrogenase inhibitor on endocrine function in the fathead minnow. *Environ. Toxicol. Chem.* **30**, 2094–2102.
- Ankley, G. T., Cavallin, J. E., Durhan, E. J., Jensen, K. M., Kahl, M. D., Makynen, E. A., Thomas, L. M., Wehmas, L. C., and Villeneuve, D. L. (2012). A time-course analysis of effects of the steroidogenesis inhibitor ketoconazole on components of the hypothalamic-pituitary-gonadal axis of fathead minnows. *Aquat. Toxicol.* **114-115**, 88–95.
- Barton, H. A., and Andersen, M. E. (1998). A model for pharmacokinetics and physiological feedback among hormones of the testicular-pituitary axis in adult male rats: A framework for evaluating effects of endocrine active compounds. *Toxicol. Sci.* **45**, 174–187.
- Breen, M. S., Villeneuve, D. L., Breen, M., Ankley, G. T., and Conolly, R. B. (2007). Mechanistic computational model of ovarian steroidogenesis to predict biochemical responses to endocrine active compounds. *Ann. Biomed. Eng.* **35**, 970–981.

- Chang, J. P., Johnson, J. D., Sawisky, G. R., Grey, C. L., Mitchell, G., Booth, M., Volk, M. M., Parks, S. K., Thompson, E., Goss, G. G., *et al.* (2009). Signal transduction in multifactorial neuroendocrine control of gonadotropin secretion and synthesis in teleosts—studies on the goldfish model. *Gen. Comp. Endocrinol.* **161**, 42–52.
- Cooper, R. L., and Kavlock, R. J. (1997). Endocrine disruptors and reproductive development: A weight-of-evidence overview. *J. Endocrinol.* **152**, 159–166.
- Daston, G. P., Cook, J. C., and Kavlock, R. J. (2003). Uncertainties for endocrine disruptors: Our view on progress. *Toxicol. Sci.* **74**, 245–252.
- Ekman, D. R., Villeneuve, D. L., Teng, Q., Ralston-Hooper, K. J., Martinović-Weigelt, D., Kahl, M. D., Jensen, K. M., Durhan, E. J., Makynen, E. A., Ankley, G. T., *et al.* (2011). Use of gene expression, biochemical and metabolite profiles to enhance exposure and effects assessment of the model androgen 17 $\beta$ -trenbolone in fish. *Environ. Toxicol. Chem.* **30**, 319–329.
- Hutchinson, T. H., Ankley, G. T., Segner, H., and Tyler, C. R. (2006). Screening and testing for endocrine disruption in fish-biomarkers as “signposts,” not “traffic lights,” in risk assessment. *Environ. Health Perspect.* **114**(Suppl. 1), 106–114.
- Kim, J., Hayton, W. L., and Schultz, I. R. (2006). Modeling the brain-pituitary-gonad axis in salmon. *Mar. Environ. Res.* **62**(Suppl.), S426–S432.
- Krishnamurthy, H., Kishi, H., Shi, M., Galet, C., Bhaskaran, R. S., Hirakawa, T., and Ascoli, M. (2003). Postendocytotic trafficking of the follicle-stimulating hormone (FSH)-FSH receptor complex. *Mol. Endocrinol.* **17**, 2162–2176.
- Levavi-Sivan, B., Bogerd, J., Mañanós, E. L., Gómez, A., and Lareyre, J. J. (2010). Perspectives on fish gonadotropins and their receptors. *Gen. Comp. Endocrinol.* **165**, 412–437.
- Li, Z., Kroll, K. J., Jensen, K. M., Villeneuve, D. L., Ankley, G. T., Brian, J. V., Sepúlveda, M. S., Orlando, E. F., Lazorchak, J. M., Kostich, M., *et al.* (2011). A computational model of the hypothalamic-pituitary-gonadal axis in female fathead minnows (*Pimephales promelas*) exposed to 17 $\alpha$ -ethynylestradiol and 17 $\beta$ -trenbolone. *BMC Syst. Biol.* **5**, 63.
- McArdle, C. A., Franklin, J., Green, L., and Hislop, J. N. (2002). Signalling, cycling and desensitisation of gonadotrophin-releasing hormone receptors. *J. Endocrinol.* **173**, 1–11.
- Miller, W. L. (1988). Molecular biology of steroid hormone synthesis. *Endocr. Rev.* **9**, 295–318.
- Miller, W. L. (2005). Minireview: Regulation of steroidogenesis by electron transfer. *Endocrinology* **146**, 2544–2550.
- Miwa, S., Yan, L., and Swanson, P. (1994). Localization of two gonadotropin receptors in the salmon gonad by in vitro ligand autoradiography. *Biol. Reprod.* **50**, 629–642.
- Murphy, C. A., Rose, K. A., and Thomas, P. (2005). Modeling vitellogenesis in female fish exposed to environmental stressors: Predicting the effects of endocrine disturbance due to exposure to a PCB mixture and cadmium. *Reprod. Toxicol.* **19**, 395–409.
- National Research Council. (2007). *Toxicity Testing in the 21st Century: A Vision and a Strategy*. National Academy Press, Washington, DC.
- Nelder, J. A., and Mead, R. (1965). A simplex method for function minimization. *Comput. J.* **7**, 308–313.
- Nichols, J. W., Fitzsimmons, P. N., Whiteman, F. W., Dawson, T. D., Babeu, L., and Juenemann, J. (2004). A physiologically based toxicokinetic model for dietary uptake of hydrophobic organic compounds by fish: I. Feeding studies with 2,2',5,5'-tetrachlorobiphenyl. *Toxicol. Sci.* **77**, 206–218.
- Nichols, J. W., McKim, J. M., Andersen, M. E., Gargas, M. L., Clewell, H. J., 3rd, and Erickson, R. J. (1990). A physiologically based toxicokinetic model for the uptake and disposition of waterborne organic chemicals in fish. *Toxicol. Appl. Pharmacol.* **106**, 433–447.
- Nichols, J. W., McKim, J. M., Lien, G. J., Hoffman, A. D., Bertelsen, S. L., and Elonen, C. M. (1996). A physiologically based toxicokinetic model for dermal absorption of organic chemicals by fish. *Fundam. Appl. Toxicol.* **31**, 229–242.
- Pechstein, B., Nagaraja, N. V., Hermann, R., Romeis, P., Locher, M., and Derendorf, H. (2000). Pharmacokinetic-pharmacodynamic modeling of testosterone and luteinizing hormone suppression by cetrorelix in healthy volunteers. *J. Clin. Pharmacol.* **40**, 266–274.
- Petkov, P. I., Temelkov, S., Villeneuve, D. L., Ankley, G. T., and Mekenyan, O. G. (2009). Mechanism-based categorization of aromatase inhibitors: A potential discovery and screening tool. *SAR QSAR Environ. Res.* **20**, 657–678.
- Ralston-Hooper, K. J., Turner, M. E., Soderblom, E. J., Villeneuve, D., Ankley, G. T., Moseley, M. A., Hoke, R. A., and Ferguson, P. L. (2013). Application of a label-free, gel-free quantitative proteomics method for ecotoxicological studies of small fish species. *Environ. Sci. Technol.* **47**, 1091–1100.
- Ramsey, J. C., and Andersen, M. E. (1984). A physiologically based description of the inhalation pharmacokinetics of styrene in rats and humans. *Toxicol. Appl. Pharmacol.* **73**, 159–175.
- Robinson, D. E., Balter, N. J., and Schwartz, S. L. (1992). A physiologically based pharmacokinetic model for nicotine and cotinine in man. *J. Pharmacokinet. Biopharm.* **20**, 591–609.
- Stocco, D. M. (2001). StAR protein and the regulation of steroid hormone biosynthesis. *Annu. Rev. Physiol.* **63**, 193–213.
- Tørnøe, C. W., Agersø, H., Senderovitz, T., Nielsen, H. A., Madsen, H., Karlsson, M. O., and Jonsson, E. N. (2007). Population pharmacokinetic/pharmacodynamic (PK/PD) modelling of the hypothalamic-pituitary-gonadal axis following treatment with GnRH analogues. *Br. J. Clin. Pharmacol.* **63**, 648–664.
- Trudeau, V. L. (1997). Neuroendocrine regulation of gonadotrophin II release and gonadal growth in the goldfish, *Carassius auratus*. *Rev. Reprod.* **2**, 55–68.
- Villeneuve, D. L., Breen M., Bencic, D. C., Cavallin, J. E., Jensen, K. M., Makynen, E. A., Thomas, L. M., Wehmas, L. C., Conolly, R. B., Ankley, G. T. (2013). Developing predictive approaches to characterize adaptive responses of the reproductive endocrine axis to aromatase inhibition: I. Data generation in a small fish model. *Toxicol. Sci.* **133**, 225–233.
- Villeneuve, D. L., Knoebel, I., Kahl, M. D., Jensen, K. M., Hammermeister, D. E., Greene, K. J., Blake, L. S., and Ankley, G. T. (2006). Relationship between brain and ovary aromatase activity and isoform-specific aromatase mRNA expression in the fathead minnow (*Pimephales promelas*). *Aquat. Toxicol.* **76**, 353–368.
- Villeneuve, D. L., Mueller, N. D., Martinović, D., Makynen, E. A., Kahl, M. D., Jensen, K. M., Durhan, E. J., Cavallin, J. E., Bencic, D., and Ankley, G. T. (2009). Direct effects, compensation, and recovery in female fathead minnows exposed to a model aromatase inhibitor. *Environ. Health Perspect.* **117**, 624–631.
- Vinggaard, A. M., Hnida, C., Breinholt, V., and Larsen, J. C. (2000). Screening of selected pesticides for inhibition of CYP19 aromatase activity in vitro. *Toxicol. In Vitro* **14**, 227–234.
- Watanabe, K. H., Jensen, K. M., Orlando, E. F., and Ankley, G. T. (2007). What is normal? A characterization of the values and variability in reproductive endpoints of the fathead minnow, *Pimephales promelas*. *Comp. Biochem. Physiol. C Toxicol. Pharmacol.* **146**, 348–356.
- Watanabe, K. H., Li, Z., Kroll, K. J., Villeneuve, D. L., Garcia-Reyero, N., Orlando, E. F., Sepúlveda, M. S., Collette, T. W., Ekman, D. R., Ankley, G. T., *et al.* (2009). A computational model of the hypothalamic-pituitary-gonadal axis in male fathead minnows exposed to 17 $\alpha$ -ethynylestradiol and 17 $\beta$ -estradiol. *Toxicol. Sci.* **109**, 180–192.
- Yaron, Z. (1995). Endocrine control of gametogenesis and spawning induction in the carp. *Aquaculture* **129**, 49–73.
- Zacharewski, T. (1998). Identification and assessment of endocrine disruptors: Limitations of in vivo and in vitro assays. *Environ. Health Perspect.* **106**(Suppl. 2), 577–582.
- Zhao, J., Mak, P., Tchoudakova, A., Callard, G., and Chen, S. (2001). Different catalytic properties and inhibitor responses of the goldfish brain and ovary aromatase isozymes. *Gen. Comp. Endocrinol.* **123**, 180–191.

## **Supplemental Data to:**

### **Developing Predictive Approaches to Characterize Adaptive Responses of the Reproductive Endocrine Axis to Aromatase Inhibition: II. Computational Modeling**

Miyuki Breen,<sup>\*,†</sup> Daniel L. Villeneuve,<sup>‡</sup> Gerald T. Ankley,<sup>‡</sup> David C. Bencic,<sup>§</sup> Michael S. Breen,<sup>¶</sup>  
Karen H. Watanabe,<sup>||</sup> Alun L. Lloyd,<sup>†</sup> Rory B. Conolly<sup>\*</sup>

<sup>\*</sup> Integrated Systems Toxicology Division, National Health and Environmental Effects Research Laboratory, U.S. Environmental Protection Agency, Research Triangle Park, NC 27711, USA (breen.miyuki@epa.gov)

<sup>†</sup> Biomathematics Graduate Program, Department of Mathematics, North Carolina State University, Raleigh, NC 27695, USA (alun\_lloyd@ncsu.edu)

<sup>‡</sup> Mid-Continent Ecology Division, National Health and Environmental Effects Research Laboratory, U.S. Environmental Protection Agency, Duluth, MN 55804, USA (villeneuve.dan@epa.gov)

<sup>§</sup> Ecological Exposure Research Division, National Exposure Research Laboratory, U.S. Environmental Protection Agency, Cincinnati, OH, USA (bencic.david@epa.gov)

<sup>¶</sup> National Exposure Research Laboratory, U.S. Environmental Protection Agency, Research Triangle Park, NC 27711, USA (breen.michael@epa.gov)

<sup>||</sup> Department of Environmental and Biomolecular Systems, Oregon Health & Science University, Beaverton, OR 97006, USA (watanabe@ebs.ogi.edu)

#### **Address correspondence to:**

Rory Conolly  
U.S. Environmental Protection Agency  
Office of Research and Development  
National Health and Environmental Effects Research Laboratory  
109 T.W. Alexander Drive, Mail B105-03  
Research Triangle Park, NC 27711  
Telephone: 919-541-9782  
Email: conolly.rory@epa.gov

## **Dynamic molecular balance equations**

### **Gill Compartment**

FAD:

$$C_{\text{FAD\_gill\_blood}} = \frac{Q_{\text{water\_gill}} C_{\text{FAD\_insp\_water}} + Q_{\text{cardiac}} C_{\text{FAD\_venous}}}{Q_{\text{cardiac}} + \frac{Q_{\text{water\_gill}}}{P_{\text{FAD\_water:blood}}}};$$

### **Brain Compartment**

E2:

$$V_{\text{brain}} \frac{dC_{\text{E2\_brain}}}{dt} = Q_{\text{brain}} \left( C_{\text{E2\_arterial}} - \frac{C_{\text{E2\_brain}}}{P_{\text{E2\_brain:blood}}} \right);$$

FAD:

$$V_{\text{brain}} \frac{dC_{\text{FAD\_brain}}}{dt} = Q_{\text{brain}} \left( C_{\text{FAD\_arterial}} - \frac{C_{\text{FAD\_brain}}}{P_{\text{FAD\_brain:blood}}} \right);$$

LH/FSH:

$$V_{\text{brain}} \frac{dC_{\text{LHFSH\_brain}}}{dt} = k_{0\_syn\_LHFSH} - k_{loss\_LHFSH} \cdot A_{\text{LHFSH\_brain}} - \frac{k_{\text{LHFSH}} \cdot A_{\text{LHFSH\_brain}}}{\left( 1 + \frac{C_{\text{E2\_brain}}}{K_{i\_E2}} \right)};$$

### **Ovary Compartment**

FAD:

$$V_{\text{ovary}} \frac{dC_{\text{FAD\_ovary}}}{dt} = Q_{\text{ovary}} \left( C_{\text{FAD\_arterial}} - \frac{C_{\text{FAD\_ovary}}}{P_{\text{FAD\_ovary:blood}}} \right);$$

$$V_{\text{ovary}} \frac{dC_{\text{E2\_ovary}}}{dt} = Q_{\text{ovary}} \left( C_{\text{E2\_arterial}} - \frac{C_{\text{E2\_ovary}}}{P_{\text{E2\_ovary:blood}}} \right) + \frac{V_{\text{max\_CYP19A}} \cdot C_{\text{T}}}{K_{\text{m\_T}} \left( 1 + \frac{C_{\text{FAD\_ovary}}}{K_{\text{i\_FAD}}} \right) + C_{\text{T}}};$$

*cyp19a*:

$$V_{\text{ovary}} \frac{dC_{\text{CYP19A}}}{dt} = \frac{V_{\text{max\_syn\_CYP19A}} \cdot C_{\text{CYP19A\_mRNA}}}{K_{\text{m\_syn\_CYP19A}} + C_{\text{CYP19A\_mRNA}}} - k_{\text{loss\_CYP19A}} \cdot A_{\text{CYP19A}};$$

Vmax of *cyp19a* (conversion of T to E2):

$$V_{\text{max\_CYP19A}} = k_{\text{cat\_CYP19A}} \cdot A_{\text{CYP19A}};$$

CYP19A mRNA:

$$V_{\text{ovary}} \frac{dC_{\text{CYP19A\_mRNA}}}{dt} = k_{\text{syn\_mRNA\_basal}} + \frac{(k_{\text{syn\_mRNA\_max}} - k_{\text{syn\_mRNA\_basal}}) C_{\text{LHFSH\_R\_LHFSH}}}{K_{\text{a\_syn\_mRNA}} + C_{\text{LHFSH\_R\_LHFSH}}} - k_{\text{loss\_mRNA}} \cdot A_{\text{CYP19A\_mRNA}};$$

## Liver Compartment

FAD:

$$V_{\text{liver}} \frac{dC_{\text{FAD\_liver}}}{dt} = Q_{\text{liver}} \left( C_{\text{FAD\_arterial}} - \frac{C_{\text{FAD\_liver}}}{P_{\text{FAD\_liver:blood}}} \right) - k_{\text{loss\_FAD}} \cdot A_{\text{FAD\_liver}};$$

E2:

$$V_{\text{liver}} \frac{dC_{\text{E2\_liver}}}{dt} = Q_{\text{liver}} \left( C_{\text{E2\_arterial}} - \frac{C_{\text{E2\_liver}}}{P_{\text{E2\_liver:blood}}} \right) - k_{\text{loss\_E2}} \cdot A_{\text{E2\_liver}};$$

## Venous Blood Compartment

LH/FSH-receptor complex:

$$\frac{dA_{\text{LHFSH\_R\_LHFSH}}}{dt} = k_{\text{LHFSH\_on}} \cdot A_{\text{LHFSH\_venous\_free}} \cdot A_{\text{R\_LHFSH\_free}} - k_{\text{LHFSH\_off}} \cdot A_{\text{LHFSH\_R\_LHFSH}},$$

where  $A_{\text{R\_LHFSH\_free}} = A_{\text{R\_LHFSH}} - A_{\text{LHFSH\_R\_LHFSH}}$

and  $A_{\text{LHFSH\_venous\_free}} = A_{\text{LHFSH\_venous}} - A_{\text{LHFSH\_R\_LHFSH}}$ ;

LH/FSH:

$$V_{\text{venous}} \frac{dC_{\text{LHFSH\_venous}}}{dt} = \frac{k_{\text{LHFSH}} \cdot A_{\text{LHFSH\_brain}}}{\left(1 + \frac{C_{\text{E2\_brain}}}{K_{\text{i\_E2}}}\right)} - k_{\text{loss\_LHFSH}} \cdot A_{\text{LHFSH\_venous\_free}};$$

E2:

$$V_{\text{venous}} \frac{dC_{\text{E2\_venous}}}{dt} = Q_{\text{liver}} \left( \frac{C_{\text{E2\_liver}}}{P_{\text{E2\_liver:blood}}} \right) + Q_{\text{ovary}} \left( \frac{C_{\text{E2\_ovary}}}{P_{\text{E2\_ovary:blood}}} \right) + Q_{\text{brain}} \left( \frac{C_{\text{E2\_brain}}}{P_{\text{E2\_brain:blood}}} \right) + Q_{\text{RoB}} \left( \frac{C_{\text{E2\_RoB}}}{P_{\text{E2\_RoB:blood}}} \right) - Q_{\text{cardiac}} C_{\text{E2\_venous}};$$

FAD:

$$V_{\text{venous}} \frac{dC_{\text{FAD\_venous}}}{dt} = Q_{\text{liver}} \left( \frac{C_{\text{FAD\_liver}}}{P_{\text{FAD\_liver:blood}}} \right) + Q_{\text{ovary}} \left( \frac{C_{\text{FAD\_ovary}}}{P_{\text{FAD\_ovary:blood}}} \right) + Q_{\text{brain}} \left( \frac{C_{\text{FAD\_brain}}}{P_{\text{FAD\_brain:blood}}} \right) + Q_{\text{RoB}} \left( \frac{C_{\text{FAD\_RoB}}}{P_{\text{FAD\_RoB:blood}}} \right) - Q_{\text{cardiac}} C_{\text{FAD\_venous}};$$

## Rest of Body Compartment

FAD:

$$V_{\text{RoB}} \frac{dC_{\text{FAD\_RoB}}}{dt} = Q_{\text{RoB}} \left( C_{\text{FAD\_arterial}} - \frac{C_{\text{FAD\_Rob}}}{P_{\text{FAD\_RoB:blood}}} \right);$$

E2:

$$V_{\text{RoB}} \frac{dC_{\text{E2\_RoB}}}{dt} = Q_{\text{RoB}} \left( C_{\text{E2\_arterial}} - \frac{C_{\text{E2\_Rob}}}{P_{\text{E2\_RoB:blood}}} \right);$$

## **Dynamic molecular balance equations for “electron transfer” hypothesis**

### **Gill Compartment**

FAD:

$$C_{\text{FAD\_gill\_blood}} = \frac{Q_{\text{water\_gill}} C_{\text{FAD\_insp\_water}} + Q_{\text{cardiac}} C_{\text{FAD\_venous}}}{Q_{\text{cardiac}} + \frac{Q_{\text{water\_gill}}}{P_{\text{FAD\_water:blood}}}};$$

### **Brain Compartment**

E2:

$$V_{\text{brain}} \frac{dC_{\text{E2\_brain}}}{dt} = Q_{\text{brain}} \left( C_{\text{E2\_arterial}} - \frac{C_{\text{E2\_brain}}}{P_{\text{E2\_brain:blood}}} \right);$$

FAD:

$$V_{\text{brain}} \frac{dC_{\text{FAD\_brain}}}{dt} = Q_{\text{brain}} \left( C_{\text{FAD\_arterial}} - \frac{C_{\text{FAD\_brain}}}{P_{\text{FAD\_brain:blood}}} \right);$$

LH/FSH:

$$V_{\text{brain}} \frac{dC_{\text{LHFSH\_brain}}}{dt} = k_{0\_syn\_LHFSH} - k_{loss\_LHFSH} \cdot A_{\text{LHFSH\_brain}} - \frac{k_{\text{LHFSH}} \cdot A_{\text{LHFSH\_brain}}}{\left( 1 + \frac{C_{\text{E2\_brain}}}{K_{i\_E2}} \right)};$$

## Ovary Compartment

FAD:

$$V_{\text{ovary}} \frac{dC_{\text{FAD\_ovary}}}{dt} = Q_{\text{ovary}} \left( C_{\text{FAD\_arterial}} - \frac{C_{\text{FAD\_ovary}}}{P_{\text{FAD\_ovary:blood}}} \right);$$

E2:

$$V_{\text{ovary}} \frac{dC_{\text{E2\_ovary}}}{dt} = Q_{\text{ovary}} \left( C_{\text{E2\_arterial}} - \frac{C_{\text{E2\_ovary}}}{P_{\text{E2\_ovary:blood}}} \right) + \frac{V_{\text{max\_CYP19A}} \cdot C_{\text{T}}}{K_{\text{m\_T}} \left( 1 + \frac{C_{\text{FAD\_ovary}}}{K_{\text{i\_FAD}}} \right) + C_{\text{T}}};$$

*cyp19a*:

$$V_{\text{ovary}} \frac{dC_{\text{CYP19A}}}{dt} = \frac{V_{\text{max\_syn\_CYP19A}} \cdot C_{\text{CYP19A\_mRNA}}}{K_{\text{m\_syn\_CYP19A}} + C_{\text{CYP19A\_mRNA}}} - k_{\text{loss\_CYP19A}} \cdot A_{\text{CYP19A}};$$

Vmax of *cyp19a* (conversion of T to E2):

$$V_{\text{max\_CYP19A}} = k_{\text{cat\_CYP19A}} \cdot A_{\text{CYP19A}};$$

CYP19A mRNA:

$$V_{\text{ovary}} \frac{dC_{\text{CYP19A\_mRNA}}}{dt} = k_{\text{syn\_mRNA\_basal}} + \frac{(k_{\text{syn\_mRNA\_max}} - k_{\text{syn\_mRNA\_basal}}) C_{\text{LHFSH\_R\_LHFSH}}}{K_{\text{a\_syn\_mRNA}} + C_{\text{LHFSH\_R\_LHFSH}}} - k_{\text{loss\_mRNA}} \cdot A_{\text{CYP19A\_mRNA}};$$

## Liver Compartment

FAD:

$$V_{\text{liver}} \frac{dC_{\text{FAD\_liver}}}{dt} = Q_{\text{liver}} \left( C_{\text{FAD\_arterial}} - \frac{C_{\text{FAD\_liver}}}{P_{\text{FAD\_liver: blood}}} \right) - k_{\text{loss\_FAD}} \cdot A_{\text{FAD\_liver}};$$

E2:

$$V_{\text{liver}} \frac{dC_{\text{E2\_liver}}}{dt} = Q_{\text{liver}} \left( C_{\text{E2\_arterial}} - \frac{C_{\text{E2\_liver}}}{P_{\text{E2\_liver: blood}}} \right) - k_{\text{loss\_E2}} \cdot A_{\text{E2\_liver}};$$

## Venous Blood Compartment

LH/FSH-receptor complex:

$$\begin{aligned} \frac{dA_{\text{LHFSH\_R\_LHFSH}}}{dt} = & k_{\text{LHFSH\_on}} \cdot A_{\text{LHFSH\_venous\_free}} \cdot A_{\text{R\_LHFSH\_free}} \\ & - k_{\text{LHFSH\_off}} \cdot A_{\text{LHFSH\_R\_LHFSH}}, \end{aligned}$$

where  $A_{\text{R\_LHFSH\_free}} = A_{\text{R\_LHFSH}} - A_{\text{LHFSH\_R\_LHFSH}}$

and  $A_{\text{LHFSH\_venous\_free}} = A_{\text{LHFSH\_venous}} - A_{\text{LHFSH\_R\_LHFSH}};$

LH/FSH:

$$V_{\text{venous}} \frac{dC_{\text{LHFSH\_venous}}}{dt} = \frac{k_{\text{LHFSH}} \cdot A_{\text{LHFSH\_brain}}}{\left( 1 + \frac{C_{\text{E2\_brain}}}{K_{\text{I\_E2}}} \right)} - k_{\text{loss\_LHFSH}} \cdot A_{\text{LHFSH\_venous\_free}} - Q_{\text{cardiac}} C_{\text{LHFSH\_venous\_free}};$$

E2:

$$\begin{aligned} V_{\text{venous}} \frac{dC_{\text{E2\_venous}}}{dt} = & Q_{\text{liver}} \left( \frac{C_{\text{E2\_liver}}}{P_{\text{E2\_liver: blood}}} \right) + Q_{\text{ovary}} \left( \frac{C_{\text{E2\_ovary}}}{P_{\text{E2\_ovary: blood}}} \right) \\ & + Q_{\text{brain}} \left( \frac{C_{\text{E2\_brain}}}{P_{\text{E2\_brain: blood}}} \right) + Q_{\text{RoB}} \left( \frac{C_{\text{E2\_RoB}}}{P_{\text{E2\_RoB: blood}}} \right) - Q_{\text{cardiac}} C_{\text{E2\_venous}}; \end{aligned}$$

FAD:

$$V_{\text{venous}} \frac{dC_{\text{FAD\_venous}}}{dt} = Q_{\text{liver}} \left( \frac{C_{\text{FAD\_liver}}}{P_{\text{FAD\_liver:blood}}} \right) + Q_{\text{ovary}} \left( \frac{C_{\text{FAD\_ovary}}}{P_{\text{FAD\_ovary:blood}}} \right) \\ + Q_{\text{brain}} \left( \frac{C_{\text{FAD\_brain}}}{P_{\text{FAD\_brain:blood}}} \right) + Q_{\text{RoB}} \left( \frac{C_{\text{FAD\_RoB}}}{P_{\text{FAD\_RoB:blood}}} \right) - Q_{\text{cardiac}} C_{\text{FAD\_venous}};$$

## Rest of Body Compartment

FAD:

$$V_{\text{RoB}} \frac{dC_{\text{FAD\_RoB}}}{dt} = Q_{\text{RoB}} \left( C_{\text{FAD\_arterial}} - \frac{C_{\text{FAD\_RoB}}}{P_{\text{FAD\_RoB:blood}}} \right);$$

E2:

$$V_{\text{RoB}} \frac{dC_{\text{E2\_RoB}}}{dt} = Q_{\text{RoB}} \left( C_{\text{E2\_arterial}} - \frac{C_{\text{E2\_RoB}}}{P_{\text{E2\_RoB:blood}}} \right);$$

## Dynamic molecular balance equations for “autocrine feedback” hypothesis

### Gill Compartment

FAD:

$$C_{\text{FAD\_gill\_blood}} = \frac{Q_{\text{water\_gill}} C_{\text{FAD\_insp\_water}} + Q_{\text{cardiac}} C_{\text{FAD\_venous}}}{Q_{\text{cardiac}} + \frac{Q_{\text{water\_gill}}}{P_{\text{FAD\_water:blood}}}};$$

### Brain Compartment

E2:

$$V_{\text{brain}} \frac{dC_{\text{E2\_brain}}}{dt} = Q_{\text{brain}} \left( C_{\text{E2\_arterial}} - \frac{C_{\text{E2\_brain}}}{P_{\text{E2\_brain:blood}}} \right);$$

FAD:

$$V_{\text{brain}} \frac{dC_{\text{FAD\_brain}}}{dt} = Q_{\text{brain}} \left( C_{\text{FAD\_arterial}} - \frac{C_{\text{FAD\_brain}}}{P_{\text{FAD\_brain:blood}}} \right);$$

LH/FSH:

$$V_{\text{brain}} \frac{dC_{\text{LHFSH\_brain}}}{dt} = k_{0\_syn\_LHFSH} - k_{\text{loss\_LHFSH}} \cdot A_{\text{LHFSH\_brain}} - \frac{k_{\text{LHFSH}} \cdot A_{\text{LHFSH\_brain}}}{\left(1 + \frac{C_{\text{E2\_brain}}}{K_{i\_E2}}\right)};$$

## Ovary Compartment

FAD:

$$V_{\text{ovary}} \frac{dC_{\text{FAD\_ovary}}}{dt} = Q_{\text{ovary}} \left( C_{\text{FAD\_arterial}} - \frac{C_{\text{FAD\_ovary}}}{P_{\text{FAD\_ovary:blood}}} \right);$$

E2:

$$V_{\text{ovary}} \frac{dC_{\text{E2\_ovary}}}{dt} = Q_{\text{ovary}} \left( C_{\text{E2\_arterial}} - \frac{C_{\text{E2\_ovary}}}{P_{\text{E2\_ovary:blood}}} \right) + \left[ \frac{V_{\text{max\_CYP19A}} \cdot C_{\text{T}}}{K_{\text{m\_T}} \left( 1 + \frac{C_{\text{FAD\_ovary}}}{K_{i\_FAD}} \right) + C_{\text{T}}} \right] \left[ \frac{A_{\text{CYP19A\_elec}}}{K_{\text{a\_transfer\_CYP19A\_elec}} + A_{\text{CYP19A\_elec}}} \right];$$

*cyp19a* electron:

$$\frac{dA_{\text{CYP19A\_elec}}}{dt} = k_{\text{syn\_CYP19A\_elec}} - k_{\text{loss\_CYP19A\_elec}} \cdot A_{\text{CYP19A\_elec}} - \left[ \frac{V_{\text{max\_CYP19A}} \cdot C_{\text{T}}}{K_{\text{m\_T}} \left( 1 + \frac{C_{\text{FAD\_ovary}}}{K_{i\_FAD}} \right) + C_{\text{T}}} \right] \left[ \frac{A_{\text{CYP19A\_elec}}}{K_{\text{a\_transfer\_CYP19A\_elec}} + A_{\text{CYP19A\_elec}}} \right];$$

*cyp19a*:

$$V_{\text{ovary}} \frac{dC_{\text{CYP19A}}}{dt} = \frac{V_{\text{max\_syn\_CYP19A}} \cdot C_{\text{CYP19A\_mRNA}}}{K_{\text{m\_syn\_CYP19A}} + C_{\text{CYP19A\_mRNA}}} - k_{\text{loss\_CYP19A}} \cdot A_{\text{CYP19A}};$$

Vmax of *cyp19a* (conversion of T to E2):

$$V_{\text{max\_CYP19A}} = k_{\text{cat\_CYP19A}} \cdot A_{\text{CYP19A}};$$

CYP19A mRNA:

$$V_{\text{ovary}} \frac{dC_{\text{CYP19A\_mRNA}}}{dt} = k_{\text{syn\_mRNA\_basal}} + \frac{(k_{\text{syn\_mRNA\_max}} - k_{\text{syn\_mRNA\_basal}}) C_{\text{LHFSH\_R\_LHFSH}}}{K_{\text{a\_syn\_mRNA}} + C_{\text{LHFSH\_R\_LHFSH}}} - k_{\text{loss\_mRNA}} \cdot A_{\text{CYP19A\_mRNA}};$$

## Liver Compartment

FAD:

$$V_{\text{liver}} \frac{dC_{\text{FAD\_liver}}}{dt} = Q_{\text{liver}} \left( C_{\text{FAD\_arterial}} - \frac{C_{\text{FAD\_liver}}}{P_{\text{FAD\_liver:blood}}} \right) - k_{\text{loss\_FAD}} \cdot A_{\text{FAD\_liver}};$$

E2:

$$V_{\text{liver}} \frac{dC_{\text{E2\_liver}}}{dt} = Q_{\text{liver}} \left( C_{\text{E2\_arterial}} - \frac{C_{\text{E2\_liver}}}{P_{\text{E2\_liver:blood}}} \right) - k_{\text{loss\_E2}} \cdot A_{\text{E2\_liver}};$$

## Venous Blood Compartment

LH/FSH receptor:

$$\frac{dA_{\text{R\_LHFSH\_surface}}}{dt} = k_{\text{R\_LHFSH\_out}} \cdot A_{\text{R\_LHFSH\_in}} - k_{\text{R\_LHFSH\_in}} \left( \frac{C_{\text{E2\_ovary}}}{K_{\text{a\_R\_LHFSH\_in}} + C_{\text{E2\_ovary}}} \right) A_{\text{R\_LHFSH\_surface}}$$

LH/FSH-receptor complex:

$$\frac{dA_{\text{LHFSH\_R\_LHFSH}}}{dt} = k_{\text{LHFSH\_on}} \cdot A_{\text{LHFSH\_venous\_free}} \cdot A_{\text{R\_LHFSH\_surface\_free}} - k_{\text{LHFSH\_off}} \cdot A_{\text{LHFSH\_R\_LHFSH}},$$

where  $A_{\text{R\_LHFSH\_surface\_free}} = A_{\text{R\_LHFSH\_surface}} - A_{\text{LHFSH\_R\_LHFSH}}$

and  $A_{\text{LHFSH\_venous\_free}} = A_{\text{LHFSH\_venous}} - A_{\text{LHFSH\_R\_LHFSH}}$ ;

LH/FSH:

$$V_{\text{venous}} \frac{dC_{\text{LHFSH\_venous}}}{dt} = \frac{k_{\text{LHFSH}} \cdot A_{\text{LHFSH\_brain}}}{\left(1 + \frac{C_{\text{E2\_brain}}}{K_{\text{i\_E2}}}\right)} - k_{\text{loss\_LHFSH}} \cdot A_{\text{LHFSH\_venous\_free}} - Q_{\text{cardiac}} C_{\text{LHFSH\_venous\_free}};$$

E2:

$$V_{\text{venous}} \frac{dC_{\text{E2\_venous}}}{dt} = Q_{\text{liver}} \left( \frac{C_{\text{E2\_liver}}}{P_{\text{E2\_liver:blood}}} \right) + Q_{\text{ovary}} \left( \frac{C_{\text{E2\_ovary}}}{P_{\text{E2\_ovary:blood}}} \right) + Q_{\text{brain}} \left( \frac{C_{\text{E2\_brain}}}{P_{\text{E2\_brain:blood}}} \right) + Q_{\text{RoB}} \left( \frac{C_{\text{E2\_RoB}}}{P_{\text{E2\_RoB:blood}}} \right) - Q_{\text{cardiac}} C_{\text{E2\_venous}};$$

FAD:

$$V_{\text{venous}} \frac{dC_{\text{FAD\_venous}}}{dt} = Q_{\text{liver}} \left( \frac{C_{\text{FAD\_liver}}}{P_{\text{FAD\_liver:blood}}} \right) + Q_{\text{ovary}} \left( \frac{C_{\text{FAD\_ovary}}}{P_{\text{FAD\_ovary:blood}}} \right) + Q_{\text{brain}} \left( \frac{C_{\text{FAD\_brain}}}{P_{\text{FAD\_brain:blood}}} \right) + Q_{\text{RoB}} \left( \frac{C_{\text{FAD\_RoB}}}{P_{\text{FAD\_RoB:blood}}} \right) - Q_{\text{cardiac}} C_{\text{FAD\_venous}};$$

## Rest of Body Compartment

FAD:

$$V_{\text{RoB}} \frac{dC_{\text{FAD\_RoB}}}{dt} = Q_{\text{RoB}} \left( C_{\text{FAD\_arterial}} - \frac{C_{\text{FAD\_Rob}}}{P_{\text{FAD\_RoB:blood}}} \right);$$

E2:

$$V_{\text{RoB}} \frac{dC_{\text{E2\_RoB}}}{dt} = Q_{\text{RoB}} \left( C_{\text{E2\_arterial}} - \frac{C_{\text{E2\_Rob}}}{P_{\text{E2\_RoB: blood}}} \right),$$

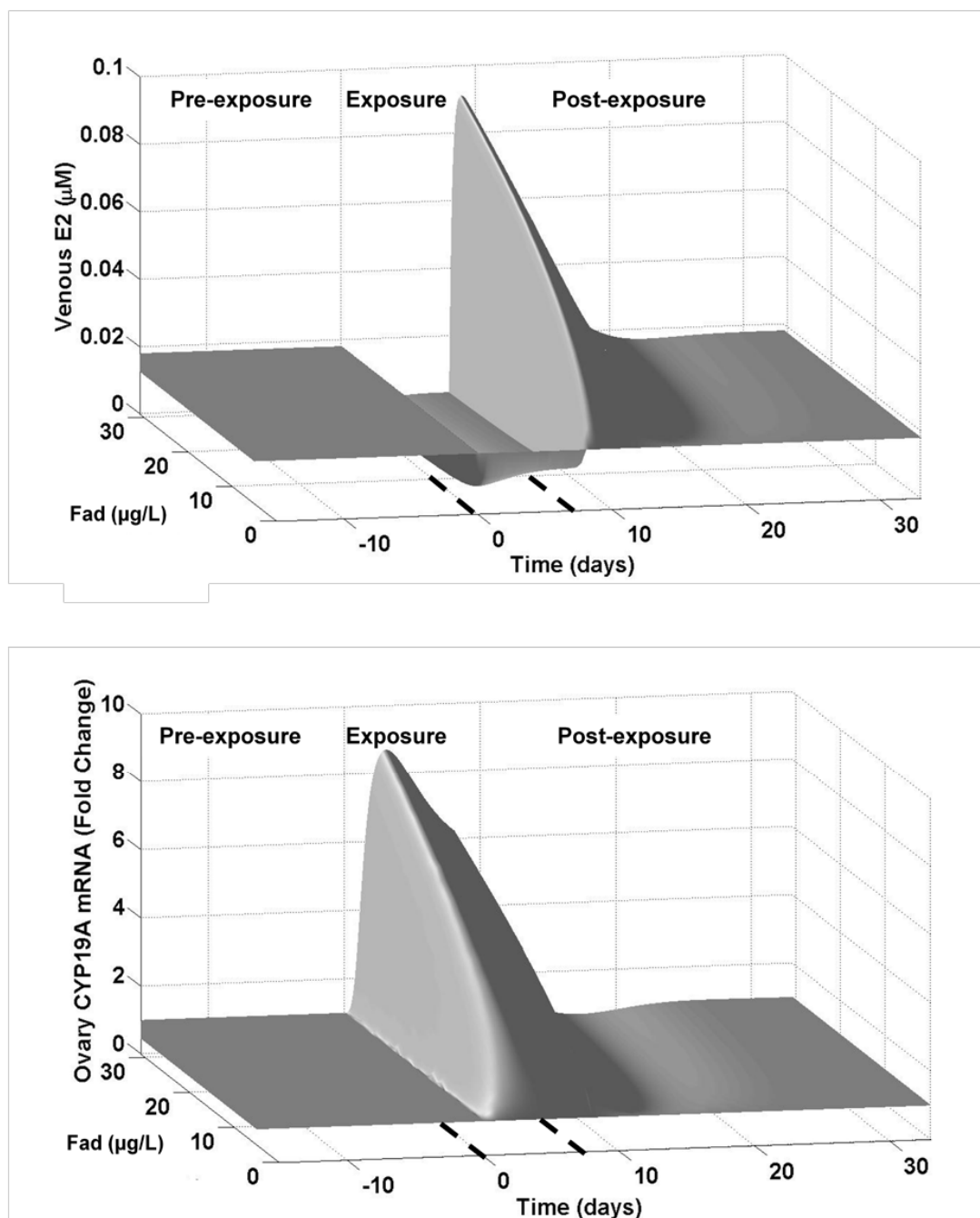
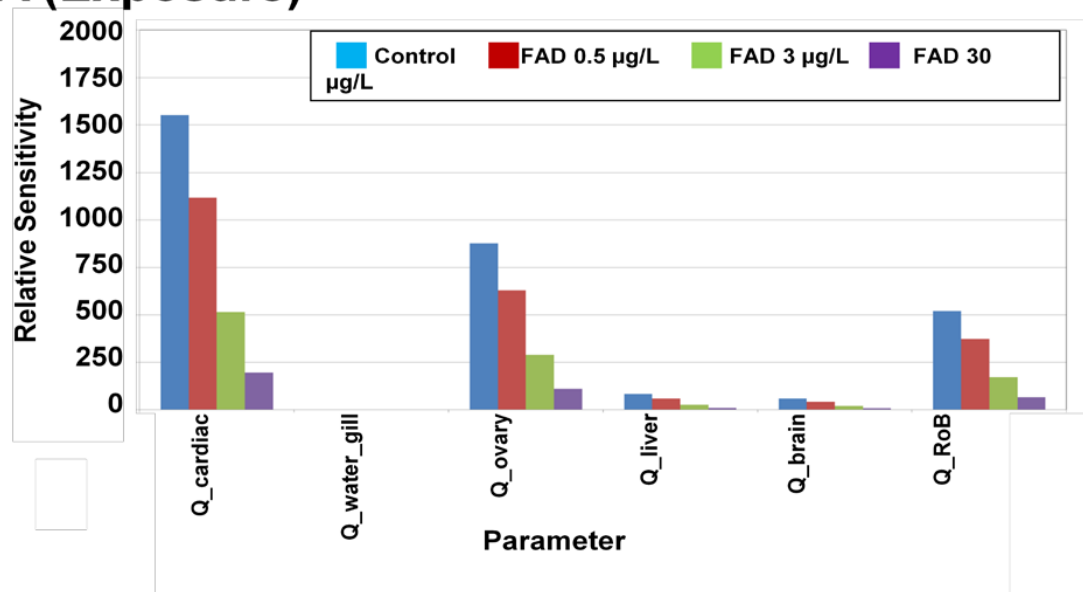


**Figure S1**

**Figure S1.** Model predictions plotted as a function of FAD concentration and time during pre-exposure (-15 – 0 days), exposure to FAD (0 – 8 days), and post-exposure (8 – 33 days) for venous E2 concentrations (A) and ovary CYP19A\_mRNA fold changes relative to controls (B).

## A (Exposure)



## B (post exposure)

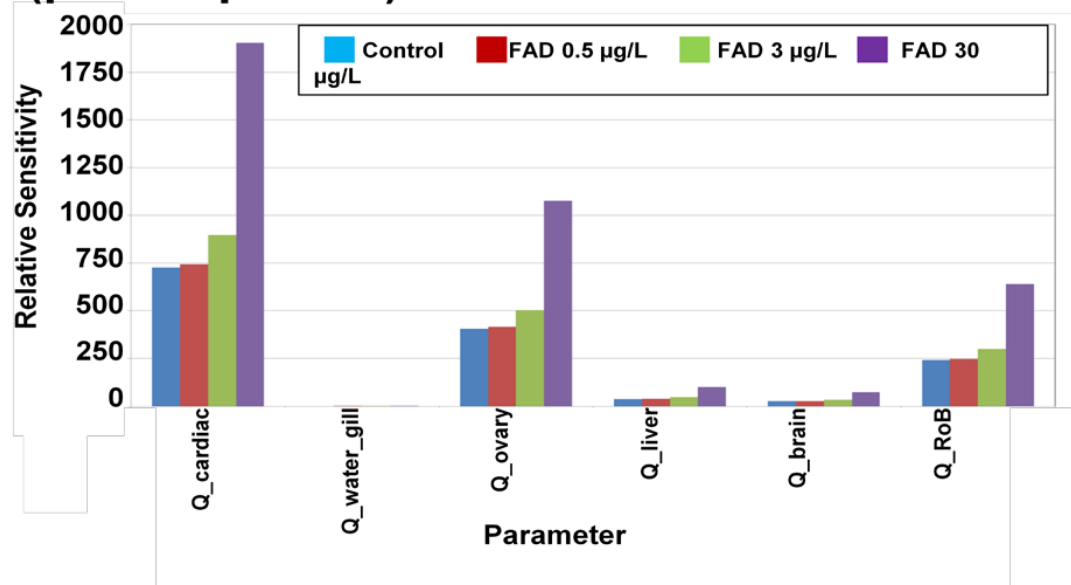
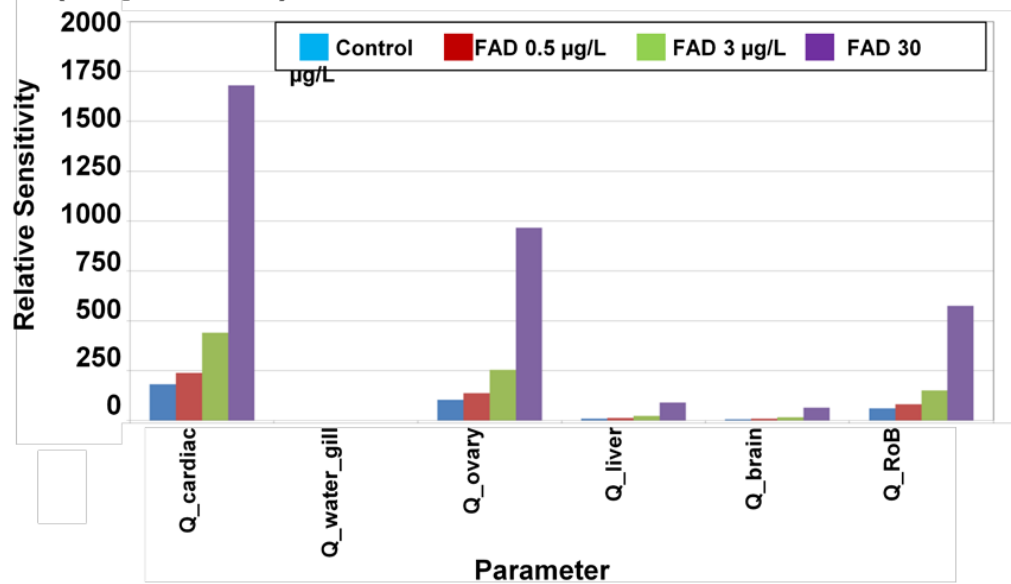


**Figure S2**

**Figure S2.** Relative sensitivities for modeled E2 plotted as a function of the 6 cardiovascular model parameters for control and three FAD concentrations (0.5, 3, and 30 µg/L). Each bar represents the  $L^2$  norm of the relative sensitivities across time during exposure (0-8 days; A) and post-exposure (8-33 days; B). The values indicate the degree to which changes in parameter values lead to changes in model outputs.

## A (exposure)



## B (post exposure)

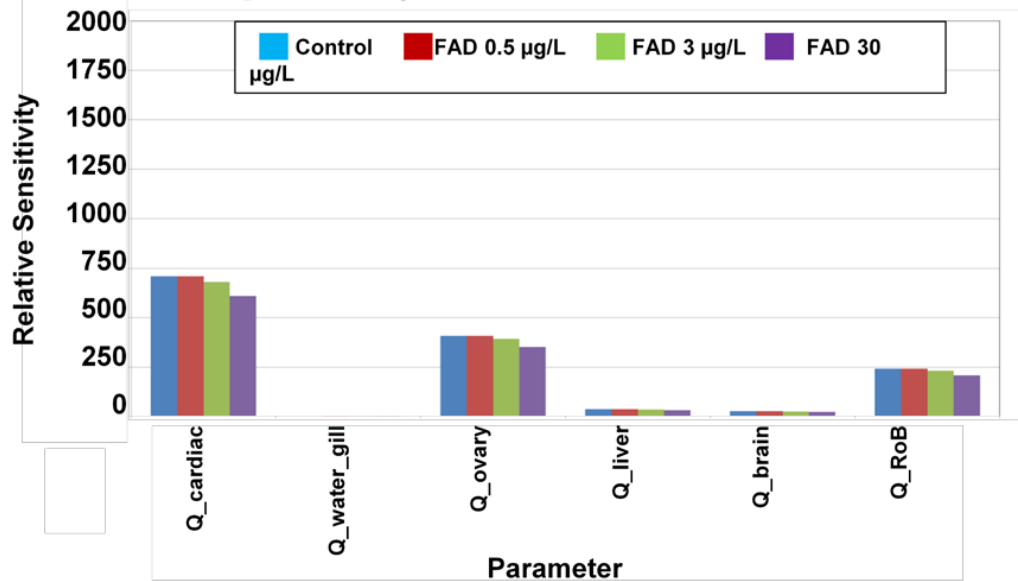


**Figure S3**

**Figure S3.** Relative sensitivities for modeled CYP19A\_mRNA plotted as a function of the 6 cardiovascular model parameters for control and three FAD concentrations (0.5, 3, and 30 µg/L). Each bar represents the  $L^2$  norm of the relative sensitivities across time during exposure (0-8 days; A) and post-exposure (8-33 days; B). The values indicate the degree to which changes in parameter values lead to changes in model outputs.

**4. COMPUTATIONAL MODEL OF THE FATHEAD MINNOW  
HYPOTHALAMIC-PITUITARY-GONADAL AXIS: INCORPORATING  
PROTEIN SYNTHESIS TO IMPROVE PREDICTABILITY OF BIOCHEMICAL  
RESPONSE TO ENDOCRINE ACTIVE CHEMICALS**

Miyuki Breen, Daniel L. Villeneuve, Gerald T. Ankley, David C. Bencic, Michael S. Breen, Karen H. Watanabe, Alun L. Lloyd, Rory B. Conolly

Be Submit to Comparative Biochemistry and Physiology – Part C: Toxicology & Pharmacology

Miyuki Breen was primarily responsible for model development, simulation, analysis of results, and manuscript writing.

# Computational Model of the Fathead Minnow Hypothalamic-Pituitary-Gonadal Axis: Incorporating Protein Synthesis in Improving Predictability of Responses to Endocrine Active Chemicals

Miyuki Breen<sup>a</sup>, Daniel L. Villeneuve<sup>b</sup>, Gerald T. Ankley<sup>b</sup>, David Bencic<sup>c</sup>, Michael S. Breen<sup>d</sup>,  
Karen H. Watanabe<sup>e</sup>, Alun L. Lloyd<sup>a</sup>, Rory B. Conolly<sup>f,\*</sup>

<sup>a</sup> Biomathematics Graduate Program, Department of Mathematics, North Carolina State University, Box 8203, Raleigh, NC 27695, USA ([mbreen@ncsu.edu](mailto:mbreen@ncsu.edu); [alun\\_lloyd@ncsu.edu](mailto:alun_lloyd@ncsu.edu))

<sup>b</sup> Mid-Continent Ecology Division, National Health and Environmental Effects Research Laboratory, U.S. Environmental Protection Agency, 6201 Congdon Blvd, Duluth, MN 55804, USA ([villeneuve.dan@epa.gov](mailto:villeneuve.dan@epa.gov); [ankley.gerald@epa.gov](mailto:ankley.gerald@epa.gov))

<sup>c</sup> Ecological Exposure Research Division, National Exposure Research Laboratory, U.S. Environmental Protection Agency, Cincinnati, OH, USA ([bencic.david@epa.gov](mailto:bencic.david@epa.gov))

<sup>d</sup> National Exposure Research Laboratory, U.S. Environmental Protection Agency, 109 TW Alexander Drive, Research Triangle Park, NC 27711, USA ([breen.michael@epa.gov](mailto:breen.michael@epa.gov))

<sup>e</sup> Division of Environmental and Biomolecular Systems, Institute of Environmental Health, Oregon Health & Science University, 3181 SW Sam Jackson Park Road HRC3, Portland, OR 97239, USA ([watanabk@ohsu.edu](mailto:watanabk@ohsu.edu))

<sup>f</sup> Integrated Systems Toxicology Division, National Health and Environmental Effects Research Laboratory, U.S. Environmental Protection Agency, 109 TW Alexander Drive, Research Triangle Park, NC 27711, USA ([conolly.rory@epa.gov](mailto:conolly.rory@epa.gov))

## Address correspondence to:

Rory Conolly  
U.S. Environmental Protection Agency  
Office of Research and Development  
National Health and Environmental Effects Research Laboratory  
109 T.W. Alexander Drive, Mail B105-03  
Research Triangle Park, NC 27711  
Telephone: 919-541-9782  
Email: [conolly.rory@epa.gov](mailto:conolly.rory@epa.gov)

## ABSTRACT

There is international concern about chemicals that alter endocrine system function in humans and/or wildlife and subsequently cause adverse effects. We previously developed a mechanistic computational model of the hypothalamic-pituitary-gonadal (HPG) axis in female fathead minnows exposed to a model aromatase inhibitor, fadrozole (FAD), to predict dose-response and time-course behaviors for apical reproductive. Initial efforts to develop a computational model describing adaptive responses to endocrine stress providing good fits to empirical plasma 17 $\beta$ -estradiol (E2) data in exposed fish were only partially successful, which suggests that additional regulatory biology processes is needed. In this study, we addressed short-comings of previous model by incorporating additional details concerning *cyp19a* (aromatase) protein synthesis into our previous model. Predictions based on the revised model were evaluated using plasma E2 concentrations and ovarian cytochrome P450 (CYP) 19A aromatase mRNA data from two fathead minnow time-course experiments with FAD, as well as from a third 4-day study. The extended model provides better fits to measured E2 time-course concentrations, and the model accurately predicts CYP19A mRNA fold changes and plasma E2 dose-response from the 4-d concentration-response study. This study suggests that aromatase protein synthesis is an important process in the biological system to model the effects of FAD exposure.

**Keywords:** endocrine disrupting chemicals, computational model, adaptation, protein synthesis, toxicology, fadrozole, hypothalamic-pituitary-gonadal axis, fish

## INTRODUCTION

There is international concern about environmental contaminants, commercial products and drugs that alter endocrine system function in humans and/or wildlife and subsequently cause adverse effects (Cooper and Kavlock, 1997; Daston *et al.*, 2003; Hutchinson *et al.*, 2006; Zacharewski, 1998). The Safe Drinking Water Act Amendments (1996) and the Food Quality Protection Act (1996) require the U.S. Environmental Protection Agency (EPA) to screen for endocrine-active chemicals in drinking water and pesticides used in food production. Based on this legislation, the EPA developed and implemented a multi-phased screening (Tier 1) and testing (Tier 2) process called the Endocrine Disruptor Screening Program (EDSP; U.S. EPA, 1998; U.S. EPA, 2009). Steroid biosynthesis inhibitors, including aromatase inhibitors, were recognized as an important class of endocrine disruptors and were selected for evaluation in the EDSP (Drenth *et al.*, 1998; Sanderson, 2006; Vinggaard *et al.*, 2000; U.S. EPA, 1998). One of the functions of EDSP Tier 2 is to characterize the dose-response of chemicals that can interact with the endocrine system, reflecting the importance of understanding the dose-response behavior of endocrine disruptors.

The dose-response and time-course (DRTC) behavior of organisms exposed to environmental chemicals are major determinants of health risk. In addition to factors like adsorption, distribution, metabolism, and elimination, physiological adaptation or compensation can be a major determinant of the occurrence of adverse effects. Understanding compensatory responses is critical to the modern practice of toxicology, particularly as the field evolves from traditional reliance on whole animal testing with apical

endpoints toward more predictive approaches anchored to an understanding of chemical modes of action. In recognition of this, a U.S. National Research Council report, *Toxicity Testing in the 21<sup>st</sup> Century: A Vision and a Strategy*, emphasizes that adaptive changes within organisms exposed to environmental stress can alter dose-response behaviors to modulate stressor effects (National Research Council, 2007). Consequently, to improve descriptions of dose-response behaviors for risk assessment, a better understanding of adaptive mechanisms is needed. Hence, a goal of our larger research effort (Ankley *et al.*, 2009) research has been to develop a computational model of adaptive mechanisms in the hypothalamic-pituitary-gonadal (HPG) axis for a model vertebrate, the fathead minnow (*Pimephales promelas*).

In initial studies, we developed a mathematical model to predict the DRTC behaviors in the HPG axis of female fathead minnows exposed to model aromatase inhibitor, fadrozole (FAD; Breen *et al.*, 2013). Fadrozole competitively inhibits the steroidogenic enzyme aromatase, a cytochrome P450 (CYP) 19A, which is rate-limiting in the conversion of testosterone (T) to 17 $\beta$ -estradiol (E2) (Miller, 1988). While FAD itself is not ecologically relevant, there are a variety of environmental contaminants that can inhibit aromatase activity and elicit similar effects (Petkov *et al.*, 2009; Vinggaard *et al.*, 2000). The initial deterministic model included a feedback regulatory loop within the HPG axis to mediate adaptive responses to endocrine-active chemical stressors by controlling the secretion of luteinizing hormone (LH) and follicle-stimulating hormone (FSH) from a generalized HP complex (Breen *et al.*, 2013). In the present paper, we build upon the previously described model to address a key limitation in its predictive ability to improve the congruence between model predictions and empirical data.

The primary focus of our previous work was on adaptive changes (compensation) in plasma E2 concentrations during FAD exposure, which resulted in a period of increased E2 production/concentration, relative to controls (an overshoot), and an “overshoot” behavior in E2 when the inhibitor was removed, particularly at lower FAD concentrations (Breen *et al.*, 2013). The main limitation of the previous HPG axis model was a large overestimation of plasma E2 concentrations for higher FAD test concentrations. In the present paper, we address this limitation by investigating protein synthesis of *cyp19a*. Because protein synthesis and degradation is responsible for amounts of *cyp19a* available for the conversion of T to E2, we extended the previous model by adding the *cyp19a* protein synthesis pathway.

The contribution of this study is the extension of the previously developed HPG axis model (Breen *et al.*, 2013). The extended model was evaluated with measurements of plasma E2 and ovarian CYP19A mRNA for eight FAD test concentrations. Comparing the model-predicted and measured data provides insights into possible feedback control mechanisms embedded in the HPG axis.

## MATERIALS AND METHODS

### *FAD exposure*

The model described in the present study incorporates data from three experiments with fathead minnows exposed to FAD. The first of these studies is described in detail by Villeneuve *et al.* (2009). Briefly, sexually-mature fathead minnows (5-6 month old), obtained from an onsite culture facility at the EPA Mid-Continent Ecology Division (Duluth, MN), were exposed to 0, 3, or 30 µg FAD/L. Fadrozole was delivered to 20 L tanks containing

10 L of test solution via a continuous flow (approximately 45 ml/min) of UV-treated, filtered Lake Superior water without use of a carrier solvent. Four male and four female fathead minnows were exposed in each tank. The experiment was initiated by transferring random groups of fish directly to tanks that had been receiving a continuous flow of test solution for approximately 48 h. Addition of fish was staggered by replicate within each treatment to permit all samples from a given exposure tank to be collected within 45 min of the desired exposure duration. Two tanks of four male and four female fish were sacrificed after 1, 2, 4, and 8 d of exposure. After 8 days of exposure, remaining fish were held in control Lake Superior water (no FAD) and sampled after 1, 2, 4, or 8 d of depuration. There were two replicate tanks for each unique exposure condition (i.e., combination of treatment and time point). Urine, plasma, liver, gonad, brain, and pituitary samples were collected and a variety of endocrine and toxicogenomic endpoints were examined. In total, Villeneuve *et al.* (2009) reported results for over 15 different endocrine-related variables. However, for the current modeling work, major endpoints of interest were plasma concentrations of E2 and ovarian expression of *cyp19a*. Notably, *cyp19a* protein concentrations were not measured.

The second experiment (Villeneuve *et al.*, 2013) was a follow-up to the study described above, only with extended time-course. Briefly, reproductively-mature fathead minnows were exposed to 0, 0.5, or 30 µg FAD/L using conditions similar to those described above. Fish were either exposed continuously and sampled after 1, 8, 12, 16, 20, 24, or 28 d of exposure or exposed for 8 d, then held in a continuous flow of clean Lake Superior water for an additional 4, 8, 12, 16, or 20 d. Various endpoints were analyzed, including plasma E2 and ovarian CYP19A mRNA.

In a third experiment (Ralston-Hooper *et al.*, 2013), fathead minnows were exposed to 0, 0.04, 0.2, 1, or 5 µg FAD/L for 4 d under conditions similar to those described above and various endpoints were analyzed, including plasma E2 concentrations.

### *Mathematical Model of the HPG-axis*

The extended computational model of the HPG axis for FAD-exposed female fathead minnow described herein is a modification of our previously-described HPG axis model (Breen *et al.*, 2013). As does the model of Breen *et al.* (2013), the extended model consists of six tissue compartments: gill, brain, ovary, liver, venous blood, and rest of body (Figure 1). These compartments, which are involved in HPG axis signaling and feedback control, are connected in a manner consistent with the cardiovascular system of fish. The model includes a generalized regulatory feedback loop within the HPG axis that mediates adaptive responses to endocrine stress from FAD. The regulatory loop controls the secretion of gonadotropins (LH and FSH) from the brain. The descriptions of each tissue compartment were previously reported by Breen *et al.* (2013), with the exception of *cyp19a* protein synthesis in the ovary (Figure 1D). Protein synthesis involves two major processes: transcription and translation. In the nucleus, transcription occurs when an RNA polymerase enzyme binds to DNA to start the formation of messenger RNA (mRNA). The mRNA then leaves the nucleus and enters the cytoplasm to bind to ribosomes. In the cytoplasm, amino acids (AA) bind to transfer RNA (tRNA) and are transported to ribosomes. At the ribosome, translation occurs when a series of tRNA molecules bind to mRNA to form a chain of AA that creates a protein (Bruce *et al.*, 2002; Campbell, 1996). In the extended model, the rate of protein synthesis from *cyp19a* is a

function of levels of mRNA, ribosomes, tRNA, and AA. Once CYP19A mRNA is transcribed for the CYP19A gene, it diffuses to a ribosome to form an mRNA-ribosome complex. The tRNAs bind to AA to form tRNA-AA complexes, which bind to the CYP19A mRNA-ribosome complex for translation of CYP19A mRNA and subsequent synthesis of the CYP19A protein. In the ovary compartment, the model has zero-order synthesis and first-order degradation of AA, and translation of *cyp19a* is described by Michaelis-Menten kinetics. The time-varying concentrations of substrates are described by dynamic mass balances. We can express the dynamic mass balance for the substrates in the compartment  $y$  with volume  $V_y$  as:

$$V_y \frac{dC_{x,y}}{dt} = P_{x,y} - U_{x,y} - D_{x,y} + I_{x,y} - S_{x,y} \quad (1)$$

where  $C_{x,y}$  is the concentration of substrate  $x$  in compartment  $y$ ,  $P_{x,y}$  is the production rate of substrate  $x$  in compartment  $y$ ,  $U_{x,y}$  is the utilization rate of substrate  $x$  in compartment  $y$ ,  $D_{x,y}$  is the degradation rate of substrate  $x$  in compartment  $y$ ,  $I_{x,y}$  is the import rate of substrate  $x$  into compartment  $y$ , and  $S_{x,y}$  is the secretion rate of substrate  $x$  from compartment  $y$ . The first two terms in the right side of Eq. (1) represent the net metabolic reaction rate of substrate  $x$ . The last two terms represent the net uptake or release rate of substrate  $x$  in compartment  $y$ . The complete set of equations for the model is provided in the Supplementary Data.

### Parameter Estimation

The model consists of physiological and biochemical parameters, including tissue compartment volumes, blood flow rates, equilibrium partition coefficients, and biochemical reaction rates (i.e. transcription, translation, metabolism, transport, and degradation). As in the previous model (Breen *et al.*, 2013), the extended model utilizes measured volumes of the major tissue compartments (ovary, liver, brain) and the whole body, and determined physiological parameter values from the literature. Based on experimental results (Villeneuve *et al.*, 2013), the equilibrium tissue:blood partition coefficients for E2, and blood:water and tissue:blood partition coefficients for FAD were assumed to be one. In the extended model, there are 28 biochemical parameters affecting the dose-response and time-course behaviors of CYP19A mRNA and E2 in FAD-exposed animals; literature-reported values were used for five parameters as in the previous model, and 23 parameters were estimated using the mean E2 concentrations from the fathead minnow studies. We utilized measured plasma E2 data from the first and second experiments for parameter estimation and ovarian CYP19A mRNA data from the first and second experiments, along with plasma E2 data from the third experiment for model validation. The definitions and values of physiological constants and fixed biochemical parameters, and the measured E2 and CYP19A mRNA data were previously described in detail by Breen *et al.* (2013).

The ordinary least squares method was used to estimate the following 23 biochemical parameters from the fathead minnow E2 time-course data (see Table 1): 15 parameters in the ovary compartment ( $k_{\text{syn\_mRNA\_basal}}$ ,  $k_{\text{syn\_mRNA\_max}}$ ,  $k_{\text{loss\_mRNA}}$ ,  $V_{\text{max\_syn\_CYP19A}}$ ,  $K_{\text{m\_syn\_CYP19A}}$ ,  $k_{\text{loss\_CYP19A}}$ ,  $K_{\text{i\_FAD}}$ ,  $K_{\text{a\_syn\_mRNA}}$ ,  $k_{\text{rib\_on}}$ ,  $k_{\text{rib\_off}}$ ,  $k_{\text{syn\_AA}}$ ,  $k_{\text{loss\_AA}}$ ,  $A_{\text{rib\_total}}$ ,  $k_{\text{tRNA\_on}}$ ,  $k_{\text{tRNA\_off}}$ ), two

parameters in the liver compartment ( $k_{\text{loss\_FAD}}, k_{\text{loss\_E2}}$ ), four parameters in the brain compartment ( $k_{0\_syn\_LHFSH}, k_{\text{loss\_LHFSH}}, k_{\text{LHFSH}}, K_{i\_E2}$ ), and two parameters in the venous blood compartment ( $k_{\text{LHFSH\_off}}, k_{\text{loss\_LHFSH}}$ ). Let  $n_d$  be the number of time points in the E2 time-course data for the  $d^{\text{th}}$  FAD dose (including control);  $C_{\text{E2,blood}}^{d,i}$  be the measured E2 plasma concentrations for the  $d^{\text{th}}$  FAD dose at the  $i^{\text{th}}$  time;  $C_{\text{E2,blood}}(t_i; C_{\text{FAD}}^d, \bar{k})$  be the model-predicted concentrations of E2 in the venous blood compartment at the  $i^{\text{th}}$  time,  $t_i$ , for the  $d^{\text{th}}$  FAD dose (including control),  $C_{\text{FAD}}^d$ , with parameter set

$$\bar{k} = (k_{\text{syn\_mRNA\_basal}}, k_{\text{syn\_mRNA\_max}}, k_{\text{loss\_mRNA}}, V_{\text{max\_syn\_CYP19A}}, K_{\text{m\_syn\_CYP19A}}, k_{\text{loss\_CYP19A}}, K_{i\_FAD}, K_{a\_syn\_mRNA}, k_{\text{rib\_on}}, k_{\text{rib\_off}}, k_{\text{syn\_AA}}, k_{\text{loss\_AA}}, A_{\text{rib\_total}}, k_{\text{tRNA\_on}}, k_{\text{tRNA\_off}}, k_{\text{loss\_FAD}}, k_{\text{loss\_E2}}, k_{0\_syn\_LHFSH}, k_{\text{loss\_LHFSH}}, k_{\text{LHFSH}}, K_{i\_E2}, k_{\text{LHFSH\_off}}, k_{\text{loss\_LHFSH}})$$

for  $d=1,2,3,4$ , and  $i=1, \dots, n_d$ . Then, the least squares estimate,

$$\bar{k}^* = (k_{\text{syn\_mRNA\_basal}}^*, k_{\text{syn\_mRNA\_max}}^*, k_{\text{loss\_mRNA}}^*, V_{\text{max\_syn\_CYP19A}}^*, K_{\text{m\_syn\_CYP19A}}^*, k_{\text{loss\_CYP19A}}^*, K_{i\_FAD}^*, K_{a\_syn\_mRNA}^*, k_{\text{rib\_on}}^*, k_{\text{rib\_off}}^*, k_{\text{syn\_AA}}^*, k_{\text{loss\_AA}}^*, A_{\text{rib\_total}}^*, k_{\text{tRNA\_on}}^*, k_{\text{tRNA\_off}}^*, k_{\text{loss\_FAD}}^*, k_{\text{loss\_E2}}^*, k_{0\_syn\_LHFSH}^*, k_{\text{loss\_LHFSH}}^*, k_{\text{LHFSH}}^*, K_{i\_E2}^*, k_{\text{LHFSH\_off}}^*, k_{\text{loss\_LHFSH}}^*),$$

is the parameter vector  $\bar{k}^*$ , which minimizes the cost function

$$J(\underline{k}) = \sum_{d=1}^4 \sum_{i=1}^{n_d} \left( C_{\text{E2,blood}}^{d,i} - C_{\text{E2,blood}}(t_i; C_{\text{FAD}}^d, \bar{k}) \right)^2. \quad (2)$$

Parameters were estimated with an iterative nonlinear optimization algorithm using MATLAB R2010a (Mathworks, Natick, MA, USA) software. We chose the Nelder-Mead simplex method for its relative insensitivity to the initial parameter values as compared to other common methods, such as Newton's method, and its robustness to discontinuities (Nelder and Mead, 1965). We confirmed convergence to the solution after the parameter search terminated.

### Sensitivity Analysis

We performed a sensitivity analysis to examine model parameter uncertainty using a previously described method (Breen *et al.*, 2013). The key purpose of sensitivity analysis is to identify the main contributors to the variation in the model outputs by ordering the parameters; parameters with high sensitivity are more important for the model output than parameters with low sensitivity. Briefly, the sensitivity function relates changes of the model output to changes in the model parameters. We calculated the relative sensitivity functions  $R_{E2,blood,k_i}(t)$  and  $R_{mRNA,ovary,k_i}(t)$  with respect to the parameters  $k_i$  for each of the model-predicted concentrations  $C_{E2, blood}$  and fold changes of CYP19A mRNA in the ovary compartment  $F_{mRNA,ovary}$ , respectively. MATLAB was used to numerically solve the partial derivatives of  $R_{E2,blood,k_i}(t)$  and  $R_{mRNA,ovary,k_i}(t)$  for control and each FAD dose. To rank the relative sensitivities, we calculated the L2 norm across time for each relative sensitivity function as described by

$$\text{L2 norm}(R_{E2,blood,k_i}) = \sqrt{\int |R_{E2,blood,k_i}(t)|^2 dt} \quad (3)$$

and

$$\text{L2 norm}(R_{mRNA,ovary,k_i}) = \sqrt{\int |R_{mRNA,ovary,k_i}(t)|^2 dt} . \quad (4)$$

## RESULTS

### *Mathematical Model of HPG-axis*

Table 1 shows the estimated biochemical parameter values determined by fitting the model predictions to the measured mean plasma E2 concentrations for all four FAD doses from the two time-course studies. The time for convergence to the solution for the nonlinear parameter estimation was typically around 4 h on an Intel Core 2 Duo processor using MATLAB.

For plasma E2 concentrations, we compared the model-predicted concentrations with the time-course measurements. Overall, the model-predicted E2 concentrations correspond closely to the mean time-course measurements for all four doses (Figure 2A-D). For the high FAD dose (30  $\mu\text{g/L}$ ), the extended model performed markedly better than the previous model (Breen *et al.*, 2013), the prediction error from the previous model is reduced by 60, 32, 81, 95, 99, 96, 27, and 14 % at 1, 2, 9, 10, 12, 16, 20, and 28 d, respectively. When compared with our initial model (Breen *et al.*, 2013), the extended model also better captured the mean time-course behavior for the 30  $\mu\text{g/L}$  FAD treatment, which was substantially reduced within 1 d of exposure to FAD, remained reduced throughout the exposure period, and rebounded at 2 d post-exposure, before returning to control levels following 8 or more d of recovery in clear water (Figure 2D). For the other FAD doses, the extended model performed similarly to the original model (Breen *et al.*, 2013). For example, in the 3  $\mu\text{g}$  FAD/L treatment, the extended model continued to capture the plasma E2 compensation during exposure, and the overshoot and return to control levels once the FAD exposure was terminated (Figure 2C).

Figure 3A shows the model-predicted venous E2 dose-response during FAD exposure on d, 1, 4, and 8. For FAD doses between 0  $\mu\text{g/L}$  and 10  $\mu\text{g/L}$ , the model predictions monotonically decreased across dose, with FAD exposure on d 1 having the lowest venous E2 concentration and d 8 having the highest venous E2 concentration, the same as the original model predicted. The model predictions continued to decrease monotonically across doses for FAD dose greater than 10  $\mu\text{g/L}$ , with E2 concentrations on d 1 decreasing slower than on d 4 and 8. As a result, FAD exposure on d 1 had the highest venous E2 concentration and d 4 and 8 had similar venous E2 concentrations at higher FAD treatments. In contrast, the previous model predictions had the lowest venous E2 concentration on FAD exposure d 1 and the highest venous E2 concentration on FAD exposure d 8 at higher FAD doses. Figure 4A provides a summary of model predictions for venous E2 concentrations plotted as a function both of FAD concentration and time.

We also compared the model-predicted and measured ovary CYP19A mRNA fold changes to validate our extended model. The model-predicted ovary CYP19A fold changes correspond closely to the time-course measurements for all four doses (Figure 2E-H). Figure 3B shows the model-predicted ovary CYP19A dose-response for FAD exposure on d 1, 4, and 8. The model predictions monotonically increased across dose, with the lowest ovary CYP19A mRNA predicted for FAD exposure on d 1: similar to in the original model. For d 4 and 8, the model predicted similar ovary CYP19A mRNA fold changes as a function of FAD dose, whereas the previous model predicted higher ovary CYP19A mRNA fold changes on d 4 than on d 8 (Breen *et al.*, 2013). Figure 4B provides an integrated summary of the

predictions for ovary CYP19A mRNA fold changes are plotted both as a function of FAD concentration and time.

Model predictions were compared to plasma E2 concentrations from the 4-d exposure study to further validate our model: this dataset was not used in the model development. Even though all five FAD doses (0, 0.04, 0.2, 1, and 5 µg FAD/L) used for model validation differed from the FAD doses used for model calibration, the model-predicted dose-response curve for venous E2 corresponds closely to measured plasma E2 (Figure 3C).

### *Sensitivity Analysis*

The relative sensitivities for modeled E2 and CYP19A mRNA, respectively, with respect to each of the 26 biochemical model parameters are shown for the control and three FAD test concentrations (0.5, 3, and 30 µg/L) during exposure and post-exposure (Figures 5 and 6). Overall, E2 (Figures 5) and CYP19A mRNA (Figures 6) are highly to moderately sensitive to 17 model parameters during exposure and post-exposure; six parameters,  $k_{\text{syn\_mRNA\_basal}}$ ,  $Ka_{\text{syn\_mRNA}}$ ,  $k_{\text{loss\_FAD}}$ ,  $k_{\text{loss\_LHFSH}}$ ,  $k_{\text{rib\_on}}$ ,  $k_{\text{rib\_off}}$  are insensitive. Of these six parameters, four ( $k_{\text{syn\_mRNA\_basal}}$ ,  $Ka_{\text{syn\_mRNA}}$ ,  $k_{\text{loss\_FAD}}$ ,  $k_{\text{loss\_LHFSH}}$ ) are also not sensitive for E2 and CYP19A mRNA in the original model (Breen *et al.*, 2013).

## **DISCUSSION**

Breen *et al.*, (2013) developed a mechanistic mathematical model for the HPG axis in female fathead minnows to predict the dose-response, time-course behaviors for endocrine

effects of the aromatase inhibitor, FAD. The model included a regulatory feedback loop within the HPG axis that facilitates adaptive responses in plasma E2 concentrations and CYP19A mRNA to FAD. The previous model captured the adaptive changes in plasma E2 concentrations occurring during exposure, and the overshoot observed post-exposure for the 3 µg/L FAD dose, along with the up-regulation of ovary CYP19A mRNA production occurring during exposure for both the low (3 µg/L) and high (30 µg/L) FAD treatment groups. However, the model did not provide good predictions of plasma E2 concentrations for the high dose (30 µg/L FAD) treatment, which was significantly reduced throughout the exposure period and substantially different from the response at the lower FAD concentrations. These experimental data and modeling results prompted us to refine the model in the current study to examine the hypothesis that an additional biological mechanism was needed. Since protein synthesis controls the amount of CYP19A involved in the conversion of T into E2, we investigated protein synthesis as a possible factor influencing compensation. Specifically, we extended the computational model of the HPG axis to include a pathway for protein synthesis to address the main limitation of the previous HPG axis model (Breen *et al.*, 2013). The extended model was evaluated with measurements of plasma E2 data and ovarian CYP19A mRNA for eight FAD test concentrations. The results support our hypothesis. By including a pathway for protein synthesis of CYP19A, the extended model significantly improved the model fit for the dynamic E2 concentrations at high FAD dose (30 µg/L FAD) treatment, while maintaining good model fits of dynamic E2 concentrations for controls and the lower doses (0.5 and 3 µg/L FAD), despite significant differences in data behavior between high and low doses. The extended model was also

capable of predicting the dynamic CYP19A mRNA fold changes for all four doses during the two time-course studies, and the venous E2 dose-response during a 4-d exposure at 0, 0.04, 0.2, 1, and 5  $\mu\text{g FAD/L}$ . Moreover, our sensitivity analysis indicates that CYP19A protein synthesis plays an important role in the revised model, since both E2 and CYP19A mRNA were highly to moderately sensitive to the parameters associated with the protein synthesis.

The extended model contributes to on going efforts to understand and simulate biological responses to endocrine active chemicals, including aromatase inhibitors. Development of a computational system model that incorporates this additional biological mechanism provides a better understanding of possible adaptive responses, which can refine descriptions of dose-response time-course behaviors that differ substantially from low dose to high dose regimes. The knowledge obtained from iterations in model development, refinement, and empirical testing can help us to better understand the biology underlying toxicological responses to endocrine active chemicals, and can be applied to help reduce the uncertainty of dose-response assessments in support of quantitative risk assessments, a need identified as critical to supporting new approaches to regulatory toxicology (National Research Council, 2007).

### **SUPPLEMENTARY DATA**

The dynamic molecular balance equations are provided as supplementary data, available online.

## **ACKNOWLEDGEMENTS**

Although this manuscript was reviewed by the U.S. Environmental Protection Agency and approved for publication, it may not reflect official Agency policy. Mention of trade names or commercial products does not constitute endorsement or recommendation for use.

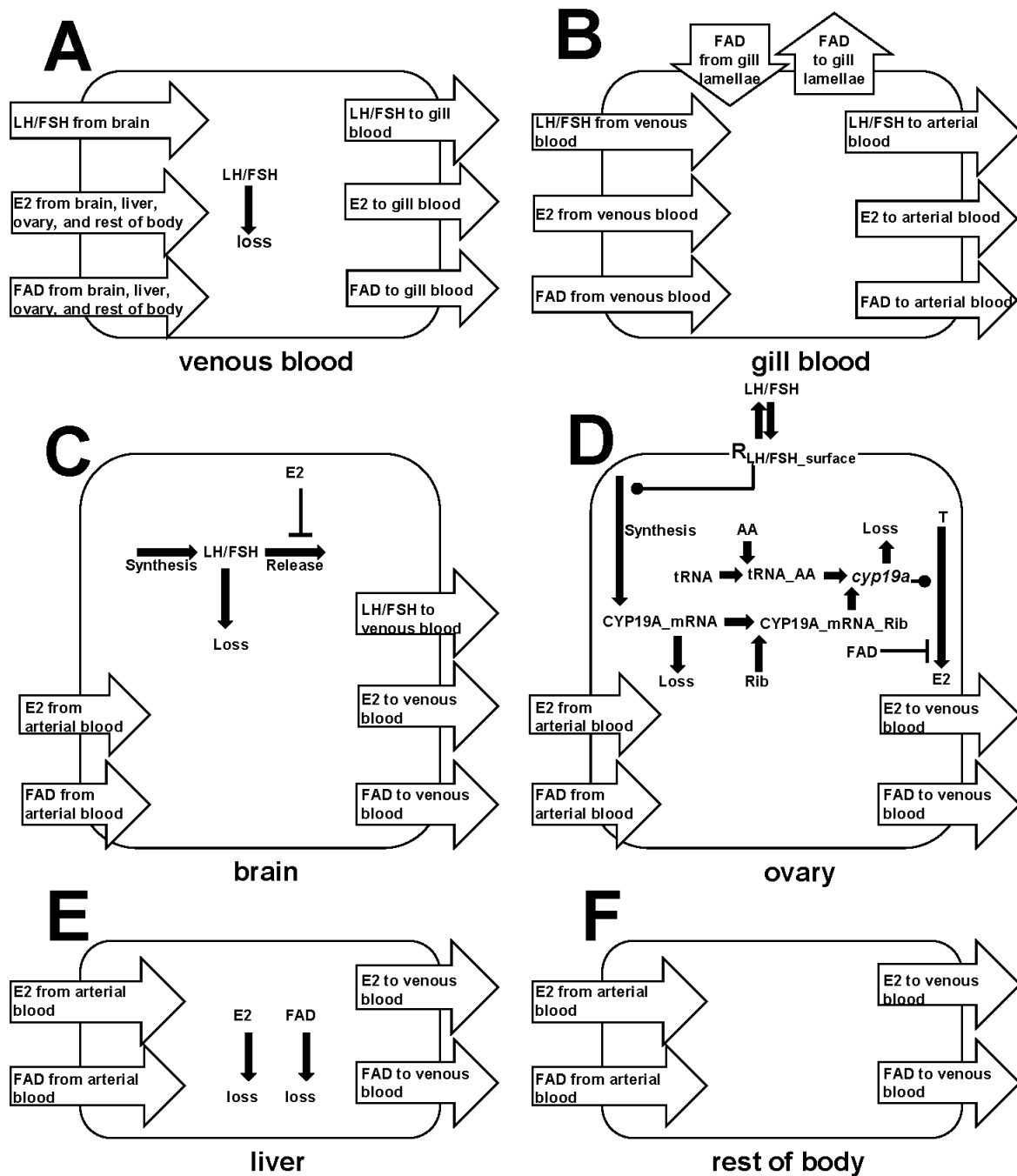


**Figure 1.** Graphical representation of biochemical processes within the six compartments of the model: venous blood (A), gill blood (B), brain (C), ovary (D), liver (E), and rest of body (F). In the venous blood (A), processes include: uptake and release of LH/FSH, E2, and FAD; degradation of LH/FSH. In the gill (B), processes include: uptake and release of LH/FSH, E2, and FAD; FAD transport from gill lamellae to gill blood. In the brain (C), processes include: uptake and release of FAD and E2; LH/FSH synthesis, release, and degradation; E2-mediated inhibition of LH/FSH release into venous blood. In the ovary (D), processes include: uptake and release of FAD and E2; reversible binding of LH/FSH in blood to LH/FSH receptors on cell membrane (surface); LH/FSH receptor-mediated activation of CYP19A\_mRNA synthesis; binding of CYP19A\_mRNA to ribosome (Rib); binding of amino acids (AA) to transfer RNA (tRNA); translation of CYP19A\_mRNA into CYP19A by CYP19A\_mRNA\_Rib complex and tRNA\_AA; degradation of CYP19A\_mRNA and CYP19A; conversion of T into E2 catalyzed by CYP19A; enzyme inhibition of CYP19A by FAD. In the liver (E), processes include: uptake and release of E2 and FAD; degradation of E2 and FAD. In the rest of body (F), processes include uptake and release of FAD and E2.

**Table 1. Estimated parameters**

Parameter Description	Symbol	Compartment	Value
Basal synthesis rate of CYP19A mRNA	$k_{\text{syn\_mRNA\_basal}}$	Ovary	$5.1 \times 10^{-7} \text{ } \mu\text{mol}\cdot\text{hr}^{-1}$
Maximum synthesis rate of CYP19A mRNA	$k_{\text{syn\_mRNA\_max}}$	Ovary	$6.8 \times 10^{-1} \text{ } \mu\text{mol}\cdot\text{hr}^{-1}$
Degradation rate of CYP19A mRNA	$k_{\text{loss\_mRNA}}$	Ovary	$2.9 \times 10^{-2} \text{ hr}^{-1}$
Maximum synthesis rate of CYP19A	$k_{\text{cat\_CYP19A\_mRNA}}$	Ovary	$5.7 \times 10^{-2} \text{ hr}^{-1}$
Michaelis constant for synthesis of CYP19A	$K_{\text{m\_syn\_CYP19A}}$	Ovary	$6.5 \times 10^4 \text{ } \mu\text{mol}\cdot\text{L}^{-1}$
Degradation rate of CYP19A	$k_{\text{loss\_CYP19A}}$	Ovary	$3.0 \times 10^{-2} \text{ hr}^{-1}$
Inhibition constant of FAD	$K_{\text{i\_FAD}}$	Ovary	$4.3 \times 10^{-3} \text{ } \mu\text{mol}\cdot\text{L}^{-1}$
Activation constant for synthesis CYP19A mRNA	$K_{\text{a\_syn\_mRNA}}$	Ovary	$6.8 \times 10^{-22} \text{ } \mu\text{mol}\cdot\text{L}^{-1}$
Total amount of ribosome	$A_{\text{rib\_total}}$	Ovary	$9.6 \times 10^{-3} \text{ } \mu\text{mol}$
Binding rate of ribosome with CYP19A mRNA	$k_{\text{rib\_on}}$	Ovary	$2.0 \times 10^1 \text{ } \mu\text{mol}^{-1}\cdot\text{hr}^{-1}$
Releasing rate of ribosome with CYP19A mRNA	$k_{\text{rib\_off}}$	Ovary	$1.8 \times 10^{-5} \text{ hr}^{-1}$
Synthesis rate of AA	$k_{\text{syn\_AA}}$	Ovary	$1.1 \times 10^1 \text{ } \mu\text{mol}\cdot\text{hr}^{-1}$
Degradation rate of AA	$k_{\text{loss\_AA}}$	Ovary	$2.1 \text{ hr}^{-1}$
Binding rate of AA with AA with tRNA	$k_{\text{tRNA\_on}}$	Ovary	$9.2 \text{ } \mu\text{mol}^{-1}\cdot\text{hr}^{-1}$
Releasing rate of AA from tRNA	$k_{\text{tRNA\_off}}$	Ovary	$7.1 \times 10^{-1} \text{ hr}^{-1}$
Degradation rate of FAD	$k_{\text{loss\_FAD}}$	Liver	$5.6 \times 10^{-1} \text{ hr}^{-1}$
Degradation rate of E2	$k_{\text{loss\_E2}}$	Liver	$4.3 \text{ hr}^{-1}$
Zero-order synthesis rate of LHFSH	$k_{0\_syn\_LHFSH}$	Brain	$5.3 \times 10^{-10} \text{ } \mu\text{mol}\cdot\text{hr}^{-1}$
Degradation rate of LHFSH	$k_{\text{loss\_LHFSH}}$	Brain	$1.4 \times 10^2 \text{ hr}^{-1}$
Releasing rate of LHFSH	$k_{\text{LHFSH}}$	Brain	$2.5 \times 10^{-3} \text{ hr}^{-1}$
Inhibition constant of E2	$K_{\text{i\_E2}}$	Brain	$4.8 \times 10^{-5} \text{ } \mu\text{mol}\cdot\text{L}^{-1}$
Releasing rate of LHFSH (blood) from LHFSH receptor (ovary)	$k_{\text{LHFSH\_off}}$	Venous Blood	$7.8 \times 10^{-1} \text{ hr}^{-1}$
Degradation rate of LHFSH	$k_{\text{loss\_LHFSH}}$	Venous Blood	$2.8 \text{ hr}^{-1}$

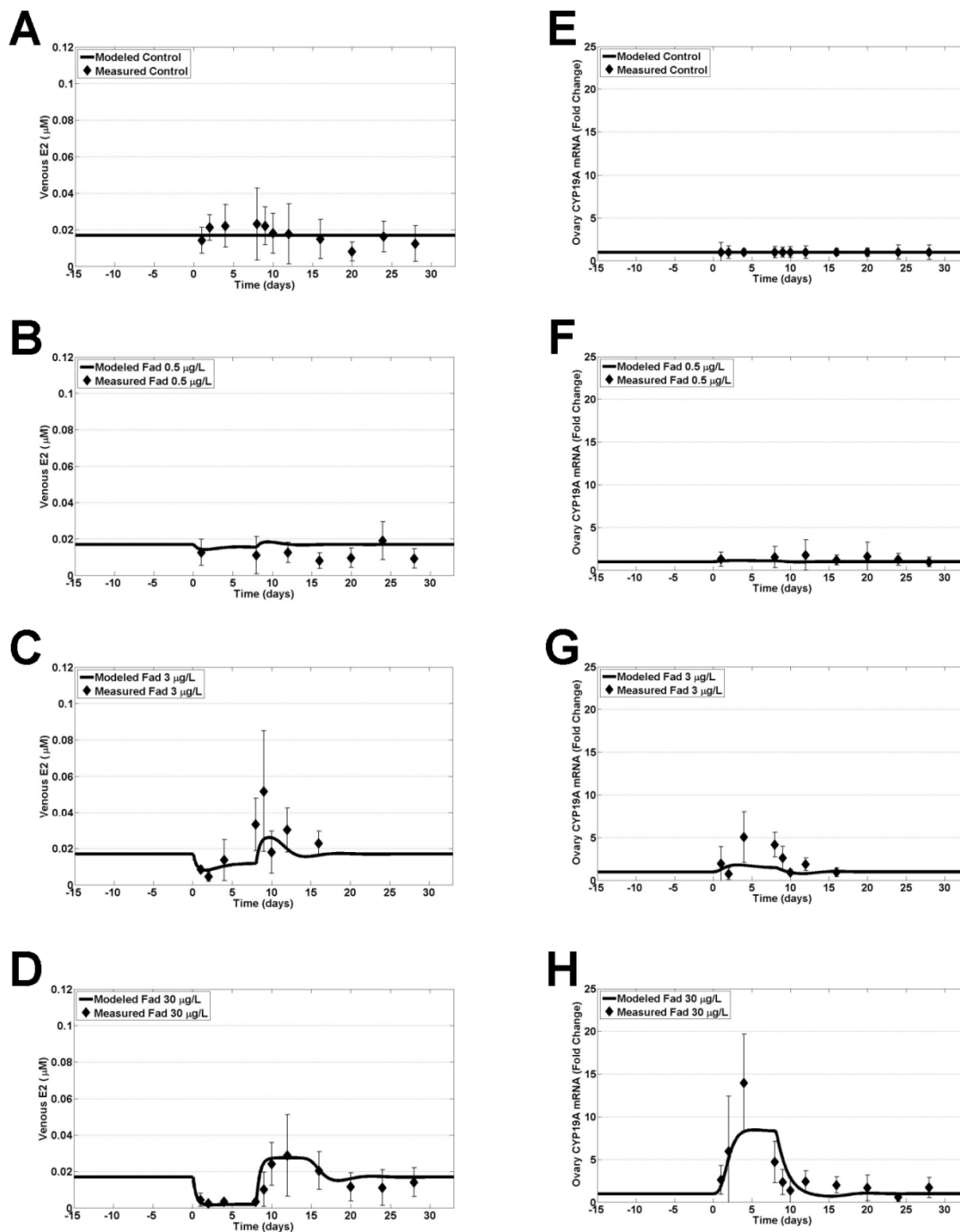


**Figure 2.** Model evaluation for control and three FAD concentrations (0.5 µg/L, 3 µg/L, and 30 µg/L). Model-predictions were plotted as a function of days during pre-exposure (-15 – 0 days), exposure to FAD (0 – 8 days), and post-exposure (8 – 33 days), and compared with measurements (mean  $\pm$  SD) for plasma E2 concentrations (A-D) and ovary CYP19A\_mRNA fold changes relative to controls (E-H). Model-predictions were compared with measurement data from two experiments: control data includes four sampling times during exposure and seven sampling times post-exposure; 0.5 µg/L - two sampling times during exposure and five sampling times post-exposure; 3 µg/L - four sampling times during exposure and four sampling times post-exposure; 30 µg/L - four sampling times during exposure and seven sampling times post-exposure. Vertical dashed lines indicate period of FAD exposure.

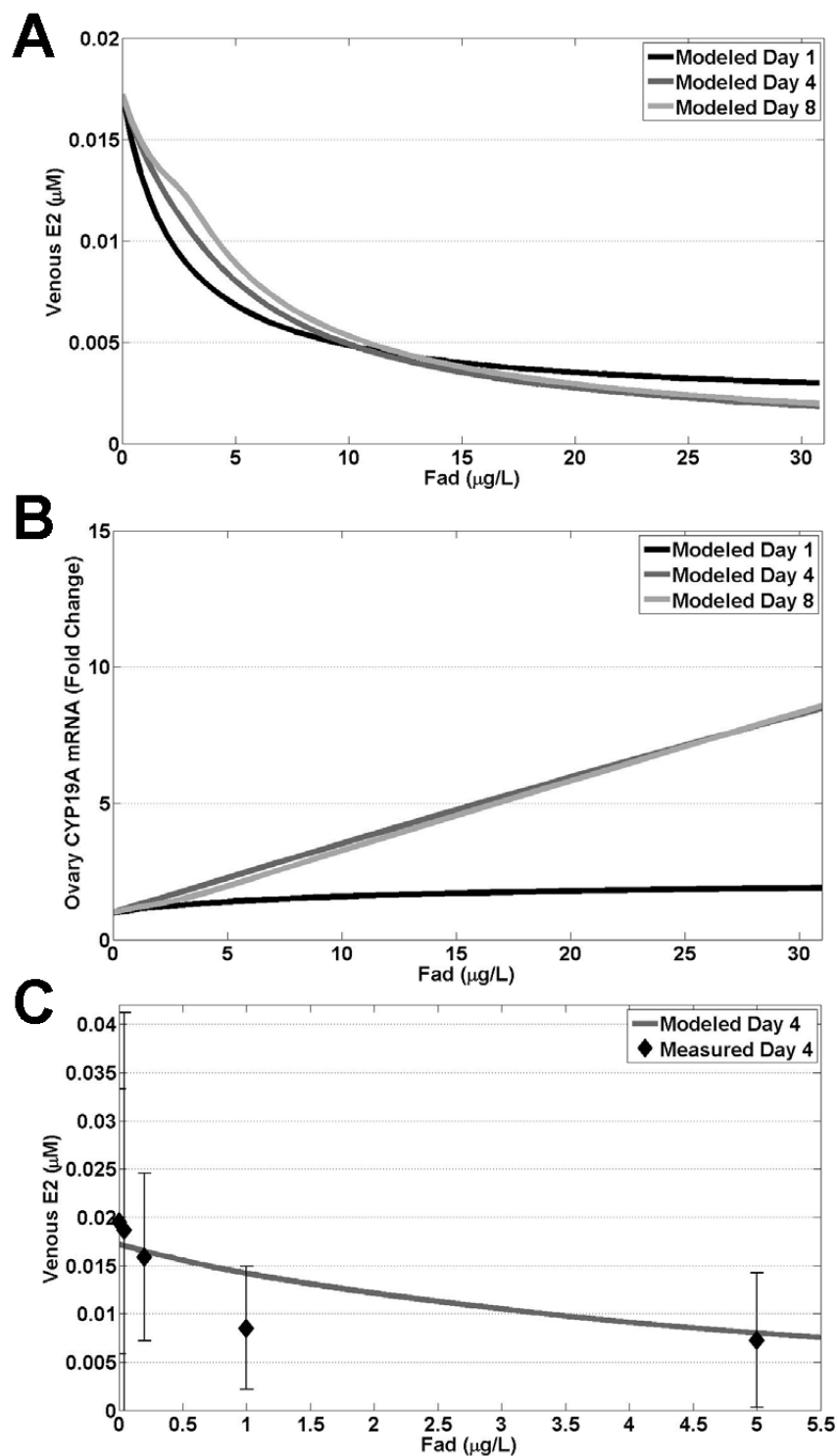


**Figure 3.** Modeled dose-response during FAD exposure. Model predictions were plotted as a function of FAD concentrations for venous E2 concentrations (A,C) and ovary CYP19A\_mRNA fold changes relative to controls (B) during exposure to FAD on days 1, 4, and 8 (2024, 2096, and 2192 hr). For day 4 (C), measured venous E2 concentrations for five FAD concentrations (0, 0.04 0.2, 1, 5  $\mu\text{g/L}$ ) with  $n=11$  or 12 were plotted with model predictions. Same model predictions are shown in A and C for FAD concentrations between 0 and 5.5  $\mu\text{g/L}$ .

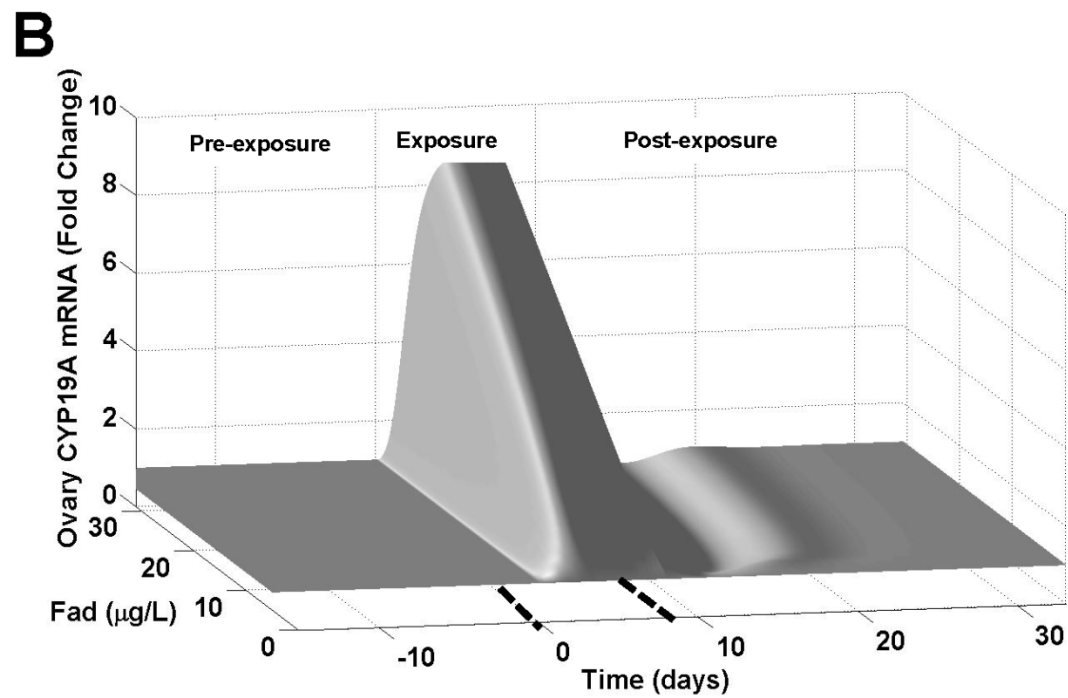
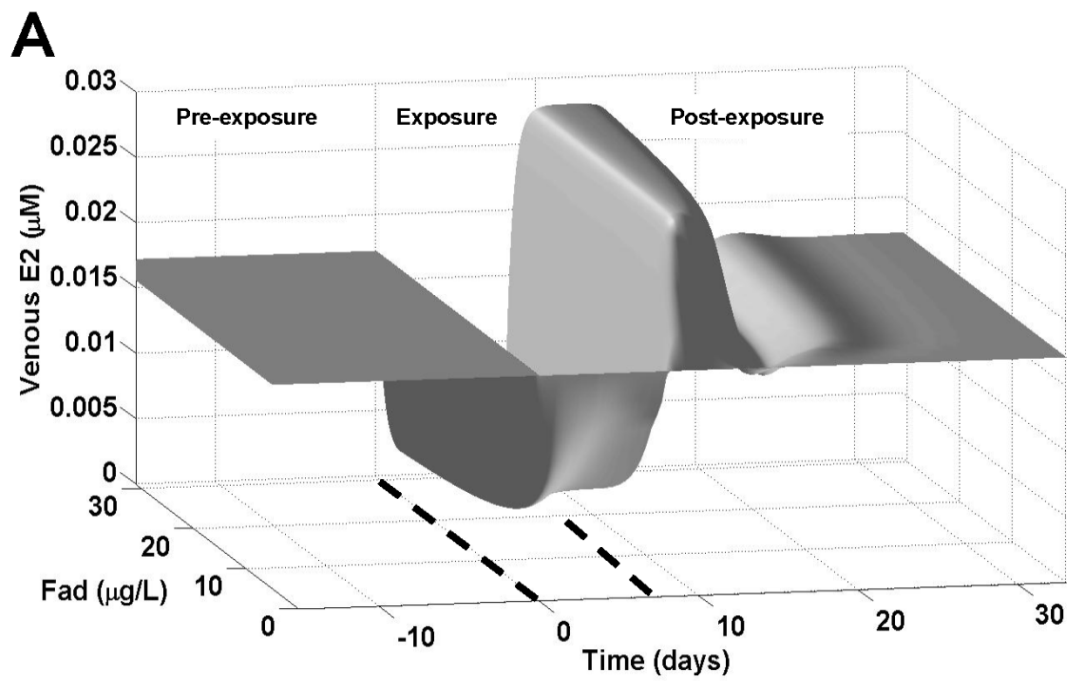


**Figure 4.** Model predictions plotted as a function of FAD concentration and time during pre-exposure (-15 – 0 days), exposure to FAD (0 – 8 days), and post-exposure (8 – 33 days) for venous E2 concentrations (A) and ovary CYP19A\_mRNA fold changes relative to controls (B).

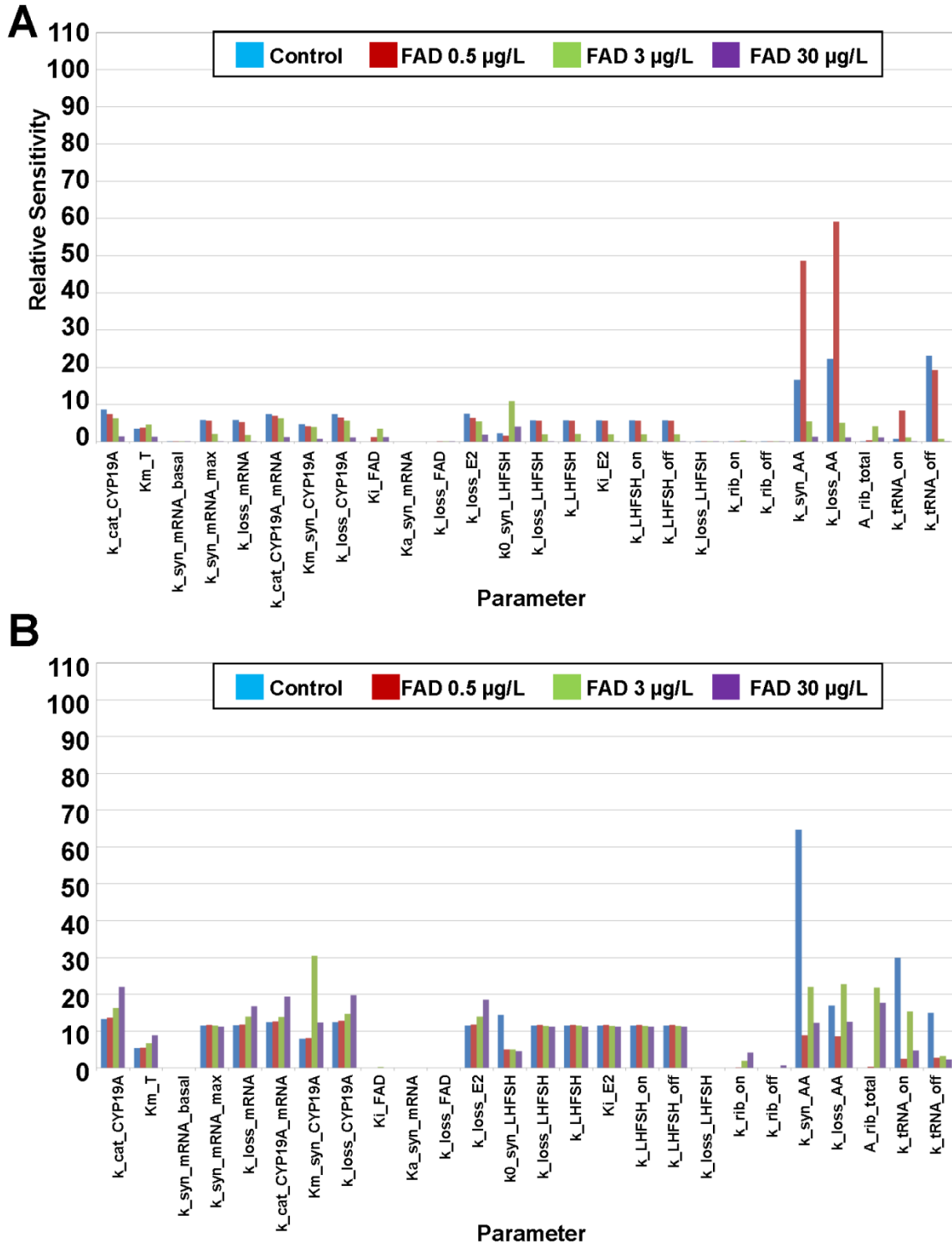


**Figure 5.** Relative sensitivities for modeled E2 plotted as a function of the 26 biochemical model parameters for control and three FAD concentrations (0.5, 3, and 30 µg/L). Each bar represents the  $L^2$  norm of the relative sensitivities across time during exposure (0 – 8 days; A) and post-exposure (8 – 33 days; B). The values indicate the degree to which changes in parameter values lead to changes in model outputs.

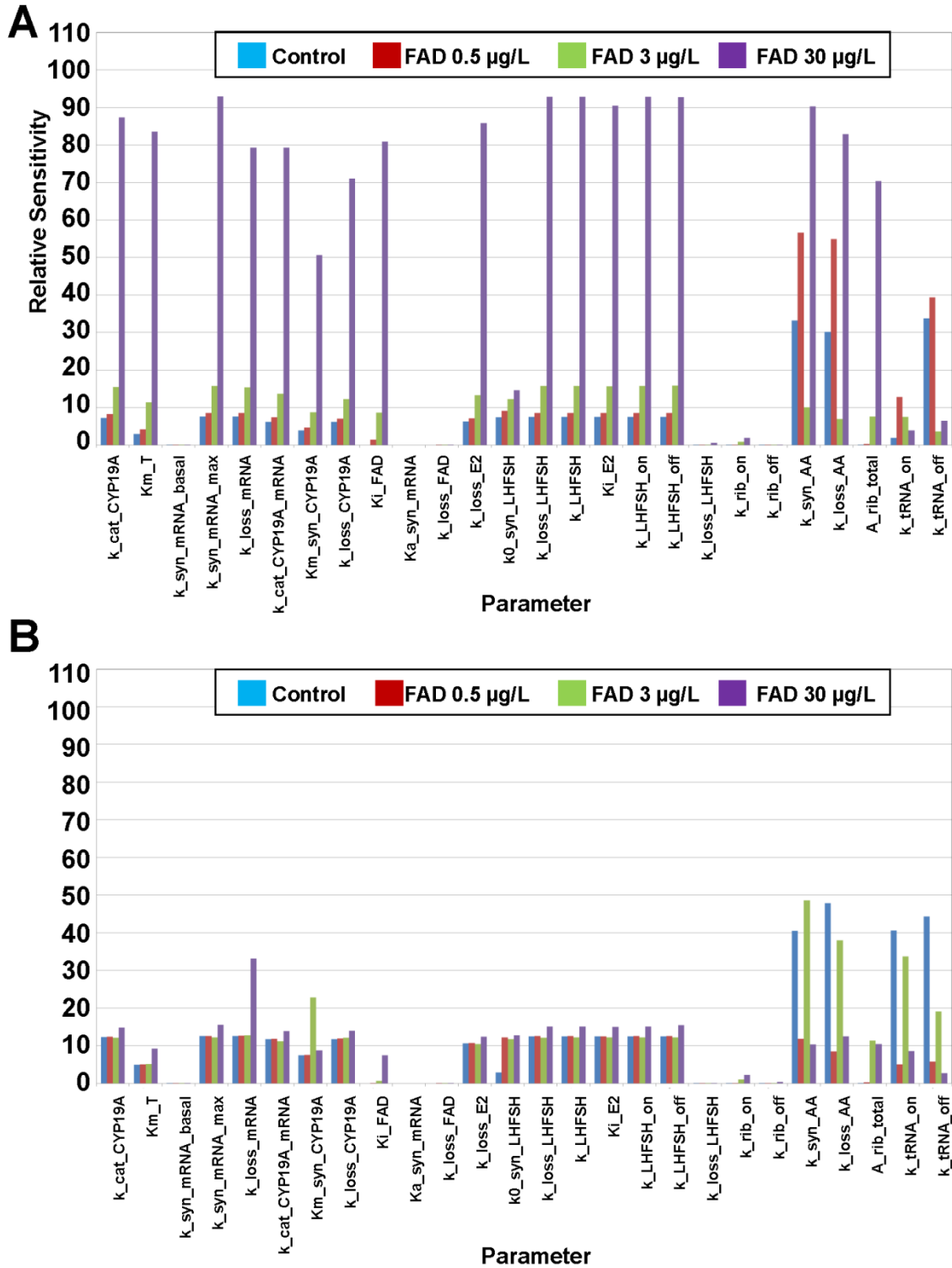


**Figure 6.** Relative sensitivities for modeled CYP19A\_mRNA plotted as a function of the 26 biochemical model parameters for control and three FAD concentrations (0.5, 3, and 30 µg/L). Each bar represents the  $L^2$  norm of the relative sensitivities across time during exposure (0 – 8 days; A) and post-exposure (8 – 33 days; B). The values indicate the degree to which changes in parameter values lead to changes in model outputs.

## REFERENCES

- Ankley, G.T., Bencic, D.C., Breen, M.S., Collette, T.W., Conolly, R.B., Denslow, N.D., Edwards, S.W., Ekman, D.R., Garcia-Reyero, N., Jensen, K.M., Lazorchak, J.M., Martinović, D., Miller, D.H., Perkins, E.J., Orlando, E.F., Villeneuve, D.L., Wang, R.L., Watanabe, K.H., 2009. Endocrine disrupting chemicals in fish: developing exposure indicators and predictive models of effects based on mechanism of action. *Aquat Toxicol.* 92, 168-178.
- Breen, M., Villeneuve, D.L., Ankley, G.T., Bencic, D.C., Breen, M.S., Watanabe, K.H., Lloyd, A.L., Conoll, R.B., 2013. Developing Predictive approaches to characterize adaptive responses of the reproductive endocrine axis to aromatase inhibition: II. Computational modeling. *Toxicol. Sci.* 133, 234-247.
- Bruce, A., Johnson, A., Lewis, J., Raff, M., Roberts, K., Walter, P., 2002. *Molecular biology of the cell*. 4th ed. Garland Science, New York, NY.
- Campbell, N.A., 1996. *Biology*. 4th ed. The Benjamin/Cummings Publishing Company, San Francisco, CA.
- Cooper, R.L., Kavlock, R.J., 1997. Endocrine disruptors and reproductive development: a weight-of-evidence overview. *J. Endocrinol.* 152, 159-166.
- Daston, G.P., Cook, J.C., Kavlock, R.J., 2003. Uncertainties for endocrine disruptors: our view on progress. *Toxicol. Sci.* 74, 245-252.
- Drenth, H.J., Bouwman, C.A., Seinen, W., Van den Berg, M.V., 1998. Effects of some persistent halogenated environmental contaminants on aromatase (CYP19) activity in the human choriocarcinoma cell line JEG-3. *Toxicol. Appl. Pharmacol.* 148, 50-55.
- Food Quality Protection Act, 1996. Public Law 104-170.
- Hutchinson, T.H., Ankley, G.T., Segner, H., Tyler, C.R., 2006. Screening and testing for endocrine disruption in fish-biomarkers as "signposts," not "traffic lights," in risk assessment. *Environ. Health Perspect.* 114, 106-114.
- Miller, W., 1988. Molecular biology of steroid hormone synthesis. *Endocr. Rev.* 9, 295-318.
- National Research Council., 2007. *Toxicity Testing in the 21st Century: A Vision and a strategy*. National Academy Press, Washington, DC
- Nelder, J.A., Mead, R., 1965. A simplex method for function minimization. *Comput. J.* 7, 308-313.

Petkov, P.I., Temelkov, S., Villeneuve, D.L., Ankley, G.T., Mekenyan, O.G., 2009. Mechanism-based categorization of aromatase inhibitors: A potential discovery and screening tool. SAR QSAR Environ. Res. 20, 657-678.

Ralston-Hooper, K.J., Turner, M.E., Soderblom, E.J., Villeneuve, D.L., Ankley, G.T., Moseley, M.A., Hoke, R.A., Ferguson, P.L., 2013. Application of a label-free, gel-free quantitative proteomics method for ecotoxicological studies of small fish species. Environ Sci Technol. 47, 1091-1100.

Safe Drinking Water Act Amendments, 1996. Public Law 104-182.

Sanderson, J. T., 2006. The steroid hormone biosynthesis pathway as a target for endocrine-disrupting chemicals. Toxicol. Sci. 94, 3-21.

U.S. Environmental Protection Agency, 1998. Endocrine Disruptor Screening Program. Federal Register. Vol. 63, No. 154, August 11, 1998, Page 42852-42855.

U.S. Environmental Protection Agency, 2009. Endocrine Disruptor Screening Program (EDSP): announcing the availability of the Tier 1 screening battery and related test guidelines. Federal Register. Vol. 74, No. 202, October 21, 2009, Page 54415-54422.

Villeneuve, D.L., Breen, M., Bencic, D.C., Cavallin, J.E., Jensen, K.M., Makynen, E.A., Thomas, L.M., Wehmas, L.C., Conoll, R.B., Ankley, G.T., 2013. Developing Predictive approaches to characterize adaptive responses of the reproductive endocrine axis to aromatase inhibition: I. Data Generation in a Small Fish Model. Toxicol. Sci. 133, 225-233.

Villeneuve, D.L., Mueller, N.D., Martinovic, D., Makynen, E.A., Kahl, M.D., Jensen, K.M., Durhan, E.J., Cavallin, J.E., Bencic, D., Ankley, G.T., 2009. Direct effects, compensation, and recovery in female fathead minnows exposed to a model aromatase inhibitor. Environ Health Perspect 117, 624-631.

Vinggaard, A.M., Hnida, C., Breinholt, V., Larsen, J.C., 2000. Screening of selected pesticides for inhibition of CYP19 aromatase activity *in vitro*. Toxicol. In Vitro. 14, 227-234.

Zacharewski T., 1998. Identification and assessment of endocrine disruptors: limitations of in vivo and in vitro assays. Environ. Health Perspect. 106, 577-582.

Supplemental Data to:

Computational Model of the Fathead Minnow Hypothalamic-Pituitary-Gonadal Axis: Role of Biological Protein Synthesis to Improve Predictability of Biochemical Response to Endocrine Active Chemicals

Miyuki Breen<sup>a</sup>, Daniel L. Villeneuve<sup>b</sup>, Gerald T. Ankley<sup>b</sup>, David Bencic<sup>c</sup>, Michael S. Breen<sup>d</sup>,  
Karen H. Watanabe<sup>e</sup>, Alun L. Lloyd<sup>a</sup>, Rory B. Conolly<sup>f,\*</sup>

<sup>a</sup> Biomathematics Graduate Program, Department of Mathematics, North Carolina State University, Box 8203, Raleigh, NC 27695, USA (mbreen@ncsu.edu)

<sup>b</sup> Mid-Continent Ecology Division, National Health and Environmental Effects Research Laboratory, U.S. Environmental Protection Agency, 6201 Congdon Blvd, Duluth, MN 55804, USA ([villeneuve.dan@epa.gov](mailto:villeneuve.dan@epa.gov))

<sup>c</sup> Ecological Exposure Research Division, National Exposure Research Laboratory, U.S. Environmental Protection Agency, Cincinnati, OH, USA (bencic.david@epa.gov)

<sup>d</sup> National Exposure Research Laboratory, U.S. Environmental Protection Agency, 109 TW Alexander Drive, Research Triangle Park, NC 27711, USA (breen.michael@epa.gov)

<sup>e</sup> Department of Environmental and Biomolecular Systems, Oregon Health & Science University, 20000 NW Walker Road, Beaverton, OR 97006, USA (watanabe@ebs.ogi.edu)

<sup>f</sup> Integrated Systems Toxicology Division, National Health and Environmental Effects Research Laboratory, U.S. Environmental Protection Agency, 109 TW Alexander Drive, Research Triangle Park, NC 27711, USA (conolly.rory@epa.gov)

**Address correspondence to:**

Rory Conolly  
U.S. Environmental Protection Agency  
Office of Research and Development  
National Health and Environmental Effects Research Laboratory  
109 T.W. Alexander Drive, Mail B105-03  
Research Triangle Park, NC 27711  
Telephone: 919-541-9782  
Email: [conolly.rory@epa.gov](mailto:conolly.rory@epa.gov)

## **Dynamic molecular balance equations**

### **Gill Compartment**

FAD:

$$C_{\text{FAD\_gill\_blood}} = \frac{Q_{\text{water\_gill}} C_{\text{FAD\_insp\_water}} + Q_{\text{cardiac}} C_{\text{FAD\_venous}}}{Q_{\text{cardiac}} + \frac{Q_{\text{water\_gill}}}{P_{\text{FAD\_water:blood}}}};$$

### **Brain Compartment**

E2:

$$V_{\text{brain}} \frac{dC_{\text{E2\_brain}}}{dt} = Q_{\text{brain}} \left( C_{\text{E2\_arterial}} - \frac{C_{\text{E2\_brain}}}{P_{\text{E2\_brain:blood}}} \right);$$

FAD:

$$V_{\text{brain}} \frac{dC_{\text{FAD\_brain}}}{dt} = Q_{\text{brain}} \left( C_{\text{FAD\_arterial}} - \frac{C_{\text{FAD\_brain}}}{P_{\text{FAD\_brain:blood}}} \right);$$

LH/FSH:

$$V_{\text{brain}} \frac{dC_{\text{LHFSH\_brain}}}{dt} = k_{0\_syn\_LHFSH} - k_{loss\_LHFSH} \cdot A_{\text{LHFSH\_brain}} - \frac{k_{\text{LHFSH}} \cdot A_{\text{LHFSH\_brain}}}{\left( 1 + \frac{C_{\text{E2\_brain}}}{K_{i\_E2}} \right)};$$

### **Ovary Compartment**

FAD:

$$V_{\text{ovary}} \frac{dC_{\text{FAD\_ovary}}}{dt} = Q_{\text{ovary}} \left( C_{\text{FAD\_arterial}} - \frac{C_{\text{FAD\_ovary}}}{P_{\text{FAD\_ovary:blood}}} \right);$$

E2:

$$V_{\text{ovary}} \frac{dC_{\text{E2\_ovary}}}{dt} = Q_{\text{ovary}} \left( C_{\text{E2\_arterial}} - \frac{C_{\text{E2\_ovary}}}{P_{\text{E2\_ovary:blood}}} \right) + \frac{V_{\text{max\_CYP19A}} \cdot C_{\text{T}}}{K_{\text{m\_T}} \left( 1 + \frac{C_{\text{FAD\_ovary}}}{K_{\text{i\_FAD}}} \right) + C_{\text{T}}};$$

CYP19A:

$$V_{\text{ovary}} \frac{dC_{\text{CYP19A}}}{dt} = \frac{V_{\text{max\_syn\_CYP19A}} \cdot C_{\text{AA\_tRNA}}}{K_{\text{m\_syn\_CYP19A}} + C_{\text{AA\_tRNA}}} - k_{\text{loss\_CYP19A}} \cdot A_{\text{CYP19A}};$$

Vmax of CYP19A (conversion of T to E2):

$$V_{\text{max\_CYP19A}} = k_{\text{cat\_CYP19A}} \cdot A_{\text{CYP19A}};$$

Amino Acids (AA):

$$V_{\text{ovary}} \frac{dC_{\text{AA}}}{dt} = k_{\text{syn\_AA}} - \frac{V_{\text{max\_syn\_CYP19A}} \cdot C_{\text{AA\_tRNA}}}{K_{\text{m\_syn\_CYP19A}} + C_{\text{AA\_tRNA}}} - k_{\text{loss\_AA}} \cdot A_{\text{AA}};$$

CYP19A mRNA:

$$V_{\text{ovary}} \frac{dC_{\text{CYP19A\_mRNA}}}{dt} = k_{\text{syn\_mRNA\_basal}} + \frac{(k_{\text{syn\_mRNA\_max}} - k_{\text{syn\_mRNA\_basal}}) C_{\text{LHFSH\_R\_LHFSH}}}{K_{\text{a\_syn\_mRNA}} + C_{\text{LHFSH\_R\_LHFSH}}} - k_{\text{loss\_mRNA}} \cdot A_{\text{CYP19A\_mRNA}};$$

CYP19A mRNA – Ribosome Complex:

$$V_{\text{ovary}} \frac{dC_{\text{CYP19A\_mRNA\_rib}}}{dt} = k_{\text{rib\_on}} \cdot A_{\text{CYP19A\_mRNA\_free}} \cdot A_{\text{rib\_free}} - k_{\text{rib\_off}} \cdot A_{\text{CYP19A\_mRNA\_rib}};$$

$$A_{\text{CYP19A\_mRNA\_free}} = A_{\text{CYP19A\_mRNA}} - A_{\text{CYP19A\_mRNA\_rib}};$$

$$A_{\text{rib\_free}} = A_{\text{rib\_total}} - A_{\text{CYP19A\_mRNA\_rib}};$$

Amino Acids – tRNA Complex:

$$V_{\text{ovary}} \frac{dC_{\text{AA\_tRNA}}}{dt} = k_{\text{tRNA\_on}} \cdot A_{\text{AA\_free}} \cdot A_{\text{tRNA\_free}} - k_{\text{tRNA\_off}} \cdot A_{\text{AA\_tRNA}};$$

$$A_{\text{AA\_free}} = A_{\text{AA}} - A_{\text{AA\_tRNA}};$$

$$A_{\text{tRNA\_free}} = A_{\text{tRNA\_total}} - A_{\text{AA\_tRNA}};$$

Vmax of CYP19A\_mRNA-rib complex (conversion of transcript (CYP19A mRNA) to protein (CYP19A)):

$$V_{\text{max\_syn\_CYP19A}} = k_{\text{cat\_CYP19A\_mRNA}} \cdot A_{\text{CYP19A\_mRNA\_rib}};$$

**Liver Compartment**

FAD:

$$V_{\text{liver}} \frac{dC_{\text{FAD\_liver}}}{dt} = Q_{\text{liver}} \left( C_{\text{FAD\_arterial}} - \frac{C_{\text{FAD\_liver}}}{P_{\text{FAD\_liver: blood}}} \right) - k_{\text{loss\_FAD}} \cdot A_{\text{FAD\_liver}};$$

E2:

$$V_{\text{liver}} \frac{dC_{\text{E2\_liver}}}{dt} = Q_{\text{liver}} \left( C_{\text{E2\_arterial}} - \frac{C_{\text{E2\_liver}}}{P_{\text{E2\_liver: blood}}} \right) - k_{\text{loss\_E2}} \cdot A_{\text{E2\_liver}};$$

## Venous Blood Compartment

LH/FSH-receptor complex:

$$\begin{aligned} \frac{dA_{\text{LHFSH\_R\_LHFSH}}}{dt} &= k_{\text{LHFSH\_on}} \cdot A_{\text{LHFSH\_venous\_free}} \cdot A_{\text{R\_LHFSH\_free}} \\ &\quad - k_{\text{LHFSH\_off}} \cdot A_{\text{LHFSH\_R\_LHFSH}}, \end{aligned}$$

where  $A_{\text{R\_LHFSH\_free}} = A_{\text{R\_LHFSH}} - A_{\text{LHFSH\_R\_LHFSH}}$

and  $A_{\text{LHFSH\_venous\_free}} = A_{\text{LHFSH\_venous}} - A_{\text{LHFSH\_R\_LHFSH}};$

LH/FSH:

$$V_{\text{venous}} \frac{dC_{\text{LHFSH\_venous}}}{dt} = \frac{k_{\text{LHFSH}} \cdot A_{\text{LHFSH\_brain}}}{\left( 1 + \frac{C_{\text{E2\_brain}}}{K_{\text{i\_E2}}} \right)} - k_{\text{loss\_LHFSH}} \cdot A_{\text{LHFSH\_venous\_free}};$$

E2:

$$V_{\text{venous}} \frac{dC_{\text{E2\_venous}}}{dt} = Q_{\text{liver}} \left( \frac{C_{\text{E2\_liver}}}{P_{\text{E2\_liver:blood}}} \right) + Q_{\text{ovary}} \left( \frac{C_{\text{E2\_ovary}}}{P_{\text{E2\_ovary:blood}}} \right) \\ + Q_{\text{brain}} \left( \frac{C_{\text{E2\_brain}}}{P_{\text{E2\_brain:blood}}} \right) + Q_{\text{RoB}} \left( \frac{C_{\text{E2\_RoB}}}{P_{\text{E2\_RoB:blood}}} \right) - Q_{\text{cardiac}} C_{\text{E2\_venous}};$$

FAD:

$$V_{\text{venous}} \frac{dC_{\text{FAD\_venous}}}{dt} = Q_{\text{liver}} \left( \frac{C_{\text{FAD\_liver}}}{P_{\text{FAD\_liver:blood}}} \right) + Q_{\text{ovary}} \left( \frac{C_{\text{FAD\_ovary}}}{P_{\text{FAD\_ovary:blood}}} \right) \\ + Q_{\text{brain}} \left( \frac{C_{\text{FAD\_brain}}}{P_{\text{FAD\_brain:blood}}} \right) + Q_{\text{RoB}} \left( \frac{C_{\text{FAD\_RoB}}}{P_{\text{FAD\_RoB:blood}}} \right) - Q_{\text{cardiac}} C_{\text{FAD\_venous}};$$

## Rest of Body Compartment

FAD:

$$V_{\text{RoB}} \frac{dC_{\text{FAD\_RoB}}}{dt} = Q_{\text{RoB}} \left( C_{\text{FAD\_arterial}} - \frac{C_{\text{FAD\_Rob}}}{P_{\text{FAD\_RoB:blood}}} \right);$$

E2:

$$V_{\text{RoB}} \frac{dC_{\text{E2\_RoB}}}{dt} = Q_{\text{RoB}} \left( C_{\text{E2\_arterial}} - \frac{C_{\text{E2\_Rob}}}{P_{\text{E2\_RoB:blood}}} \right);$$

## 5. COMMENTARY ON THE PARAMETER IDENTIFICATION ISSUE

Mathematical modeling of biological systems and their response to chemical exposures plays a key role to enhance the interpretation and quantitative application of biological measurement data in risk assessments and drug development. Computational models are considered the central element in systems biology, which allows us to better understand complex biological systems by means of *in silico* experiments, model predictions, and hypothesis generation (Chris *et al.*, 2011). Since it is often not possible to measure key model parameters directly, these parameters need to be obtained from an estimation process by data fitting, and this process is a critical step in model development (Chris *et al.*, 2011; Saccomani *et al.*, 2011). However, mathematical models that describe biological systems are often complex nonlinear dynamic models with many unknown parameters (Saccomani *et al.*, 2011). Given the complexity of biological mechanisms in combination with the limited amount of quantitative biological data, it is important in the model development process to infer how well model parameters can be determined. The mismatch between the complexity of the models and the limited available data can lead to ill-conditioned inverse problems (Burth *et al.*, 1999). Hence, parameter estimation can be a challenging mathematical and computational problem (Chris *et al.*, 2011).

The main source of difficulties to estimate unknown parameters is the lack of identifiability, which is an important aspect of model development (Chris *et al.*, 2011; Jacquez and Greif, 1985). For the models to be identifiable, a unique solution of the inverse problem for all the free parameters must exist (Chris *et al.*, 2011; Jacquez and Greif, 1985). Therefore, it is not possible to assign unique values for all the unknown parameters when the model has

identifiability issues (Chis *et al.*, 2011). Identifiability can be of particular importance when many of the model parameters have biological meaning, and these parameter values have implications in biological or public health contexts, e.g. estimating the basic reproductive number,  $R_0$ , in epidemiological models (Chis *et al.*, 2011; Eisenberg *et al.*, 2013). Hence, identifiability of estimated model parameters and their uncertainties need to be addressed.

Parameter identification issues can be classified into two types: structural (a priori) non-identifiability and practical (a posteriori or data-based) non-identifiability (Chis *et al.*, 2011; Saccomani, 2013). Structural non-identifiability arises when some model parameters cannot be uniquely determined in the best-case scenario of noise-free data (Chis *et al.*, 2011; Eisenberg *et al.*, 2013; Saccomani, 2013). For instance, when the model is structurally non-identifiable, it is not possible to estimate two or more parameters in the model separately (Capaldi *et al.*, 2012), but only some combination of parameters. Moreover a structural non-identifiable model might contain unnecessary parameters. These parameters might be not identifiable since the model does not depend at all on the parameters. Structural identifiability is a necessary condition for estimating parameters in model development for real-life situations, which use data with inevitable noise and possibly insufficient data length (Eisenberg *et al.*, 2013; Saccomani, 2013). Practical non-identifiability arises when we lack information in the available experimental data (Chis *et al.*, 2011; Saccomani, 2013). We often encounter severe constraints on experimental design when we attempt to develop mathematical models of biological systems (Saccomani, 2013). To model biological systems, practical identifiability issues frequently occur due to estimating parameters with an insufficient sample size, since it is expensive and time consuming to collect large

experimental data, especially for *in vivo* studies. In addition, mathematical modeling of biological systems often includes complicated non-linear terms such as Michaelis-Menten and Hill kinetics in their model equations, which requires appropriate data to capture both an early exponential growth and a saturation phase. The lack of appropriate data could be another common source of practical non-identifiability.

The most noticeable cause of non-identifiability is due to over-parameterization of models (Catchpole *et al.*, 1997). Parameter redundancy occurs when a model has too many parameters (Cole *et al.*, 2010). We could also have parameter redundancy in the practical

sense with complicated non-linear terms such as Michaelis-Menten kinetics,  $v = \frac{V_{\max} S}{S + K_m}$ ,

e.g. the parameters  $V_{\max}$  and  $K_m$  cannot be estimated independently when  $S \ll K_m$ , since

$v \approx \left( \frac{V_{\max}}{K_m} \right) S$ . For a parameter redundant model, a set of model parameters can be expressed

in terms of a smaller set of parameters (Catchpole *et al.*, 1997; Little *et al.*, 2010).

In our study, mathematical modeling of biological systems was performed by using a system of nonlinear ordinary differential equations. The mathematical models were developed based on knowledge of biological mechanisms, and model parameters were estimated using biological data generated from experiments. It is essential in the model development process to infer how well model parameters can be determined and the uncertainty of the estimated model parameters given the complexity of biological mechanisms in combination with the limited amount of quantitative biological data. Thus, the estimation of unknown model parameters, identifiability, and uncertainty quantification play

a central role in the model development. To quantify the uncertainties of estimated model parameters in our study, standard errors of estimated model parameters for the extended H295R steroidogenesis model of Chapter 2 and the first HPG axis model of Chapter 3 were calculated. Moreover, we examined identifiability of the first HPG axis model of Chapter 3.

### Standard Error and Correlation Coefficient Calculation

To quantify the uncertainties of the estimated model parameters in our models, standard errors and relative standard errors of the estimated model parameters were calculated. In addition, we calculated the correlation matrix of the model parameters. We followed the development and notation laid out in Banks *et al.* (2009) to describe the standard error and correlation coefficient calculations. The statistical model is defined as

$$\bar{Y}_j = \bar{f}(t_j, \bar{\theta}) + \bar{\varepsilon}_j, \quad j = 1, \dots, n, \quad (1)$$

where  $\bar{f}(t_j, \bar{\theta})$  is our deterministic model and  $\bar{\varepsilon}_j$  are the errors. The ordinary least squares

estimator  $\hat{\theta}$  is obtained by minimizing the cost function  $\sum_{j=1}^n [\bar{y}_j - \bar{f}(t_j, \bar{\theta})]^T [\bar{y}_j - \bar{f}(t_j, \bar{\theta})]$ ,

$$\hat{\theta} = \arg \min_{\bar{\theta}} \sum_{j=1}^n [\bar{y}_j - \bar{f}(t_j, \bar{\theta})]^T [\bar{y}_j - \bar{f}(t_j, \bar{\theta})]. \quad (2)$$

Then, the  $m \times p$  sensitivity matrix  $D_j(\bar{\theta})$  is given by

$$D_j(\bar{\theta}) = \begin{pmatrix} \frac{\partial f_1(t_j, \bar{\theta})}{\partial \bar{\theta}_1} & \frac{\partial f_1(t_j, \bar{\theta})}{\partial \bar{\theta}_2} & \dots & \frac{\partial f_1(t_j, \bar{\theta})}{\partial \bar{\theta}_p} \\ \frac{\partial f_2(t_j, \bar{\theta})}{\partial \bar{\theta}_1} & \frac{\partial f_2(t_j, \bar{\theta})}{\partial \bar{\theta}_2} & \dots & \frac{\partial f_2(t_j, \bar{\theta})}{\partial \bar{\theta}_p} \\ \vdots & \vdots & \ddots & \vdots \\ \frac{\partial f_m(t_j, \bar{\theta})}{\partial \bar{\theta}_1} & \frac{\partial f_m(t_j, \bar{\theta})}{\partial \bar{\theta}_2} & \dots & \frac{\partial f_m(t_j, \bar{\theta})}{\partial \bar{\theta}_p} \end{pmatrix}, \quad j = 1, \dots, n, \quad (3)$$

where  $m$  is the number of states of the system. The estimated variance of error matrix is given by

$$\hat{V} = \text{var}(\bar{\varepsilon}_j) = \text{diag} \left( \frac{1}{n-p} \sum_{j=1}^n [\bar{y}_j - \bar{f}(t_j, \bar{\theta})][\bar{y}_j - \bar{f}(t_j, \bar{\theta})]^T \right), \quad (4)$$

which is an unbiased estimator. The variance-covariance matrix is described by

$$\hat{\Sigma} = \Omega^{-1}, \quad (5)$$

where  $\Omega = \sum_{j=1}^n D_j^T(\bar{\theta}) \hat{V}^{-1} D_j(\bar{\theta})$ . Using the variance-covariance matrix, we obtain the standard

errors  $SE(\hat{\theta}_k)$  for the  $k^{th}$  element of  $\hat{\theta}$  by

$$SE(\hat{\theta}_k) \approx \sqrt{\hat{\Sigma}_{kk}}, \quad k = 1, \dots, p, \quad (6)$$

and the correlation matrix  $P$  by

$$P = M^{-1} \hat{\Sigma} M^{-1}, \quad (7)$$

where  $M = \sqrt{\text{diag}(\hat{\Sigma})}$ .

Standard errors and relative standard errors for the estimated transport equilibrium parameters and the estimated parameters of the metabolic pathway in the extended H295R

model of Chapter 2 are shown in Table 1 and Table 2, respectively. Overall, relative standard errors for the estimated parameters of the metabolic pathway were much smaller than estimated transport equilibrium parameters. The relative standard errors for all the estimated parameters of metabolic pathway were very small, less than 3.3%, except one parameter  $k_{14}$ . The model parameter,  $k_{14}$ , had very large uncertainty. We believe the large uncertainty is due to the existence of two paths to create E2 in our model, namely the E1 pathway and the T pathway. Based on the sensitivity analysis results, the E1 pathway appears to be the preferred pathway for E2 synthesis, as compared to the T pathway (Breen *et al.*, 2011). The relative standard errors for all of the estimated transport equilibrium parameters were also small, less than 15.9%, except one parameter  $q_{28}$  having a larger value of 65.78%. The absolute values of each element of the correlation matrix for the metabolic pathway are shown in Figure 1. Taking the absolute value of the correlation coefficient measures the strength of the relationship. Overall, most pairs of estimated parameters have very little or no correlation. The correlation matrix for the estimated transport equilibrium parameters is the identity matrix since transport equilibrium parameters are independent of each other, which implies that their covariance is zero.

We encountered a problem when we attempted to calculate the standard errors and the correlation matrix of the estimated model parameters of the HPG axis model of Chapter 3. As described earlier, existence and invertibility of the matrix  $\Omega$  in Equation (6) is required in order to calculate the standard errors and the correlation matrix. However, this required condition is rather easily violated in practice (Banks *et al.*, 2009). We were unable to invert the matrix  $\Omega$  without a warning of potential inaccurate results using Matlab, since the matrix

was ill-conditioned. Hence, we were incapable of obtaining stable estimates of the standard errors and the correlation matrix. This result suggests that the estimated model parameters in the HPG axis model suffer from parameter identifiability issues. Therefore, identifiability of the HPG axis model of Chapter 3 was examined.

**Table 1. Estimated transport equilibrium parameters, standard errors, and relative standard errors**

Parameter	Value	SE	Relative SE (%)
q <sub>19</sub>	0.0129	0.0007	5.43
q <sub>20</sub>	0.0052	0.0003	5.77
q <sub>21</sub>	0.0412	0.0028	6.80
q <sub>22</sub>	0.0558	0.0019	3.41
q <sub>23</sub>	0.0911	0.0027	2.96
q <sub>24</sub>	0.0605	0.0087	14.38
q <sub>25</sub>	0.0212	0.0014	6.60
q <sub>26</sub>	0.0423	0.0067	15.84
q <sub>27</sub>	0.0676	0.0023	3.40
q <sub>28</sub>	0.0377	0.0248	65.78
q <sub>29</sub>	0.0400	0.0024	6.00
q <sub>30</sub>	0.0267	0.0009	3.37
q <sub>31</sub>	0.0443	0.0015	3.39
q <sub>32</sub>	0.0351	0.0020	5.70

**Table 2. Estimated parameters of metabolic pathway, standard errors, and relative standard errors**

Parameter	Value	SE	Relative SE (%)
$k_0$	0.0139	0.0000	0
$k_1$	0.0163	0.0000	0
$k_2$	0.0105	0.0000	0
$k_3$	0.7573	0.0006	0.08
$k_4$	1.2683	0.0028	0.22
$k_5$	0.8139	0.0007	0.09
$k_6$	11.1525	0.0280	0.25
$k_7$	7.2168	0.0013	0.02
$k_8$	0.1765	0.0058	3.29
$k_9$	1.7537	0.0085	0.48
$k_{10}$	0.0476	0.0006	1.26
$k_{11}$	6.4794	0.0019	0.03
$k_{12}$	12.1879	0.0173	0.14
$k_{13}$	0.5948	0.0008	0.13
$k_{14}$	0.0005	0.2013	40260.00
$k_{15}$	0.0910	0.0008	0.88
$k_{16}$	0.6367	0.0038	0.60
$k_{17}$	0.2471	0.0001	0.04
$k_{18}$	0.1215	0.0004	0.33
$k_{41}$	63.5659	0.0000	0
$k_{42}$	25.2075	0.0000	0

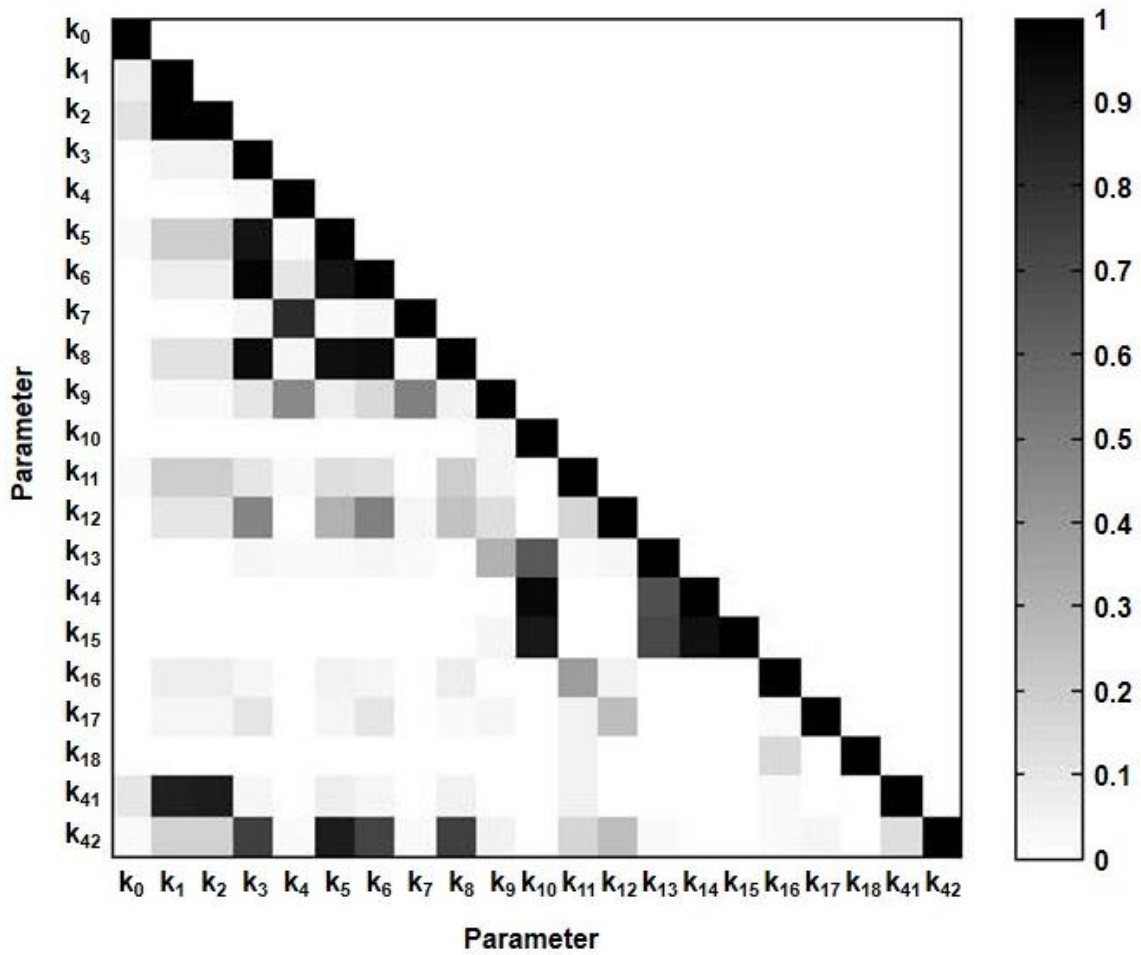


Figure 1: Heat map of correlation coefficients for metabolic pathway parameters of the H295R model. The heat map shows the absolute value of each element of the correlation matrix.

### Identifiability Analysis

As discussed earlier, we could encounter practical identifiability issues due to the insufficient data available for an inverse problem. Collecting biological data is often difficult and costly (Capaldi *et al.*, 2012). Our HPG axis model is a representation of the endocrine system of an organism (i.e., fish) based on *in vivo* experimental results. The HPG model was developed from detailed analysis of the underlying biological system, which involves a

relatively large number of biologically interesting parameters. On the other hand, the data available from *in vivo* experiments are typically not large. It is the nature of *in vivo* studies that experiments are expensive and time consuming, and that biological systems at the organismal level are highly complex. The HPG axis model has 16 model parameters to estimate from 26 data points. Therefore, the ratio between the number of observables and the number of parameters in our HPG axis model is low. To examine the possibility of insufficient data, we generated a larger dataset by simulation under a best case scenario. We obtained computer-generated data from the model simulation without any noise for each of the 16 state variables, sampled every 24 hours for 34 hours, and at 3 doses, and model parameters were re-estimated with this dataset. These estimated parameter values did not change substantially from the estimated HPG axis model parameters shown in Chapter 3. Moreover, we were still unable to invert the matrix  $\Omega$  in Equation (6) without a warning of potential inaccurate results using Matlab, since the matrix was ill-conditioned. Even though we used the best case scenario of a large dataset to re-estimate model parameters, we were still unable to obtain stable estimates of the standard errors and correlation matrix for the HPG axis model.

We could also encounter structural identifiability issues. One of the potential causes of non-identifiability is due to over-parameterization of models, causing some of parameters to be unidentifiable. Under these conditions, reduced model and combinations of parameters can be estimated even when individual parameters may not be estimated (Eisenberg *et al.*, 2013). Therefore, one way to overcome this issue is to use the subset selection method to reduce the number of parameters to be estimated in the model (Burth *et al.*, 1999). To apply

subset selection, the model parameters are partitioned into well-conditioned and ill-conditioned parameters: well-conditioned parameters are the parameters likely to be estimated reliably, whereas ill-conditioned parameters are the remaining parameters that are likely to be causing the inverse problem to be ill-conditioned (Burth *et al.*, 1999). Ill-conditioned model parameters are fixed at prior estimated values, while the remaining well-conditioned parameters are re-estimated using the same dataset (Burth *et al.*, 1999). This approach may introduce the bias by fixing the ill-conditioned parameters to prior estimates, but could lead to major improvements on the parameter estimation over full-order estimation (Burth *et al.*, 1999). We implemented the subset selection method for our HPG axis model using the L2 norm results of the sensitivity analysis. Small perturbations in the highly sensitive parameters result in large changes in the model output, whereas substantial variations in the relatively insensitive parameters result in only small changes in the model output (Reich, 1981; Li *et al.*, 1996). Parameters could become identifiable when insensitive parameters are fixed a priori (Li *et al.*, 1996). Thus, we selected a subset of parameters to be re-estimated by ordering parameters according to the L2 norm results of the sensitivity analysis, and fixing the insensitive parameters to prior estimates. First, we fixed four insensitive parameters ( $k_{\text{syn\_mRNA\_basal}}$ ,  $K_{\text{a\_syn\_mRNA}}$ ,  $k_{\text{loss\_FAD}}$ ,  $k_{\text{loss\_LHFSH}}$ ) to prior estimated values and then re-estimated 12 sensitive parameters ( $k_{\text{syn\_mRNA\_max}}$ ,  $k_{\text{loss\_mRNA}}$ ,  $V_{\text{max\_syn\_CYP19A}}$ ,  $K_{\text{m\_syn\_CYP19A}}$ ,  $k_{\text{loss\_CYP19A}}$ ,  $K_{\text{i\_FAD}}$ ,  $K_{\text{a\_syn\_mRNA}}$ ,  $k_{\text{loss\_E2}}$ ,  $k_{0\_syn\_LHFSH}$ ,  $k_{\text{LHFSH}}$ ,  $K_{\text{i\_E2}}$ ,  $k_{\text{LHFSH\_off}}$ ). We were still unable to invert the matrix  $\Omega$  in Equation (6) without a warning of potential inaccurate results using Matlab, since the matrix was ill-conditioned. Next, we halved the number of parameters to be re-estimated, choosing 6 parameters to be

re-estimated from 12 sensitive parameters and fixing the remaining 12 parameters to prior estimated values. We tried every combination of 6 sensitive parameters, but were still unable to invert the matrix  $\Omega$ . Even with this substantial reduction in the number of estimated model parameters, we were still unable to obtain stable estimates of the standard errors and correlation matrix for the HPG axis model.

We also used a Monte Carlo approach to investigate parameter identifiability for the HPG axis model. First, we generated 100 data sets by adding small noise to the simulated hourly model output based on the published results, and model parameters were re-estimated using the generated data set. Then, the matrix  $\Omega$  was created and we removed, in turn, row  $i$  and column  $i$  from the matrix (i.e., treating parameter  $i$  as if it were known.) Based on the set of matrices generated, we then selected which parameter to eliminate from the estimation process, either by finding which matrix had the largest condition number (i.e. “hardest” to invert) or which of the resulting variance/covariance matrices yielded the largest correlation between some pair of parameters. Using this approach, we could remove, one-by-one, “troublesome” parameters. In many instances, the matrix  $\Omega$  was not positive definite until many parameters were removed. And in some instances, most of the parameters had to be removed, leaving only a set of four, five, or six parameters that were identifiable, despite the fact that this procedure was based on idealized scenarios. These results are in agreement with the subset selection analysis, which showed the inability of obtaining stable estimates of the standard errors and correlation matrix for the HPG axis model. Based on the results from several analyses to examine potential identifiability issues, we believe that our HPG axis model had non-identifiable parameters. Hence, we are unable to estimate all 16 parameters

reliably. Work is ongoing to investigate the issue of identifiability in more detail for this model.

Currently, the vast majority of biological models are nonlinear and dynamic, including the biological models developed in this study. Ideally, one would like to establish the domain of validity of the identifiability algorithm. However, this may not be possible (Saccomani et al., 2010). Testing the identifiability of general non-linear dynamic models is an extremely challenging mathematical problem (Chis *et al.*, 2011). In addition, it may also not be possible to distinguish between non-identifiability and lack of convergence of the iterative optimization algorithm used for parameter estimation (Saccomani et al., 2010), which could further complicate the investigation of identifiability. Moreover, we also need to consider designing the experiment to improve the ability to estimate the model parameters. An optimized experimental design is necessary to improve the estimability of the relevant parameters in biological models. Identifiability and optimal sampling design are linked steps in parameter estimation (Jacquez and Greif, 1985).

## REFERENCES

- Banks HT, Davidian M, Samuels JR, Sutton KL. (2009). An Inverse Problem Statistical Methodology Summary. In *Mathematical and Statistical Estimation Approaches in Epidemiology*. DOI 10.1007/978-90-481-2313-1\_11. Springer Science+Business Media B.V. 249-302.
- Breen M, Breen MS, Terasaki N, Yamazaki M, Lloyd AL, Conolly RB. (2011). Mechanistic Computational Model of Steroidogenesis in H295R Cells: Role of Oxysterols and Cell Proliferation to Improve Predictability of Biochemical Response to Endocrine Active Chemical-Metyrapone. *Toxicol Sci.* **123**, 80-93.

- Burth M, Verghese GC, Velez-Reyes M. (1999). Subset selection for improved parameter estimation in on-line identification of a synchronous generator. *IEEE Trans Power Syst.* **14**, 218-225.
- Capaldi A, Behrend S, Berman B, Smith J, Wright J, Lloyd AL. (2012). Parameter estimation and uncertainty quantification for an epidemic model. *Math Biosci Eng.* **9**, 553-576.
- Catchpole EA, Morgan BJT. (1997). Detecting parameter redundancy. *Biometrika.* **84**, 187-196.
- Chis O, Banga J, Balsa-Canto E. (2011). GenSSI: a Software Toolbox for Structural Identifiability Analysis of Biological Models. *Bioinformatics.* **27**, 2610-2611.
- Chis O, Banga J, Balsa-Canto E. (2011). Structural identifiability of systems biology models: a critical comparison of methods. *PLoS One.* **6**, e27755.
- Cole DJ, Morgan BJT, Titterton DM. (2010). Determining the Parametric Structure of Models. *Math Biosci.* **228**, 16-30.
- Eisenberg MC, Robertson SL, Tien JH. (2013). Identifiability and estimation of multiple transmission pathways in cholera and waterborne disease. *J Theor Biol.* **324**, 84-102.
- Jacquez J, Greif P. (1985). Numerical Parameter Identifiability and Estimability. *Math Biosci.* **77**, 201-227.
- Li SC, Lewandowsky S, DeBrunner, VE. (1996). Using parameter sensitivity and interdependence to predict model scope and falsifiability. *J Exp Psychol Gen.* **125**, 360-369.
- Little MP, Heidenreich WF, Li G. (2010). Parameter Identifiability and Redundancy: Theoretical Considerations. *PLoS One.* **5**, e8915.
- Reich JG. (1974). Analysis of kinetic and binding measurements I. information content of kinetic data. *Studia Biophysica*, **42**, 165-180.
- Reich JG. (1974). Analysis of kinetic and binding measurements IV. Redundancy of Model Parameters. *Studia Biophysica*, **43**, 91-107.
- Reich JG. (1981). On Parameter Redundancy in Curve Fitting of Kinetic Data. *Kinet Data Anal.* 39-50.
- Saccomani MP, Audoly S, Bellu G, D'Angiò L. (2011). Examples of Testing Global Identifiability of Biological and Biomedical Models with the DAISY Software. *Comput Biol Med.* **40**, 402-407.

Saccomani MP. (2013). Structural vs Practical Identifiability in System Biology. *IWBBIO*. 305-313.

## 6. CONCLUSIONS

We have developed mechanistic computational models to predict the biochemical responses of vertebrate endocrine systems to EACs in collaboration with government, academia, and industry within the United States and internationally. Specifically, we developed (1) a model of the metabolic network of adrenal steroidogenesis in human cells to predict the synthesis and secretion of adrenocortical steroids and their dynamic dose-response to EACs, and (2) a model of the HPG axis in female fathead minnows to predict dose-response and time-course behaviors for endocrine effects of EACs. A variety of environmental contaminants and pharmaceuticals are known to act as EACs, which have the potential to alter endocrine homeostasis leading to adverse effects in exposed vertebrates including humans. In order to assess environmental risk, exposures must be linked to effects of EACs. It is critical to establish a causal relationship between exposures and adverse effects of EACs in order to understand the result of molecular and biochemical changes. The development of predictive mechanistic computational models allows for more accurate and efficient quantitative evaluations of the chemical toxicants to help overcome challenges in ecological and human risk assessments, and to improve quantitative risk assessments. The integration of mathematical and computational models with the technology of molecular biology and chemistry enabled us to improve the ability to predict the effects in exposed vertebrates. In collaboration with experimental scientists, the use of data from laboratory experiments allowed us to develop and evaluate mathematical models of biochemical signaling and metabolic pathways, which could be utilized for predicting human health and ecological outcomes from exposures to chemical toxicants. Moreover, the use of *in vitro*

experimental methods together with our computational model support the recommendations of the National Research Council report on the vision of toxicology in the 21<sup>st</sup> century with the use of *in vitro* systems that can: (1) provide broad coverage of chemicals, mixtures, and outcomes; (2) reduce the cost and time of testing; (3) use fewer animals; and (4) develop more robust scientific basis to assess health effects from environmental chemicals.

In particular, our research demonstrates the need for a close collaboration between modelers and biologists/toxicologists to successfully develop and evaluate mechanistic computational models that can predict and improve the understanding of the mechanisms for dose-response behavior of EACs. Data needed by the modelers (e.g., ovary volume measurements) were obtained experimentally. In turn, model simulations helped generate testable hypotheses that directed further laboratory work. The application and refinement of these models are proceeding in much the same way. As experimental data is generated, it informs the refinement of these models and its adaptation for other applications. In turn, use of these models for those applications leads to additional hypotheses that can be tested to inform our understanding and the impact of chemical stressors on important biological processes. Our dose-response models for human adrenal cells and fish exposed to EACs support both human health and ecological risk assessments by advancing our understanding of the biological effects of chemicals considered harmful to the public and ecosystems, which include many EACs. Both of these models and the approaches taken for their development represent innovative and highly transferrable products that address critical needs for improved predictive risk assessments related to EACs.

The mechanistic computational models developed in our research have several potential applications. First, these models will help to improve our understanding of the biochemical responses to EAC, and could be used to identify predictive biomarkers indicative of adverse effects. Second, these models could be used as a basis to predict the potentially adverse effects of environmental EAC that interact with components of the modeled biological pathways. Furthermore, the mechanistic information incorporated in the models could help to more accurately extrapolate dose-response curves from high dose data to lower doses that are often more environmentally relevant. These applications can help overcome challenges in both ecological and human risk assessments since the modeled biological pathways are conserved across vertebrates (e.g., human, fish).

There are some limitations to our mechanistic computational models. In particular, our model of the HPG axis had some parameter identification challenges. Mathematical models are simplified representations of the systems and processes in which we are interested. Even though the use of an *in vivo* experimental method linked to our computational model provided us with valuable biological information, we had limited data available due to the expense and time constraints of the *in vivo* study. The small sample size used for parameter estimation could contribute to the uncertainty in the parameter values.

In our study, the primary use of models is to make predictions. The ability to forecast the unseen outcome under different situations provides us with vital information. However, the meaning and relevance of the model parameters may be compromised under parameter identification issues. It is a requirement for parameter estimation that all parameters in a model are identifiable on the basis of the observed data. The absence of identifiable

parameters implies that we cannot distinguish between different values of parameters on the basis of the observed data. Even though it is possible to estimate parameter values even when not all parameters are identifiable, the estimated parameters may not be reliable. The simplest way to solve the problem of parameter estimation with non-identifiable parameters is to predetermine the values of other parameters in the model which could influence the parameters being estimated by other means, and hold these parameters to be predetermined fixed values. However, even this simplest approach requires additional data or knowledge in order to predetermine these parameter values soundly. The exploration of identifiability is a major task, which needs to be addressed in future research.

## APPENDICES

## Appendix A

### **COMPUTATIONAL MODEL OF STEROIDOGENESIS IN HUMAN H295R CELLS TO PREDICT BIOCHEMICAL RESPONSE TO ENDOCRINE-ACTIVE CHEMICALS: MODEL DEVELOPMENT FOR METYRAPONE**

Michael S. Breen, Miyuki Breen, Natsuko Terasaki, Makoto Yamazaki, Rory B. Conolly

Published in Environmental Health Perspectives: 2010; 118: 265-272

Publication of this article lies in the public domain

Miyuki Breen was primarily responsible for assistance of model development, simulation, analysis of results, and manuscript writing.

# Computational Model of Steroidogenesis in Human H295R Cells to Predict Biochemical Response to Endocrine-Active Chemicals: Model Development for Metirapone

Michael S. Breen,<sup>1</sup> Miyuki Breen,<sup>2,3</sup> Natsuko Terasaki,<sup>4</sup> Makoto Yamazaki,<sup>4</sup> and Rory B. Conolly<sup>2</sup>

<sup>1</sup>National Exposure Research Laboratory and <sup>2</sup>National Center for Computational Toxicology, U.S. Environmental Protection Agency, Research Triangle Park, North Carolina, USA; <sup>3</sup>Biomathematics Program, Department of Statistics, North Carolina State University, Raleigh, North Carolina, USA; <sup>4</sup>Safety Research Laboratory, Mitsubishi Tanabe Pharma Corporation, Kisarazu, Chiba, Japan

**BACKGROUND:** An *in vitro* steroidogenesis assay using the human adrenocortical carcinoma cell line H295R is being evaluated as a possible screening assay to detect and assess the impact of endocrine-active chemicals (EACs) capable of altering steroid biosynthesis. Data interpretation and their quantitative use in human and ecological risk assessments can be enhanced with mechanistic computational models to help define mechanisms of action and improve understanding of intracellular concentration–response behavior.

**OBJECTIVES:** The goal of this study was to develop a mechanistic computational model of the metabolic network of adrenal steroidogenesis to estimate the synthesis and secretion of adrenal steroids in human H295R cells and their biochemical response to steroidogenesis-disrupting EAC.

**METHODS:** We developed a deterministic model that describes the biosynthetic pathways for the conversion of cholesterol to adrenal steroids and the kinetics for enzyme inhibition by metirapone (MET), a model EAC. Using a nonlinear parameter estimation method, the model was fitted to the measurements from an *in vitro* steroidogenesis assay using H295R cells.

**RESULTS:** Model-predicted steroid concentrations in cells and culture medium corresponded well to the time-course measurements from control and MET-exposed cells. A sensitivity analysis indicated the parameter uncertainties and identified transport and metabolic processes that most influenced the concentrations of primary adrenal steroids, aldosterone and cortisol.

**CONCLUSIONS:** Our study demonstrates the feasibility of using a computational model of steroidogenesis to estimate steroid concentrations *in vitro*. This capability could be useful to help define mechanisms of action for poorly characterized chemicals and mixtures in support of predictive hazard and risk assessments with EACs.

**KEY WORDS:** endocrine-disrupting chemicals, H295R cells, mathematical model, mechanistic computational model, metirapone, sensitivity analysis, steroid biosynthesis. *Environ Health Perspect* 118:265–272 (2010). doi:10.1289/ehp.0901107 available via <http://dx.doi.org/> [Online 16 October 2009]

There is international concern about the potential for various environmental contaminants and commercial products to alter endocrine system function and contribute to adverse effects in humans and wildlife (Cooper and Kavlock 1997; Daston et al. 2003; Hutchinson et al. 2006; Zacharewski 1998). The Safe Drinking Water Act Amendments (1996) and the Food Quality Protection Act (1996) require screening for endocrine-disrupting properties of chemicals in drinking water and pesticides used in food production. In response to this legislation, the U.S. Environmental Protection Agency developed and implemented an endocrine disruptor screening program. The effort focuses on the effects of chemicals that mimic hormones by acting as agonists or antagonists of estrogen and androgen hormone receptors (Chu et al. 2009; Henley and Korach 2006), and other endocrine-active chemicals (EACs) that can cause effects by non-receptor-mediated mechanisms (Harvey and Everett 2003; Ulleras et al. 2008; Villeneuve et al. 2007). In this article, we describe a mechanistic computational model of steroidogenesis that can be used to estimate the biochemical effect

of EACs that can modulate the activity of steroidogenic enzymes and the subsequent concentrations of steroid hormones.

Steroids have an important role in several physiologic and pathologic processes, such as stress response, development, metabolism, electrolyte regulation, reproduction, and hormone-sensitive cancers (Portier 2002; Ulleras et al. 2008). Steroids are derived from cholesterol (CHOL) and are synthesized primarily in the adrenal cortex, ovaries, testes, and placenta through a series of biochemical reactions mediated by multiple cytochrome P450 (CYP) enzymes and hydroxysteroid dehydrogenases (HSDs) (Miller 1988; Payne and Hales 2004). Exposure to various environmental EACs can alter the activity of these steroidogenic enzymes and the subsequent production rate of steroids (Sanderson 2006; Sanderson et al. 2002; Walsh et al. 2000). To better understand the intracellular mechanisms underlying the concentration–response behavior of steroidogenesis-disrupting chemicals, we are developing mechanistic computational steroidogenesis models that describe chemical-mediated biological perturbations at the biochemical level.

Data for our computational model were obtained from an *in vitro* steroidogenesis assay using the human adrenocortical carcinoma cell line H295R. The H295R cells express all the key enzymes for steroidogenesis and the ability to produce all the adrenocortical steroids (Gazdar et al. 1990; Rainey et al. 1994; Staels et al. 1993). The expression of steroidogenic genes in H295R cells is well correlated to the expression in normal human adrenal (Oskarsson et al. 2006). The H295R cell line has been widely used to study adrenocortical function, regulation of steroidogenesis, and screening of EACs (Gracia et al. 2006; Hecker and Giesy 2008; Muller-Vieira et al. 2005; Sanderson et al. 2002; Ulleras et al. 2008). The H295R assay system is being developed and evaluated by several international laboratories as a possible steroidogenesis screening approach (Hecker et al. 2007). This assay coupled with a mechanistic computational model supports the recommendations by the National Research Council (2007) on the vision of toxicology in the 21st century with the use of *in vitro* systems that can *a*) provide broad coverage of chemicals, mixtures,

Address correspondence to M.S. Breen, U.S. Environmental Protection Agency, Office of Research and Development, National Exposure Research Laboratory, 109 T.W. Alexander Dr., Mail E205-02, Research Triangle Park, NC 27711 USA. Telephone: (919) 541-9409. Fax: (919) 541-9444. E-mail: [breen.michael@epa.gov](mailto:breen.michael@epa.gov)

Supplemental Material is available online (doi:10.1289/ehp.0901107.S1 via <http://dx.doi.org/>).

This modeling work was performed at the U.S. Environmental Protection Agency (Research Triangle Park, NC, USA). The experiments were performed in cooperation with the Mitsubishi Tanabe Pharma Corporation (Kisarazu, Chiba, Japan). We thank D. Villeneuve, R. Kavlock, and J. Blacato for their assistance and many helpful suggestions.

M.B. was supported by the Environmental Protection Agency Cooperative Training Program in Environmental Sciences Research with North Carolina State University, Training Agreement CT833235-01-0.

Although the manuscript was reviewed by the U.S. Environmental Protection Agency and approved for publication, it may not necessarily reflect official agency policy. Mention of trade names or commercial products does not constitute endorsement or recommendation for use.

N.T. and M.Y. are employed by Mitsubishi Tanabe Pharma Corporation. The other authors declare they have no competing financial interests.

Received 19 June 2009; accepted 16 October 2009.

and outcomes; *b*) reduce the cost and time of testing; *c*) use fewer animals; and *d*) develop a more robust scientific basis to assess health effects from environmental agents.

A mechanistic mathematical model of steroidogenesis has several potential applications. First, this type of model can enhance the interpretation of data from *in vitro* steroidogenesis assays by helping to define mechanisms of action for poorly characterized chemicals and mixtures of chemicals in support of *in vitro* EAC screening methods. Second, this model can help guide low-concentration extrapolations of *in vitro* concentration–response curves. Third, the model can help formulate hypotheses and design critical experiments. Fourth, a model that predicts the response of the major adrenal steroids [e.g., cortisol (CORT), aldosterone (ALDO)] to EACs can be coupled to multiorgan systems models, which include regulatory feedback of the hypothalamus–pituitary–adrenal axis and the renal–angiotensin–aldosterone system, in support of *in vivo* EAC screening methods.

Other steroidogenesis models have been previously reported. Murphy et al. (2005) developed a model for vitellogenesis, a steroid-controlled process, in female fish. To model ovarian steroidogenesis, all reactions between the release of gonadotropin and the production of testosterone were combined and mathematically described by one Hill equation. Selgrade and Schlosser (1999) developed a mathematical model to predict plasma levels of estradiol during different stages of the menstrual cycle in women. Estradiol concentrations were modeled as a weighted sum of luteinizing hormone, growth follicle stage, and preovulatory stage. However, these models lack a mechanistic metabolic pathway of steroid biosynthesis at the biochemical level. Breen et al. (2007) developed a mechanistic computational model of ovarian

steroidogenesis. Metabolic reaction and transport rates were estimated from ovary explants of a small fish. Becker et al. (1980) developed a probabilistic model of the metabolic pathway for testicular steroidogenesis. Transition probabilities for the reactions in the pathway were estimated from *ex vivo* preparations of rat and rabbit testes. However, ovarian and testicular steroidogenesis does not include the metabolic pathways for the major adrenal steroids, aldosterone and cortisol.

In this study, we developed a mechanistic computational model of the adrenal metabolic and transport processes that mediate steroid synthesis and secretion and the kinetics for enzyme inhibition by the competitive steroidogenic enzyme inhibitor metyrapone (MET), a model EAC.

## Materials and Methods

We first describe the *in vitro* steroidogenesis experiments, and then the mathematical model and procedures for parameter estimation.

**Steroidogenesis assay with H295R cells.** We performed two experimental studies with H295R cells: a control study with samples analyzed at five time points (0, 8, 24, 48, and 72 hr) and a MET study with two MET concentrations (1 and 10  $\mu$ M) with samples analyzed at four time points [8, 24, 48, and 72 hr; see Supplemental Material for details (doi:10.1289/ehp.0901107.S1 via <http://dx.doi.org/>)]. Briefly, the medium and cells were separately removed from four replicate wells at each time point. The cells were dissolved in 100  $\mu$ L distilled water and sonicated to produce a cell lysate. Steroid concentrations in the medium and cell lysate were measured using liquid chromatography/mass spectrometry for 12 steroids [pregnenolone (PREG), 17 $\alpha$ -hydroxypregnenolone (HPREG), dehydroepiandrosterone (DHEA), progesterone (PROG), 17 $\alpha$ -hydroxyprogesterone (HPROG), androstenedione (DIONE), testosterone (T), deoxycorticosterone (DCORTICO), corticosterone (CORTICO), ALDO, 11-deoxycortisol (DCORT), and CORT] and using enzyme-linked immunosorbent assay for two additional steroids [estrone ( $E_1$ ) and 17 $\beta$ -estradiol ( $E_2$ )]. The quantitative ranges for each steroid in the cells and medium are provided in Table 1 of the Supplemental Material (doi:10.1289/ehp.0901107.S1).

**Estimation of cell volume.** To estimate the volume of the cells per well, we performed a cell morphology study following the same experimental method as the previously described steroidogenesis assay for both controls and the two concentrations of MET (1 and 10  $\mu$ M). At post-stimuli incubation periods of 0, 24, 48, and 72 hr, cells were separated from the medium and removed from six replicate wells. The mean cell diameter and mean cell circularity in each well were measured using a cell

analyzer (Vi-CELL XR, Beckman Coulter, Fullerton, CA, USA). Because the mean circularity of the separated cells was always  $\geq 90\%$ , a spherical cell shape was assumed with a volume  $V_{\text{indiv\_cell}}$  expressed as

$$V_{\text{indiv\_cell}} = \frac{4}{3}\pi\left(\frac{d}{2}\right)^3, \quad [1]$$

where  $d$  is the mean measured cell diameter (14.20  $\mu$ m). This yielded a  $V_{\text{indiv\_cell}}$  of 1,499  $\mu\text{m}^3$ . To determine the mean volume of cells per well,  $V_{\text{cell}}$ , we multiplied  $V_{\text{indiv\_cell}}$  by the number of cells per well.

**Compensation of steroid dilution in cell lysate.** To compensate for dilution of the steroids by 0.1 mL distilled water,  $V_{\text{water}}$ , added to the cell lysate, we determined the concentration of steroid  $x$  in cells,  $C_{\text{cell},x}(t)$ , by multiplying the measured concentration of steroid  $x$  in the cell lysate,  $C_{\text{lysate},x}(t)$ , by the dilution factor  $V_{\text{lysate}}/V_{\text{cell}}$ , where the volume of the cell lysate,  $V_{\text{lysate}}$ , is the sum of  $V_{\text{cell}}$  and  $V_{\text{water}}$ .

**Overview of mathematical H295R steroidogenesis model.** The computational model is based on an *in vitro* steroidogenesis experimental design with two compartments: culture medium and H295R cells (Figure 1). The model consists of steroid transport and metabolic pathways. The transport pathways include cellular uptake of CHOL (steroid precursor) and MET and the import and secretion of 14 adrenal steroids (PREG, HPREG, DHEA, PROG, HPROG, DIONE, T, DCORTICO, CORTICO, ALDO, DCORT, CORT,  $E_1$ , and  $E_2$ ). The metabolic pathway includes conversion of CHOL into the 14 adrenal steroids and inhibition of steroidogenic enzymes by MET. Development of various aspects of the model is described in detail below.

**Import of CHOL, the precursor for all steroid hormones.** Cholesterol is transported to the inner mitochondrial membrane, which is the site for the first metabolic reaction of steroid biosynthesis. This transport process consists of two main steps. First, CHOL is imported into the cell mainly by the low-density-lipoprotein-receptor-mediated lysosomal pathway (Brown and Goldstein 1986; Chang et al. 2006; Gallegos et al. 2000). Second, CHOL is delivered to the inner mitochondrial membrane by the intracellular sterol carrier protein-2, steroidogenic acute regulatory (StAR) protein, and peripheral benzodiazepine receptor (Chang et al. 2006; Gallegos et al. 2000; Maxfield and Wustner 2002). We model the transport rate of CHOL from the medium as a first-order process (Figure 1B).

**Metabolic pathway.** The metabolic pathway in the H295R cells that converts CHOL into the 14 adrenal steroids consists of 17 enzymatic reactions catalyzed by nine different proteins (Figure 1A) (Payne and Hales 2004). All

**Table 1.** Estimated transport equilibrium parameter values (dimensionless) and  $R^2$  values from model fit of steroids corresponding to given  $q$  parameters.

Parameter	Value	$R^2$
$q_{19}$	0.0048	0.98
$q_{20}$	0.0019	0.97
$q_{21}$	0.0140	0.99
$q_{22}$	0.0171	0.99
$q_{23}$	0.0268	0.98
$q_{24}$	0.0229	0.97
$q_{25}$	0.0072	0.99
$q_{26}$	0.0141	0.97
$q_{27}$	0.0201	0.99
$q_{28}$	0.0174	0.70
$q_{29}$	0.0124	0.99
$q_{30}$	0.0084	0.98
$q_{31}$	0.0130	0.98
$q_{32}$	0.0108	0.99
$q_{40}$	0.0171	— <sup>a</sup>

<sup>a</sup>MET transport equilibrium ( $q_{40}$ ) set to CORTICO transport equilibrium ( $q_{27}$ ); see "Results" for details.

metabolic reactions occur in the smooth endoplasmic reticulum except conversion of CHOL to PREG, which occurs in the inner mitochondrial membrane (Agarwal and Auchus 2005; Miller and Strauss 1999). Intergorganelle transports are not included in the model because we assumed these processes are not rate limiting. Because the metabolic reactions are predominantly irreversible, the reverse reaction rates are set to zero (Becker et al. 1980). We assume the substrate concentration is much less than the Michaelis constant (substrate concentration that yields a half-maximal reaction rate). Thus, the rate of product formation increases linearly with substrate concentration as described by a first-order rate constant (Figure 1B).

**Steroid transport pathway.** The transport of the steroids between the cells and medium is mediated by multiple transport mechanisms, including nonvesicular and vesicular processes (Chang et al. 2006; Maxfield and Wustner 2002; Neufeld et al. 1996). Because the concentration of the newly synthesized steroids in the cells is probably insufficient to saturate the multiple steroid transport mechanisms during the experiments, we model the rates of secretion and uptake for each steroid as reversible first-order processes [ $k_{+x}$  and  $k_{-x}$  for secretion and uptake of steroid  $x$ , respectively; see Supplemental Material, Figure 1 (doi:10.1289/ehp.0901107.S1)].

**Uptake and enzyme inhibition by MET.** Various EACs can directly inhibit the steroidogenic enzymes in the metabolic pathway. In this study, we examined the steroid response of H295R cells to exposures from MET, an EAC that is a competitive inhibitor of CYP11- $\beta$ -hydroxylase (CYP11B1), which catalyzes two different reactions in the metabolic pathway: conversion of DCORTICO to CORTICO, and conversion of DCORT to CORT (Figure 1A) (Harvey and Everett 2003; Harvey et al. 2007). We assume that MET diffuses into the cells and reaches equilibrium with the MET concentration in the medium:

$$C_{MET,cell}(t) = q_{40} C_{MET,med}(t), \quad [2]$$

where  $C_{MET,cell}$  and  $C_{MET,med}$  are the cell and medium MET concentrations at time  $t$ , respectively, and  $q_{40}$  is the partition coefficient (Figure 1B). To account for the volumes of the cells,  $V_{cell}$ , and medium,  $V_{med}$ , the molecular balance equation

$$V_{cell} C_{MET,cell}(t) + V_{med} C_{MET,med}(t) = V_{cell} C_{MET,cell}(0) + V_{med} C_{MET,med}(0), \quad [3]$$

is solved for  $C_{MET,cell}(t)$  and substituted into Equation 2 with  $C_{MET,cell}(0) = 0$  to yield

$$C_{MET,cell}(t) = \left( \frac{q_{40}}{1 + q_{40} V_{cell}/V_{med}} \right) C_{MET,med}(0). \quad [4]$$

For the two CYP11B1 enzymatic reactions competitively inhibited by MET, the kinetic parameters  $k_{16}$  and  $k_{17}$  are respectively divided by  $\alpha_{CORTICO} = 1 + (C_{MET,cell}/k_{41})$  and  $\alpha_{CORT} = 1 + (C_{MET,cell}/k_{42})$  with MET inhibition constants  $k_{41}$  and  $k_{42}$  (Figure 1B).

**Dynamic molecular balances.** The time courses of the steroids are described by dynamic molecular balance equations [see Supplemental Material (doi:10.1289/ehp.0901107.S1)]. The dynamic molecular balance equations for the steroids in cells and medium are

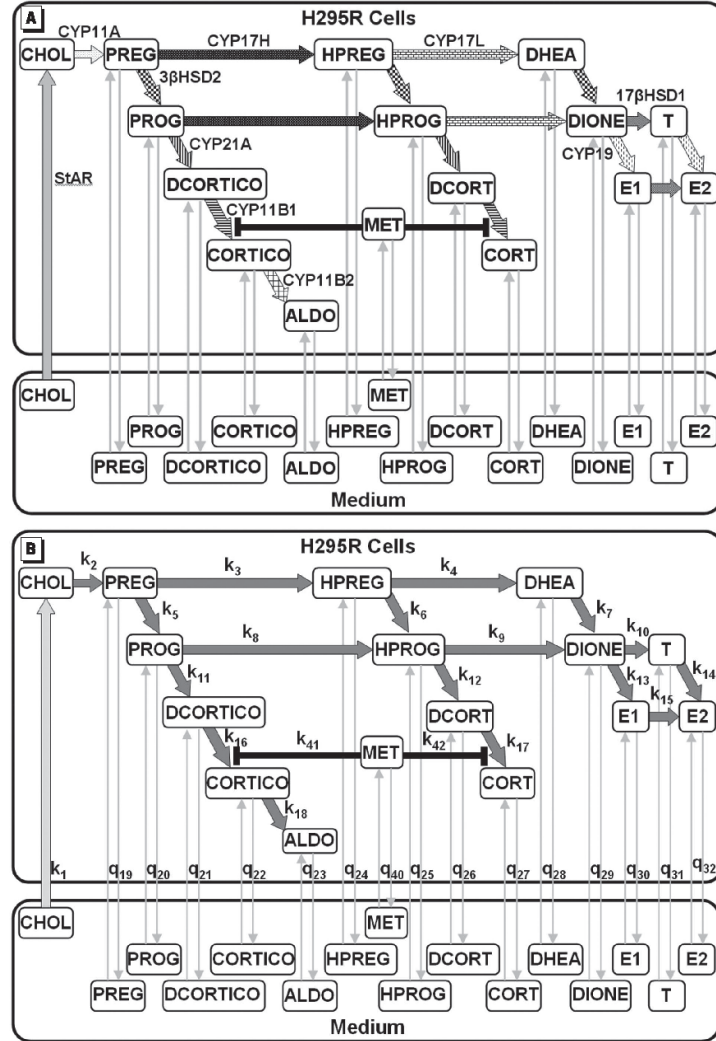


**Figure 1.** (A) Conceptual steroidogenesis model for control and MET-exposed H295R cells. The model consists of two compartments: culture medium and H295R cells. Cellular uptake of CHOL from medium is depicted by the broad gray arrow labeled with the StAR protein. Reversible steroid transport between medium and cells is depicted by bidirectional thin gray arrows. Irreversible metabolic reactions in the cells are depicted by arrows, with each pattern representing a unique enzyme. Enzymes are labeled next to reactions they catalyze: CYP450 side-chain-cleavage (CYP11A), CYP450c17- $\alpha$ -hydroxylase (CYP17H), CYP450c17,20-lyase (CYP17L), 3- $\beta$ -hydroxydehydrogenase type 2 (3 $\beta$ HSD2), 17 $\beta$ -hydroxydehydrogenase type 1 (17 $\beta$ HSD1), CYP450 aromatase (CYP19), CYP450 21- $\alpha$ -hydroxylase (CYP21A), CYP450 11- $\beta$ -hydroxylase type 1 (CYP11B1), and aldosterone synthase (CYP11B2). Steroids are PREG, HPREG, DHEA, PROG, HPROG, DIONE, T, E1, E2, DCORTICO, CORTICO, ALDO, DCORT, and CORT. The EAC MET is shown as enzyme inhibitor of CYP11B1. (B) A graphical representation of the parameters for the mathematical H295R steroidogenesis model, which consists of first-order rate constants for CHOL uptake into the cells,  $k_1$ , and for each metabolic process,  $k_2$ – $k_{18}$ . For the quasi-equilibrium analysis, the equilibrium constants are  $q_{19}$ – $q_{32}$ . Partition coefficient for MET is  $q_{40}$ . Enzyme inhibition constants for MET are  $k_{41}$  and  $k_{42}$  for CORTICO and CORT pathways, respectively.

$$V_{\text{cell}} \frac{dC_{x,\text{cell}}}{dt} = P_{x,\text{cell}} - U_{x,\text{cell}} + I_{x,\text{cell}} - S_{x,\text{cell}} \quad [5]$$

and

$$V_{\text{med}} \frac{dC_{x,\text{med}}}{dt} = S_{x,\text{cell}} - I_{x,\text{cell}} \quad [6]$$

where  $C_{x,\text{cell}}$  and  $C_{x,\text{med}}$  are the concentrations of steroid  $x$  in cells and medium, respectively;  $P_{x,\text{cell}}$  and  $U_{x,\text{cell}}$  are the production and use rates of steroid  $x$  in cells, respectively;  $I_{x,\text{cell}}$  and  $S_{x,\text{cell}}$  are the cell import and secretion rates of steroid  $x$ , respectively. The first two terms on the right side of Equation 5 represent the net metabolic reaction rate of steroid  $x$ . The last two terms represent the net cellular uptake or release rate of steroid  $x$ .

**Quasi-equilibrium analysis.** We assume that the steroid concentrations in the cells and medium are operating near equilibrium. There is good experimental evidence to support this assumption. First, the time-course data from the control and MET-exposed cells show that some steroid concentrations in the medium increase for 48 hr but then decrease at 72 hr. Because the cells can secrete and import steroids, the steroid transport is probably reversible. Second, the time-course data from the control and MET studies show remarkably similar dynamic behavior for each steroid concentration in the cells and its corresponding concentration in medium. For each steroid, a comparison between the simultaneous measurements in the cells and medium shows that a linear regression line (y-intercept set to zero) closely fits the data [see Supplemental Material, Figure 2 (doi:10.1289/ehp.0901107.S1)]. This linear correlation between concentrations in the cells and medium is clearly evident with large  $R^2$  values for each steroid transport parameter (Table 1). This is good evidence that the steroid transport between the cells and medium

is rapid and reversible. Therefore, we assume that the steroid concentrations in the cells and medium reach equilibrium after a short transient time. Because the steroids are also involved in the metabolic pathway of steroidogenesis, this is considered a quasi-equilibrium.

To examine the quasi-equilibrium behavior, the reversible transport rates ( $k_{+x}$  and  $k_{-x}$  for secretion and import of steroid  $x$ , respectively) are assumed to be much faster than the metabolic reaction rates. After a short period of time, the concentration of steroid  $x$  in the cells and medium reaches equilibrium:

$$\frac{C_{x,\text{med}}}{C_{x,\text{cell}}} = \frac{k_{+x}}{k_{-x}} = q_x \quad [7]$$

where  $q_x$  is the equilibrium constant. We can sum the mass (molecules) of steroid  $x$  in the cells and medium to yield

$$\begin{aligned} & \frac{d(V_{\text{cell}} C_{x,\text{cell}} + V_{\text{med}} C_{x,\text{med}})}{dt} \\ &= \frac{d(V_{\text{cell}} + V_{\text{med}} q_x) C_{x,\text{cell}}}{dt} \\ &= P_{x,\text{cell}} - U_{x,\text{cell}} \end{aligned} \quad [8]$$

The simplified system of equations consists of a differential equation for each steroid in the cells,

$$\frac{dC_{x,\text{cell}}}{dt} = \frac{1}{V_{\text{cell}} + V_{\text{med}} q_x} (P_{x,\text{cell}} - U_{x,\text{cell}}) \quad [9]$$

and an algebraic equation for each steroid in the medium,

$$C_{x,\text{med}} = q_x C_{x,\text{cell}} \quad [10]$$

The model consists of 14 transport equilibrium constants ( $q_{19}, q_{20}, \dots, q_{32}$ ), 17 metabolic rate constants ( $k_2, k_3, \dots, k_{18}$ ), a CHOL import rate ( $k_1$ ), two enzyme inhibition constants for MET ( $k_{41}, k_{42}$ ), and the partition coefficient for MET ( $q_{40}$ ). These dynamic molecular balance equations for quasi-equilibrium and 35 parameters are used in all subsequent analyses [see Supplemental Material (doi:10.1289/ehp.0901107.S1)].

**Parameter estimation.** The parameters for the two pathways (steroid transport pathway and metabolic pathway) were independently estimated using the mean concentrations from replicate experiments. For the steroid transport pathway, the equilibrium constants ( $q_{19}, q_{20}, \dots, q_{32}$ ), were estimated with the time-course data from the control and MET studies using the direct least squares solution for Equation 10:

$$q_x^* = [C_{x,\text{cell}}' C_{x,\text{cell}}]^{-1} C_{x,\text{cell}}' C_{x,\text{med}} \quad [11]$$

where  $q_x^*$  is the least squares estimate of the equilibrium constant for steroid  $x$ , and  $C_{x,\text{cell}}' = [C_{x,\text{cell}}(t = 0, d = 0) \dots C_{x,\text{cell}}(t = 8, d = 0) \dots C_{x,\text{cell}}(t = 72, d = 10)]$  and  $C_{x,\text{med}}' = [C_{x,\text{med}}(t = 0, d = 0) \dots C_{x,\text{med}}(t = 8, d = 0) \dots C_{x,\text{med}}(t = 72, d = 10)]$  are the measured concentrations in the cell and medium, respectively, at time  $t$  for the MET dose  $d$  for  $d = 0, 1$ , and  $10 \mu\text{M}$ .

For the metabolic pathway, the parameters ( $k_1, k_2, \dots, k_{18}, k_{41}, k_{42}$ ) were estimated with the time-course data from the control and MET studies using the weighted least squares method. Let  $C_{x,\text{cell}}(t_i; C_{\text{MET},\text{med}}^d, \underline{k})$  be the model-predicted concentrations of steroid  $x$  in the cells at the  $i$ th time  $t_i$  for the  $d$ th MET dose (including control)  $C_{\text{MET},\text{med}}^d$  with parameter set  $\underline{k} = (k_1, k_2, \dots, k_{18}, k_{41}, k_{42})$ . Let  $C_{x,\text{cell}}^i$  be the measured concentration of steroid  $x$  in the cells at the  $i$ th time  $t_i$  for the  $d$ th MET dose (including control)  $C_{\text{MET},\text{med}}^d$ , and let  $\underline{C}_{x,\text{cell}}^d$  be the mean measured concentration across time where  $d = 1, \dots, 3$  and  $i = 1, \dots, 5$ . Then, the weighted least squares estimate,  $\underline{k}^* = (k_1^*, k_2^*, \dots, k_{18}^*, k_{41}^*, k_{42}^*)$ , is the parameter values  $\underline{k}$ , which minimizes the cost function

$$J(\underline{k}) = \sum_{x=1}^5 \sum_{d=1}^3 \sum_{i=1}^5 \frac{1}{C_{x,\text{cell}}^d} \left[ C_{x,\text{cell}}^i - C_{x,\text{cell}}(t_i; C_{\text{MET},\text{med}}^d, \underline{k}) \right]^2 \quad [12]$$

Parameters for the metabolic pathway were estimated with an iterative optimization algorithm using MATLAB R2009a (Mathworks, Natick, MA, USA) software. We chose the Nelder-Mead simplex method for its relative insensitivity to the initial parameter values compared with other common methods, such as Newton's method, and its robustness to discontinuities (Nelder and Mead 1965). Convergence to the solution was confirmed after the parameter search terminated.

**Sensitivity analysis.** We performed a sensitivity analysis to examine model uncertainty. The sensitivity function relates the changes of the model output to changes in the model parameters. To rank the sensitivity functions, we calculated relative sensitivity functions  $R_{x,\text{med},k_i}$  with respect to parameter  $k_i$  for each of the model-predicted concentrations in the medium  $C_{x,\text{med}}$  as described by

$$R_{x,\text{med},k_i} = \left( \frac{k_i}{C_{x,\text{med}}} \right) \frac{\partial C_{x,\text{med}}}{\partial k_i} \quad [13]$$

Substituting Equation 10 into Equation 13 yields

$$R_{x,\text{med},k_i} = \left( \frac{k_i}{C_{x,\text{cell}}} \right) \frac{\partial C_{x,\text{cell}}}{\partial k_i} \quad [14]$$

The relative sensitivities  $R_{x,\text{med},q_i}$  with respect to parameter  $q_i$  for each of the model-predicted concentrations in the medium  $C_{x,\text{med}}$  are

$$R_{x,\text{med},q_i} = \left( \frac{q_i}{C_{x,\text{med}}} \right) \frac{\partial C_{x,\text{med}}}{\partial q_i} \quad [15]$$

**Table 2.** Estimated parameter values of metabolic pathway.

Parameter	Value	Unit
$k_1$	0.0049	$\text{hr}^{-1}$
$k_2$	0.0230	$\text{hr}^{-1}$
$k_3$	0.9448	$\text{hr}^{-1}$
$k_4$	$2.7 \times 10^{-9}$	$\text{hr}^{-1}$
$k_5$	0.8522	$\text{hr}^{-1}$
$k_6$	13.2263	$\text{hr}^{-1}$
$k_7$	0.0020	$\text{hr}^{-1}$
$k_8$	$3.1 \times 10^{-5}$	$\text{hr}^{-1}$
$k_9$	3.1479	$\text{hr}^{-1}$
$k_{10}$	0.0367	$\text{hr}^{-1}$
$k_{11}$	6.8701	$\text{hr}^{-1}$
$k_{12}$	13.6062	$\text{hr}^{-1}$
$k_{13}$	0.5482	$\text{hr}^{-1}$
$k_{14}$	0.0003	$\text{hr}^{-1}$
$k_{15}$	0.0828	$\text{hr}^{-1}$
$k_{16}$	0.5627	$\text{hr}^{-1}$
$k_{17}$	0.2396	$\text{hr}^{-1}$
$k_{18}$	0.0847	$\text{hr}^{-1}$
$k_{41}$	18.1767	nM
$k_{42}$	8.2661	nM

Substituting Equation 10 into Equation 15 yields

$$R_{x,med,q_i} = \begin{cases} \left( \frac{q_i}{C_{x,cell}} \right) \frac{\partial C_{x,cell}}{\partial q_i}, & i \neq x \\ \left( \frac{q_x}{C_{x,cell}} \right) \frac{\partial C_{x,cell}}{\partial q_x} + 1, & i = x \end{cases} \quad [16]$$

Using MATLAB, partial derivatives were numerically determined for  $C_{x,cell}$  with respect to each parameter, and relative sensitivity functions were calculated as shown in Equations 14 and 16 for control and each MET dose. To rank the relative sensitivities, we calculated the L2 norm across time for each relative sensitivity function as described by

$$L2norm(R_{x,med,q_i}) = \sqrt{\int |R_{x,med,q_i}(t)|^2 dt} \quad [17]$$

and

$$L2norm(R_{x,med,q_i}) = \sqrt{\int |R_{x,med,q_i}(t)|^2 dt} \quad [18]$$

Magnitudes of the relative sensitivities relate the degree to which changes in parameters values lead to changes in model outputs.

## Results

**Transport pathway.** Table 1 shows the estimated parameter values and  $R^2$  values for the model evaluation of the transport pathway. The MET transport equilibrium ( $q_{40}$ ) could not be determined from the data because MET was not measured in the cells. Therefore, we set ( $q_{40}$ ) equal to CORTICO transport equilibrium ( $q_{22}$ ) because the previously measured partition coefficients for MET ( $\chi_{logP} =$

2.0) and CORTICO ( $\chi_{logP} = 1.9$ ) are similar [PubChem Database (National Center for Biotechnology Information 2003)]. The transport equilibrium model predictions correspond well to the mean steroid concentrations measured in the cells and medium with large  $R^2$  values (Table 1). For DCORTICO, the transport equilibrium model closely fits the measured concentrations in the cells and medium [see Supplemental Material, Figure 2 (doi:10.1289/ehp.0901107.S1)]. Across time, the model-predicted and measured DCORTICO concentrations in medium also correspond well [see Supplemental Material, Figure 3 (doi:10.1289/ehp.0901107.S1)]. Similar results were observed for the other steroids. The close fit of a transport equilibrium model to the data indicates that the steroid concentrations in the cells and medium reach equilibrium after a short time.

**Metabolic pathway.** Table 2 shows the estimated parameter values for the metabolic pathway. The time for convergence to the solution for the iterative parameter estimation was typically 24 min on an Intel Core 2 Duo processor computer using MATLAB.

For control cells, we compared model-predicted steroid concentrations with time-course measurements. Overall, the model-predicted concentrations correspond well to the mean time-course data in cells [see Supplemental Material, Figure 4 (doi:10.1289/ehp.0901107.S1)] and in medium (Figure 2). For two steroids (PROG and PREG) with mean measurements that increase until 48 hr and then sharply decrease at 72 hr, the model underestimated at 48 hr and overestimated at

72 hr (Figure 2B,E). For DCORTICO, the model underestimated the mean measurements at 8, 24, and 48 hr (Figure 2D). For DHEA, all model-predicted and measured concentrations in the cells were below the minimum level of quantification [see Supplemental Material, Figure 4 (doi:10.1289/ehp.0901107.S1)]. Therefore, the ability of the model to accurately correspond to the time-varying concentrations of DHEA measured in the medium is limited with the assumed quasiequilibrium between the cells and medium. The model-predicted DHEA concentrations in the medium correspond well with the average time-course behavior of the measurements (Figure 2B).

For MET-exposed cells, we compared model-predicted steroid concentrations with time-course measurements after incubation with MET. For the steroids (CORTICO, ALDO, and CORT) downstream from the enzyme inhibited by MET (CYP11B1), the model-predicted concentrations closely correspond to the mean time-course measurements in cells [see Supplemental Material, Figure 5 (doi:10.1289/ehp.0901107.S1)] and in medium (Figure 3A–C), which decrease as MET increases. For the steroids (DCORTICO and DCORT) immediately upstream from CYP11B1, the model-predicted concentrations compare well with the mean time-course data in cells [see Supplemental Material (doi:10.1289/ehp.0901107.S1)] and in medium (Figure 3D,E), which remain approximately unchanged at 8, 24, and 48 hr as MET increases and then slightly increase at 72 hr as MET increases. For the other steroids further upstream from CYP11B1, the

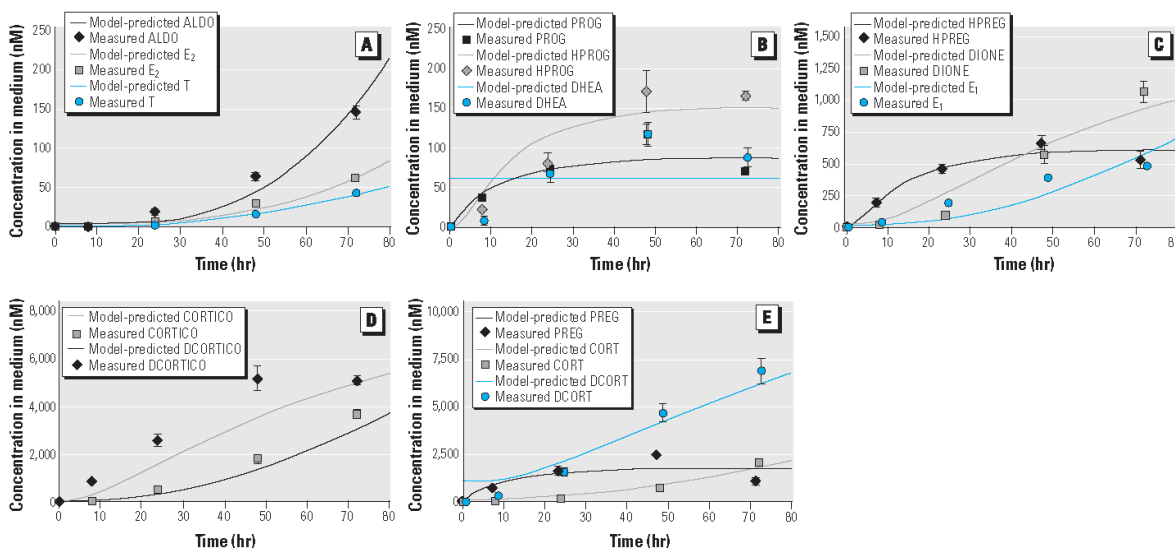


**Figure 2.** Model evaluation of metabolic and transport pathways for control study. Model-predicted concentrations in medium were plotted as a function of time and compared with concentrations (mean  $\pm$  SD) measured at five sampling times for steroids: ALDO, E<sub>2</sub>, and T (A); PROG, HPROG, and DHEA (B); HPREG, DIONE, and E<sub>1</sub> (C); CORTICO and DCORTICO (D); and PREG, CORT, and DCORT (E).

model-predicted and measured concentrations remained approximately unchanged from controls as MET increases (data not shown).

**Sensitivity analysis.** Figure 4 shows the relative sensitivities for two steroids. Odd- and even-numbered parameters are shown in Figure 4A and 4B, respectively. For ALDO, two parameters ( $k_{18}$ ,  $q_{22}$ ) were highly sensitive at each MET dose, and six parameters were moderately sensitive, with their sensitivity decreased ( $k_2$ ,  $k_5$ ,  $k_{16}$ ,  $q_{21}$ ) or increased ( $k_{41}$ ,  $q_{40}$ ) as MET increased. For CORT, two parameters ( $k_{17}$ ,  $q_{27}$ ) were highly sensitive at each MET dose, and five parameters ( $k_2$ ,  $k_3$ ,  $k_{26}$ ,  $q_{40}$ ,  $q_{42}$ ) were moderately sensitive with their sensitivity decreased as MET increased. The HPREG pathway appears to be the preferred pathway for CORT synthesis because CORT was more sensitive to the HPREG pathway ( $k_3$ ,  $k_6$ ) and less sensitive to the PROG pathway ( $k_5$ ,  $k_8$ ). The sensitivity of ALDO and CORT can indicate the uncertainty of the parameters. The parameters with high sensitivity tend to have less uncertainty compared with parameters with low sensitivity.

## Discussion

We developed a mechanistic mathematical model and estimated metabolic and transport parameters for adrenal steroidogenesis to estimate synthesis and transport of the steroids and their dynamic concentration–response to the EAC MET. In the H295R cells and medium, the model-predicted steroid concentrations closely correspond to the time-course data from control experiments and

dynamic concentration–response data from experiments with MET-exposed cells. The quasi-equilibrium assumption reduced the complexity of the model while maintaining the model's predictive ability.

**Advantages of mechanistic model.** The potential importance of the model is due to the use of mechanistic information at the biochemical level. Our mechanistic model includes each enzymatic reaction in the metabolic pathway. Under control conditions, the rate-limiting step is the transport of CHOL from the outer to inner mitochondrial membrane (Chang et al. 2006; Miller and Strauss 1999). For EAC-exposed cells, one or more steps in the pathway can become rate limiting, depending on the EAC concentration and enzyme inhibition strength. Some chemicals inhibit a single specific steroidogenic enzyme, whereas others inhibit multiple enzymes (Harvey et al. 2007). After further development, our model should increase insight into mechanisms of steroidogenic-active chemicals with unknown mechanisms of action and mixtures of chemicals. Furthermore, laboratory experiments are often performed with EACs at higher doses than typical human exposures because of the quantification limits of the assay. Low concentration extrapolations of concentration–response curves may be inaccurate if not guided by mechanistic models (Conolly and Lutz 2004).

The experiments used to fit and evaluate this model included time-course measurements of each adrenal steroid in both the cells and medium. In addition, the mechanism of action for MET, the EAC used in this study,

was previously characterized as a potential CYP11B1 enzyme inhibitor. These “data-rich” experiments allow us to fit and evaluate the model for each steroid. After further refinement and evaluation of the model for other EAC with different mechanisms of action, the model could be then applied for rapid *in vitro* EAC screening methods, which measure only a few steroids. The refined model would help identify mechanisms of action for poorly characterized EAC and extrapolate concentration–response curves in support of human hazard and risk assessments.

The model assumption of quasi-equilibrium has several advantages. It reduces the number of model parameters and the number of differential equations in the mathematical model by replacing some of them with algebraic equations. Also, it decouples the system of equations for the metabolic and transport pathways to allow the set of parameters for each pathway to be independently estimated. Moreover, it reduces the complexity of the more general model while preserving its important features and facilitating model analysis.

**In vitro steroidogenesis assay.** As shown with *in vitro* data, H295R cells can provide the data needed for comparison with model predictions. H295R cell experiments eliminate the feedback of the hypothalamus–pituitary–adrenal axis, which allows discrimination among different modes of action for EACs. This *in vitro* assay can identify direct effects at the molecular and biochemical level and distinguish them from general stress-induced effects observed with *in vivo* rodent assays. Furthermore, cell assays allow for the use of

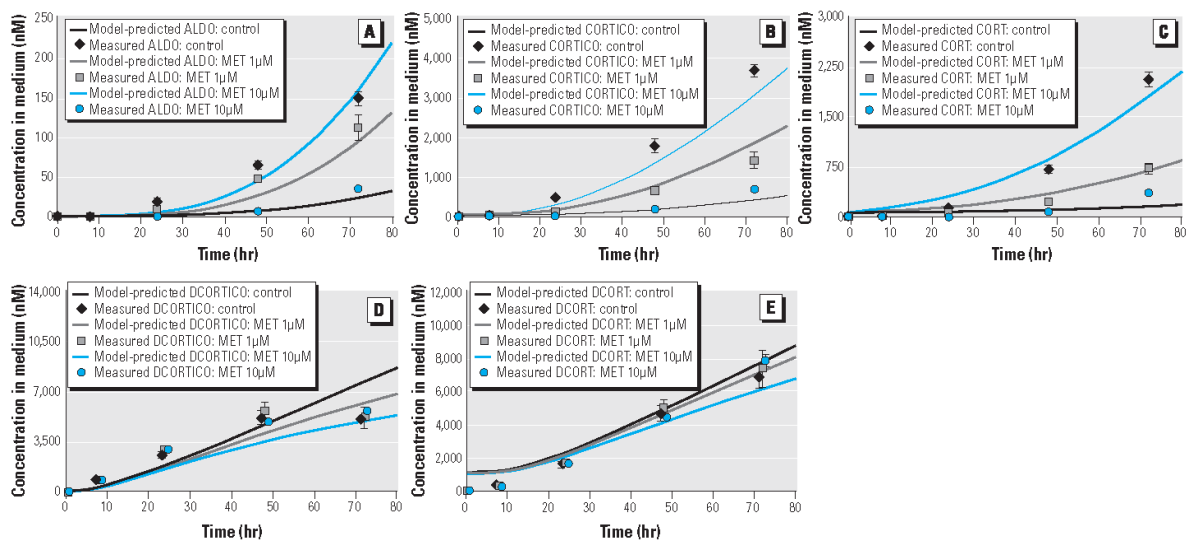


**Figure 3.** Model evaluation of metabolic and transport pathways for control and two MET concentrations (1  $\mu$ M and 10  $\mu$ M). Model-predicted concentrations in medium were plotted as a function of time and compared with concentrations (mean  $\pm$  SD) measured at five sampling times for steroids: ALDO (A), CORTICO (B), CORT (C), DCORTICO (D), and DCORT (E). For controls, model-predicted and measured steroid concentrations are the same as shown in Figure 2.

RNA interference-mediated gene knock-downs, gene knockouts, or steroid precursors to selectively block or bypass certain reactions and isolate regions of the steroidogenic pathway for refinement of parameter estimates.

**Dynamic concentration-response behavior.** The model closely matched three dynamic concentration-response behaviors observed in these experiments. First, the concentration of the steroids (CORTICO, ALDO, CORT) downstream from CYP11B1 (enzyme inhibited by MET) decreased as MET increased (Figure 3A–C). Second, the concentrations of steroids (DCORTICO and DCORT) immediately upstream of CYP11B1 slightly increased or remained constant as MET increased (Figure 3D,E). This small concentration increase in the model predictions and mean measurements is due to the decrease in the conversion rate of DCORTICO into CORTICO and of DCORT into CORT and the subsequent pooling of the substrates. Third, all the other steroids were unaffected by MET.

Our research goal is to better understand the dose-response behavior of EACs. Our

approach is to develop computational mechanistic models that describe the biological perturbations at the biochemical level and integrate information toward higher levels of biological organization. This approach will ultimately enable predictions of *in vivo* dose responses. To achieve this goal, further refinement of the model will be needed based on additional model-guided experiments, such as cell proliferation and viability, gene regulation, and upstream signaling.

**Limitations.** Although our model predictions compare well with the experimental data, the model-predicted concentrations of three steroids (PROG, PREG, and DCORTICO) do not correspond for a few measurements. For control experiments, the model underestimated PROG and PREG concentrations at 48 hr and overestimated them at 72 hr (Figure 2B,E), and underestimated DCORTICO concentrations at 8, 24, and 48 hr (Figure 2D). For MET experiments, DCORTICO did not correspond at 72 hr after incubation with 10  $\mu$ M MET (Figure 3D). Instead of a small increase in DCORTICO as predicted by the model, MET

had little or no effect on DCORTICO. Time-course measurements for these three steroids showed an increase in the mean concentrations until 48 hr, and then a sharp decrease (PROG and PREG) or no change (DCORTICO) at 72 hr. A possible source of these discrepancies is the model assumption of no saturation in the metabolic pathway; our model uses first-order enzyme kinetics. We plan to investigate a model with Michaelis-Menten enzyme kinetics that may improve the model fit.

## Conclusions

Our study demonstrates the ability of a newly developed mechanistic computational model of adrenal steroidogenesis to estimate the synthesis and secretion of adrenal steroids in human H295R cells, and their dynamic concentration-response to the EAC MET. Model-predicted steroid concentrations in the cells and medium closely correspond to the time-course measurements from control and MET-exposed cells. This capability could enhance the interpretation of data from *in vitro* steroidogenesis assays by helping to define mechanisms of action for poorly characterized chemicals and mixtures in support of *in vitro* EAC screening systems for predictive hazard assessments.

## REFERENCES

- Agarwal AK, Auchus RJ. 2005. Minireview: cellular redox state regulates hydroxysteroid dehydrogenase activity and intracellular hormone potency. *Endocrinology* 146:2531–2538.
- Becker S, Chubb C, Ewing L. 1980. Mathematical model of steroidogenesis in rat and rabbit testes. *Am J Physiol* 239:R184–R195.
- Breen MS, Villeneuve DL, Breen M, Ankley GT, Conolly RB. 2007. Mechanistic computational model of ovarian steroidogenesis to predict biochemical responses to endocrine active compounds. *Ann Biomed Eng* 35:970–981.
- Brown MS, Goldstein JL. 1986. A receptor-mediated pathway for cholesterol homeostasis. *Science* 232:34–47.
- Chang TY, Chang CC, Ohgami N, Yamauchi Y. 2006. Cholesterol sensing, trafficking, and esterification. *Annu Rev Cell Dev Biol* 22:129–157.
- Chu WL, Shiizaki K, Kawanishi M, Kondo M, Yagi T. 2009. Validation of a new yeast-based reporter assay consisting of human estrogen receptors  $\alpha/\beta$  and coactivator SRC-1: application for detection of estrogenic activity in environmental samples. *Environ Toxicol* 24:513–521.
- Conolly RB, Lutz WK. 2004. Nonmonotonic dose-response relationships: mechanistic basis, kinetic modeling, and implications for risk assessment. *Toxicol Sci* 77:151–157.
- Cooper RL, Kavlock RJ. 1997. Endocrine disruptors and reproductive development: a weight-of-evidence overview. *J Endocrinol* 152:159–166.
- Daston GP, Cook JC, Kavlock RJ. 2003. Uncertainties for endocrine disruptors: our view on progress. *Toxicol Sci* 74:245–252.
- Food Quality Protection Act of 1996. 1996. Public Law 104–170.
- Gallegos AM, Schoer JK, Starodub O, Kier AB, Billheimer JT, Schroeder F. 2000. A potential role for sterol carrier protein-2 in cholesterol transfer to mitochondria. *Chem Phys Lipids* 105:9–29.
- Gazdar AF, Die HK, Shackleton CH, Chen TR, Triche TJ, Myers CE, et al. 1990. Establishment and characterization of a human adrenocortical carcinoma cell line that expresses multiple pathways of steroid biosynthesis. *Cancer Res* 50:5488–5496.
- Gracia T, Hilscherova K, Jones PD, Newsted JL, Zhang X, Hecker M, et al. 2006. The H295R system for evaluation

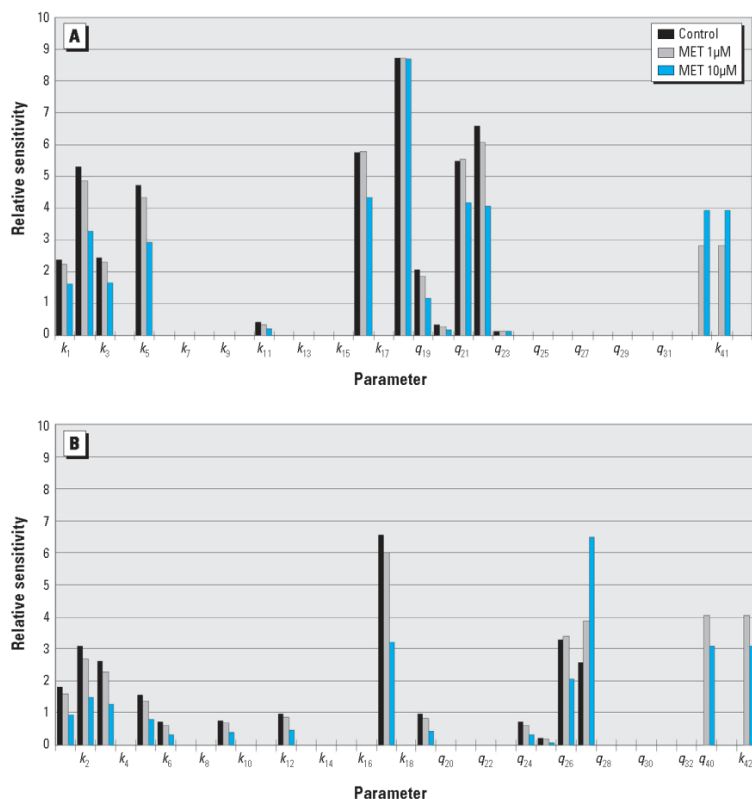


**Figure 4.** Relative sensitivities for model-predicted steroids ALDO (A) and CORT (B), plotted as a function of the 35 model parameters ( $k_1$ – $k_{18}$ ,  $q_{19}$ – $q_{32}$ ,  $k_{40}$ – $k_{42}$ ) for control and two MET concentrations (1 and 10  $\mu$ M). Each bar represents the L2 norm of the relative sensitivities across time (0–80 hr) and indicates the degree to which changes in parameter values lead to changes in model outputs. Odd- and even-numbered parameters are shown in A and B, respectively.

- of endocrine-disrupting effects. *Ecotoxicol Environ Saf* 65:293–305.
- Harvey PW, Everett DJ. 2003. The adrenal cortex and steroidogenesis as cellular and molecular targets for toxicity: critical omissions from regulatory endocrine disrupter screening strategies for human health? *J Appl Toxicol* 23:61–87.
- Harvey PW, Everett DJ, Springall CJ. 2007. Adrenal toxicology: a strategy for assessment of functional toxicity to the adrenal cortex and steroidogenesis. *J Appl Toxicol* 27:103–115.
- Hecker M, Giesy JP. 2008. Novel trends in endocrine disruptor testing: the H295R steroidogenesis assay for identification of inducers and inhibitors of hormone production. *Anal Bioanal Chem* 390:287–291.
- Hecker M, Hollert H, Cooper R, Vinggaard AM, Akahori Y, Murphy M, et al. 2007. The OECD validation program of the H295R steroidogenesis assay for the identification of in vitro inhibitors and inducers of testosterone and estradiol production. Phase 2: inter-laboratory pre-validation studies. *Environ Sci Pollut Res* 14(special issue 1):23–30.
- Henley DV, Korach KS. 2006. Endocrine-disrupting chemicals use distinct mechanisms of action to modulate endocrine system function. *Endocrinology* 147(suppl 6):S25–S32.
- Hutchinson TH, Ankley GT, Segner H, Tyler CR. 2006. Screening and testing for endocrine disruption in fish-biomarkers as “signposts,” not “traffic lights,” in risk assessment. *Environ Health Perspect* 114(suppl 1):106–114.
- Maxfield FR, Wustner D. 2002. Intracellular cholesterol transport. *J Clin Invest* 110:891–898.
- Miller WL. 1988. Molecular biology of steroid hormone synthesis. *Endocr Rev* 9:295–318.
- Miller WL, Strauss JF 3rd. 1999. Molecular pathology and mechanism of action of the steroidogenic acute regulatory protein, STAR. *J Steroid Biochem Mol Biol* 69:131–141.
- Muller-Vieira U, Angotti M, Hartmann RW. 2005. The adrenocortical tumor cell line NCI-H295R as an in vitro screening system for the evaluation of CYP11B2 (aldosterone synthase) and CYP11B1 (steroid-11 $\beta$ -hydroxylase) inhibitors. *J Steroid Biochem Mol Biol* 96:259–270.
- Murphy CA, Rose KA, Thomas P. 2005. Modeling vitellogenesis in female fish exposed to environmental stressors: predicting the effects of endocrine disturbance due to exposure to a PCB mixture and cadmium. *Reprod Toxicol* 19:395–409.
- National Center for Biotechnology. 2003. PubChem Database. Available: <http://pubchem.ncbi.nlm.nih.gov> [accessed 1 March 2009].
- National Research Council. 2007. *Toxicity Testing in the 21st Century: A Vision and a Strategy*. Washington, DC:National Academy Press.
- Nelder JA, Mead R. 1965. A simplex method for function minimization. *Comput J* 7:308–313.
- Neufeld EB, Cooney AM, Pitha J, Dawidowicz EA, Dwyer NK, Pentchev PG, et al. 1996. Intracellular trafficking of cholesterol monitored with a cyclodextrin. *J Biol Chem* 271:21604–21613.
- Oskarsson A, Ulleras E, Plant KE, Hinson JP, Goldfarb PS. 2006. Steroidogenic gene expression in H295R cells and the human adrenal gland: adrenotoxic effects of lindane in vitro. *J Appl Toxicol* 26:484–492.
- Payne AH, Hales DB. 2004. Overview of steroidogenic enzymes in the pathway from cholesterol to active steroid hormones. *Endocr Rev* 25:947–970.
- Portier CJ. 2002. Endocrine dismodulation and cancer. *Neuro Endocrinol Lett* 23(suppl 2):43–47.
- Rainey WE, Bird IM, Mason JL. 1994. The NCI-H295 cell line: a pluripotent model for human adrenocortical studies. *Mol Cell Endocrinol* 100:45–50.
- Safe Drinking Water Act Amendments of 1996. 1996. Public Law 104–182.
- Sanderson JT. 2006. The steroid hormone biosynthesis pathway as a target for endocrine-disrupting chemicals. *Toxicol Sci* 94:3–21.
- Sanderson JT, Boerma J, Lansbergen GW, van den Berg M. 2002. Induction and inhibition of aromatase (CYP19) activity by various classes of pesticides in H295R human adrenocortical carcinoma cells. *Toxicol Appl Pharmacol* 182:44–54.
- Selgrade JF, Schlosser PM. 1999. A model for the production of ovarian hormones during the menstrual cycle. *Fields Inst Commun* 21:429–446.
- Staels B, Hum DW, Miller WL. 1993. Regulation of steroidogenesis in NCI-H295 cells: a cellular model of the human fetal adrenal. *Mol Endocrinol* 7:423–433.
- Ulleras E, Ohlsson A, Oskarsson A. 2008. Secretion of cortisol and aldosterone as a vulnerable target for adrenal endocrine disruption—screening of 30 selected chemicals in the human H295R cell model. *J Appl Toxicol* 28:1045–1053.
- Villeneuve DL, Ankley GT, Makynen EA, Blake LS, Greene KJ, Higley EB, et al. 2007. Comparison of fathead minnow ovary explant and H295R cell-based steroidogenesis assays for identifying endocrine-active chemicals. *Ecotoxicol Environ Saf* 68:20–32.
- Walsh LP, Kuratko CN, Stocco DM. 2000. Econazole and miconazole inhibit steroidogenesis and disrupt steroidogenic acute regulatory (StAR) protein expression post-transcriptionally. *J Steroid Biochem Mol Biol* 75:229–236.
- Zacharewski T. 1998. Identification and assessment of endocrine disruptors: limitations of in vivo and in vitro assays. *Environ Health Perspect* 106(suppl 2):577–582.

**Supplemental Material to:**

**Computational Model of Steroidogenesis in Human H295R Cells to Predict Biochemical Response to Endocrine Active Chemicals: Model Development for Metyrapone**

Michael S. Breen,<sup>1\*</sup> Miyuki Breen,<sup>2,3</sup> Natsuko Terasaki,<sup>4</sup> Makoto Yamazaki,<sup>4</sup> Rory B. Conolly<sup>2</sup>

<sup>1</sup> National Exposure Research Laboratory, U.S. Environmental Protection Agency, 109 T.W. Alexander Drive, Mail E205-02, Research Triangle Park, NC 27711, USA

<sup>2</sup> National Center for Computational Toxicology, U.S. Environmental Protection Agency, Research Triangle Park, NC 27711, USA

<sup>3</sup> Biomathematics Program, Department of Statistics, North Carolina State University, Raleigh, NC 27695, USA

<sup>4</sup> Safety Research Laboratory, Mitsubishi Tanabe Pharma Corporation, Kisarazu, Chiba 292-0818, Japan

## **1. Steroidogenesis Assay with H295R cells**

NCI H295R human adrenocortical carcinoma cells (American Type Culture Collection, Manassas, VA, USA) were grown in 1:1 mixture of Dulbecco's modified Eagle's medium (Invitrogen Corporation, Carlsbad, CA, USA) and Ham's F12 medium (MP Biomedicals Inc, Irvine, CA, USA) containing 15 mM HEPES (Dojindo Laboratories, Kumamoto, Japan), 0.00625 mg/ml insulin (Sigma-Aldrich, Inc., St. Louis, MO, USA), 0.00625 mg/ml transferrin (Sigma-Aldrich, Inc., St. Louis, MO, USA), 30 nmol/L sodium selenite (Wako Pure Chemical Industries, Ltd., Osaka, Japan), 1.25 mg/ml bovine serum albumin (Sigma-Aldrich, Inc., St. Louis, MO, USA), 0.00535 mg/ml linoleic acid (Sigma-Aldrich, Inc., St. Louis, MO, USA), 2.5 % Nu-Serum I (Becton, Dickinson and Company, Franklin Lakes, NJ, USA), 100 U/mL penicillin (Meiji Seika Kaisha, Ltd., Tokyo, Japan) and 100 mg/L streptomycin (Meiji Seika Kaisha Ltd., Tokyo, Japan) at 37°C in a 5% CO<sub>2</sub> atmosphere. Cells were grown in 225 cm<sup>2</sup> flask (Asahi Techno Glass Corporation, Chiba, Japan) to about 80 % confluence, and then split using 0.025% Trypsin (MP Biomedicals Inc, Irvine, California)- 0.02 % EDTA solution (Dojindo Laboratories, Kumamoto, Japan).

The control and MET exposure experiments were conducted in 6-well tissue culture plates (Becton, Dickinson and Company, Franklin Lakes, NJ, USA). A cell suspension of 2 ml containing 6x10<sup>5</sup> cells was placed in each well. Each experiment had four replicates per time sample. The test plates were then incubated at 37°C in a 5% CO<sub>2</sub> atmosphere. After incubation for 72 hr, the medium was changed to either 2 ml of supplemented medium, which was 1:1 mixture of Dulbecco's modified Eagle's medium and Ham's F12 medium (Invitrogen Corporation, Carlsbad, CA, USA) containing 0.00625 mg/ml insulin, 0.00625 mg/ml transferrin, 30 nmol/L sodium selenite, 1.25 mg/ml bovine serum albumin, 0.00535 mg/ml linoleic acid, 10 % FBS (Invitrogen Corporation, Carlsbad, CA, USA), 100 U/mL penicillin and 100 mg/L streptomycin, with 50 nM of adrenocorticotropin (ACTH, Sigma-Aldrich, Inc., St. Louis, MO, USA), 20 µM of forskolin (Sigma-Aldrich, Inc., St.

Louis, MO, USA), 100 nM of angiotensin II (EMD Chemicals Inc., Darmstadt, Germany) and 0.1% of dimethyl sulfoxide (DMSO, Wako Pure Chemical Industries, Ltd., Osaka, Japan), in the case of the control experiments, or 2 ml of MET-treated supplemented medium. Dilutions of a MET (Sigma-Aldrich, Inc., St. Louis, MO, USA) stock solution were prepared directly in supplemented medium to generate two test concentrations of MET (1 and 10  $\mu$ M). After changing the medium, the test plates were incubated at 37°C with a 5% CO<sub>2</sub> atmosphere, and the experiments were initiated. At incubation periods of 8, 24, 48, and 72 hr for the control and MET experiments, the medium and cells were separately removed from four replicate wells. The cells were dissolved in 100  $\mu$ l of distilled water and sonicated to produce a cell lysate.

The concentrations of twelve steroids (PREG, HPREG, DHEA, PROG, HPROG, DIONE, T, DCORTICO, CORTICO, ALDO, DCORT, CORT) in the medium and cell lysate were measured using liquid chromatography/mass spectrometry (LC-MS/MS). The LC-MS/MS systems consisted of a LC10A VP series (Shimadzu, Kyoto, Japan) and API4000 (Applied Biosystems, Foster City, CA, USA.). The steroids were extracted from the medium and cell lysate by ethyl acetate and separated on LC by acetonitrile and formic acid. MS/MS parameters were optimized using multiple reaction monitoring (MRM) mode for every steroids in positive electrospray ionization. The medium and cell lysate volumes were 500  $\mu$ L and 70  $\mu$ L, respectively, and LC-MS/MS running time was 17.5 min/sample. The concentrations of two additional steroids (E1, E2) in the medium and cell lysate were measured using enzyme-linked immunosorbent assay (ELISA) with commercial kits (Wako Pure Chemical Industries, Ltd., Osaka, Japan). The concentration of cholesterol in the medium and cell lysate was measured using a commercial kit (Wako Pure Chemical Industries, Ltd., Osaka, Japan) based on cholesterol oxidase method (Allain et al. 1974).

## 2. Dynamic molecular balance equations in cells and medium

CHOL in cells:

$$V_{\text{cell}} \frac{dC_{\text{CHOL,cell}}(t)}{dt} = k_1 V_{\text{med}} C_{\text{CHOL,med}}(t) - k_2 V_{\text{cell}} C_{\text{CHOL,cell}}(t);$$
$$C_{\text{CHOL,cell}}(0) = 1.88 \times 10^7 \text{ nM}$$

PREG in cells:

$$V_{\text{cell}} \frac{dC_{\text{PREG,cell}}(t)}{dt} = k_2 V_{\text{cell}} C_{\text{CHOL,cell}}(t) - (k_3 + k_5 + k_{+19}) V_{\text{cell}} C_{\text{PREG,cell}}(t) + k_{-19} V_{\text{med}} C_{\text{PREG,med}}(t);$$
$$C_{\text{PREG,cell}}(0) = 9.45 \times 10^3 \text{ nM}$$

HPREG in cells:

$$V_{\text{cell}} \frac{dC_{\text{HPREG,cell}}(t)}{dt} = k_3 V_{\text{cell}} C_{\text{PREG,cell}}(t) - (k_4 + k_6 + k_{+24}) V_{\text{cell}} C_{\text{HPREG,cell}}(t) + k_{-24} V_{\text{med}} C_{\text{HPREG,med}}(t);$$
$$C_{\text{HPREG,cell}}(0) = 0$$

DHEA in cells:

$$V_{\text{cell}} \frac{dC_{\text{DHEA,cell}}(t)}{dt} = k_4 V_{\text{cell}} C_{\text{HPREG,cell}}(t) - (k_7 + k_{+28}) V_{\text{cell}} C_{\text{DHEA,cell}}(t) + k_{-28} V_{\text{med}} C_{\text{DHEA,med}}(t);$$
$$C_{\text{DHEA,cell}}(0) = 3.49 \times 10^3 \text{ nM}$$

PROG in cells:

$$V_{\text{cell}} \frac{dC_{\text{PROG,cell}}(t)}{dt} = k_5 V_{\text{cell}} C_{\text{PREG,cell}}(t) - (k_8 + k_{11} + k_{+20}) V_{\text{cell}} C_{\text{PROG,cell}}(t) + k_{-20} V_{\text{med}} C_{\text{PROG,med}}(t);$$
$$C_{\text{PROG,cell}}(0) = 32.10 \text{ nM}$$

HPRG in cells:

$$V_{\text{cell}} \frac{dC_{\text{HPRG,cell}}(t)}{dt} = k_6 V_{\text{cell}} C_{\text{HPREG,cell}}(t) + k_8 V_{\text{cell}} C_{\text{PROG,cell}}(t) - (k_9 + k_{12} + k_{+25}) V_{\text{cell}} C_{\text{HPRG,cell}}(t) + k_{-25} V_{\text{med}} C_{\text{HPRG,med}}(t);$$
$$C_{\text{HPRG,cell}}(0) = 101.83 \text{ nM}$$

DIONE in cells:

$$V_{\text{cell}} \frac{dC_{\text{DIONE,cell}}(t)}{dt} = k_7 V_{\text{cell}} C_{\text{DHEA,cell}}(t) + k_9 V_{\text{cell}} C_{\text{HPROG,cell}}(t) - (k_{10} + k_{13} + k_{+29}) V_{\text{cell}} C_{\text{DIONE,cell}}(t) + k_{-29} V_{\text{med}} C_{\text{DIONE,med}}(t);$$

$$C_{\text{DIONE,cell}}(0) = 2.33 \times 10^3 \text{ nM}$$

T in cells:

$$V_{\text{cell}} \frac{dC_{\text{T,cell}}(t)}{dt} = k_{10} V_{\text{cell}} C_{\text{AD,cell}}(t) - (k_{14} + k_{+31}) V_{\text{cell}} C_{\text{T,cell}}(t) + k_{-31} V_{\text{med}} C_{\text{T,med}}(t)$$

$$C_{\text{T,cell}}(0) = 0$$

E1 in cells:

$$V_{\text{cell}} \frac{dC_{\text{E1,cell}}(t)}{dt} = k_{13} V_{\text{cell}} C_{\text{DIONE,cell}}(t) - (k_{15} + k_{+30}) V_{\text{cell}} C_{\text{E1,cell}}(t) + k_{-30} V_{\text{med}} C_{\text{E1,med}}(t)$$

$$C_{\text{E1,cell}}(0) = 2.09 \times 10^3 \text{ nM}$$

E2 in cells:

$$V_{\text{cell}} \frac{dC_{\text{E2,ovv}}(t)}{dt} = k_{14} V_{\text{cell}} C_{\text{T,cell}}(t) + k_{15} V_{\text{cell}} C_{\text{E1,cell}}(t) - k_{+32} V_{\text{cell}} C_{\text{E2,cell}}(t) + k_{-32} V_{\text{med}} C_{\text{E2,med}}(t)$$

$$C_{\text{E2,cell}}(0) = 424.17 \text{ nM}$$

DCORTICO in cells:

$$V_{\text{cell}} \frac{dC_{\text{DCORTICO,cell}}(t)}{dt} = k_{11} V_{\text{cell}} C_{\text{PROG,cell}}(t) - \left( \frac{k_{16}}{\alpha_{\text{CORTICO}}} + k_{+21} \right) V_{\text{cell}} C_{\text{DCORTICO,cell}}(t) + k_{-21} V_{\text{med}} C_{\text{DCORTICO,med}}(t)$$

$$C_{\text{DCORTICO,cell}}(0) = 835.01 \text{ nM}$$

CORTICO in cells:

$$V_{\text{cell}} \frac{dC_{\text{CORTICO,cell}}(t)}{dt} = \frac{k_{16}}{\alpha_{\text{CORTICO}}} V_{\text{cell}} C_{\text{DCORTICO,cell}}(t) - (k_{18} + k_{+22}) V_{\text{cell}} C_{\text{CORTICO,cell}}(t) + k_{-22} V_{\text{med}} C_{\text{CORTICO,med}}(t)$$

$$C_{\text{CORTICO,cell}}(0) = 2.27 \times 10^3 \text{ nM}$$

ALDO in cells:

$$V_{\text{cell}} \frac{dC_{\text{ALDO,cell}}(t)}{dt} = k_{18} V_{\text{cell}} C_{\text{CORTICO,cell}}(t) - k_{+23} V_{\text{cell}} C_{\text{ALDO,cell}}(t) + k_{-23} V_{\text{med}} C_{\text{ALDO,med}}(t)$$

$$C_{\text{ALDO,cell}}(0) = 0$$

DCORT in cells:

$$V_{\text{cell}} \frac{dC_{\text{DCORT,cell}}(t)}{dt} = k_{12} V_{\text{cell}} C_{\text{HPROG,cell}}(t) - \left( \frac{k_{17}}{\alpha_{\text{CORT}}} + k_{+26} \right) V_{\text{cell}} C_{\text{DCORT,cell}}(t) + k_{-26} V_{\text{med}} C_{\text{DCORT,med}}(t)$$

$$C_{\text{DCORT,cell}}(0) = 7.56 \times 10^4 \text{ nM}$$

CORT in cells:

$$V_{\text{cell}} \frac{dC_{\text{CORT,cell}}(t)}{dt} = \frac{k_{17}}{\alpha_{\text{CORT}}} V_{\text{cell}} C_{\text{DCORT,cell}}(t) - k_{+27} V_{\text{cell}} C_{\text{CORT,cell}}(t) + k_{-27} V_{\text{med}} C_{\text{CORT,med}}(t)$$

$$C_{\text{CORT,cell}}(0) = 3.43 \times 10^3 \text{ nM}$$

CHOL in medium:

$$\frac{dC_{\text{CHOL,med}}(t)}{dt} = -k_1 C_{\text{CHOL,med}}(t); \quad C_{\text{CHOL,med}}(0) = 8.11 \times 10^4 \text{ nM}$$

PREG in medium:

$$V_{\text{med}} \frac{dC_{\text{PREG,med}}(t)}{dt} = k_{+19} V_{\text{cell}} C_{\text{PREG,cell}}(t) - k_{-19} V_{\text{med}} C_{\text{PREG,med}}(t); \quad C_{\text{PREG,med}}(0) = 0.85 \text{ nM}$$

HPREG in medium:

$$V_{\text{med}} \frac{dC_{\text{HPREG,med}}(t)}{dt} = k_{+24} V_{\text{cell}} C_{\text{HPREG,cell}}(t) - k_{-24} V_{\text{med}} C_{\text{HPREG,med}}(t); \quad C_{\text{HPREG,med}}(0) = 69.45 \text{ nM}$$

DHEA in medium:

$$V_{\text{med}} \frac{dC_{\text{DHEA,med}}(t)}{dt} = k_{+28} V_{\text{cell}} C_{\text{DHEA,cell}}(t) - k_{-28} V_{\text{med}} C_{\text{DHEA,med}}(t); \quad C_{\text{DHEA,med}}(0) = 0$$

PROG in medium:

$$V_{\text{med}} \frac{dC_{\text{PROG,med}}(t)}{dt} = k_{+20} V_{\text{cell}} C_{\text{PROG,cell}}(t) - k_{-20} V_{\text{med}} C_{\text{PROG,med}}(t); \quad C_{\text{PROG,med}}(0) = 0.03 \text{ nM}$$

HPROG in medium:

$$V_{\text{med}} \frac{dC_{\text{HPROG,med}}(t)}{dt} = k_{+25} V_{\text{cell}} C_{\text{HPROG,cell}}(t) - k_{-25} V_{\text{med}} C_{\text{HPROG,med}}(t); \quad C_{\text{HPROG,med}}(0) = 0$$

DIONE in medium:

$$V_{\text{med}} \frac{dC_{\text{DIONE,med}}(t)}{dt} = k_{+29} V_{\text{cell}} C_{\text{DIONE,cell}}(t) - k_{-29} V_{\text{med}} C_{\text{DIONE,med}}(t); \quad C_{\text{DIONE,med}}(0) = 0.80 \text{ nM}$$

T in medium:

$$V_{\text{med}} \frac{dC_{\text{T,med}}(t)}{dt} = k_{+31} V_{\text{cell}} C_{\text{T,cell}}(t) - k_{-31} V_{\text{med}} C_{\text{T,med}}(t); \quad C_{\text{T,med}}(0) = 0.80 \text{ nM}$$

E1 in medium:

$$V_{\text{med}} \frac{dC_{\text{E1,med}}(t)}{dt} = k_{+30} V_{\text{cell}} C_{\text{E1,cell}}(t) - k_{-30} V_{\text{med}} C_{\text{E1,med}}(t); \quad C_{\text{E1,med}}(0) = 0.11 \text{ nM}$$

E2 in medium:

$$V_{\text{med}} \frac{dC_{\text{E2,med}}(t)}{dt} = k_{+32} V_{\text{cell}} C_{\text{E2,cell}}(t) - k_{-32} V_{\text{med}} C_{\text{E2,med}}(t); \quad C_{\text{E2,med}}(0) = 1.21 \text{ nM}$$

DCORTICO in medium:

$$V_{\text{med}} \frac{dC_{\text{DCORTICO,med}}(t)}{dt} = k_{+21} V_{\text{cell}} C_{\text{DCORTICO,cell}}(t) - k_{-21} V_{\text{med}} C_{\text{DCORTICO,med}}(t); \quad C_{\text{DCORTICO,med}}(0) = 0 \text{ nM}$$

CORTICO in medium:

$$V_{\text{med}} \frac{dC_{\text{CORTICO,med}}(t)}{dt} = k_{+22} V_{\text{cell}} C_{\text{CORTICO,cell}}(t) - k_{-22} V_{\text{med}} C_{\text{CORTICO,med}}(t); \quad C_{\text{CORTICO,med}}(0) = 0.11 \text{ nM}$$

ALDO in medium:

$$V_{\text{med}} \frac{dC_{\text{ALDO,med}}(t)}{dt} = k_{+23} V_{\text{cell}} C_{\text{ALDO,cell}}(t) - k_{-23} V_{\text{med}} C_{\text{ALDO,med}}(t); \quad C_{\text{ALDO,med}}(0) = 0.91 \text{ nM}$$

DCORT in medium:

$$V_{\text{med}} \frac{dC_{\text{DCORT,med}}(t)}{dt} = k_{+26} V_{\text{cell}} C_{\text{DCORT,cell}}(t) - k_{-26} V_{\text{med}} C_{\text{DCORT,med}}(t); \quad C_{\text{DCORT,med}}(0) = 0 \text{ nM}$$

CORT in medium:

$$V_{\text{med}} \frac{dC_{\text{CORT,med}}(t)}{dt} = k_{+27} V_{\text{cell}} C_{\text{CORT,cell}}(t) - k_{-27} V_{\text{med}} C_{\text{CORT,med}}(t); \quad C_{\text{CORT,med}}(0) = 0.03 \text{ nM}$$

### 3. Molecular balance equations for quasi-equilibrium

CHOL in cells:

$$V_{\text{cell}} \frac{dC_{\text{CHOL,cell}}(t)}{dt} = k_1 V_{\text{med}} C_{\text{CHOL,med}}(t) - k_2 V_{\text{cell}} C_{\text{CHOL,cell}}(t); \quad C_{\text{CHOL,cell}}(0) = 1.88 \times 10^7 \text{ nM}$$

PREG in cells:

$$\frac{dC_{\text{PREG,cell}}(t)}{dt} = \left( \frac{1}{V_{\text{cell}} + V_{\text{med}} q_{19}} \right) \left[ k_2 V_{\text{cell}} C_{\text{CHOL,cell}}(t) - (k_3 + k_5) V_{\text{cell}} C_{\text{PREG,cell}}(t) \right]; \quad C_{\text{PREG,cell}}(0) = 9.45 \times 10^3 \text{ nM}$$

HPREG in cells:

$$\frac{dC_{\text{HPREG,cell}}(t)}{dt} = \left( \frac{1}{V_{\text{cell}} + V_{\text{med}} q_{24}} \right) \left[ k_3 V_{\text{cell}} C_{\text{PREG,cell}}(t) - (k_4 + k_6) V_{\text{cell}} C_{\text{HPREG,cell}}(t) \right]; \quad C_{\text{HPREG,cell}}(0) = 0$$

DHEA in cells:

$$\frac{dC_{\text{DHEA,cell}}(t)}{dt} = \left( \frac{1}{V_{\text{cell}} + V_{\text{med}} q_{28}} \right) \left[ k_4 V_{\text{cell}} C_{\text{HPREG,cell}}(t) - k_7 V_{\text{cell}} C_{\text{DHEA,cell}}(t) \right]; \quad C_{\text{DHEA,cell}}(0) = 3.49 \times 10^3 \text{ nM}$$

PROG in cells:

$$\frac{dC_{\text{PROG,cell}}(t)}{dt} = \left( \frac{1}{V_{\text{cell}} + V_{\text{med}}q_{20}} \right) \left[ k_5 V_{\text{cell}} C_{\text{PREG,cell}}(t) - (k_8 + k_{11}) V_{\text{cell}} C_{\text{PROG,cell}}(t) \right]; C_{\text{PROG,cell}}(0) = 32.10 \text{ nM}$$

HPROG in cells:

$$\frac{dC_{\text{HPROG,cell}}(t)}{dt} = \left( \frac{1}{V_{\text{cell}} + V_{\text{med}}q_{25}} \right) \left[ k_6 V_{\text{cell}} C_{\text{HPREG,cell}}(t) + k_8 V_{\text{cell}} C_{\text{PROG,cell}}(t) - (k_9 + k_{12}) V_{\text{cell}} C_{\text{HPROG,cell}}(t) \right]$$

$$C_{\text{HPROG,cell}}(0) = 101.83 \text{ nM}$$

DIONE in cells:

$$\frac{dC_{\text{DIONE,cell}}(t)}{dt} = \left( \frac{1}{V_{\text{cell}} + V_{\text{med}}q_{29}} \right) \left[ k_7 V_{\text{cell}} C_{\text{DHEA,cell}}(t) + k_9 V_{\text{cell}} C_{\text{HPROG,cell}}(t) - (k_{10} + k_{13}) V_{\text{cell}} C_{\text{DIONE,cell}}(t) \right]$$

$$C_{\text{DIONE,cell}}(0) = 2.33 \times 10^3 \text{ nM}$$

T in cells:

$$\frac{dC_{\text{T,cell}}(t)}{dt} = \left( \frac{1}{V_{\text{cell}} + V_{\text{med}}q_{31}} \right) \left[ k_{10} V_{\text{cell}} C_{\text{DIONE,cell}}(t) - k_{14} V_{\text{cell}} C_{\text{T,cell}}(t) \right]; C_{\text{T,cell}}(0) = 0$$

E1 in cells:

$$\frac{dC_{\text{E1,cell}}(t)}{dt} = \left( \frac{1}{V_{\text{cell}} + V_{\text{med}}q_{30}} \right) \left[ k_{13} V_{\text{cell}} C_{\text{DIONE,cell}}(t) - k_{15} V_{\text{cell}} C_{\text{E1,cell}}(t) \right]; C_{\text{E1,cell}}(0) = 2.09 \times 10^3 \text{ nM}$$

E2 in cells:

$$\frac{dC_{\text{E2,ov}}(t)}{dt} = \left( \frac{1}{V_{\text{cell}} + V_{\text{med}}q_{32}} \right) \left[ k_{14} V_{\text{cell}} C_{\text{T,cell}}(t) + k_{15} V_{\text{cell}} C_{\text{E1,cell}}(t) \right]; C_{\text{E2,cell}}(0) = 424.17 \text{ nM}$$

DCORTICO in cells:

$$\frac{dC_{\text{DCORTICO,cell}}(t)}{dt} = \left( \frac{1}{V_{\text{cell}} + V_{\text{med}} q_{21}} \right) \left[ k_{11} V_{\text{cell}} C_{\text{PROG,cell}}(t) - \left( \frac{k_{16}}{\alpha_{\text{CORTICO}}} \right) V_{\text{cell}} C_{\text{DCORTICO,cell}}(t) \right]; \quad C_{\text{DCORTICO,cell}}(0) = 835.01 \text{ nM}$$

CORTICO in cells:

$$\frac{dC_{\text{CORTICO,cell}}(t)}{dt} = \left( \frac{1}{V_{\text{cell}} + V_{\text{med}} q_{22}} \right) \left[ \frac{k_{16}}{\alpha_{\text{CORTICO}}} V_{\text{cell}} C_{\text{DCORTICO,cell}}(t) - k_{18} V_{\text{cell}} C_{\text{CORTICO,cell}}(t) \right]; \quad C_{\text{CORTICO,cell}}(0) = 2.27 \times 10^3 \text{ nM}$$

ALDO in cells:

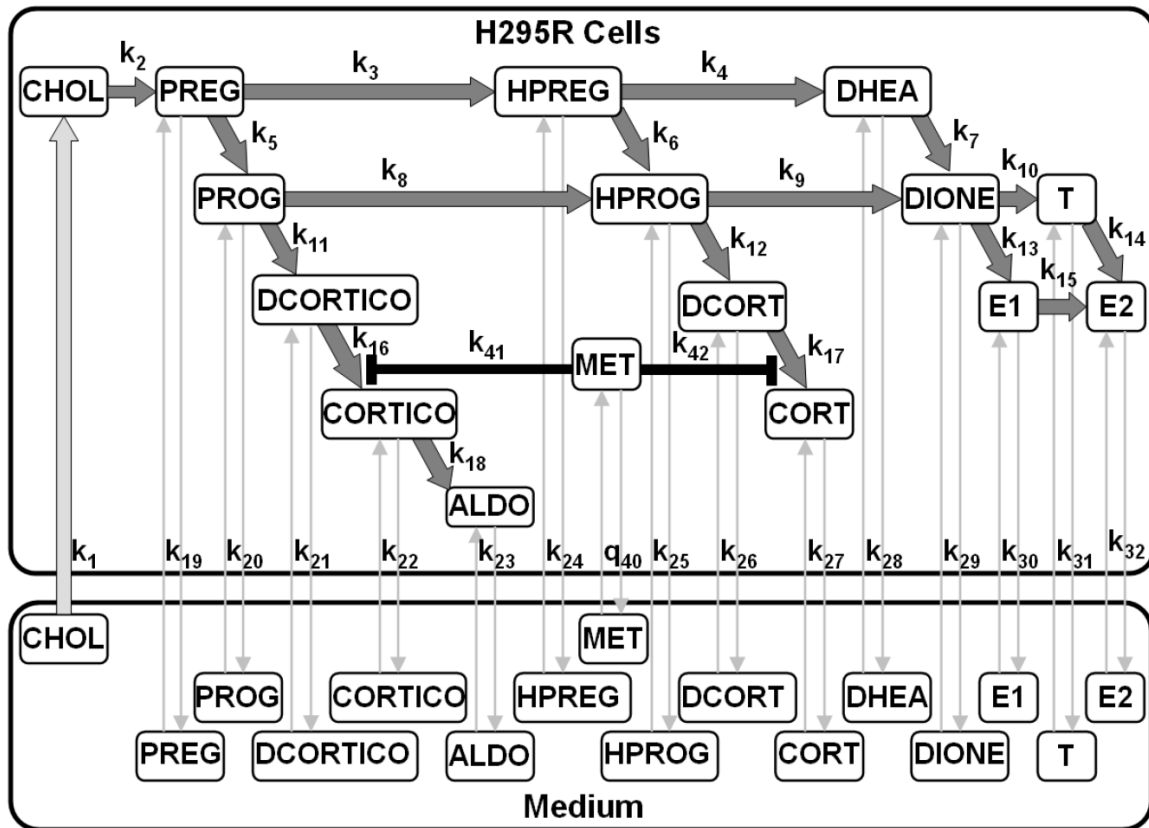
$$\frac{dC_{\text{ALDO,cell}}(t)}{dt} = \left( \frac{1}{V_{\text{cell}} + V_{\text{med}} q_{23}} \right) \left[ k_{18} V_{\text{cell}} C_{\text{CORTICO,cell}}(t) \right]; \quad C_{\text{ALDO,cell}}(0) = 0$$

DCORT in cells:

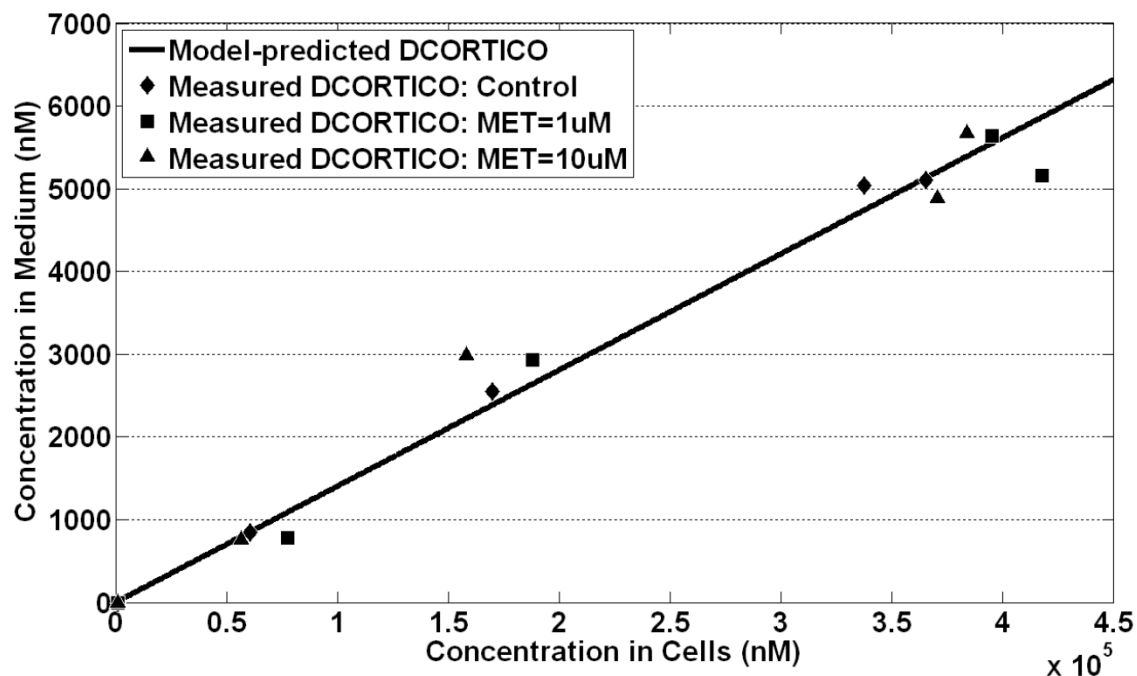
$$\frac{dC_{\text{DCORT,cell}}(t)}{dt} = \left( \frac{1}{V_{\text{cell}} + V_{\text{med}} q_{26}} \right) \left[ k_{12} V_{\text{cell}} C_{\text{HPROG,cell}}(t) - \left( \frac{k_{17}}{\alpha_{\text{CORT}}} \right) V_{\text{cell}} C_{\text{DCORT,cell}}(t) \right]; \quad C_{\text{DCORT,cell}}(0) = 7.56 \times 10^4 \text{ nM}$$

CORT in cells:

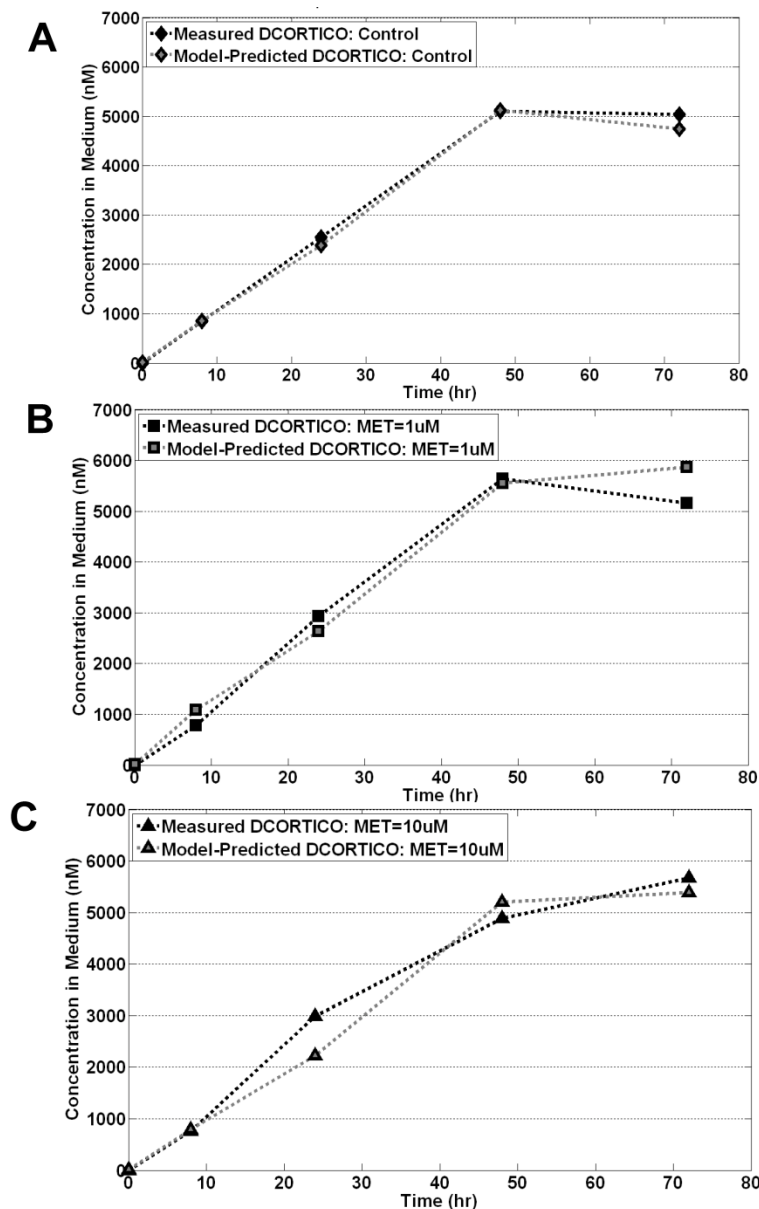
$$\frac{dC_{\text{CORT,cell}}(t)}{dt} = \left( \frac{1}{V_{\text{cell}} + V_{\text{med}} q_{27}} \right) \left[ \frac{k_{17}}{\alpha_{\text{CORT}}} V_{\text{cell}} C_{\text{DCORT,cell}}(t) \right]; \quad C_{\text{CORT,cell}}(0) = 3.43 \times 10^3 \text{ nM}$$



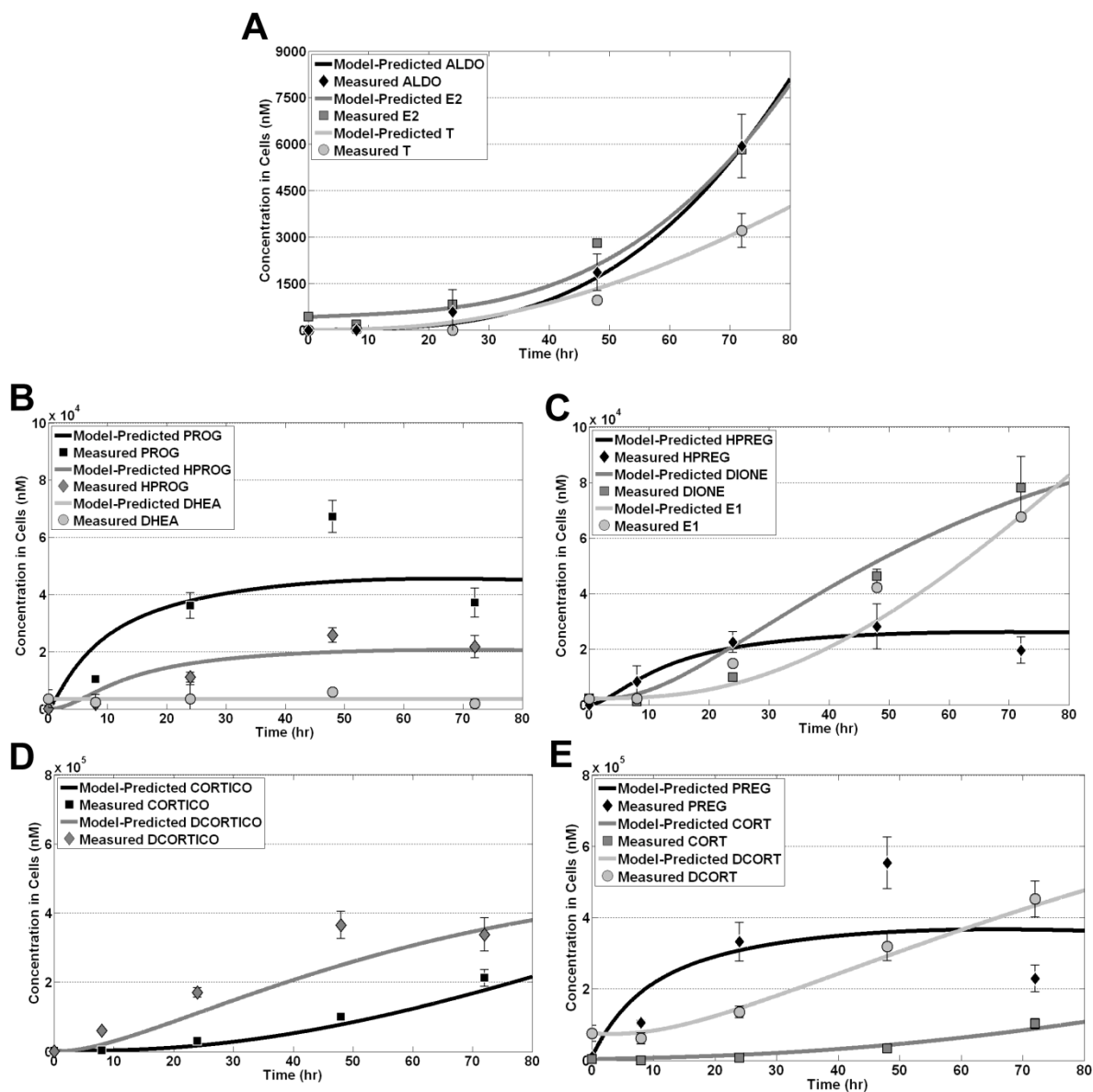
**Supplemental Material, Figure 1.** Graphical representation of the parameters for the mathematical H295R steroidogenesis model. First-order rate constant for cholesterol uptake into the cells is  $k_1$ . First-order rate constants for metabolic processes are:  $k_2 - k_{18}$ . Reversible first-order rate constants for transport processes ( $k_{+x}$  and  $k_{-x}$  for secretion and import of steroid x; respectively) are  $k_{19} - k_{32}$ . Enzyme inhibition constants for MET are  $k_{41}$  and  $k_{42}$  for CORTICO and CORT pathways, respectively.



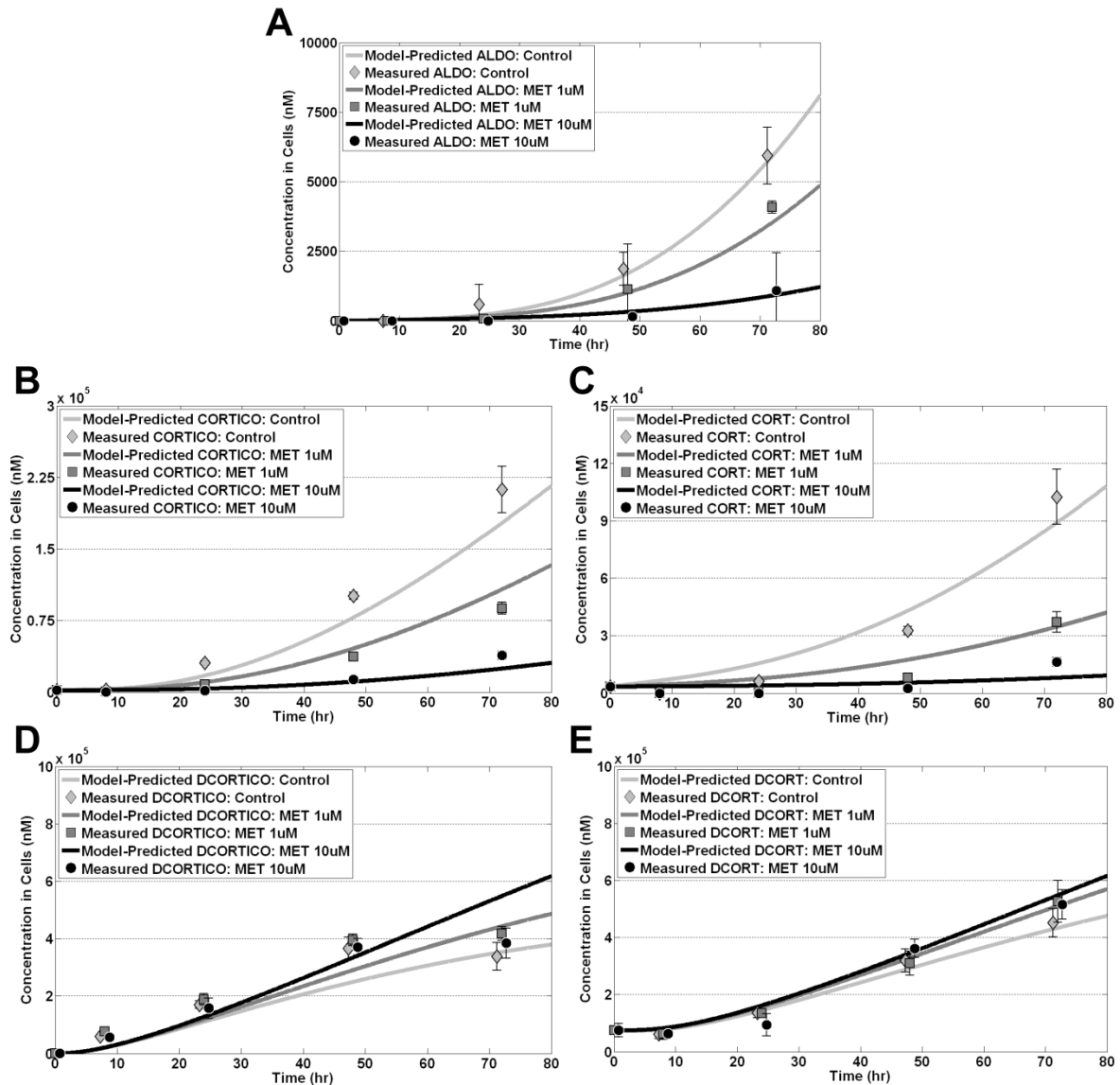
**Supplemental Material, Figure 2.** Comparison of transport equilibrium model-predictions (linear regression line) with measurements in cells and medium. Model-predicted DCORTICO concentrations in medium were plotted as a function of DCORTICO concentrations in cells, and compared with mean concentrations measured at five sampling times for control and two MET concentrations.



**Supplemental Material, Figure 3.** Model evaluation of transport pathway. Comparison of transport equilibrium model-predictions with time-course measurements in medium from control (A) and two MET concentrations: 1  $\mu$ M (B) and 10  $\mu$ M (C). Model-predicted and mean measured DCORTICO concentrations in medium were plotted at five time points after incubation of cells with MET. Model-predicted DCORTICO concentrations in medium were estimated from mean measured concentrations in cells at each corresponding time point. Dotted lines represent linear interpolations between model-predicted and measured concentrations. Measured steroid concentrations are same as shown in Supplemental Material, Figure 2.



**Supplemental Material, Figure 4.** Model evaluation of metabolic pathway for control experiments. Model-predicted concentrations in cells were plotted as a function of time, and compared with concentrations (mean and standard deviation) measured at five sampling times for steroids: ALDO, E2, T (A); PROG, HPROG, DHEA (B); HPREG, DIONE, E1 (C); CORTICO, DCORTICO (D); PREG, CORT, DCORT (E).



**Supplemental Material, Figure 5.** Model evaluation of metabolic pathway for control and MET-exposed cells. Model-predicted concentrations in cells were plotted as a function of time, and compared with concentrations (mean and standard deviation) measured at five sampling times for steroids: ALDO (A), CORTICO (B), CORT (C), DCORTICO (D), DCORT (E). For controls, model-predicted and measured steroid concentrations are same as shown in Supplemental Material, Figure 5.

**Supplemental Material, Table 1. Quantitative ranges for steroids in cells and medium**

Steroid	Quantitative range (nM)	
	Cells	Medium
PREG	$1.3 \times 10^4 - 1.3 \times 10^6$	$15.8 - 1.6 \times 10^3$
HPREG	$1.2 \times 10^4 - 1.2 \times 10^6$	$15.0 - 1.5 \times 10^3$
DHEA	$1.4 \times 10^4 - 1.4 \times 10^6$	$17.3 - 1.7 \times 10^3$
PROG	$2.6 \times 10^3 - 1.3 \times 10^6$	$3.2 - 1.6 \times 10^3$
HPROG	$2.4 \times 10^3 - 1.2 \times 10^6$	$3.0 - 1.5 \times 10^3$
DIONE	$2.8 \times 10^3 - 1.4 \times 10^6$	$3.5 - 1.7 \times 10^3$
T	$2.8 \times 10^3 - 1.4 \times 10^6$	$3.5 - 1.7 \times 10^3$
E1	$1.6 \times 10^3 - 1.5 \times 10^5$	$5.5 - 5.5 \times 10^2$
E2	$5.0 \times 10^2 - 1.0 \times 10^4$	$5.5 - 1.1 \times 10^2$
DCORTICO	$1.2 \times 10^4 - 6.1 \times 10^6$	$15.1 - 7.6 \times 10^3$
CORTICO	$1.2 \times 10^4 - 5.9 \times 10^6$	$14.4 - 7.2 \times 10^3$
ALDO	$2.2 \times 10^3 - 1.1 \times 10^6$	$2.8 - 1.4 \times 10^3$
DCORT	$1.2 \times 10^4 - 5.9 \times 10^6$	$14.4 - 7.2 \times 10^3$
CORT	$1.1 \times 10^4 - 5.6 \times 10^6$	$13.8 - 6.9 \times 10^3$

## Appendix B

### **DEVELOPING PREDICTIVE APPROACHES TO CHARACTERIZE ADAPTIVE RESPONSES OF THE REPRODUCTIVE ENDOCRINE AXIS TO AROMATASE INHIBITION: I. DATA GENERATION IN A SMALL FISH MODEL**

Daniel L. Villeneuve, Miyuki Breen, David C. Bencic, Jenna E. Cavallin, Kathleen M. Jensen, Elizabeth A. Makynen, Linnea M. Thomas, Leah C. Wehmas, Rory B. Conolly, Gerald T. Ankley

Published in Toxicological Sciences: 2013; 133: 225-233

Reprinted with permission from Oxford University Press

Miyuki Breen was primarily responsible for assistance of experiment design based on the computational model of HPG axis preliminary results, and coordination of manuscript writing and submission as a companion paper of part II. Computational Modeling.

# Developing Predictive Approaches to Characterize Adaptive Responses of the Reproductive Endocrine Axis to Aromatase Inhibition: I. Data Generation in a Small Fish Model

Daniel L. Villeneuve,<sup>\*,1</sup> Miyuki Breen,<sup>†</sup> David C. Bencic,<sup>‡</sup> Jenna E. Cavallin,<sup>\*,§</sup> Kathleen M. Jensen,<sup>\*</sup> Elizabeth A. Makynen,<sup>\*</sup> Linnea M. Thomas,<sup>\*,2</sup> Leah C. Wehmas,<sup>\*,3</sup> Rory B. Conolly,<sup>¶</sup> and Gerald T. Ankley<sup>\*</sup>

<sup>\*</sup>United States Environmental Protection Agency, Mid-Continent Ecology Division, Duluth, Minnesota 55804; <sup>†</sup>Biomathematics Program, Department of Statistics, North Carolina State University, Raleigh, North Carolina 27695; <sup>‡</sup>United States Environmental Protection Agency, Ecological Exposure Research Division, Cincinnati, Ohio 45268; <sup>§</sup>ORISE Research Participation Program, United States Environmental Protection Agency, Mid-Continent Ecology Division, Duluth, Minnesota 55804; and <sup>¶</sup>United States Environmental Protection Agency, Integrated Systems Toxicology Division, Research Triangle Park, North Carolina 27711.

<sup>1</sup>To whom correspondence should be addressed at US EPA Mid-Continent Ecology Division, 6201 Congdon Blvd, Duluth, MN 55804. Fax: (218) 529-5003. E-mail: [villeneuve.dan@epa.gov](mailto:villeneuve.dan@epa.gov).

<sup>2</sup>Present address: U.S. Fish and Wildlife Service, Region 3, 5600 American Blvd West, Suite 990 Bloomington, MN 55437-1458.

<sup>3</sup>Present address: Environmental Health Sciences Center, Oregon State University, Corvallis, OR 97331-7302.

Received December 4, 2012; accepted February 27, 2013

Adaptive or compensatory responses to chemical exposure can significantly influence *in vivo* concentration-duration-response relationships. This study provided data to support development of a computational dynamic model of the hypothalamic-pituitary-gonadal axis of a model vertebrate and its response to aromatase inhibitors as a class of endocrine active chemicals. Fathead minnows (*Pimephales promelas*) were either exposed to the aromatase inhibitor fadrozole (0.5 or 30 µg/l) continuously for 1, 8, 12, 16, 20, 24, or 28 days or exposed for 8 days and then held in control water (no fadrozole) for an additional 4, 8, 12, 16, or 20 days. The time course of effects on ovarian steroid production, circulating 17β-estradiol (E2) and vitellogenin (VTG) concentrations, and expression of steroidogenesis-related genes in the ovary was measured. Exposure to 30 µg fadrozole/l significantly reduced plasma E2 and VTG concentrations after just 1 day and those effects persisted throughout 28 days of exposure. In contrast, *ex vivo* E2 production was similar to that of controls on day 8–28 of exposure, whereas transcripts coding for aromatase and follicle-stimulating hormone receptor were elevated, suggesting a compensatory response. Following cessation of fadrozole exposure, *ex vivo* E2 and plasma E2 concentrations exceeded and then recovered to control levels, but plasma VTG concentrations did not, even after 20 days of depuration. Collectively these data provide several new insights into the nature and time course of adaptive responses to an aromatase inhibitor that support development of a computational model (see companion article).

**Key Words:** steroidogenesis; endocrine disruption; reproduction; alternative species; compensation; time course.

Aromatase (cytochrome P450 [CYP] 19) catalyzes a key rate-limiting step in estrogen biosynthesis—conversion of C19

androgens such as androstenedione or testosterone (T) to C18 estrogens such as estrone or 17β-estradiol (E2) (Miller, 1988). From a therapeutic perspective, aromatase inhibitors have been sought and developed primarily to treat estrogen-dependent cancers. However, aromatase has also been recognized as a target for chemical contaminants in the environment. For example, numerous fungicides, certain polychlorinated biphenyls, polychlorinated dibenzo-*p*-dioxins, organotin, etc. have been reported to inhibit aromatase activity, at least *in vitro* (Drenth *et al.*, 1998; Sanderson, 2006; Vinggaard *et al.*, 2000). This has led to recognition of aromatase inhibitors as an important class of endocrine disruptors and inclusion of screening for aromatase inhibitors specifically, and steroid biosynthesis inhibitors more broadly, in the Endocrine Disruptor Screening Program of United States Environmental Protection Agency (U.S. EPA) (<http://www.epa.gov/endo/>). *In vitro* aromatase inhibition assays have also been incorporated into nascent high-throughput screening programs such as ToxCast (Reif *et al.*, 2010). As chemicals are screened in these programs, identification of additional environmental contaminants that inhibit aromatase activity can be expected. Based on adverse outcome pathway knowledge developed by our research program, such chemicals are likely to function as reproductive toxicants in fish (Ankley *et al.*, 2010).

Indeed, previous study has demonstrated that *in vivo* exposure to aromatase inhibitors can cause reproductive impairment in fish (Ankley *et al.*, 2002, 2005; Sun *et al.*, 2007). Based on endpoints measured in fish at multiple levels of biological organization, an adverse outcome pathway has been defined whereby aromatase inhibition leads to decreased estrogen synthesis in

the gonad, decreased concentrations of circulating E2, reduced hepatic vitellogenesis, reduced uptake of vitellogenin (VTG) into oocytes, impaired oocyte growth, and ultimately decreased fecundity (Ankley *et al.*, 2010). Early life exposures to aromatase inhibitors have also been reported to cause adverse effects on growth, eye development, sexual differentiation, and sperm quality in zebrafish (Hamad *et al.*, 2007; McAllister and Kime, 2003), as well as complete sex reversal in *Xenopus laevis* (Olmstead *et al.*, 2009). In birds, exposure to aromatase inhibitors has been linked to altered behavior and impaired osteogenesis (Deng *et al.*, 2010; Wacker *et al.*, 2008). Additionally, gestational exposures of rodents to aromatase inhibitors have been associated with *in utero* developmental abnormalities and altered sexual behaviors in adulthood (Gerardin *et al.*, 2008; Tiboni *et al.*, 2008). Collectively, given the important role of estrogens in many aspects of developmental, reproductive, and behavioral biology, it is clear that chemical inhibition of aromatase poses a potential risk *in vivo* to a diversity of vertebrates. However, the challenge of understanding at what concentrations and under what exposure conditions adverse *in vivo* effects are likely to occur remains.

To more effectively utilize *in vitro* aromatase inhibition data for quantitative risk assessment and predictive toxicology, there is a need to develop computational models that can support prediction of complex concentration-duration-response relationships that may occur *in vivo* (Villeneuve and Garcia-Reyero, 2011). To address this, our research team has conducted a series of time-course experiments to characterize direct effects of exposure to endocrine active chemicals (EACs) such as aromatase inhibitors, adaptive/compensatory responses that occur during exposure, and the rapidity and extent to which organisms recover following exposure (Ankley *et al.*, 2009a,b; Ekman *et al.*, 2011; Villeneuve *et al.*, 2009). In earlier studies in which fathead minnows were exposed to 3 or 30 µg fadrozole/l for 1, 2, 4, or 8 days, followed by varying durations of depuration (experiment 1; Villeneuve *et al.*, 2009) or exposed to 2, 5, 15 or 50 µg fadrozole/l for 7 days (Villeneuve *et al.*, 2006), we documented a series of ovarian gene expression changes consistent with a compensatory feedback response to declining E2 concentrations. Although we observed some recovery in both rates of E2 production and plasma E2 concentrations, circulating concentrations of VTG did not return to control levels, even after 8 days of depuration, and after 21 days of continuous exposure, reproductive impacts were still observed (Ankley *et al.*, 2002; Villeneuve *et al.*, 2009).

This study had four primary objectives. First, we tested the hypothesis that plasma VTG concentrations in female fathead minnows would return to control levels over a more extended depuration/recovery period. Second, we sought to evaluate whether compensatory responses observed in an 8-day exposure would be sustained over a longer period of continuous exposure. Third, we wanted to examine the dynamics of the compensatory responses at a lower fadrozole concentration (i.e., 0.5 µg fadrozole/l) that had been used in the previous studies (e.g., experiment 1; Villeneuve *et al.*, 2006, 2009).

Finally, we wanted to measure the concentrations of fadrozole in plasma. Collectively, these data contribute to increased understanding of the nature and time course of compensatory responses and recovery processes that can affect concentration-duration-response relationships and toxicological outcomes for aromatase inhibitors. The results also inform the development of computational models of the hypothalamic-pituitary-gonadal axis in fish that could support the use of data from *in vitro* screening assays to predict probable reproductive outcomes in fish. The initial steps toward development of such a model are described in the companion article by Breen *et al.* (2013).

## MATERIALS AND METHODS

**Fadrozole exposure.** Sexually mature adult fathead minnows (*Pimephales promelas*; 5–6 months old), obtained from an onsite culture facility at the U.S. EPA Mid-Continent Ecology Division (Duluth, MN), were exposed to 0, 0.5, or 30 µg fadrozole/l. Solvent-free solutions of fadrozole were delivered to 20-l tanks containing 10 l of test solution via a continuous flow (approximately 45 ml/min) of UV-treated, filtered Lake Superior water. Four male and four female fathead minnows were exposed in each tank. The experiment was initiated by transferring random groups of fish directly to tanks that had been receiving a continuous flow of test solution for approximately 48 h. Addition of fish was staggered by replicate within each treatment to permit all samples from a given exposure tank to be collected within 45 min of the desired exposure duration. Fish were either exposed continuously and sampled after 1, 8, 12, 16, 20, 24, or 28 days of exposure or exposed for 8 days, after which chemical delivery ceased and the tanks received a continuous flow of control Lake Superior water (no fadrozole) for an additional 4, 8, 12, 16, or 20 days (Supplementary fig. 1), with fadrozole concentrations steadily diminishing as the volume in the tank was exchanged (6.5 water exchanges per day at 45 ml/min flow rate). There were two replicate tanks for each unique exposure condition (i.e., combination of treatment and time point). Fish survival, water temperature, and dissolved oxygen concentrations were monitored daily in all test tanks. Flow rates and pH were monitored one to two times each week.

Fadrozole concentrations in exposure tanks were measured on 19 occasions over the course of the experiment. Water from control tanks was also analyzed for fadrozole on 14 occasions over the study duration. Fadrozole concentrations in the tank water were quantified by high-pressure liquid chromatography (LC) with mass spectral (MS) detection. The LC/MS (1946 LC/MSD, Agilent, Wilmington, DE) method consisted of injecting 50 µl of tank water onto a Kinetex C18 2.0 × 50 mm column (Phenomenex, Torrance, CA) held at 25°C with an isocratic elution using a mobile phase of 50% 0.025M ammonium acetate buffer/methanol at a flow rate of 200 µl/min. Fadrozole was measured in the selective ion monitoring mode using the response of positive ions 224 and 225 amu, with an atmospheric pressure photoionization source with a toluene dopant. Recoveries (mean ± SD) in water samples spiked with 0.43 and 21.8 µg fadrozole/l, respectively, were 98 ± 3% (*n* = 30) and 101 ± 4% (*n* = 28). Average percent agreement among duplicates was 97 ± 3% (*n* = 59). The method detection limit was 0.05 µg/l.

On appropriate sampling days, fish were euthanized in a buffered solution of tricaine methanesulfonate (MS-222; Finquel, Argent, Redmond, WA). Whole-body wet weight was measured, and urine was collected from males using nonheparinized microcapillary tubes. The presence or absence of sperm in each urine sample was noted and urine was stored at –80°C for future metabolomic analyses (e.g., Collette *et al.*, 2010). Blood was collected from both males and females using heparinized microhematocrit tubes then centrifuged to separate the plasma. Plasma samples were stored at –80°C until analyzed. For males, the remaining carcass (sans urine and blood) was wrapped in solvent-rinsed aluminum foil and stored at –20°C for tissue residue analysis. For females, liver tissue was removed, snap frozen in liquid nitrogen, and stored at –80°C. Ovary tissue was removed, weighed, and then split into three subsamples. A 16 ± 8 mg (mean ± SD) portion of the center of the right ovary was transferred

to a glass test tube containing 500  $\mu$ l medium 199 (M2520; Sigma, St Louis, MO) supplemented with 0.1mM isobutylmethylxanthine (Sigma I7018) and 1  $\mu$ g 25-hydroxycholesterol (Sigma)/ml for use in an *ex vivo* steroid production assay. The entire left ovary and the anterior portion of the right ovary was snap frozen in liquid nitrogen and stored at  $-80^{\circ}\text{C}$  for subsequent metabolomic analysis, whereas the posterior portion of the right ovary was similarly frozen and stored for RNA extraction. Female brain tissue was removed, snap frozen, and stored at  $-80^{\circ}\text{C}$ . Pituitary glands ( $< 0.5$  mg) were removed with a fine forceps, transferred to 100  $\mu$ l RNAlater (Ambion, Austin, TX) and stored at  $-20^{\circ}\text{C}$ . All dissection tools were washed with RNaseZap (Ambion) between samples to prevent cross-contamination and/or RNA degradation. All procedures involving animals were reviewed and approved by the U.S. EPA Animal Care and Use Committee in accordance with Animal Welfare Act and Interagency Research Animal Committee guidelines.

An additional set of tanks loaded with four males and four females per tank, as above, were included in the overall experimental design to allow for measurement of fadrozole concentrations in plasma. Fish in these tanks were exposed to 0.5 or 30  $\mu$ g fadrozole/l for 1 day, 8 days, or 8 days followed by a single day of depuration or to control Lake Superior water for 8 days. There were two replicate tanks per time  $\times$  treatment combination. However, unlike in the main experiment, only blood samples were collected from these fish. After blood collection, the rest of the carcass was preserved intact and stored at  $-20^{\circ}\text{C}$  for possible tissue residue analysis. Plasma was prepared by centrifugation and samples stored at  $-80^{\circ}\text{C}$  for subsequent determination of plasma fadrozole concentrations. For fadrozole quantification, 15  $\mu$ l of plasma was combined with 50  $\mu$ l acetonitrile, vortexed, and then sonicated for 15 min. Following sonication, samples were centrifuged for 10 min at  $12,000 \times g$  at  $0^{\circ}\text{C}$ , and the supernatant was transferred to a clean sample vial. The remaining extract was subjected to a second round of extraction with 100  $\mu$ l of 50% acetonitrile/water and the supernatant of the second round of extraction combined with the first. The volume was brought to 500  $\mu$ l, and 50  $\mu$ l of the resulting final extract was injected into the LC/MS. The subsequent fadrozole quantification was the same as that described for the tank water. The effective method detection limit for plasma fadrozole measurements was 0.3 pg/ $\mu$ l.

**Biochemical analyses.** Plasma VTG concentrations were quantified by enzyme-linked immunosorbent assay using a polyclonal antibody to fathead minnow VTG and purified fathead minnow VTG as a standard (Korte *et al.*, 2000). *Ex vivo* steroid production assays were conducted using methods adapted from McMaster *et al.* (1995) as described previously (Ankley *et al.*, 2007; Martinovic *et al.*, 2008). Steroids were extracted from medium (*ex vivo*) or plasma samples by liquid-liquid extraction with diethyl ether and quantified by radioimmunoassay (Jensen *et al.*, 2001). For culture medium samples from *ex vivo* steroid production assays, both E2 and T were quantified; however, due to limited volumes, only E2 could be quantified in female plasma.

**Gene expression analyses.** Relative abundance of mRNA transcripts coding for aromatase (*cyp19a1a*), follicle-stimulating hormone receptor (*fshr*), cytochrome P450 cholesterol side-chain cleavage (*cyp11a*), and steroidogenic acute regulatory protein (*star*) in ovaries was measured by real-time quantitative PCR (QPCR). Ovary samples were extracted and DNase treated (DNA free; Applied Biosystems/Ambion), and then 250 ng total RNA was reverse transcribed to cDNA and transcripts were quantified by Dynamo Sybargreen (Bio-Rad, Hercules, CA) using methods and reaction conditions detailed previously (Biales *et al.*, 2007). Primer specificity was determined through melting curve analysis. Both minus reverse transcription and no-template controls were used to confirm a lack of genomic DNA contamination and/or primer dimer formation. Relative quantity values, unadjusted for amplification efficiency, were calculated using the  $2^{-\Delta\Delta\text{CT}}$  method (Livak and Schmittgen, 2001) using 18S rRNA as a normalizer. QuantumRNA Universal 18S primers (Ambion) were used for 18S rRNA, and all other primer sequences used for the analyses are provided as Supplementary table 1.

**Statistical analysis.** Analyses were conducted such that samples from all relevant treatment groups (i.e., control, continuously exposed to 0.5 or 30  $\mu$ g fadrozole/l, and 8 days exposed to 0.5 or 30  $\mu$ g fadrozole/l then depurated/

allowed to recover [0.5R, 30R]) for each time point were analyzed in the same assay (e.g., radioimmunoassay and QPCR), whereas samples from different time points were often analyzed in separate assays. As a result, interassay variability was generally not a factor in comparisons among treatments but could contribute increased variability to comparisons among time points. Therefore, unless otherwise stated, statistical analyses were focused on comparisons within rather than between time points. Data normality was evaluated using a Kolmogorov-Smirnov test. Homogeneity of variance was evaluated using Levene's test. Data conforming to parametric assumptions were analyzed using one-way ANOVA followed by Duncan's multiple range test. Data that did not conform to parametric assumptions were either transformed to meet parametric criteria or analyzed using a nonparametric Kruskal-Wallis test followed by Dunn's nonparametric *post hoc* test. There were no significant differences among replicate tanks within a treatment group and time point for the endpoints examined. Therefore, individual fish were considered the unit of replication for statistical purposes. Differences were considered significant at  $p < 0.05$  unless otherwise noted.

## RESULTS

Measured concentrations of fadrozole in the 0.5 and 30  $\mu$ g/l treatment tanks over the course of the study (mean  $\pm$  SD) were  $0.35 \pm 0.03$  ( $n = 158$ ) and  $25.3 \pm 1.0$  ( $n = 158$ )  $\mu$ g/l, respectively. No fadrozole was detected ( $< 0.05$   $\mu$ g/l) in water from control tanks. In tanks where fish were exposed to 0.5  $\mu$ g fadrozole/l for 8 days, followed by depuration (0.5R treatments), fadrozole concentrations were nondetectable by day 12 (i.e., after 4 days of depuration) and remained so throughout the rest of depuration. In contrast, in tanks where fish were exposed to 30  $\mu$ g fadrozole/l for 8 days, followed by depuration (30R treatments), 0.1  $\mu$ g fadrozole/l could be detected after 4 days of depuration (exposure day 12), and small fadrozole peaks, estimated as less than 0.02  $\mu$ g fadrozole/l, were detected after 8 days of depuration (exposure day 16). However, after 12 days of depuration, all fadrozole concentrations were less than the method detection limit of 0.05  $\mu$ g/l, and no discernible fadrozole peaks were evident on the chromatograms.

After 1 day of exposure to 30  $\mu$ g fadrozole/l, measured plasma concentrations (mean  $\pm$  SD) were  $30.3 \pm 8.8$  pg fadrozole/ $\mu$ l in males ( $n = 4$ ) and  $26.7 \pm 7.4$  pg fadrozole/ $\mu$ l in females ( $n = 3$ ). After 8 days of exposure to 30  $\mu$ g fadrozole/l, plasma concentrations were  $27.7 \pm 6.0$  pg fadrozole/ $\mu$ l in males ( $n = 6$ ) and  $21.9 \pm 4.5$  pg fadrozole/ $\mu$ l ( $n = 6$ ) in females. After a single day of depuration, those concentrations had dropped to  $1.43 \pm 0.95$  pg fadrozole/ $\mu$ l in males ( $n = 4$ ) and  $2.07 \pm 0.32$  pg fadrozole/ $\mu$ l in females ( $n = 3$ ). No fadrozole was detected in plasma from males or females exposed to control Lake Superior water for 8 days (detection limit, 0.3 pg/ $\mu$ l).

Fish survival was high over the duration of the study. No males and just two of 304 females in the study died prior to sampling. Mean ( $\pm$  SD) temperature of the water in the test tanks was  $25.5 \pm 0.6^{\circ}\text{C}$ . Mean ( $\pm$  SD) dissolved oxygen concentration was  $6.2 \pm 0.6$  mg/l, and pH was  $7.58 \pm 0.16$ . There were no significant treatment-related differences in survival or water quality conditions.

Exposure to fadrozole had significant effects on plasma E2 concentrations in females but only in those exposed to 30  $\mu$ g

fadrozole/l (Fig. 1A). Plasma E2 concentrations were significantly reduced within 1 day of exposure to 30  $\mu$ g fadrozole/l. After 8 days of exposure, plasma E2 concentrations in females exposed to 30  $\mu$ g fadrozole/l had rebounded slightly and were not significantly different from those in control females. However, for those females exposed to 30  $\mu$ g fadrozole/l continuously for 12 or more days, plasma E2 concentrations remained significantly reduced. In females exposed to 30  $\mu$ g fadrozole/l for 8 days, then exposed to control Lake Superior water over subsequent days, plasma E2 concentrations rebounded dramatically and were actually significantly greater than those detected in control females 4 and 8 days postexposure, before returning to control levels following 12 or more days of depuration/recovery (Fig. 1A). Plasma E2 concentrations in females exposed to 0.5  $\mu$ g fadrozole/l (nominal) were not significantly different from those in control females (Fig. 1B).

Concentrations of the estrogen-responsive protein, VTG, in female plasma were significantly affected at both 0.5 and 30  $\mu$ g/l fadrozole concentrations (Figs. 1C and 1D). Exposure to 30  $\mu$ g fadrozole/l reduced plasma VTG concentrations

more than 2.4-fold within 24 h and over 40-fold within 8 days. Plasma VTG concentrations remained significantly depressed (> 65- to 400-fold) in the females continuously exposed beyond 8 days. For females exposed to 30  $\mu$ g fadrozole/l for 8 days and control water on subsequent days, plasma VTG concentrations generally remained significantly depressed compared with controls (except 16 days postexposure; day 24). However, the VTG concentrations in those fish were only about 1.5- to 2.5-fold less than those in control fish. That was similar to the magnitude of VTG depression observed in fish exposed continuously to 0.5  $\mu$ g fadrozole/l for 12 or more days (Fig. 1D). As in fish exposed to the greater concentration of fadrozole, depuration in Lake Superior water after 8 days of exposure to 0.5  $\mu$ g fadrozole/l resulted in some recovery of VTG concentrations compared with fish that were continuously exposed; however, they still tended to be lower than those in females never exposed to fadrozole.

In addition to effects on circulating concentrations of E2 and VTG, steroid production by ovary tissue was affected by the *in vivo* exposure to fadrozole (Figs. 2A and 2B). *Ex vivo*

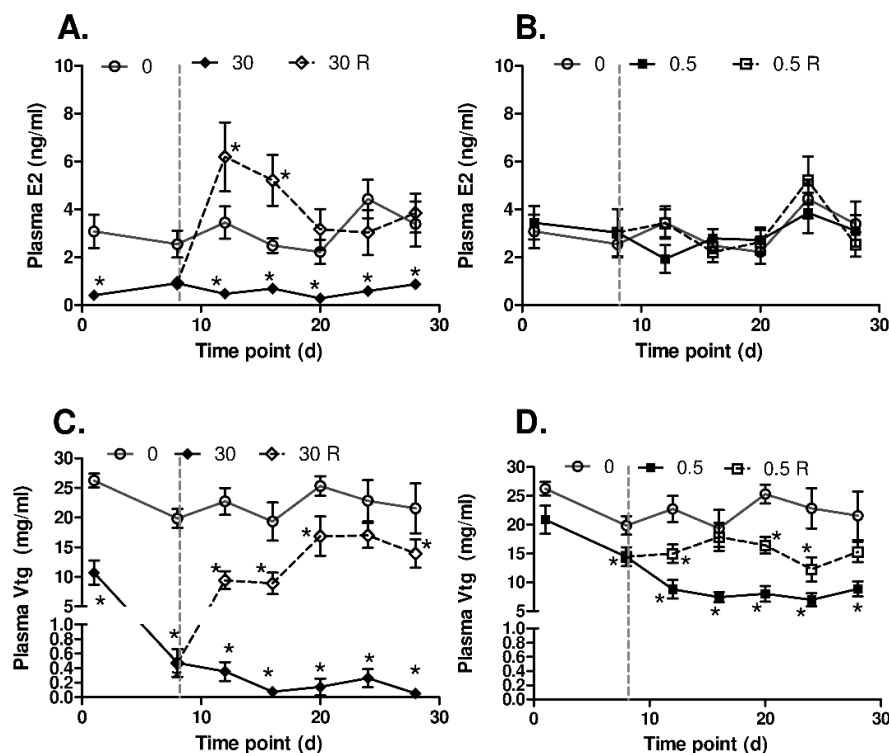
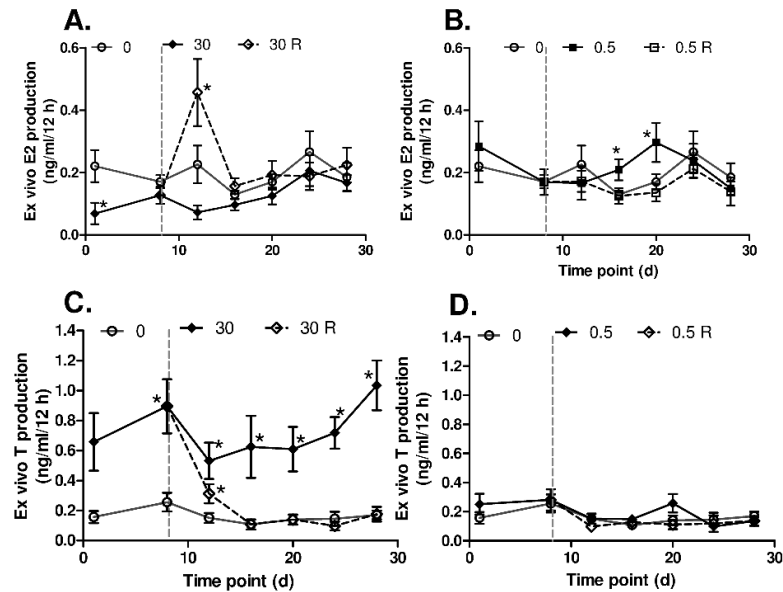


FIG. 1. Concentrations of 17 $\beta$ -estradiol (E2; panels A and B) and vitellogenin (VTG; panels C and D) measured in the plasma of female fathead minnows exposed to 0, 0.5 (panels B and D), or 30  $\mu$ g (panels A and C) fadrozole/l either continuously for 1, 8, 12, 16, 20, 24, or 28 days, or exposed to 0.5 or 30  $\mu$ g fadrozole/l for 8 days followed by an additional 4, 8, 12, 16, or 20 days of depuration in control Lake Superior water (no fadrozole; 0.5 R, 30 R). Error bars represent SE and  $n = 8$  for most conditions (treatment  $\times$  time point combinations). Vertical dashed line indicates cessation of chemical delivery to 0.5 R and 30 R treatments. \* indicates statistically significant difference from control (0) within time point.



**FIG. 2.** *Ex vivo* production of 17 $\beta$ -estradiol (E2; panels A and B) and testosterone (T; panels C and D) by ovary tissue collected from female fathead minnows exposed to 0, 0.5 (panels B and D), or 30  $\mu$ g fadrozole/l either continuously for 1, 8, 12, 16, 20, 24, or 28 days, or exposed to 0.5 or 30  $\mu$ g fadrozole/l for 8 days followed by an additional 4, 8, 12, 16, or 20 days of depuration in control Lake Superior water (no fadrozole; 0.5 R, 30 R). Error bars represent SE and  $n = 8$  for most conditions (treatment  $\times$  time point combinations). Vertical dashed line indicates cessation of chemical delivery to 0.5 R and 30 R treatments. \* indicates statistically significant difference from control (0) within time point.

E2 production by ovary tissue was significantly reduced after 24 h of exposure to 30  $\mu$ g fadrozole/l. However, in contrast with plasma E2 concentrations, that significant effect did not persist when the exposure period was extended beyond 8 days. What was similar to the plasma E2 effect was the significant increase in *ex vivo* E2 production by ovary tissue collected from fish that were exposed for 8 days, and then held in control water only for the subsequent 4 days. Over the 12-h incubation period, ovary tissue from these fish produced, on average, twice as much E2 as ovary tissue from control fish and 6.5 times more than ovary tissue from fish exposed continuously for 12 days. *Ex vivo* T production was also significantly affected (Figs. 2C and 2D). Specifically, ovary tissue from females exposed to 30  $\mu$ g fadrozole/l for 8 or more days produced, on average, about five times more T than ovary tissue from control fish. In the fish exposed to 30  $\mu$ g fadrozole/l for 8 days before being held in control water, *ex vivo* T production returned to the control range within 8 days postexposure.

At the molecular level, there was significant modulation of the abundance of two transcripts coding for proteins thought to be key for production of E2 by the fish ovary. In the females that experienced significant reductions in circulating E2 concentrations (i.e., those exposed continuously to 30  $\mu$ g fadrozole/l), both *cyp19a1a* and *fshr* expressions were significantly elevated throughout the entire exposure duration (except day 1 in the case of *cyp19a1a*; Fig. 3). The abundance of transcripts coding

for StAR and CYP11A was not significantly affected by fadrozole exposure (Supplementary fig. 2).

## DISCUSSION

In an earlier study (experiment 1), Villeneuve *et al.* (2009) reported that exposure to 3 or 30  $\mu$ g fadrozole/l caused significant reductions in *ex vivo* E2 production and plasma E2 concentrations within 24 h and that over subsequent days of exposure (through day 8), effects on *ex vivo* E2 production (both doses) and plasma E2 concentrations (3  $\mu$ g fadrozole/l only) gradually decreased. The gradual reduction in impact was accompanied by rapid and persistent increases in the expression of *cyp19a1a* and *fshr* (particularly at the 30  $\mu$ g/l concentration) and more transient upregulation of *star* and *cyp11a* (Villeneuve *et al.*, 2009). After fadrozole delivery ceased, there was a period of increased *ex vivo* E2 production compared with the controls, suggesting that E2 production rates by the gonad had increased as part of a compensatory response to aromatase inhibition by fadrozole. This study (experiment 2) largely confirmed those initial results. *Ex vivo* E2 production and plasma E2 concentrations in fish exposed to 30  $\mu$ g fadrozole/l recovered slightly from exposure day 1 to exposure day 8, such that on day 8 the effect of fadrozole was not statistically significant (Figs. 1A and 2A). Fish exposed to 30  $\mu$ g fadrozole/l for

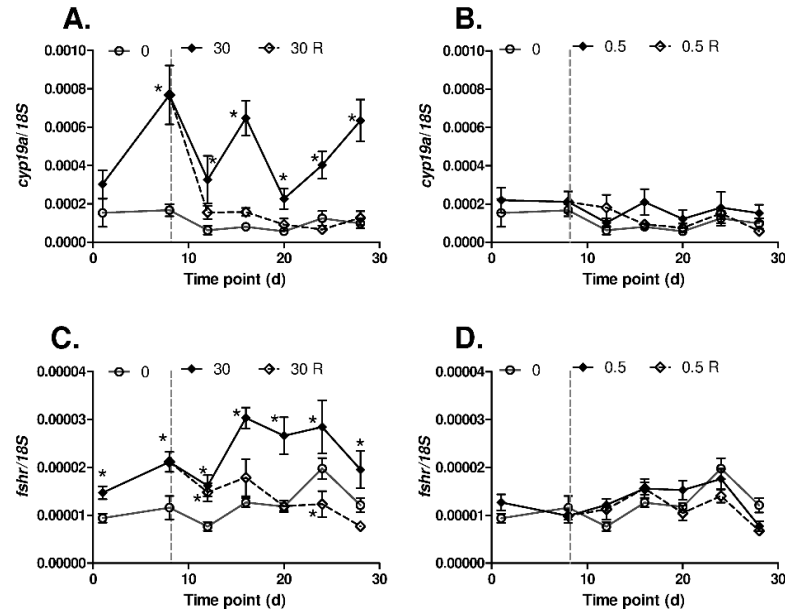


**FIG. 3.** Relative abundance of *cyp19a* (panels A and B) and *fshr* (panels C and D) transcripts detected in the ovaries of female fathead minnows exposed to 0, 0.5 (panels B and D), or 30 (panels A and C)  $\mu\text{g}$  fadrozole/l either continuously for 1, 8, 12, 16, 20, 24, or 28 days, or exposed to 0.5 or 30  $\mu\text{g}$  fadrozole/l for 8 days followed by an additional 4, 8, 12, 16, or 20 days of depuration in control Lake Superior water (no fadrozole; 0.5 R, 30 R). Relative transcript abundance normalized to 18S rRNA. Error bars represent SE and  $n = 8$  for most conditions (treatment  $\times$  time point combinations). Vertical dashed line indicates cessation of chemical delivery to 0.5 R and 30 R treatments. \* indicates statistically significant difference from control (0) within time point.

8 days followed by control water on subsequent days exhibited a period during which their *ex vivo* and plasma E2 concentrations exceeded those of the controls, again, suggesting that the fish had mounted a compensatory response to the stressor. Just as in the previous study (experiment 1), both *cyp19a* and *fshr* expression, thought to be localized primarily within the granulosa cells, increased in response to fadrozole exposure. Additionally, this study (experiment 2) showed that this change in gene expression was sustained over the entire period of time that the fadrozole exposure was continued. In contrast, the more transient increases in *cyp11a* and *star* transcripts (Villeneuve *et al.*, 2009), both of which are thought to be localized primarily in the theca cells, were not observed in this study. Given that elevated *ex vivo* production of T was observed in both this study (experiment 2) and the previous one (experiment 1; Villeneuve *et al.*, 2009), it is not clear whether increased expression of *cyp11a* and *star* is not a consistent response to aromatase inhibition and/or declining E2 concentrations or whether the timing of sample collection in this study (experiment 2) simply missed this more transient upregulation. Either way, there were several distinct consistencies between this study (experiment 2) and that of Villeneuve *et al.* (2009) (experiment 1), which suggest a mechanism of compensation that should be incorporated into dynamic concentration-response models intended to predict effects of aromatase inhibitors.

In addition to confirming reproducibility of our previous study with fadrozole, the current, more temporally intensive study (experiment 2) enabled a more thorough mechanistic evaluation of compensatory responses to aromatase inhibition. For example, in experiment 1, Villeneuve *et al.* (2009) noted that although plasma VTG concentrations recovered considerably over the 8 days depuration/recovery period included in that study, concentrations of the lipoprotein never returned to control levels (Villeneuve *et al.*, 2009). Therefore, we were curious whether full recovery of circulating VTG concentrations would occur over a more extended recovery period as this has significant implications for predicting/modeling the potential reproductive impacts of aromatase inhibition in fish (Miller *et al.*, 2007; Li *et al.*, 2011a,b). We found that even when the depuration period was extended 2.5 times longer than that in experiment 1 (Villeneuve *et al.*, 2009), plasma VTG concentrations did not return to levels comparable to those in females that had never been exposed to fadrozole (Fig. 1C) despite the fact that plasma E2 concentrations had fully recovered or even exceeded those of control fish (Fig. 1A). Remarkably, even at the lower concentration of fadrozole (0.5  $\mu\text{g}/\text{l}$ ), which caused no discernible effect on plasma E2 concentrations (Fig. 1B), some reduction in VTG concentrations was evident over roughly half of the depuration/recovery phase of the experiment (Fig. 1D). These results suggest that, of the endpoints examined in this

study (experiment 2), plasma VTG concentrations were the most sensitive to the effects of fadrozole. Furthermore, even modest effects on VTG concentrations were quite persistent, further affirming the utility of VTG concentrations, in female fish, as a useful biomarker (Miller *et al.*, 2007). This extended duration of VTG depression following a transient exposure to an aromatase inhibitor can, in theory, be incorporated into modeling efforts. However, remaining uncertainties as to just how long the VTG depression may persist and the subtle mechanisms through which VTG production is reduced even at concentrations that cause no detectable change in E2 production or circulation make accurate modeling of VTG responses challenging.

A second major question that arose from our previous time course study with fadrozole (experiment 1) was whether the apparent compensatory response that led to a recovery in *ex vivo* E2 production and plasma concentrations (at least for the 3 µg fadrozole/l treatment; Villeneuve *et al.*, 2009) could be sustained over a longer exposure duration. At the molecular level, the response in this study (experiment 2) was maintained, with increased *cyp19a1a* and *fshr* being sustained throughout the duration of fadrozole exposure. *Ex vivo* E2 production was maintained at a level that was not significantly different from the control. However, consistent with experiment 1 (Villeneuve *et al.*, 2009), neither plasma E2 nor VTG concentrations recovered despite what might be viewed as successful compensation, at least in terms of *ex vivo* steroid production. This is consistent with results of a 21-day reproduction experiment with fadrozole in which exposure to concentrations greater than 10 µg fadrozole/l caused significant reductions in plasma E2 and VTG concentrations and associated reductions in fish fecundity (Ankley *et al.*, 2002). Unfortunately, the 0.5 µg fadrozole/l treatment concentration included in this study (experiment 2) did not cause significant reductions in *ex vivo* E2 production or plasma E2 concentrations, so it was not feasible to directly discern whether compensation could be successfully maintained at lower fadrozole concentrations. However, the VTG effect at the 0.5 µg/l concentration does suggest that some impact was occurring, even if it could not be resolved statistically for endpoints other than VTG. Thus, at present, although there is evidence that some compensatory response to fadrozole exposure occurs, it is not clear that it ultimately does much to mitigate the potential negative effects on plasma VTG production and, ultimately, reproduction, in long-term exposures.

This study (experiment 2) also provided critical knowledge concerning the kinetics of fadrozole uptake and excretion in fish as it relates to the responses observed *in vivo*. Based on fadrozole's estimated log Kow of 3.20 (estimated using KOWWIN v. 1.67; <http://www.epa.gov/opptintr/exposure/pubs/episuite.htm>) and assuming strictly branchial uptake and elimination, one would predict an equilibrium blood:water partition coefficient ( $P_{BW}$ ) of 35 (Fitzsimmons *et al.*, 2001). Total measured concentrations in plasma (not differentiating free fadrozole from protein bound) were approximately equal to

water concentrations, suggesting rapid metabolism of fadrozole by fathead minnows. This was further supported by the plasma data that showed that fadrozole was rapidly cleared from the body during depuration. Based on these results, it appears that for modeling purposes, plasma concentrations of fadrozole can be assumed to be similar to water concentrations under steady-state conditions.

Finally, although it did not relate directly to our initial study objectives or hypotheses, the time-dependent profile of *cyp19a1a* expression in fish exposed continuously to 30 µg fadrozole/l was notable. Increased *cyp19a1a* expression can be viewed as one of the primary compensatory responses to declining E2 concentrations. Over the course of the 28-day exposure, average *cyp19a1a* expression, although elevated, seemed to oscillate. Although interesting in its own right, what was even more remarkable was that plasma E2 concentrations followed a parallel time-dependent pattern (Fig. 4). *Ex vivo* E2 production, which, in a cause-effect sense, would be considered more temporally proximal to *cyp19a1a* expression, did not closely parallel the *cyp19a1a* expression profile (Supplementary fig. 3). Although by no means definitive, these behaviors raise the question of whether circulating E2 concentrations have a direct influence on *cyp19a1a* expression in the fathead minnow ovary. As opposed to *cyp19a1b*, which is an isoform of the aromatase gene predominantly expressed in brain and known to be regulated by estrogen responsive elements, the *cyp19a1a* isoform is not thought to contain a functional estrogen responsive element as part of its gene regulatory region (Callard *et al.*, 2001; Kishida and Callard, 2001). Therefore, there is currently no evidence to suggest that direct interaction of E2 with the estrogen receptor in ovary tissue could account for the parallel profiles. However, it has been suggested that T can stimulate follicle-stimulating hormone-independent expression of *cyp19*

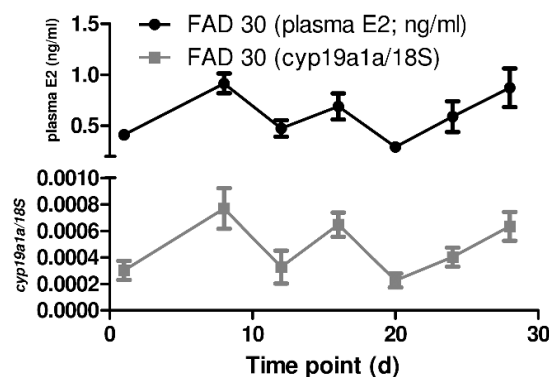


FIG. 4. Comparison of the time-dependent profile of *cyp19a1a* transcript abundance (normalized to 18S rRNA) with the time-dependent profile of plasma 17β-estradiol (E2) concentrations in female fathead minnows continuously exposed to 30 µg fadrozole/l for 1, 8, 12, 16, 20, 24, or 28 days. Error bars represent SE and  $n = 8$  for most conditions (treatment × time point combinations). Y-axis is split to allow measurements made in different units to be displayed on the same graph.

in mammalian granulosa cells via interaction with liver receptor homolog-1 LRH-1 (Wu *et al.*, 2011). It is not known whether a similar mechanism operates in fish, nor was it feasible to measure circulating T concentrations in the females from this study due to limited available plasma volumes. Nonetheless, the *ex vivo* T production results suggest that excess accumulation of T in ovary tissue and/or plasma was possible. Assuming that impaired ability to aromatize T to E2 was the major cause of the nearly fivefold increase in *ex vivo* T release from the ovaries of fish exposed to 30 µg fadrozole/l, one could hypothesize that direct, local, T-dependent regulation of *cyp19a1a* expression could yield an oscillatory expression pattern. Such regulation, if it exists, would be an important regulatory pathway to include in a mechanistic model of steroidogenesis. Thus, follow-up investigations are warranted.

As a whole, these data contribute to on-going efforts to understand and model biological responses to EACs, like aromatase inhibitors. Development of computational system models that incorporate knowledge concerning the compensatory feedback mechanisms that modulate the impacts of EACs can lead to improved prediction of complex concentration-duration-response behaviors. If appropriately coupled to complementary toxicokinetic models, such computational system models have potential to aid the extrapolation of *in vitro* toxicity pathway assay data into probabilistic predictions of potential adverse outcome(s). Additionally, iterations of model development and empirical testing can lead to an improved understanding of the biology underlying toxicological responses to EACs and other environmental contaminants (see companion paper; Breen *et al.* 2013).

#### SUPPLEMENTARY DATA

Supplementary data are available online at <http://toxsci.oxfordjournals.org/>.

#### FUNDING

United States Environmental Protection Agency, Office of Research and Development; National Health and Environmental Effects Research Laboratory; National Exposure Research Laboratory; National Center for Computational Toxicology.

#### ACKNOWLEDGMENTS

Additional technical support for aspects of this work was provided by Michael D. Kahl, Elizabeth J. Durhan, Carlisle A. LaLone, Elizabeth K. Medlock, Sara M. Seidl, Sarah Y. Skolness, and Matthew A. Weberg. The authors thank Michael Hornung for reviewing an earlier draft of this paper. This manuscript has been reviewed in accordance with official U.S. EPA policy. Mention of products and trade names does not indicate endorsement by the federal government. Conclusions

drawn in this study neither constitute nor necessarily reflect U.S. EPA policy.

#### REFERENCES

- Ankley, G. T., Bencic, D. C., Breen, M. S., Collette, T. W., Conolly, R. B., Denslow, N. D., Edwards, S. W., Ekman, D. R., Garcia-Reyero, N., Jensen, K. M., *et al.* (2009a). Endocrine disrupting chemicals in fish: Developing exposure indicators and predictive models of effects based on mechanism of action. *Aquat. Toxicol.* **92**, 168–178.
- Ankley, G. T., Bencic, D. C., Cavallin, J. E., Jensen, K. M., Kahl, M. D., Makynen, E. A., Martinovic, D., Mueller, N. D., Wehmas, L. C., and Villeneuve, D. L. (2009b). Dynamic nature of alterations in the endocrine system of fathead minnows exposed to the fungicide prochloraz. *Toxicol. Sci.* **112**, 344–353.
- Ankley, G. T., Bennett, R. S., Erickson, R. J., Hoff, D. J., Hornung, M. W., Johnson, R. D., Mount, D. R., Nichols, J. W., Russom, C. L., Schmieder, P. K., *et al.* (2010). Adverse outcome pathways: A conceptual framework to support ecotoxicology research and risk assessment. *Environ. Toxicol. Chem.* **29**, 730–741.
- Ankley, G. T., Jensen, K. M., Durhan, E. J., Makynen, E. A., Butterworth, B. C., Kahl, M. D., Villeneuve, D. L., Linnam, A., Gray, L. E., Cardon, M., *et al.* (2005). Effects of two fungicides with multiple modes of action on reproductive endocrine function in the fathead minnow (*Pimephales promelas*). *Toxicol. Sci.* **86**, 300–308.
- Ankley, G. T., Jensen, K. M., Kahl, M. D., Makynen, E. A., Blake, L. S., Greene, K. J., Johnson, R. D., and Villeneuve, D. L. (2007). Ketoconazole in the fathead minnow (*Pimephales promelas*): Reproductive toxicity and biological compensation. *Environ. Toxicol. Chem.* **26**, 287–296.
- Ankley, G. T., Kahl, M. D., Jensen, K. M., Hornung, M. W., Korte, J. J., Makynen, E. A., and Leino, R. L. (2002). Evaluation of the aromatase inhibitor fadrozole in a short-term reproduction assay with the fathead minnow (*Pimephales promelas*). *Toxicol. Sci.* **67**, 121–130.
- Biales, A. D., Bencic, D. C., Flick, R. W., Lazorchak, J., and Lattier, D. L. (2007). Quantification and associated variability of induced vitellogenin gene transcripts in fathead minnow (*Pimephales promelas*) by quantitative real-time polymerase chain reaction assay. *Environ. Toxicol. Chem.* **26**, 287–296.
- Breen, M., Villeneuve, D. L., Ankley, G. T., Bencic, D. C., Breen, M. S., Watanabe, K. H., Lloyd, A. L., and Conolly, R. B. (2013). Developing Predictive approaches to characterize adaptive responses of the reproductive endocrine axis to aromatase inhibition: II. Computational modeling. *Toxicol. Sci.* **133**, 234–247.
- Callard, G. V., Tchoudakova, A. V., Kishida, M., and Wood, E. (2001). Differential tissue distribution, developmental programming, estrogen regulation and promoter characteristics of *cyp19* genes in teleost fish. *J. Steroid Biochem. Mol. Biol.* **79**, 305–314.
- Collette, T. W., Teng, Q., Jensen, K. M., Kahl, M. D., Makynen, E. A., Durhan, E. J., Villeneuve, D. L., Martinović-Weigelt, D., Ankley, G. T., and Ekman, D. R. (2010). Impacts of an anti-androgen and an androgen/anti-androgen mixture on the metabolite profile of male fathead minnow urine. *Environ. Sci. Technol.* **44**, 6881–6886.
- Deng, Y. F., Chen, X. X., Zhou, Z. L., and Hou, J. F. (2010). Letrozole inhibits the osteogenesis of medullary bone in prelay pullets. *Poult. Sci.* **89**, 917–923.
- Drenth, H. J., Bouwman, C. A., Seinen, W., and Van den Berg, M. (1998). Effects of some persistent halogenated environmental contaminants on aromatase (CYP19) activity in the human choriocarcinoma cell line JEG-3. *Toxicol. Appl. Pharmacol.* **148**, 50–55.
- Ekman, D. R., Villeneuve, D. L., Teng, Q., Ralston-Hooper, K. J., Martinović-Weigelt, D., Kahl, M. D., Jensen, K. M., Durhan, E. J., Makynen, E. A., Ankley, G. T., *et al.* (2011). Use of gene expression, biochemical and metabolite profiles to enhance exposure and effects assessment of the model androgen 17β-trenbolone in fish. *Environ. Toxicol. Chem.* **30**, 319–329.

- Fitzsimmons, P. N., Fernandez, J. D., Hoffman, A. D., Butterworth, B. C., and Nichols, J. W. (2001). Branchial elimination of superhydrophobic organic compounds by rainbow trout (*Oncorhynchus mykiss*). *Aquat. Toxicol.* **55**, 23–34.
- Gerardin, D. C., Piffer, R. C., Garcia, P. C., Moreira, E. G., and Pereira, O. C. (2008). Effects of maternal exposure to an aromatase inhibitor on sexual behaviour and neurochemical and endocrine aspects of adult male rat. *Reprod. Fertil. Dev.* **20**, 557–562.
- Hamad, A., Kluk, M., Fox, J., Park, M., and Turner, J. E. (2007). The effects of aromatase inhibitors and selective estrogen receptor modulators on eye development in the zebrafish (*Danio rerio*). *Curr. Eye Res.* **32**, 819–827.
- Jensen, K. M., Korte, J. J., Kahl, M. D., Pasha, M. S., and Ankley, G. T. (2001). Aspects of basic reproductive biology and endocrinology in the fathead minnow (*Pimephales promelas*). *Comp. Biochem. Physiol. C Toxicol. Pharmacol.* **128**, 127–141.
- Kishida, M., and Callard, G. V. (2001). Distinct cytochrome P450 aromatase isoforms in zebrafish (*Danio rerio*) brain and ovary are differentially programmed and estrogen regulated during early development. *Endocrinology* **142**, 740–750.
- Korte, J. J., Kahl, M. D., Jensen, K. M., Mumtaz, S. P., Parks, L. G., LeBlanc, G. A., and Ankley, G. T. (2000). Fathead minnow vitellogenin: Complementary DNA sequence and messenger RNA and protein expression after 17 $\beta$ -estradiol treatment. *Environ. Toxicol. Chem.* **19**(4), 972–981.
- Li, Z., Kroll, K. J., Jensen, K. M., Villeneuve, D. L., Ankley, G. T., Brian, J. V., Sepúlveda, M. S., Orlando, E. F., Lazorchak, J. M., Kostich, M., et al. (2011a). A computational model of the hypothalamic: Pituitary: gonadal axis in female fathead minnows (*Pimephales promelas*) exposed to 17 $\alpha$ -ethynylestradiol and 17 $\beta$ -trenbolone. *BMC Syst. Biol.* **5**, 63.
- Li, Z., Wang, Y., Peng, K., Chen, L., and Chu, S. (2011b). (E)-3-(2-Bromophen-yl)-1-(3,4-dimethoxy-phen-yl)prop-2-en-1-one. *Acta Crystallogr. Sect. E. Struct. Rep. Online* **68**(Pt 3), 6776.
- Livak, K. J., and Schmittgen, T. D. (2001). Analysis of relative gene expression data using real-time quantitative PCR and the 2<sup>-</sup>(Delta Delta C(T)) Method. *Methods* **25**, 402–408.
- Martinovic, D., Blake, L. S., Durhan, E. J., Greene, K. J., Kahl, M. D., Jensen, K. M., Makynen, E. A., Villeneuve, D. L., and Ankley, G. T. (2008). Reproductive toxicity of vinclozolin in the fathead minnow: Confirming an anti-androgenic mode of action. *Environ. Toxicol. Chem.* **27**, 478–488.
- McAllister, B. G., and Kime, D. E. (2003). Early life exposure to environmental levels of the aromatase inhibitor tributyltin causes masculinisation and irreversible sperm damage in zebrafish (*Danio rerio*). *Aquat. Toxicol.* **65**, 309–316.
- McMaster, M. E., Munkittrick, K. R., Jardine, J. J., Robinson, R. D., and Van Der Kraak, G. J. (1995). Protocol for measuring in vitro steroid production by fish gonadal tissue. *Canadian Technical Report of Fisheries and Aquatic Sciences 1961*. Department of Fisheries and Oceans, Burlington, Ontario, Canada.
- Miller, W. L. (1988). Molecular biology of steroid hormone synthesis. *Endocr. Rev.* **9**, 295–318.
- Miller, D. H., Jensen, K. M., Villeneuve, D. L., Kahl, M. D., Makynen, E. A., Durhan, E. J., and Ankley, G. T. (2007). Linkage of biochemical responses to population-level effects: A case study with vitellogenin in the fathead minnow (*Pimephales promelas*). *Environ. Toxicol. Chem.* **26**, 521–527.
- Olmstead, A. W., Kosian, P. A., Korte, J. J., Holcombe, G. W., Woodis, K. K., and Degitz, S. J. (2009). Sex reversal of the amphibian, *Xenopus tropicalis*, following larval exposure to an aromatase inhibitor. *Aquat. Toxicol.* **91**, 143–150.
- Reif, D. M., Martin, M. T., Tan, S. W., Houck, K. A., Judson, R. S., Richard, A. M., Knudsen, T. B., Dix, D. J., and Kavlock, R. J. (2010). Endocrine profiling and prioritization of environmental chemicals using ToxCast data. *Environ. Health Perspect.* **118**, 1714–1720.
- Sanderson, J. T. (2006). The steroid hormone biosynthesis pathway as a target for endocrine-disrupting chemicals. *Toxicol. Sci.* **94**, 3–21.
- Sun, L., Zha, J., Spear, P. A., and Wang, Z. (2007). Toxicity of the aromatase inhibitor letrozole to Japanese medaka (*Oryzias latipes*) eggs, larvae and breeding adults. *Comp. Biochem. Physiol. C Toxicol. Pharmacol.* **145**, 533–541.
- Tiboni, G. M., Marotta, F., Rossi, C., and Giampietro, F. (2008). Effects of the aromatase inhibitor letrozole on in utero development in rats. *Hum. Reprod.* **23**, 1719–1723.
- Villeneuve, D. L., and Garcia-Reyero, N. (2011). Vision & strategy: Predictive ecotoxicology in the 21<sup>st</sup> century. *Environ. Toxicol. Chem.* **30**, 1–8.
- Villeneuve, D. L., Knoebel, I., Kahl, M. D., Jensen, K. M., Hammermeister, D. E., Greene, K. J., Blake, L. S., and Ankley, G. T. (2006). Relationship between brain and ovary aromatase activity and isoform-specific aromatase mRNA expression in the fathead minnow (*Pimephales promelas*). *Aquat. Toxicol.* **76**, 353–368.
- Villeneuve, D. L., Mueller, N. D., Martinović, D., Makynen, E. A., Kahl, M. D., Jensen, K. M., Durhan, E. J., Cavallin, J. E., Bencic, D., and Ankley, G. T. (2009). Direct effects, compensation, and recovery in female fathead minnows exposed to a model aromatase inhibitor. *Environ. Health Perspect.* **117**, 624–631.
- Vinggaard, A. M., Hnida, C., Breinholt, V., and Larsen, J. C. (2000). Screening of selected pesticides for inhibition of CYP19 aromatase activity in vitro. *Toxicol. In Vitro* **14**, 227–234.
- Wacker, D. W., Schlenger, B. A., and Wingfield, J. C. (2008). Combined effects of DHEA and fadrozole on aggression and neural VIP immunoreactivity in the non-breeding male song sparrow. *Horm. Behav.* **53**, 287–294.
- Wu, Y. G., Bennett, J., Talla, D., and Stocco, C. (2011). Testosterone, not 5 $\alpha$ -dihydrotestosterone, stimulates LRH-1 leading to FSH-independent expression of Cyp19 and P450<sub>scc</sub> in granulosa cells. *Mol. Endocrinol.* **25**, 656–668.

## SUPPLEMENTARY DATA

### ***Investigation of Adaptive Responses in Female Fathead Minnows (*Pimephales promelas*) Exposed to an Aromatase Inhibitor to Support Computational Modeling of the Hypothalamic-Pituitary-Gonadal Axis and 21<sup>st</sup> Century Toxicity Testing***

Daniel L. Villeneuve<sup>\*1</sup>, Miyuki Breen<sup>†</sup>, David C. Bencic<sup>‡</sup>, Jenna E. Cavallin<sup>\*2</sup>, Kathleen M. Jensen<sup>\*</sup>, Elizabeth A. Makynen<sup>\*</sup>, Linnea M. Thomas<sup>\*</sup>, Leah C. Wehmas<sup>\*</sup>, Rory B. Conolly<sup>§</sup>, Gerald T. Ankley<sup>\*</sup>

\* United States Environmental Protection Agency, Mid-Continent Ecology Division, 6201 Congdon Blvd., Duluth, MN, 55804, USA.

† Biomathematics Program, Department of Statistics, North Carolina State University, Raleigh, NC, 27695, USA.

‡ United States Environmental Protection Agency, Ecological Exposure Research Division, 26 W. Martin Luther King Drive, Cincinnati, OH, 45268, USA.

§ United States Environmental Protection Agency, Integrated Systems Toxicology Division, 109 T.W. Alexander Drive, Mail E205-02, Research Triangle Park, NC 27711, USA.

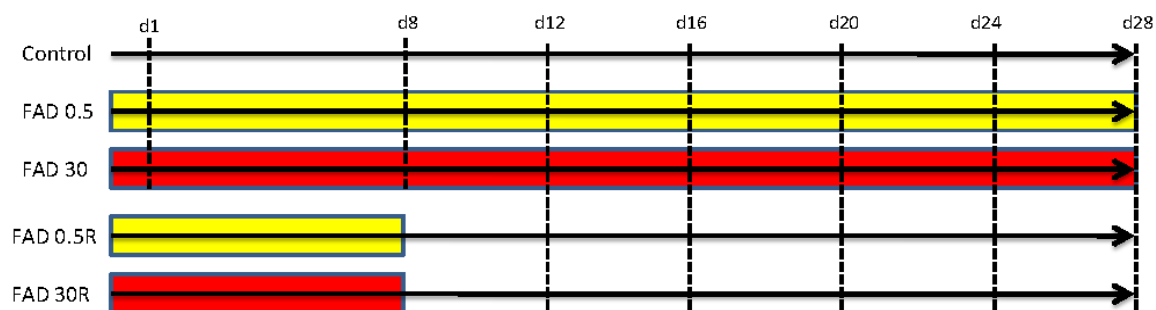
## SUPPLEMENTARY DATA

Table S1. Primers used for real-time quantitative polymerase chain reaction (QPCR) assays.

Primer ID	Sequence (5'→ 3')	Reference (if applicable)
<b>CYP11A_F</b>	CGACACCCGGACTTGCA	(Villeneuve et al. 2007)
<b>CYP11A_R</b>	CACGTCTCCTTTAGAGGTGATACG	(Villeneuve et al. 2007)
<b>FSHR_F</b>	CCCCATCGTTCTGGACATCT	(Villeneuve et al. 2007)
<b>FSHR_R</b>	GAAGCTTAAGGGTCCACAGCAT	(Villeneuve et al. 2007)
<b>StAR_F</b>	CTTGAACAGCAAACAGATGACCTT	(Villeneuve et al. 2007)
<b>StAR_R</b>	CTCCCCCATTTGTTCCATGT	(Villeneuve et al. 2007)
<b>CYP19A_F</b>	CATGCAGAAAACTCGACCA	n/a
<b>CYP19A_R</b>	GCTCCGACCAGCTAAAACAG	n/a
<b>18S-fw</b>	AATGTCTGCCCTATCAACTTTC	(Filby and Tyler 2005)
<b>18S-rv</b>	TGGATGTGGTAGCCGTTTC	(Filby and Tyler 2005)

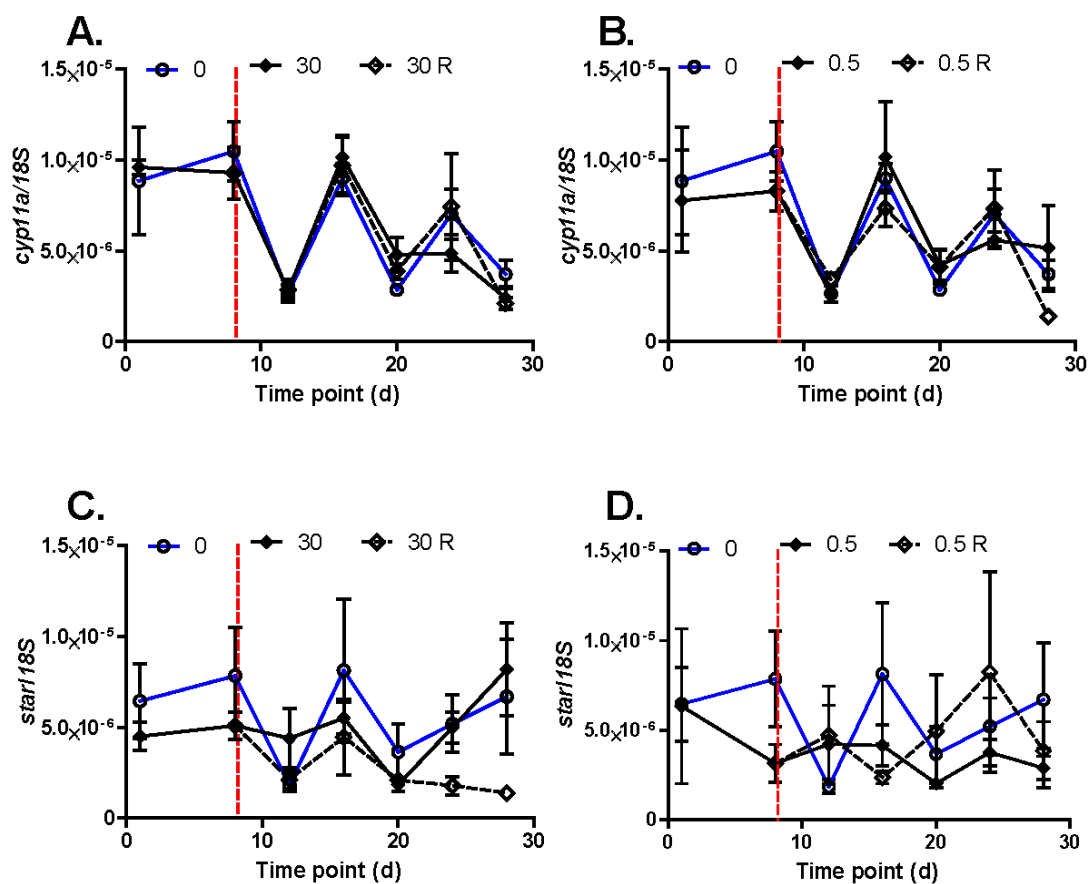
## SUPPLEMENTARY DATA

Figure S1. Diagram of experimental design. Boxes indicate the period of exposure to 0.5 (yellow) or 30  $\mu\text{g}$  (red) fadrozole (FAD)/L, respectively. The lack of a box indicates exposure to control water only. Intersection of vertical dashed lines with the horizontal arrows indicates the days on which samples were collected for each treatment group.



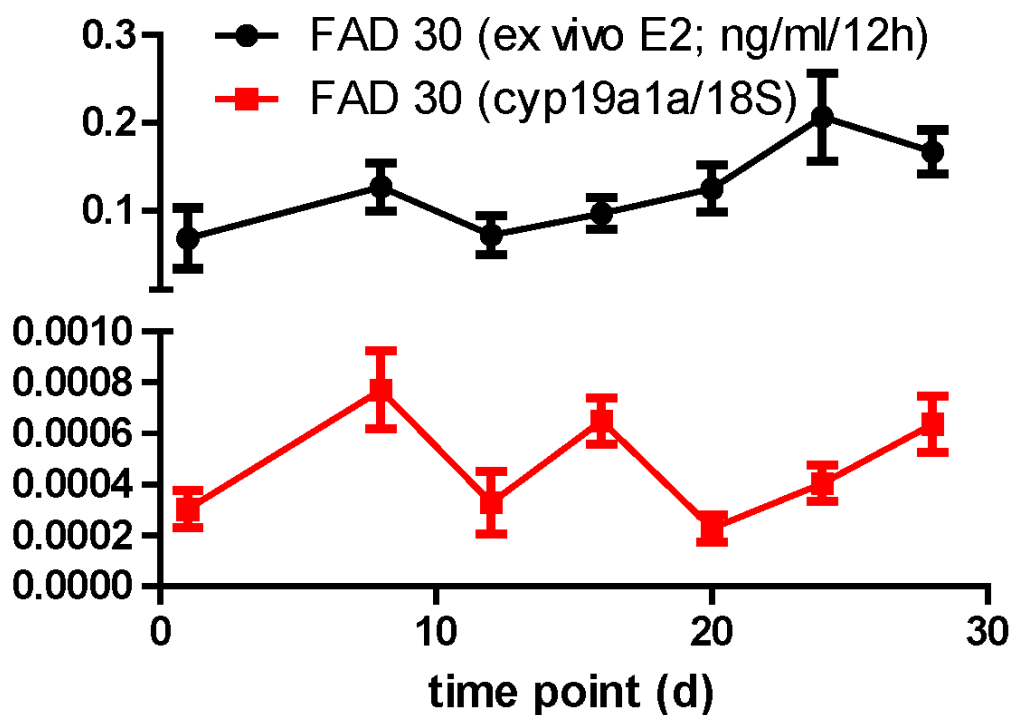
# SUPPLEMENTARY DATA

Figure S2. Relative abundance of *cyp11a* (A, B) and *star* (C, D) transcripts detected in the ovaries of female fathead minnows exposed to 0, 0.5 (B, D), or 30  $\mu$ g (A, C) fadrozole/L continuously for 1, 8, 12, 16, 20, 24, or 28 d, or exposed to 0.5 or 30  $\mu$ g fadrozole/L for 8 d followed by an additional 4, 8, 12, 16, or 20 d of depuration in control Lake Superior water (no fadrozole; 0.5 R, 30 R). Relative transcript abundance normalized to 18S rRNA. Error bars represent SE. n=8 for most conditions (treatment x time-point combinations). Vertical dashed line indicates cessation of chemical delivery to 0.5 R and 30 R treatments.



# SUPPLEMENTARY DATA

Figure S3. Comparison of the time-dependent profile of *cyp19a1a* transcript abundance (normalized to 18S rRNA) with the time-dependent profile of ex vivo E2 production in female fathead minnows continuously exposed to 30 µg fadrozole/L for 1, 8, 12, 16, 20, 24, or 28 d. Error bars represent SE. n=8 for most conditions (treatment x time-point combinations). Y-axis is split to allow measurements made in different units to be displayed on the same graph.



## SUPPLEMENTARY DATA

### REFERENCES

- Villeneuve, D. L., Blake, L. S., Brodin, J. D., Greene, K. J., Knoebl, I., Miracle A. L., et al. (2007). Transcription of key genes regulating gonadal steroidogenesis in control and ketoconazole- or vinclozolin-exposed fathead minnows. *Toxicol. Sci.* **98**(2), 395-407.
- Filby, A., Tyler, C. (2005). Molecular characterization of estrogen receptors 1, 2a, and 2b and their tissue and ontogenic expression profiles in fathead minnow (*Pimephales promelas*). *Biol. Reprod.* **73**, 648-662.